Stabilising Suppressor of Cytokine Signalling 3 (SOCS3) Protein Levels to Limit Neointimal Hyperplasia

Kirsten Margaret Anderson Munro
MSci, MRes

Thesis submitted in fulfilment of the requirements for the Degree of Doctor of Philosophy

April 2016

School of Medical, Veterinary and Life Sciences
Institute of Cardiovascular and Medical Sciences
University of Glasgow

Supervisor: Professor T.M. Palmer
Co-supervisor: Professor A.H. Baker

Summary

Suppressor of cytokine signalling 3 (SOCS3) is a potent inhibitor of the mitogenic, migratory and pro-inflammatory pathways responsible for the development of neointimal hyperplasia (NIH), a key contributor to the failure of vascular reconstructive procedures. However, the protein levels of SOCS3, and therefore its potential to reduce NIH, is limited by its ubiquitylation and high turnover by the proteasome. I hypothesised that stabilisation of endogenous SOCS3 by inhibiting its ubiquitylation has the potential to limit vascular inflammation and NIH. Consequently, the aim of this PhD was to identify the mechanisms promoting the rapid turnover of SOCS3.

Initial experiments involved the identification of residues involved in regulating the turnover of SOCS3 at the proteasome. I assessed the ubiquitylation status of a panel of FLAG tagged SOCS3 truncation mutants and identified a C-terminal 44 amino acid region required for SOCS3 ubiquitylation. This region localised to the SOCS box which is involved in binding Elongin B/C and the formation of a functional E3 ubiquitin ligase complex. However, the single lysine residue at position 173, located within this 44 amino acid region, was not required for ubiquitylation. Moreover, Emetine chase assays revealed that loss of either Lys173 or Lys6 (as documented in the literature) had no significant effect on SOCS3 stability 8 hrs post emetine treatment.

As mutagenesis studies failed to identify key sites of ubiquitylation responsible for targeting SOCS3 to the proteasome, LC-MS-MS analysis of a SOCS3 co-immunoprecipitate was employed. These data were searched for the presence of a Gly-Gly doublet (+114 Da mass shift) and revealed 8 distinct sites of ubiquitylation (Lys23, Lys28, Lys40, Lys85, Lys91, Lys173, Lys195, Lys206) on SOCS3 however Lys6 ubiquitylation was not detected.

As multiple Lys residues were ubiquitylated, I hypothesised that only a Lys-less SOCS3, in which all 8 Lys residues were mutated to Arg, would be resistant to ubiquitylation. Compared to WT SOCS3, Lys-less SOCS3 was indeed found to be completely resistant to ubiquitylation, and significantly more stable than WT SOCS3. These changes occurred in the absence of any detrimental effect on the ability of Lys-less SOCS3 to interact with the Elongin B/C components required to generate a functional E3 ligase complex. In addition,

both WT and Lys-less SOCS3 were equally capable of inhibiting cytokine-stimulated STAT3 phosphorylation upon co-expression with a chimeric EpoR-gp130 receptor.

To assess whether SOCS3 auto-ubiquitylates I generated an L189A SOCS3 mutant that could no longer bind the Elongins and therefore form the E3 ligase complex required for ubiquitylation. A denaturing IP to assess the ubiquitylation status of this mutant was performed and revealed that, despite an inability to bind the Elongins, the L189A mutant was poly-ubiquitylated similar to WT SOCS3. Together these data suggested that SOCS3 does not auto-ubiquitylate and that a separate E3 ligase must regulate SOCS3 ubiquitylation.

This study sought to identify the E3 ligase and deubiquitylating (DUB) enzymes controlling the ubiquitylation of SOCS3. Our initial strategy was to develop a tool to screen an E3 ligase/DUB library, using an siARRAY, to sequentially knockdown all known E3 ligases in the presence of a SOCS3-luciferase fusion protein or endogenous SOCS3 in a high content imaging screening platform. However, due to a poor assay window (<2) and non-specific immunoreactivity of SOCS3 antibodies available, these methods were deemed unsuitable for screening purposes. In the absence of a suitable tool to screen the si-ARRAY, LC-MS-MS analysis of a SOCS3 co-immunoprecipitate (co-IP) was investigated. I performed a SOCS3 under conditions which preserved protein-protein interactions, with the aim of identifying novel E3 ligase and/or DUBs that could potentially interact with SOCS3.

These data were searched for E3 ligase or DUB enzymes that may interact with SOCS3 in HEK293 cells and identified two promising candidates i) an E3 ligase known as HectD1 and ii) a DUB known as USP15. This thesis has demonstrated that in the presence of HectD1 overexpression, a slight increase in K63-linked polyubiquitylation of SOCS3 was observed. Mutagenesis also revealed that an N-terminal region of SOCS3 may act as a repressor of this interaction with HectD1. Additionally, USP15 was shown to reduce SOCS3 polyubiquitylation in a HEK293 overexpression system suggesting this may act as a DUB for SOCS3. The C-terminal region of SOCS3 was also shown to play a major role in the interaction with USP15.

The original hypothesis of this thesis was that stabilisation of endogenous SOCS3 by inhibiting its ubiquitylation has the potential to limit vascular inflammation and NIH.

Consistent with this hypothesis, immunohistochemistry visualisation of SOCS3, in human saphenous vein tissue derived from CABG patients, revealed that while SOCS3 was present throughout the media of these vessels the levels of SOCS3 within the neointima was reduced. Finally, preliminary data supporting the hypothesis that SOCS3 overexpression may limit the proliferation, but not migration, of human saphenous vein smooth muscle cells (HSVSMCs) is presented.

It is expected that multiple E3 ligases and DUBs will contribute to the regulation of SOCS3 turnover. However, the identification of candidate E3 ligases or DUBs that play a significant role in SOCS3 turnover may facilitate the development of peptide disruptors or gene therapy targets to attenuate pathological SMC proliferation. A targeted approach, inhibiting the interaction between SOCS3 and identified E3 ligase, that controls the levels of SOCS3, would be expected to reduce the undesirable effects associated with global inhibition of the E3 ligase involved.

Table of Contents

List of Tables

List of Figures

Acknowledgement

Thank you to my supervisor Professor Tim Palmer for his guidance and scientific expertise throughout this PhD project. Thank you also to my co-supervisor Professor Andy Baker for his advice and supervision with respect to the vascular component of this projected David Sumpton at the Beatson Institute thank you for all your help with the mass spectrometry analysis.

I would also like to extend a special thank you to Dr Claire Rutherford and my fellow PhD student Claire Speirs for all their help and support over the last 3 years. Your banter in the lab made those gels run all the more quick and I will miss our karaoke outings on a Friday night or trips “doon the water” to Gourock.

To my shinty team Glasgow Mid Argyll, especially Katie and Laura, our road trips across Scotland are the highlight of my weekend and I don’t know where I’d be without you all.

Finally I would like to thank my family. Mum and dad thank you for all your love and support throughout my university career. To my loving husband Jonathan thank you for listening to every presentation, telling me to stop waving my hands and troubleshooting every PCR reaction with me. You are always positive and taught me to believe in myself so for that I will be forever in your debt. Last but not least to my beautiful daughter Sophie Elizabeth you have been my inspiration to complete this thesis and have been kind enough to give me 8 hours sleep at night. You have been so well behaved for granny and grandma during my write up and your cheeky smile lights up the room on my study breaks. It is for my family that I have completed this thesis.

Via, Veritas, Vita

Author's Declaration

I declare that this thesis has been written entirely by me and that all work has been performed by me unless otherwise acknowledged. Dr David Sumpton performed the LC-MS-MS experiments and data analysis. Mrs Nicola Britton fixed and paraffin embedded the HSV tissue. Furthermore, this work has not been previously submitted for any other degree.

Kirsten M.A.Munro
April 2016.

Abbreviations

A	ACE	Angiotensin-converting enzyme
	ACN	Acetonitrile
	AMBIC	Ammonium bicarbonate
	APC	Adenomatous polyposis coli
	APS	Ammonium persulphate
	ASM.5	Angiosacroma.5 cell line
	AW	Assay window
B	BCA	Bicinchoninic acid
	BMS	Bare metal stent
	BSA	Bovine serum albumin
	BSF-2	B cell stimulatory factor 2
C	CABG	Coronary artery bypass grafts
	CAST	M-calpain inhibitor calpastatin
	CCA	Cholangiocarcinoma
	CHD	Coronary heart disease
	CIS	Cytokine-inducible *src homology 2* (SH2)-domain containing protein
	CMV	Cytomegalovirus
	Co-IP	Co-immunoprecipitation
	CP-SOCS3	Cell penetrable-socs3
	CRL	Cullin-ring-ligase
	CUL5	Cullin-5
	CVD	Cardiovascular disease
	CYLD	Cylindromatosis
D	DES	Drug eluting stent
	DMEM	Dulbecco's modified eagle's medium
	DMSO	Dimethyl sulfoxide

	DTT	Dithiothreitol
	DUB	Deubiquitylase
E	E.coli	Escherichia coli
	EC	Endothelial cell
	ECL	Enhanced chemiluminescence
	ECS^{SOCS3}	Elongin-Cullin-$Socs^{socs3}$
	EGFR	Epidermal growth factor receptor
	EPAC-1	Exchange protein directly activated by camp-1
	Epo	Erythropoeitin
	ERK	Extracellular signal-regulated kinase
	ESS	Extended SH2 subdomain
F	FAK1	Focal adhesion kinase 1
	FBS	Foetal bovine serum
	FCS	Foetal calf serum
	FN	Fibronectin
G	GAPDH	Glyceraldehyde 3-phosphate dehydrogenase
	G-CSFR	Granulocyte colony-stimulating factor receptor
	GEF	Guanine nucleotide exchange factor
	Gp130R	Glycoprotein 130 receptor
H	HAEC	Human aortic endothelial cells
	HAT	Histone acetytransferase
	HCC	Hepatocellular carcinoma
	HDAC	Histone deacetylase
	HECT E3 ligase	Homology to the E6AP C Terminus E3 ligase
	HEK	Human embryonic kidney
	HMG-CoA	3-hydroxy-3-methylglutaryl coenzyme A
	HRP	Horseradish peroxidase
	HSVEC	Human saphenous vein endothelial cells
	HUVEC	Human umbilical vein endothelial cell

I	IDO	Indoleamine 2,3-dioxygenase
	IDOL	Inducible degrader of the LDL receptor
	IFNγ	Interferon γ
	IGF-1	Insulin growth factor i
	IGFIR	Insulin-like Growth Factor I Receptor
	IHC	Immunohistochemistry
	IL6	Interleukin 6
	IMA	Internal mammary artery
	IP	Immunoprecipitation
	IRS1/2	Insulin receptor substrate 1/2
	ISR	In-stent restenosis
J	JAK	Janus kinase
K	KIR	Kinase inhibitory region
	KO	Knock out
L	LAR	Luciferase assay reagent
	LB broth	Luria Bertani broth
	LC-MS	Liquid chromatography mass spectrometery
	LDL	Low-density lipoprotein
	LPS	Lipopolysaccharide
	LV	Lentivirus
M	MAPK	Mitogen-activated protein kinase
	MEF	Mouse embryonic fibroblast
	MI	Myocardial infarction
	MMP	Matrix metalloproteinase
	MOI	Multiplicity of infection
	MPN	Myeloproliferative neoplasms

N	NAE	Neddylation activation enzyme
	NDB	Non-denaturing buffer
	NEDD8	Neural precursor cell expressed, developmentally down-regulated 8
	NFκB	Nuclear factor kappa B
	NIH	Neointimal hyperplasia
	NPC	Nucleopore complex
O	ORF	Open reading frame
P	PAGE	Polyacrylamide gel electrophoresis
	PBS	Phosphate buffered saline
	PCI	Percutaneous coronary intervention
	PCR	Polymerase chain reaction
	PDGF	Platelet-derived growth factor
	PEI	Polyethylenimine
	PFA	Paraformaldehyde
	PIAS	Protein inhibitors of activated STAT
	PKA	Protein kinase A
	PMSF	Phenylmethylsulphonyl fluoride
	PSGL-1	P-selectin glycoprotein ligand 1
	PTM	Post-translational modification
	PTP	Protein tyrosine phosphatases
R	RBR E3 ligase	RING-between ring-RING E3 ligase
	RING domain E3 ligase	Really Interesting New Gene domain E3 ligase
	RIPA	Radioimmunoprecipitation assay
	RTK	Receptor tyrosine kinase
S	SDS	Sodium dodecyl sulphate
	SH2	Src homology 2
	SHP	SH2-containing protein tyrosine phosphatase
	SIGLEC	Sialic acid-binding Ig-like lectin 7

	SMC	Smooth muscle cell
	SNP	Single nucleotide polymorphism
	SOCS	Suppressors of cytokine signalling
	STAT	Signal transducer and activator of transcription
	SUMO	Small ubiquitin-like modifier
	SV	Saphenous vein
T	TBS	Tris-buffered saline
	TIA	Transient ischaemic attack
U	UBL	Ubiquitin-like proteins
	UPS	Ubiquitin-proteasome system
	UTF	Untransfected
V	VE	Vascular endothelium
	VEGF	Vascular endothelial growth factor
	VSMC	Vascular smooth muscle cell
W	WT	Wild type

1 Introduction

1.1 Cardiovascular disease

Though lipid-lowering (e.g. statins) and antihypertensive (e.g. angiotensin-converting enzyme (ACE) inhibitor) therapies have significantly reduced the risk of developing cardiovascular diseases (CVD), these debilitating conditions still accounted for approximately 17.5 million deaths worldwide in 2012 [1]. In 2014, CVD was responsible for 27% of all UK deaths, 70,000 of which were attributed to coronary heart disease (CHD) specifically [2]. CHD is defined as the process by which "the walls of the coronary arteries become narrowed by the gradual accumulation of fatty material called atheroma" [2]. In some patients, statins and ACE inhibitors may no longer provide an effective therapy for the prevention of CHD. As such, surgical revascularisation may be required including coronary artery bypass grafts (CABG), balloon angioplasty or stent implantation (also known as percutaneous coronary intervention [PCI]). However, in-stent restenosis (ISR) is detectable in ~12% of stent implants at 1 year follow-up [3] and it is estimated that >50% of CABG procedures fail within 10 years [4]. Patients may be at risk of further myocardial infarctions and require repeat re-vascularisation procedures. Currently around 17,000 CABG and 92,000 PCI procedures are carried out in the UK each year therefore finding ways to increase the patency of these interventions would have a significant impact [2].

1.1.1 CHD-Atherosclerosis pathogenesis

There are three discrete layers of the artery including the adventitia, media and intima (Figure1-1). Atherosclerosis may be described as "hardening of the arteries"[5] and is a direct result of atheroma plaque formation within the intimal layer of the blood vessel [6]. An endothelial monolayer lines this intimal region, forming the luminal surface, and therefore prevents cells within the blood from being exposed to tissue factors that may promote clotting. As such, maintaining the integrity of the endothelium is vital to preserve the artery function. However, hypertension or prolonged exposure to elevated circulating low-density lipoprotein (LDL) cholesterol and pro-inflammatory cytokines may increase the permeability of this endothelial monolayer [6] (Figure 1-2). As a result, LDL cholesterol accumulates within the intimal layer of the artery and promotes the recruitment of monocytes. Circulatory monocytes adhere to the blood vessel wall and cross the

endothelial barrier to the intima where they differentiate into macrophages. Tissue macrophages are thought to further increase the absorption of LDL from the circulation (via scavenger receptors) and give rise to “lipid-laden foam cells” which are a hallmark of atheromatous plaques [6]. As the disease progresses, the plaque expands through the activation, proliferation and migration of SMCs from the media to the intimal layer of the blood vessel. Commonly a fibrous cap forms on the luminal surface of the plaque and the composition of both structures determine the risk or vulnerability of the plaque to rupture. Vulnerable plaques have a lipid rich core and show a degree of neovascularisation, intra-plaque haemorrhage and calcification [7, 8]. Importantly, the fibrous cap is extremely thin with a reduced SMC and collagen content [9]. It is thought that proteolytic enzymes known as matrix metalloproteases (MMPs) within the plaques are responsible for digestion of the fibrous cap ECM and so can promote rupture [10]. Consequently, tissue factors are exposed resulting in the recruitment of platelets involved in the formation of thrombi [8]. The atherosclerotic vessel may become partially or completely occluded resulting in ischaemia of the tissue supplied by this vessel. In the case of the coronary artery this would result in a myocardial infarction and requires reperfusion in order limit irreversible damage to the myocardium.

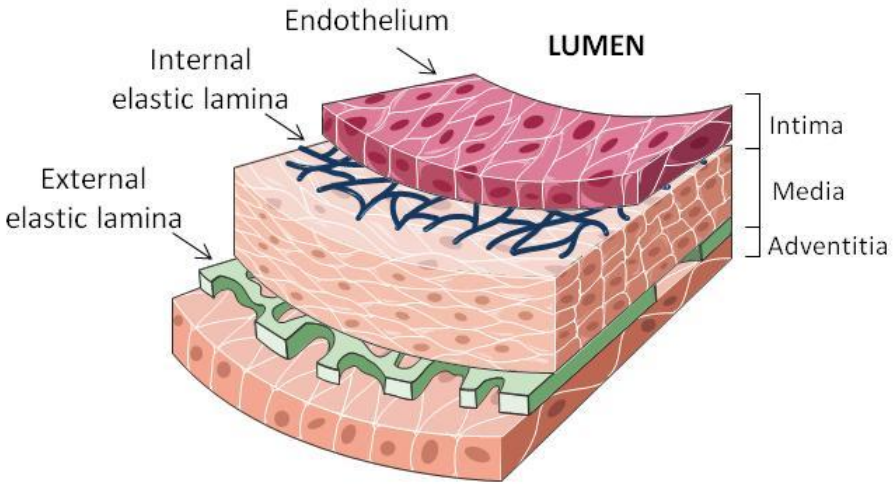

Figure 1-1: Structure of the arterial wall

The outermost adventitial layer contains connective tissue, fibroblasts and mast cells [6]. In contrast, the medial layer is composed largely of smooth muscle cells (SMCs) and the smaller intimal layer of extracellular matrix (ECM). In man the intima also contains some SMCs [6]. The intimal layer is lined by a monolayer of endothelial cells forming the endothelium which provides an interface between the circulation and the arterial wall. Figure adapted from Servier Medical Art http://servier.com/Powerpoint-image-bank.

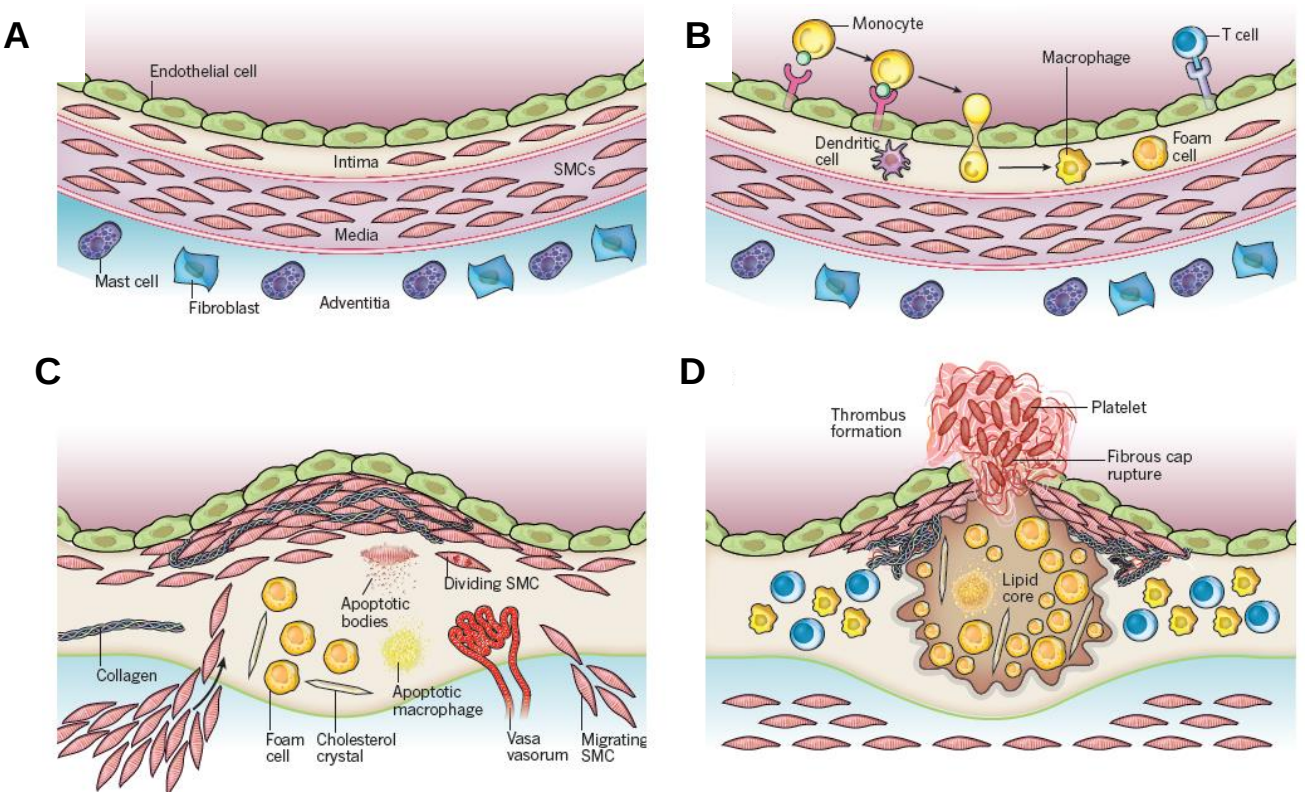

Figure 1-2: Formation of the atherosclerotic plaque.

(a) Initially the intimal region of the blood vessel is relatively small. However, chronic hypertension or exposure to high levels of cholesterol (LDL) and pro-inflammatory cytokines may lead to endothelial dysfunction. (b) The endothelial monolayer becomes "leaky" allowing LDL to enter and accumulate within the intimal layer and provides a substrate for oxidative enzymes. The resulting oxidised lipids promote the expression of leukocyte adhesion receptors and the production of chemokines by the now activated endothelial cells [11]. Various inflammatory cells such as macrophages are recruited to this site promoting the expansion of the atheromatous plaque within the inner layer of the artery and so narrowing the lumen. (c) Smooth muscle cell (SMC) migration from the media to the intima then contributes to (d) fibrous cap formation which is susceptible to rupture and may result in thrombus formation. Figure reproduced from [6] with permission.

1.1.2 Revascularisation of atherosclerotic vessels

Statins serve as a competitive inhibitor of the 3-hydroxy-3-methylglutaryl coenzyme A (HMG-CoA) reductase enzyme that is required for cholesterol synthesis [12]. A meta-analysis study involving more than 30,000 patients from 5 different trials, revealed that statin treatment reduced LDL synthesis by 28% and was associated with a 31% decrease in the risk of an adverse coronary event [13]. As such, the cholesterol lowering "statin" family provide the first-line pharmacological therapy for the treatment and prevention of cardiovascular diseases such as atherosclerosis [14]. However, where pharmacological management of atherosclerosis is unsuccessful, surgical intervention may be required to achieve effective revascularisation. Following a myocardial infarction, ischaemic damage to the blood vessel supplying the heart (coronary artery) is irreversible. As such, coronary artery bypass grafting (CABG) procedures in which the internal mammary artery (IMA) is grafted onto the left anterior descending coronary artery, or more commonly saphenous vein (SV) to other coronary vessels, is largely successful at restoring function [15]. However, these conduits are susceptible to atherosclerosis and neointimal hyperplasia (NIH), and thus requiring further intervention [16]. In 2004, one study compared the long term patency of IMA versus SV grafts and revealed that while 85% of IMA conduits were patent at 10 years follow up, only 61% of SV grafts were functional [15]. A more recent review of clinical trial data revealed that 50% of all SV conduits failed within 10 years and patients therefore required repeat revascularisation procedures [17].

An alternative strategy for the treatment of atherosclerotic vessels is the use of percutaneous coronary intervention (PCI) procedures such as stenting (Figure 1-3). A stent is a "mesh-like" cylindrical structure which is inserted into the diseased artery and expanded in order to restore the diameter of the lumen and therefore blood flow through the vessel [18]. However, the success of this revascularisation procedure has been limited due to the damage to the blood vessel wall that may result during stent deployment leading to NIH. NIH is defined as "the abnormal migration and proliferation of VSMCs with associated deposition of extracellular connective tissue matrix" [19] and may lead to the accelerated re-narrowing of the blood vessel (stenosis). During stent deployment, endothelial denudation exposes the vessel lining to mitogens in the blood or cytokines released by inflammatory cells, therefore driving VSMC exit from the quiescent phase [20]. Figure 1-4 summarises the steps involved in the development of ISR caused by neointimal thickening of the arterial wall.

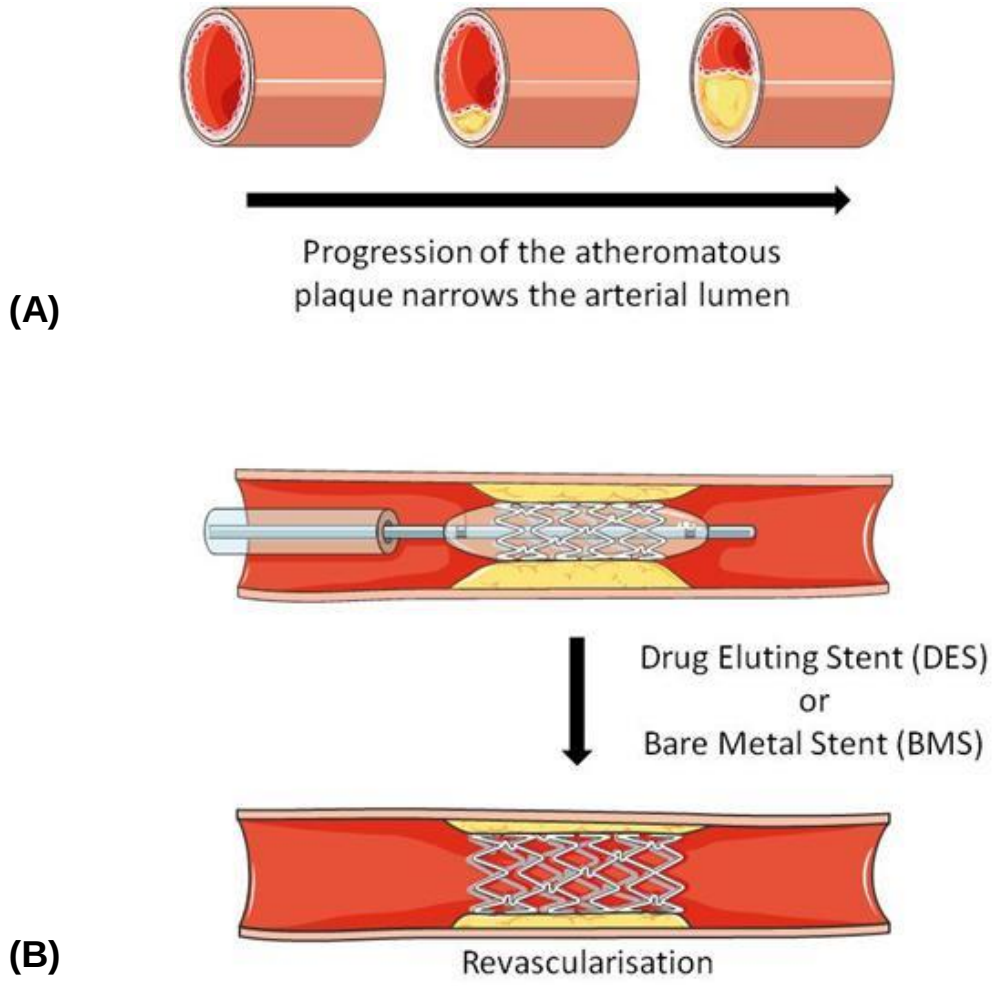

Figure 1-3: Stent revascularisation of the artery

(A) Progression of the atheromatous plaque within the lining of the coronary arterial wall may lead to complete occlusion (myocardial infarction [MI]) and is often fatal. Plaques which are refractory to statin treatment may require PCI procedures such as stenting. (B) Stent implant involves balloon angioplasty in which balloon inflation drives the expansion of the stent. The balloon catheter is removed and the expanded stent physically holds the artery open restoring blood flow to the tissues supported by the artery. The cardiologist may choose to insert a bare metal stent (BMS) or drug-eluting stent (DES). Figure A-B adapted from Servier Medical Art.

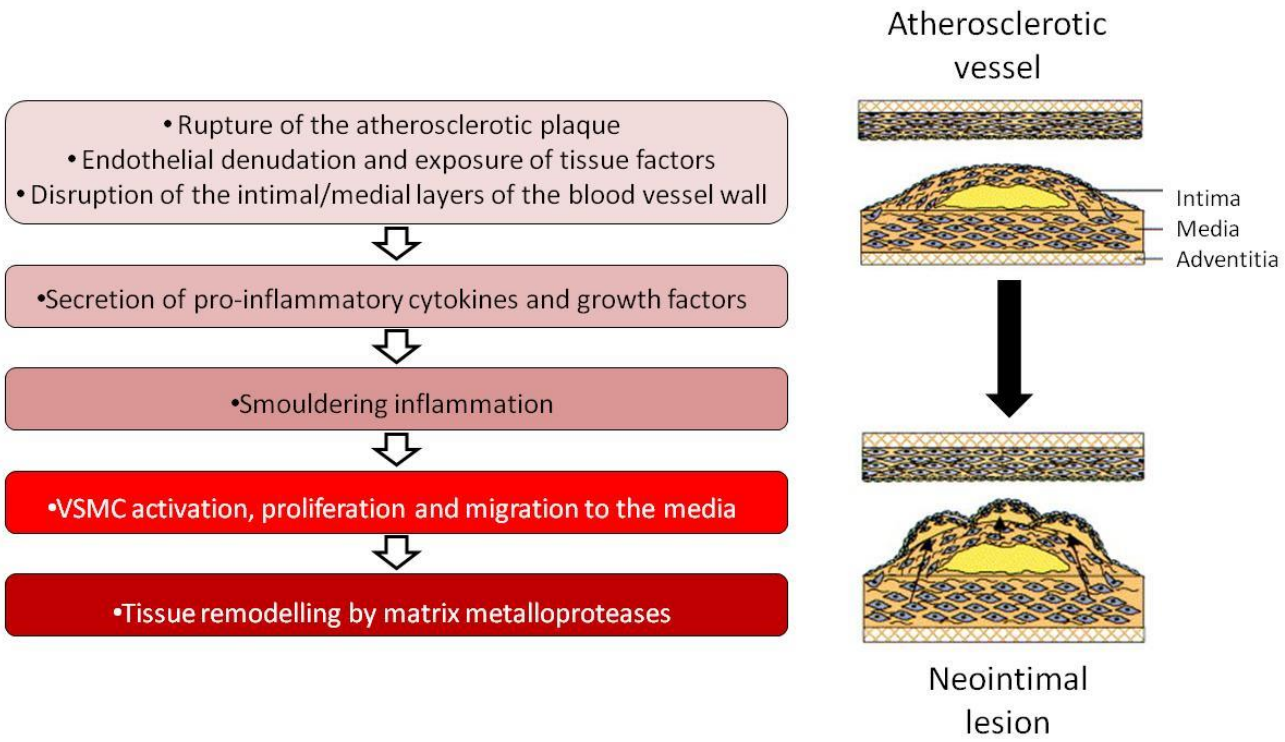

Figure 1-4: In-stent restenosis is driven by NIH thickening of the injured arterial wall which may be initiated following stent deployment

Stent deployment or balloon angioplasty procedures induce mechanical injury to the blood vessel wall. This includes the disruption of the endothelial monolayer lining the lumen of the vessel (denudation) and disruption to the intimal and medial layers of the inner wall [21]. Following this, pro-inflammatory mediators and mitogenic growth factors are released. VSMCs exit the resting (G_0) phase of the cell cycle, proliferate and migrate from the media to the intima driving neointimal lesion formation and vessel remodelling ultimately reducing the lumen diameter. Integrity of the endothelial layer lining the lumen is important as loss of this barrier promotes platelet adhesion and thrombosis. Following CABG procedures, thickening of the saphenous vein wall is an adaptation to the higher arterial pressure experienced [17]. However, following endothelial denudation there is no barrier to limit VSMC proliferation and migration. Neointimal lesions enlarge, reducing the lumen diameter, and reducing blood flow to the myocardium. Figure adapted from [22] with permission.

Despite the emergence of drug-eluting stents (DES), which release anti-proliferative compounds to inhibit this cell growth, neointimal lesions may still form within the stent (in-stent restenosis; ISR) impeding blood flow once again [23]. Moreover, drugs such as rapamycin non-selectively inhibit EC as well as SMC proliferation thus preventing re-endothelialisation at sites of injury caused by stent deployment [24]. This increases the risk of in-stent thrombosis therefore current guidelines recommend dual anti-platelet therapies such as aspirin and platelet $P2Y_{12}$ inhibitor [25]. Though the rate of ISR remains low, it is the increase in number of patients undergoing stent procedures that translates to a large number of patients requiring repeat revascularisation due to ISR [23]. Without further intervention, complete vessel occlusion may result and is often fatal.

ISR is one of the major drawbacks of BMS implants. However, the development of DESs was shown to reduce the incidence of this complication [26, 27]. In spite of this, a study which compared the long term patency of two DESs (Taxus and Cypher) with BMSs revealed that delayed healing of the stented vessel was significantly greater in patients that received the DES [28]. This short-coming was as a result of "late stent thrombosis" within the vessel. Damage to the arterial wall during stenting may expose tissue factor, fibronectin and collagen present in the media and adventitia, thus promoting thrombosis [22]. Simultaneously, locally secreted growth factors and cytokines induce VSMC entry into the S phase of the cell cycle, driving proliferation and migration to the intima and thereby contributing to the neointimal lesion. Joner and co-workers [28] proposed that anti-proliferative compounds inhibit the wound healing response of the arterial wall that results following stent implant [28]. The length of the stent (enlarged area of pathology) correlated linearly with an increase in the likelihood of thrombosis. It was hypothesised that deployment of a longer stent was technically more challenging and that the struts may not insert into the vessel wall flush across the entire length, and as a result pre-disposes the vessel to thrombus formation [28]. Conversely, according to the literature late stent thrombosis in patients with BMSs is relatively rare [26]. As such, patient compliance with two anti-platelet treatments is essential in order to reduce the incidence of thrombus formation within the DES vessels [28].

1.2 Cytokine signalling

1.2.1 Interleukin 6 classic vs. trans-signalling

Interleukin 6 (IL6) was first described in 1986 though it was initially referred to as B-cell stimulatory factor (BSF-2) responsible for the promotion of antibody secretion by B cells [29]. IL6 is a soluble protein, with a molecular weight of ~21kDa, produced by various cell types including fibroblasts, endothelial cells and immune cells such as monocytes and T-cells [30]. In addition, IL6 is a cytokine that has the ability to interact with a membrane bound or soluble form of the IL6 receptor (IL6R). The IL6R is an 80kDa protein that is not ubiquitously expressed, rather its expression is limited to the cell surface of hepatocytes and various subsets of white blood cell subtypes [31]. Interestingly, in 1990, Hibi and co-workers demonstrated that the IL6-mediated ligand activation of the IL6R requires the association with a gp130 dimer in order to drive intracellular signalling (e.g. the JAK/STAT pathway) [32]. A Jurkat T cell line was initially shown to be unresponsive to IL6 exposure *in vitro*. However, transfection with an IL6R-expressing construct resulted in a modest increase in the number of high and low affinity binding sites for IL6. Importantly, the overexpression of both the IL6R and gp130 resulted in a synergistic, 5 fold increase in the number of high affinity binding sites for IL6 [32]. This provided evidence to support the role of the gp130 in IL6 classic signalling i.e. where both the IL6R and gp130 are expressed on the cell surface.

Interestingly, IL6 trans-signalling via gp130 facilitates the IL6-mediated activation of JAK/STAT signalling in cells which do not express the endogenous membrane-localised IL6R (reviewed in [31]). Trans-signalling involves IL6 binding to a soluble IL6R (sIL6R) to form the IL6-sIL6R complex in the circulation. The sIL6R is thought to be synthesised following i) alternative splicing of IL6Rα mRNA [33, 34] or ii) matrix metalloprotease (ADAM17 or ADAM10) shedding of a sIL6R from the cell surface of IL6R-expressing hepatocytes and monocytes [35, 36]. Moreover, the literature proposes that while IL6 classic signalling mediates an anti-inflammatory and regenerative response required for activities such as wound healing, trans-signalling is thought to shift toward a pro-inflammatory response [30, 31, 37]. Accordingly, pro-inflammatory IL6 trans-signalling must be appropriately controlled via regulation by protein inhibitors of activated STAT (PIAS), protein tyrosine phosphatases (PTPs) and members of the suppressor of cytokine signalling (SOCS) family.

1.3 Suppressors of cytokine signalling (SOCS)

SOCS3-mediated regulation of IL6-JAK/STAT signalling was of specific interest to this project and is therefore described in detail. The literature describes 8 members of the Suppressor of Cytokine Signalling (SOCS) family including SOCS1-7 and the cytokine-inducible *src homology 2* (SH2)-domain containing protein (CIS) [38]. All members of the SOCS family contain a C-terminal SOCS box in addition to an SH2 domain however only SOCS1 and SOCS3 possess an N-terminal kinase inhibitory region (KIR) which is required for the inhibition of receptor-associated JAKs (Figure 1-5). The contrasting structural organisation of SOCS family members is related to their diverse functions. CIS, SOCS1, SOCS2, and SOCS3 are predominantly involved in cytokine receptor regulation in contrast to SOCS4, SOCS5, SOCS6 and SOCS7 which, for the most part, are involved in receptor tyrosine kinase (RTK) regulation [39].

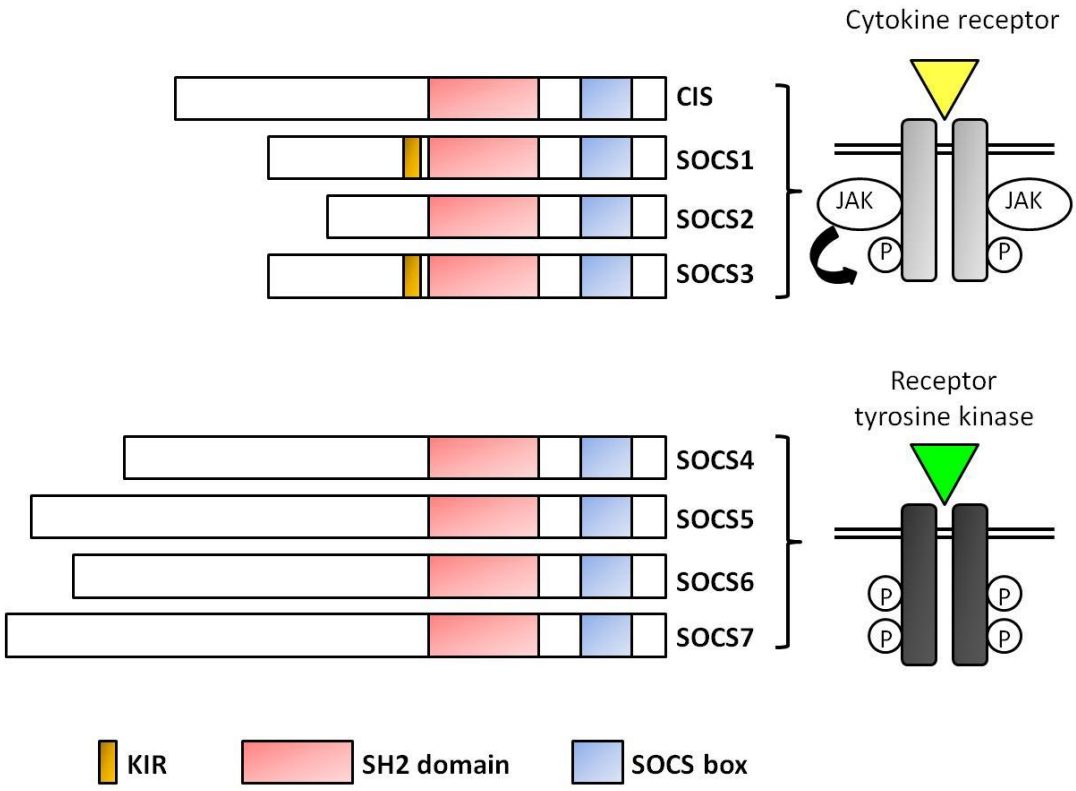

Figure 1-5: The structural organisation of members of the SOCS family

SOCS1-3 and CIS are largely involved in the negative regulation of signalling events at cytokine receptors. Cytokine receptors do not possess intrinsic kinase domains and therefore rely on receptor associated kinases such as the JAKs for activation and downstream signalling. Conversely, receptor tyrosine kinases (RTKs) possess an intrinsic kinase domain and following ligand activation, by growth factors for example, SOCS4-7 may be involved in the negative regulation of downstream signalling events. Of note, SOCS1 and SOCS3 share a similar domain structure in that the KIR is located in the C-terminus. Figure adapted from [39] and [40] with permission.

The first member of the SOCS family described in the literature was CIS which was shown to interact with activated IL3 and erythropoietin receptors (EpoR) [41]. Subsequently, SOCS1 (initially referred to as JAK-binding protein (JAB)) was identified in a yeast 2 hybrid screen using the JH1 domain of JAK2 as bait [42]. At the same time, Starr and co-workers reported the cloning of SOCS1 in addition to two structurally related proteins denoted SOCS2 and SOCS3 based on the order of their discovery [43]. $SOCS1^{-/-}$ knockout mice died as neonates (2-3 weeks of age) and this was later shown to be due to the hyperactivation of interferon γ (IFNγ) signalling pathways resulting in multiorgan disease [44]. Mice in which the SOCS1 and IFNγ gene were knocked out ($SOCS1^{-/-}$, $IFN\gamma^{-/-}$) or $SOCS1^{-/-}$ knockout mice injected with antibodies raised against IFNγ were protected from disease and premature mortality [44]. As such, SOCS1 is largely associated with the negative regulation of IFNγ signalling events. SOCS3 knockout mice ($SOCS3^{-/-}$) died during embryogenesis at day 11-13 therefore SOCS3 is non-redundant [45]. Though embryo development progressed as normal, malformations in the placental tissue meant the embryo could no longer be supported [45]. As such, *in vivo* SOCS3 investigations require conditional knockouts (typically using a Cre-lox system) or gene knockdown (e.g. using short hairpin (sh) RNA) techniques for spatio-temporal regulation of expression. Though SOCS1 and SOCS3 share structural similarities such as the presence of the N-terminal KIR, they regulate diverse signalling pathways which may vary with cell type. For the purpose of this PhD project, SOCS3-mediated inhibition of IL6-JAK/STAT signalling was of most interest and is discussed in detail.

1.3.1 SOCS3 orchestrates a negative feedback loop with the JAK-STAT pathway

SOCS3 is a key regulator of the JAK/STAT pathway and expression is driven by STAT transcription factors forming a non-redundant negative feedback loop (Figure 1-6). Interestingly, the Kinase Inhibitory Region (KIR) present in the short N-terminal region of SOCS-1 and 3 were shown to interact with and inhibit JAK1, JAK2 and TYK2 activity. Following ligand activation, cytokine receptors dimerise at the plasma membrane [46]. Cytosolic Janus Kinases (JAKs) are recruited and activated via trans-phosphorylation events (Figure 1-6). Subsequently, JAK phosphorylates the intracellular domain of the cytokine receptor providing docking sites for Src homology 2 (SH2) domain containing proteins such as signal transducer and activator of transcription 3 (STAT3). The

JAK/STAT pathway proceeds (Figure1-6) with SOCS3 forming a negative feedback loop, the disruption of which may promote an uncontrolled pro-inflammatory response.

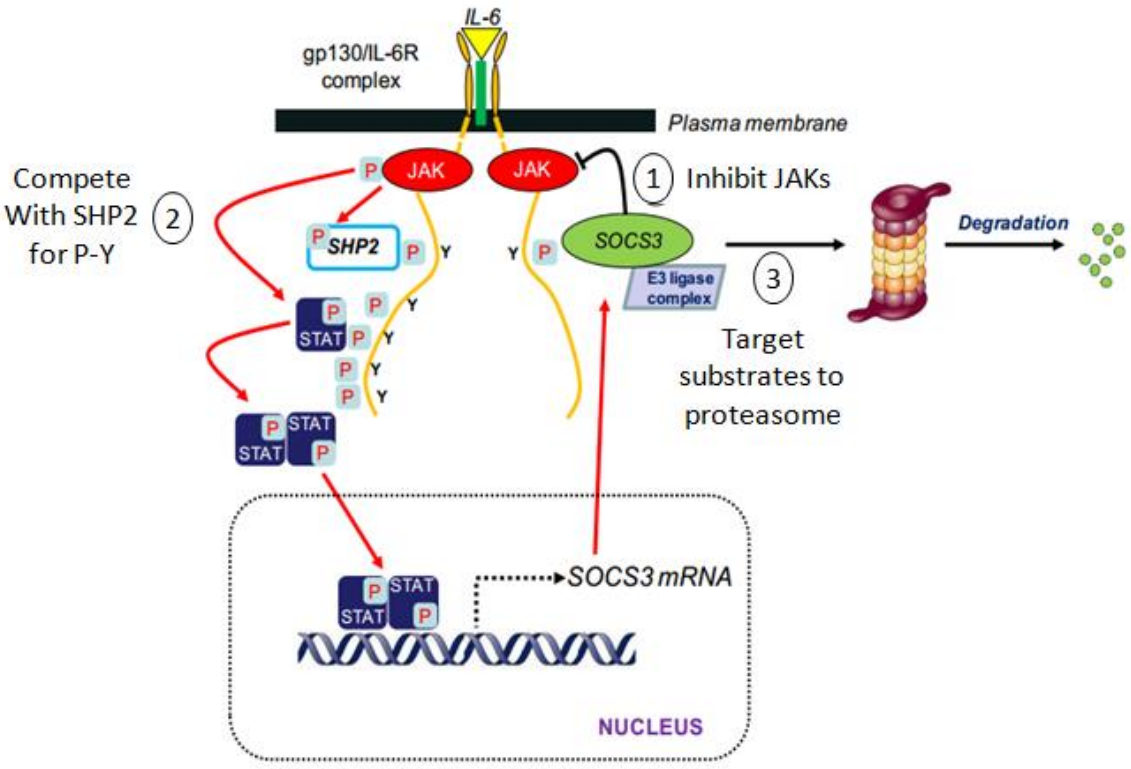

Figure 1-6: The JAK/STAT-SOCS3 negative feedback loop

Circulatory IL6 interacts with a soluble or membrane bound isoform of the IL6 receptor α (IL6Rα). The activated IL6Rα subsequently dimerises with the glycoprotein 130 receptor (gp130R) on the plasma membrane initiating the activation of receptor associated JAKs. JAK activation (trans-autophosphorylation) and the subsequent phosphorylation of pYXXQ motifs, on the gp130R cytoplasmic tail, provides phosphotyrosine (pY) docking sites for the STAT proteins. Following recruitment to the gp130R, STAT3 is phosphorylated by receptor associated JAKs promoting the dissociation and dimerisation of STAT3. The STAT3 dimer then translocates to the nucleus where it functions as a transcription factor driving the expression of genes involved in proliferation. STAT3 also drives the expression of SOCS3 which may (1) inhibit JAKs directly, (2) compete with SHP2 for pY residues (potentially switching off the Ras-MAPK pathway) or (3) target proteins to the proteasome for degradation. SOCS3 expression is therefore induced by the very pathway that they inhibit (JAK/STAT) forming a negative feedback system. Modified from [47] with permission.

1.3.2 Structural organisation of the SOCS3 protein provides an insight into its function

The domain structure of SOCS3 is illustrated in Figure 1-7. The central SH2 domain is involved in substrate recognition whereby SOCS3 interacts with phosphotyrosine (pY)

residues on target proteins. The KIR is located at the N-terminus of the protein and plays a major role in the SOCS3-mediated inhibition of receptor associated JAKS (section 1.3.7.4). To date, the SOCS box motif has been described in over 70 proteins and is involved in targeting substrates for degradation [48]. This is due to the ability of the C-terminal SOCS box to bind adaptor proteins (Elongin B and C) which provides a platform for the formation of a multi-subunit E3 ligase complex (involving Cul5 and Rbx2) which catalyses the ubiquitylation of substrates bound by the SOCS3 SH2 domain (section 1.3.8).

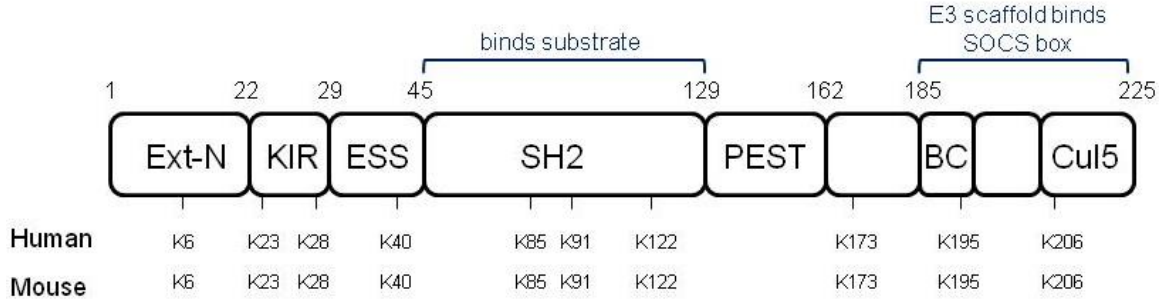

Figure 1-7: Schematic of SOCS3 protein structure

The SOCS3 protein is 225 amino acids in length with a molecular weight of ~25-27kDa. SOCS3 contains an extended N-terminal region (Ext-N), Kinase Inhibitory Region (KIR), Extended SH2 subdomain (ESS), SH2 domain, PEST sequence (rich in Pro (P), Glu (E), Ser (S), and Thr (T) residues) and the C-terminal SOCS box which contains the so-called "BC box" and "Cul5 box". The KIR may be involved in the direct inhibition of JAKs. The SH2 domain is involved in substrate (phospho-Tyr) recognition. The PEST domain is involved in protein degradation and stability. The BC box and Cul5 box are located within the SOCS box and bind Elongin B and C and Cul5 respectively. The SOCS box provides a platform for the formation of an E3 ligase complex. The location of all known Lys residues (K) for both human (http://www.uniprot.org/uniprot/O14543) and mouse (http://www.uniprot.org/uniprot/O35718) SOCS3 is shown. Figure adapted from [49] with permission.

Interestingly, the SH2 domain allows SOCS3 to associate with various membrane-bound receptors and, in some instances, regulate their downstream signalling pathways (summarised in Table 1-1).

Receptor interacting with SOCS3	Function of SOCS3	Literature reference
Erythropoietin Receptor (EpoR)	The negative regulation of Epo signalling in erythropoeisis.	[50], [51]
Leptin Receptor (LeptinR, ObRb)	Inhibition of leptin signalling. Outcompetes SHP-2 for Y985 to switch off ERK activation.	[52, 53]
Insulin-like Growth Factor I Receptor (IGFIR)	SOCS family members (CIS and SOCS1-3) are thought to exhibit functional redundancy in the negative regulation of IGFIR signalling.	[54], [55]
Granulocyte Colony-Stimulating Factor Receptor (G-CSFR)	Involved in G-CSFR downregulation by targeting the receptor for lysosomal degradation.	[56]
Gp130 Receptor (Gp130R)	Inhibition of Gp130R signalling (JAK-STAT pathway). Outcompetes SHP-2 for pY757 (mouse) or pY759 (human).	[57, 58]

Table 1-1: Receptors known to interact with SOCS3 and the functional consequence in cell signalling pathways.

The SH2 domain of SOCS3 facilitates the recognition and binding to phosphotyrosines (pY) with specificity defined by the surrounding residues [59]. For example, inhibition of leptin signalling by SOCS3 required a hydrophobic (water repelling) residue 2 positions upstream of the target pY on the cytoplasmic tail of the leptin receptor [52].

SOCS3 may be induced by various cytokine and growth factor stimuli. The following section reviews the role of SOCS3 as a negative regulator of various signalling pathways.

1.3.3 Erythropoietin signalling

Erythropoietin (Epo) is a hormone produced by the kidney and following ligand activation of the EpoR, the JAK/STAT pathway is initiated driving the proliferation and maturation of erythrocytes (erythropoiesis) [60]. In 2000, Sasaki *et al* demonstrated that SOCS3 could

interact with both the EpoR (pY401) and receptor associated JAK2 [50]. As a result, SOCS3 was shown to outcompete STAT5 for the pY401 docking site and terminated the proliferation of a pro B cell line (Ba/F3) used in the study. Following this discovery, a higher affinity interaction between SOCS3 and the EpoR was identified at the pY429/pY431 motif located on the intracellular domain of the EpoR [51]. The authors proposed that SOCS3 may therefore compete with the PTP SHP-1 for pY429/pY431 however this was not investigated further. Interestingly, Hookham and co-workers described the hyper-phosphorylation of SOCS3 by a constitutively active JAK2 mutant (V617F) found in many myeloproliferative neoplasms (MPN) [61]. This study reported that SOCS3 could no longer negatively regulate Epo signalling in the presence of the JAK2 V617F mutant resulting in the uncontrolled proliferation of cells that contributed to the disease [61]. Similarly, Elliot and co-workers reproduced these data and demonstrated that other JAK2 mutations, found in MPN patients, could also evade SOCS3-mediated inhibition [62]. However, this area remains controversial as Haan and colleagues provide conflicting evidence that showed JAK2 V617F was sensitive to SOCS3 inhibition in Human Embryonic Kidney 293 (HEK293) cells expressing the EpoR [63]. The sensitivity of JAK V617F to SOCS3 may therefore depend on the cell type under investigation.

Nevertheless, it is clear that SOCS3 plays a key role in the negative regulation of Epo signalling. A Japanese MPN patient with a SOCS3 (F136L) germ line mutation and somatic JAK2 deletion (N542-E543) has now been described [64]. Interestingly, *in vitro* experiments revealed that cells expressing SOCS3 (F136L) displayed increased EPO-induced proliferation and may therefore promote disease progression [64].

1.3.4 Leptin signalling

Leptin is a cytokine, encoded by the obese (*ob*) gene, involved in energy homeostasis through the regulation of feeding behaviour [65]. As such, perturbation through leptin resistance or mutation of leptin signalling components may contribute to the development of obesity: an important risk factor for cardiovascular morbidity and mortality. Interestingly, SOCS3 has been shown to inhibit leptin receptor signalling by competing for pY985 with SHP2 on the intracellular domain of the receptor [52]. Consequently, SHP2 activation cannot proceed and therefore the ERK/MAPK pathway remains switched off. More recently, Pedroso and co-workers conducted a study involving conditional neuronal SOCS3 knockout mice [53]. These data revealed that the SOCS3-depleted mice were

resistant to diet-induced insulin resistance and that SOCS3 may therefore represent a useful inhibitory target for the treatment of type II diabetes.

1.3.5 Insulin-like growth factor I signalling

The Insulin-like growth factor I receptor (IGFIR) is a receptor tyrosine kinase that is activated upon Insulin Growth Factor I (IGF-I) ligand binding [55]. IGFIR has a variety of roles including the promotion of cell proliferation and differentiation amongst others. As such, increased IGFIR signalling has been implicated in the progression of cancers such as breast cancer [66] and prostate cancer [67]. Though IGFIR has been a therapeutic target of interest for many years, the efficacy of inhibitors for this pathway in clinical trials has been largely underwhelming [68].

Previously, yeast-two hybrid analysis and *in vitro* co-immunoprecipitation studies confirmed that SOCS3 was constitutively bound to IGFIR [54]. Following IGF-I stimulation, SOCS3 was then tyrosine phosphorylated suggesting that SOCS3 may be a substrate for the IGFIR. However the functional consequence of this post-translational modification to SOCS3 was not investigated further. Moreover, in a HEK293T overexpression system, four members of the SOCS family (CIS and SOCS1-3) were shown to inhibit JAK1/2-mediated STAT3 activation at the IGIFR [55]. Though SOCS1 and SOCS3 were shown to be more potent negative regulators of the JAK/STAT pathway, this provided an example of functional redundancy within the SOCS family. Loss of negative regulation by SOCS3 may not be associated with aberrant signalling. It then follows that therapeutic strategies have largely been centred around monoclonal antibodies raised against the IGFIR as opposed to pharmacological interventions downstream [68].

1.3.6 Granulocyte Colony-Stimulating Factor signalling

Granulocyte Colony-Stimulating Factor (G-CSF) is a cytokine which plays central role in the proliferation of neutrophil precursor cells [69]. SOCS3 was shown to dock specifically at pY729 on the activated G-CSFR and promote the Lys632 ubiquitylation of the receptor [56]. Consequently, the G-CSFR was internalised into an endosome and was targeted for lysosomal degradation. This SOCS3-mediated receptor internalisation and therefore downregulation was responsible for the attenuation of G-CSF signalling thereby regulating the proliferation and differentiation of neutrophil precursor cells. Interestingly, a recent

review conducted by White and Nicola noted that conditional SOCS3 KO studies failed to describe pathologies associated with the loss of SOCS3-mediated regulation of G-CSF signalling and that this may suggest functional redundancy amongst SOCS family members [49].

1.3.7 The mechanism of SOCS3-mediated IL6-gp130R-JAK/STAT inhibition

1.3.7.1 SOCS3 docks at pY757 on the intracellular domain of the gp130R

Following the induction of SOCS3 by a STAT driven promoter, SOCS3 was shown to dock at pY757 (mouse equivalent to Y759 in humans) on the intracellular domain of the activated gp130R [57]. To map the site of SOCS3-gp130R interaction, Nicholson *et al* generated a chimeric erythropoietin/glycoprotein 130 receptor (Epo/Gp130R) construct and employed a panel of luciferase reporter genes as a readout of receptor activity [57]. The Epo/Gp130R chimera is composed of the erythropoietin receptor extracellular domain fused to the trans-membrane and intracellular domain of the glycoprotein-130 receptor. Stimulation of cells transfected with erythropoietin (epo) induces a gp130R response at the chimeric receptor only as HEK293 cells do not express an endogenous EpoR. Interestingly, mutation of the Epo/Gp130R Y757 site (Tyr757phe) resulted in a “four-fold” increase in receptor activity despite SOCS3 overexpression. Furthermore, in order to achieve 50% inhibition at the chimeric receptor, the amount of SOCS3 required at the mutant receptor (Tyr757Phe) was >10-fold greater (50ng) than that of the WT receptor (4ng). Importantly, loss of Y757 on gp130R did not result in 100% loss of JAK/STAT inhibition, suggesting the direct inhibition of JAK2 by SOCS3 may still proceed [57]. Together these data confirmed that pY757 on the intracellular domain of the gp130R played a major role in SOCS3-mediated inhibition of IL6-JAK/STAT signalling.

1.3.7.2 The dual interaction of SOCS3 with the gp130R and JAK2 facilitates the negative regulation of the JAK/STAT pathway.

Binding affinity experiments revealed that SOCS3 had a dissociation constant (K_D) of 42nM for pY757 on the intracellular domain of the activated gp130 receptor signifying a high affinity interaction [57]. Subsequent competitive binding assays confirmed that the interaction of SOCS3 with a JAK2 peptide was “10,000 fold weaker” than that of SOCS3

with the gp130R pY757 containing peptide. Collectively, these data suggested that SOCS3 mediated inhibition of IL6-JAK/STAT signalling may initially involve SOCS3 docking at pY757 on the cytoplasmic tail of gp130R as opposed to direct inhibition of JAK2 [57].

More recently, the crystallisation of a SOCS3-JAK2-gp130R complex revealed that SOCS3 interacts with both receptor and receptor-associated JAK simultaneously [70]. This may explain Nicholson and co-workers' previous observation that the Epo/Gp130R mutant (Tyr757Phe) required a t>10-fold greater concentration of SOCS3 to achieve 50% inhibition at the chimeric receptor [57]. The availability of a pY757 docking site on gp130 allowed SOCS3 to form a higher affinity SOCS3-JAK2-gp130R complex [70]. In fact, Kershaw *et al* hypothesised that if the concentration of cytosolic SOCS3 were great enough (>1μM) this would bypass the requirement for simultaneous binding of SOCS3 to JAK2 and Gp130R. Indeed, the Nicholson paper, published in 2000, demonstrated that at higher concentrations of SOCS3 JAK/STAT inhibition was still observed even with the introduction of a Y757F mutation.

1.3.7.3 JAK3 is resistant to inhibition by SOCS3

SOCS3 exerts an inhibitory function on receptor associated JAK1, JAK2 and TYK2 in contrast to JAK3 which was not sensitive to SOCS3 inhibition [59]. Mutagenesis studies revealed this was due to the absence of the hydrophobic amino acid sequence (GQM) in the JAK3 protein insertion loop [59]. The GQM sequence is highly conserved across vertebrate species (zebrafish to humans) for JAK1, JAK2 and TYK2 with the exception of zebrafish TYK2 which contains a "GQT" motif as opposed to "GQM" (Figure1-8) [71]. At the expected GQM motif position (1071-1073) the amino acid sequence of JAK3 shows a high degree of variability across the species (Figure 1-8).

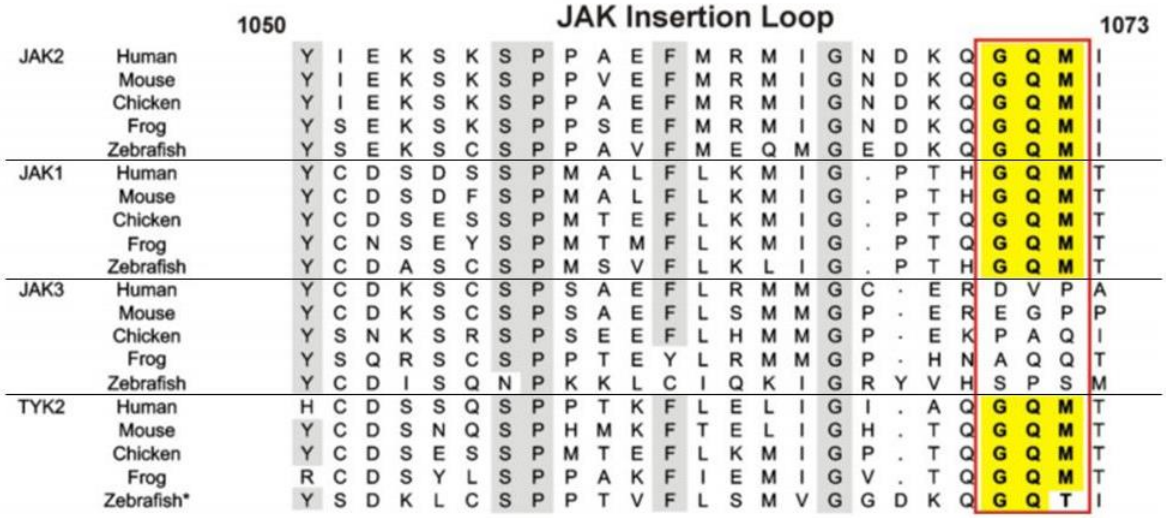

Figure 1-8: The GQM sequence is located on the JAK insertion loop of JAK2, Jak1 and TYK2
Sequence alignment of the JAK insertion loop revealed JAK3 did not contain the "GQM" motif and comprised a high degree of sequence variation. The "GQM" motif was highly conserved across the species for JAK1, JAK2 and TYK2 suggesting SOCS3 may interact with all three molecules. Figure modified from [71] with permission.

Interestingly, Babon *et al* hypothesised that the absence of JAK3 sequence conservation in this region indicated that other members of the SOCS family were not involved in the regulation of JAK3 activity [71]. In recent years, zebrafish have provided a useful model organism for cardiovascular disease [72-74]. As such, the high degree of JAK sequence conservation between man and zebrafish is an encouraging observation and may facilitate the translation of future SOCS3 studies *in vivo*. However, sequencing of the zebrafish genome has identified two SOCS3 genes- SOCS3a (Accession: ZDB-GENE-030131-7349]) and SOCS3b (Accession: ZDB-GENE-040426-2528]) which may complicate *in vivo* studies. The GQM sequence, at position 1071-1073, on JAK2 is located within the JAK insertion loop and facilitates the binding of SOCS3 via the ESS, SH2 and KIR domain collectively (Figure1-7)[70]. However, following the crystallisation of the SOCS3-JAK2-gp130R complex, Kershaw *et al* noted that following SOCS3 docking, at the GQM motif, minimal structural changes were observed in JAK2 [70].

1.3.7.4 The role of the SOCS3 kinase inhibitory region (KIR)

Importantly, the N-terminal KIR of SOCS3 was shown to associate with, and therefore block, the substrate binding domain of JAK2 [70]. For that reason, the authors described SOCS3 as a "pseudosubstrate" of JAK2 as cognate substrates could no longer interact.

Interestingly, SOCS3 inhibition of JAK2 was lost upon mutation of a key residue (Phe25Ala) within the KIR of SOCS3 [70]. Moreover, deletion of the first three residues within the KIR led to a rightward log order increase in the IC_{50} for SOCS3-mediated inhibition of JAK2 . Finally, the crystal structure of the SOCS3-JAK2-gp130R complex revealed that a positively charged residue within SOCS3 (Arg21) flanks the KIR and interacts with the JAK2 substrate binding domain serving as a phosphomimetic. The "pseudosubstrate" hypothesis was confirmed when mutation of the first three residues of the KIR (19-21) to tyrosine residues led to the phosphorylation of SOCS3 at these sites i.e. SOCS3 could be transformed into a JAK2 substrate. Together these data confirmed the significance of the KIR. However SOCS3 was not shown to be a direct inhibitor of JAK2 activity, rather SOCS3 appears to act as a pseudosubstrate that blocks the access of *bona fide* JAK2 substrates.

1.3.7.5 SOCS3 may outcompete JAK/STAT components for phosphotyrosine docking sites.

It is likely the JAK-STAT pathway involves significant cross-talk with the MAPK pathway and this is supported by the fact that many ligands activate both pathways [75]. In fact, mutagenesis experiments, in which JAK association with a cytokine receptor was abolished, revealed ERK/MAPK activation was also lost [76].

SH2-containing protein tyrosine phosphatase (SHP) enzymes were initially described in 1991 [77] and are known to provide an additional layer of regulation for cytokine signalling [78]. The literature describes two distinct SHP isoforms (SHP-1 and SHP-2) which function by removing the charged phosphate group of pY residues on the intracellular domain of activated receptors. Interestingly, SHP-2 is synthesised in an inactive conformation that requires a post-translational modification, cysteine oxidation, in order to achieve the active conformation (Figure1-9) [79]. Once active, the protein tyrosine phosphatase SHP-2 can dock at target pY residues and in turn positively or negatively regulate signalling pathways.

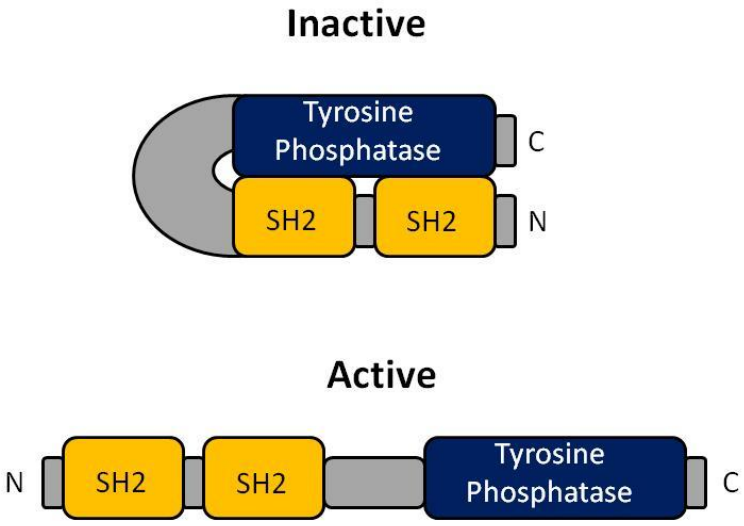

Figure 1-9: SHP-2 protein tyrosine phosphatase activation

SHP-2 contains two n-terminal SH2 domains which facilitate the interaction with phosphotyrosine (pY) residues on target substrates. SHP-2 also contains a C-terminal tyrosine phosphatase domain which removes phosphate groups from target pY residues. In the inactive state, the SH2 domains of SHP-2 interact with the phosphatase domain rendering it catalytically inactive. However, following the oxidation of a C-terminal cysteine residue on SHP-2 a conformational change is induced releasing the SH2 domains from the phosphatase domain. SHP-2 is now catalytically active. Modified from [79] with permission.

Following its activation, SHP-2 has the ability to activate the Ras-ERK1,2 pathway as depicted in Figure 1-10 [80]. Conversely SHP-2 was also shown to de-phosphorylate STAT5A and thus may also function as a negative regulator of the JAK/STAT pathway [81]. Interestingly, SOCS3 may compete with SHP-2 for pY759 on the intracellular domain of the gp130 receptor [58]. As a result of the SOCS3-pY759 interaction, SHP-2 can no longer activate the Ras-ERK1,2 signal cascade therefore limiting the expression of mitogenic gene profiles (Figure1-10).

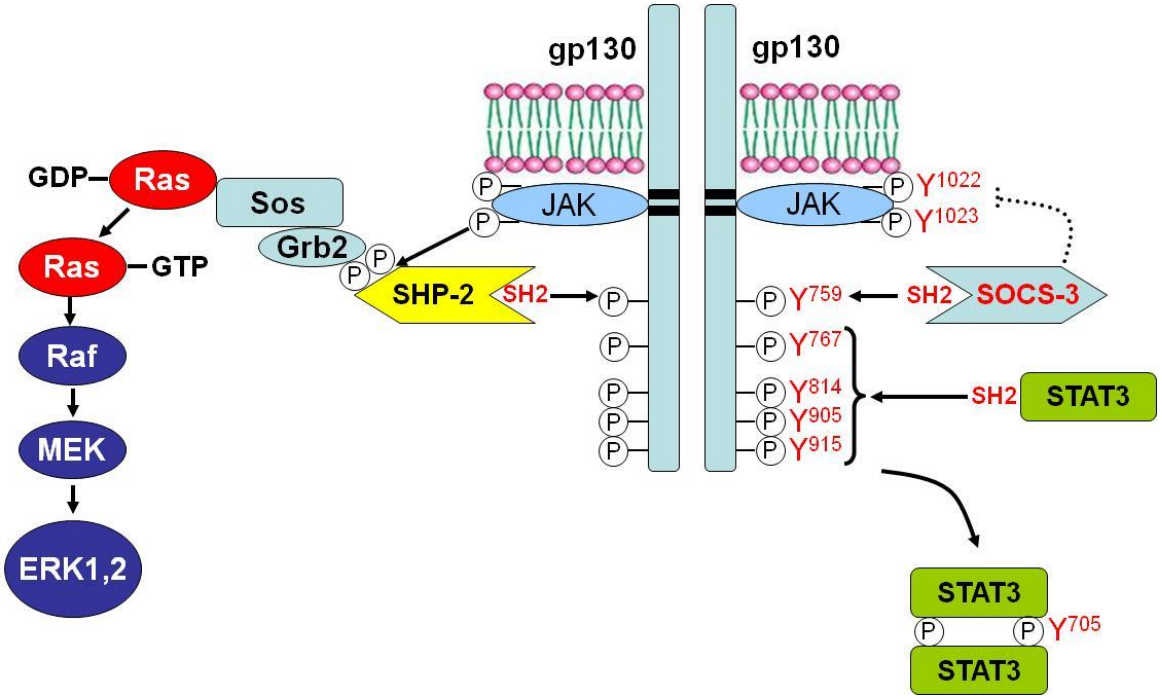

Figure 1-10: SHP-2 mediated activation of the Ras-ERK1,2 pathway

Circulatory IL6 interacts with a soluble or membrane bound isoform of the IL6 receptor α (IL6Rα). The activated IL6Rα subsequently dimerises with the glycoprotein 130 receptor (gp130R) on the plasma membrane initiating the activation of receptor associated JAKs. JAK activation (trans-autophosphorylation) and the subsequent phosphorylation of the YSTV motif, on the gp130R cytoplasmic tail, provides a phosphotyrosine (pY759 in humans or equivalent pY757 in mouse) docking site for SHP-2. SHP-2 is subsequently phosphorylated by the receptor associated JAKs leading to the recruitment of Grb2 (growth-factor-receptor-bound protein 2) which is bound to Sos (son-of-sevenless). Sos serves as a guanine nucleotide exchange factor (GEF) for the Ras protein and therefore activates Ras by generating Ras-GTP. Subsequently the ERK1/2-MAPK pathway is activated driving the expression of genes involved in proliferation, differentiation and development [80]. However, SOCS3 may compete with SHP-2 for pY759 on the gp130R and so inhibits activation of the Ras-ERK1.2 pathway by SHP-2 [58]. Figure reproduced from [82] with permission.

1.3.8 SOCS3 targets substrates for degradation

Ubiquitylation is a post-translational modification in which a single ubiquitin moiety or a chain of ubiquitin molecules are transferred to Lys residues on specific protein substrates [83]. Interestingly, the C-terminus of SOCS3 contains a 40 residue SOCS box region [49, 84] which provides a platform for the assembly of an Elongin-Cullin-SOCS^{SOCS3} (ECS^{SOCS3}) ubiquitin ligase complex (Figure 1-11B) [48]. Following ECS^{SOCS3} ligase complex formation, the ubiquitin-activating (E1) and ubiquitin-conjugating (E2) enzymes are recruited and catalyse the polyubiquitylation of target proteins that specifically interact with SOCS3 [85]. As mentioned previously, SOCS3 binds to phospho-Tyr sites on target proteins via its SH2 domain, while the SOCS box provides the platform for ECS^{SOCS-3} ligase complex formation and the interacting protein now provides a substrate for ubiquitylation.

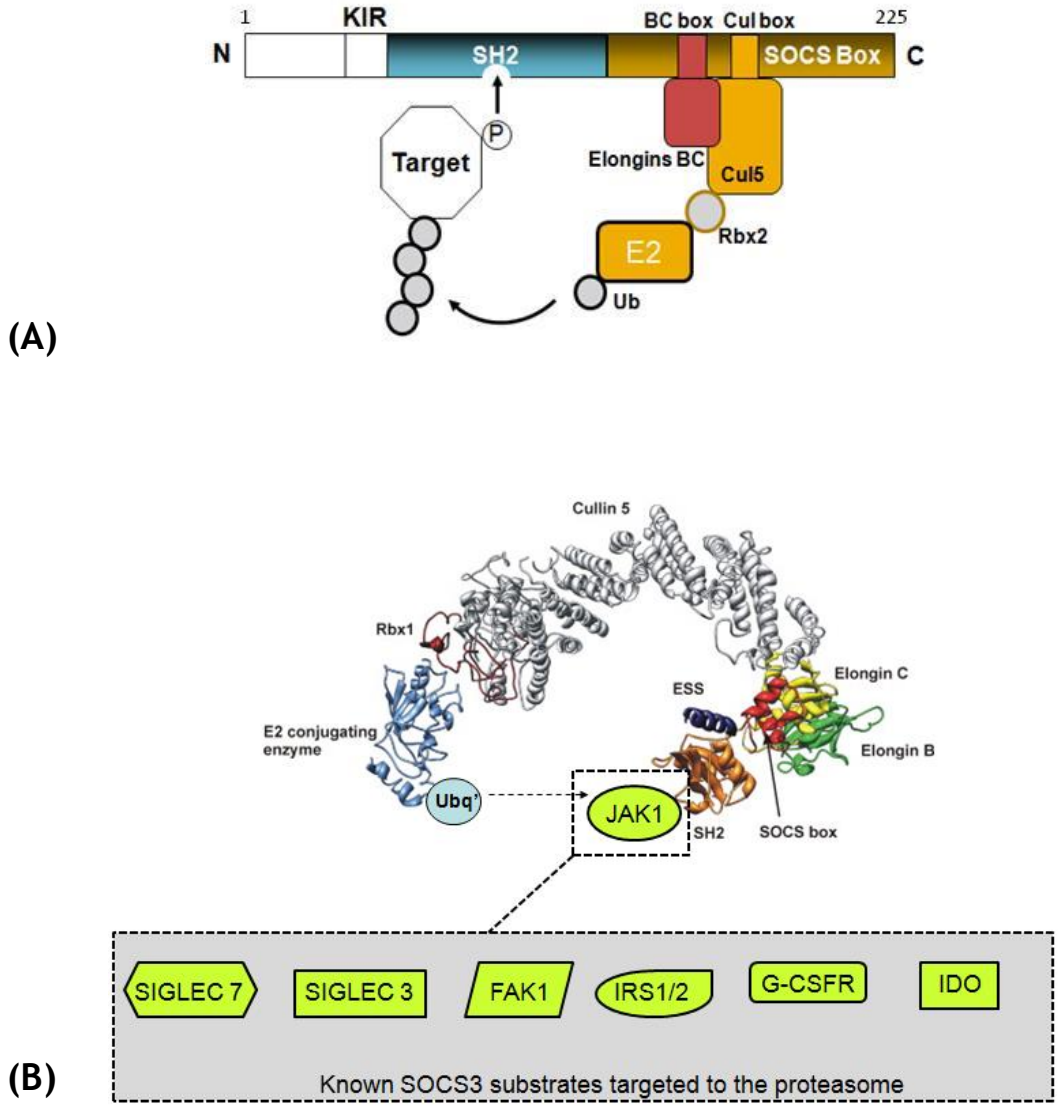

Figure 1-11: Schematic of the SOCS3 protein and formation of the E3 ubiquitin ligase complex

(A) Schematic of the SOCS3 protein structure. The SH2 domain binds phosphotyrosine residues on substrate proteins. Within the SOCS box, the BC box binds Elongin B and Elongin c providing the platform for the ubiquitin ligase machinery. The SOCS3 substrate bound by its SH2 domain may now be ubiquitylated and targeted to the proteasome. KIR denotes kinase inhibitory region. (B) Formation of the ECSSOCS-3 ubiquitin ligase complex. Initially Elongin B and C bind the C terminal BC-box of SOCS3 and recruit Cullin-5 to the scaffold. Cullin-5 then interacts with RING finger domain of Rbx 2 to form the E3 ligase complex. Rbx2 recruits the E2 conjugating enzyme bringing ubiquitin (7.6KDa) and substrate in close proximity for ligation (ubiquitylation) by the E3 ligase [86]. Lys48 linked ubiquitylated substrates are then targeted to the 26S proteasome for degradation. Mono-ubiquitination provides a weaker but sufficient signal for degradation than poly-ubiquitin chain formation. Known SOCS3 substrates from in vitro investigations have been reviewed previously [47]. Sialic acid-binding Ig-like lectin 7 (SIGLEC 7); Janus kinase 1 (JAK1); sialic acid-binding Ig-like lectin 3 (SIGLEC 3); focal adhesion kinase 1 (FAK1); insulin receptor substrate 1/2 (IRS1/2); granulocyte colony-stimulating factor receptor (G-CSFR); indoleamine 2,3-dioxygenase (IDO). Figure 1-11 A adapted from [49] and B adapted from [48] with permission.

Table 1-2 summarises the proteins known to interact with SOCS3 that are subsequently targeted for degradation (recently reviewed by our group [47]). Of these, six are known to be targeted for degradation by the proteasome (expression was stabilised in the presence of a proteasome inhibitor). Conversely, the Granulocyte Colony-Stimulating Factor Receptor (G-CSFR) provides an example of SOCS3-mediated receptor downregulation via ubiquitin-mediated lysosomal degradation [56].

Substrate targeted for proteasomal degradation	Function of SOCS3	Literature reference
Indolaemine 2,3-dioxygenase (IDO)	Targets IDO for proteasomal degradation in CD8+ dendritic cells (DCs). Induced murine tolerogenic DCs to become immunogenic.	[87]
Insulin Receptor Substrate 1/2 (IRS-1/2)	Targets IRS-1/2 for proteasomal degradation. Impaired insulin signalling. May contribute to insulin resistance and/or diabetes.	[88, 89]
Sialic Acid-Binding Immunoglobulin-Like-Lectin (Siglec)-7	Targets Siglec-7 for proteasomal degradation. Inhibition of Siglec-7-mediated Ba/F3 cell proliferation.	[90]
CD33	Targets CD33 for proteasomal degradation. Loss of CD33 mediated inhibition of Ba/F3 cell proliferation.	[91]
Janus Kinase 1 (JAK1)	Loss of the SOCS box enhanced the accumulation of P-JAK1. SOCS3 may target hyper-phosphorylated JAK1 for proteasomal degradation in murine embryonic stem cells.	[92]
Focal Adhesion Kinase 1 (FAK1)	FAK1 Y397 interacted with SOCS3 and was subsequently targeted for proteasomal degradation. Y397F mutagenesis stabilised FAK1 expression in the presence of SOCS3.	[93]
Substrate targeted for lysosomal degradation		
Granulocyte Colony-Stimulating Factor Receptor (G-CSFR)	Interacts with Y729 on G-CSFR. Lys 632 ubiquitylation targets G-CSFR for lysosomal degradation. Receptor downregulation. Switch off G-CSFR signalling.	[56]

Table 1-2: SOCS3 substrates targeted for degradation. Table adapted from [47].

1.3.9 The mechanism of SOCS3 turnover

1.3.9.1 Proteasomal degradation

The exact mechanisms responsible for SOCS3 protein turnover remain unknown. However it is likely that multiple routes of SOCS3 proteolysis exist and the contribution of each will vary between cell systems. Several studies have described the rapid turnover of SOCS3 via the 26S proteasome [94-96]. As a polyubiquitylated substrate, SOCS3 has a short biological half-life of ~40-120 mins which is cell type dependent [97]. The use of pharmacological inhibitors of the proteasome such as MG132, LLnL and epoxomicin has been instrumental in establishing its important role in SOCS3 turnover.

In 1999, Zhang and co-workers were the first to describe the stabilisation of the SOCS3 in the presence of a proteasome inhibitor [96]. A macrophage cell line (J774) was stimulated with IL-6 with or without the proteasome inhibitor LLnL over a 180 min time period to induce endogenous SOCS3 expression, SOCS3 protein levels increased between the 30 and 180 min time points in the presence of LLnL. Conversely, in the control group, SOCS3 expression peaked at the 60 min time point after which SOCS3 protein levels declined. However, as immunoblot analysis was conducted on SOCS3 IP samples and densitometry analysis was not performed, the significance of these data were not verified.

Later in 2003, another study identified the proteasome as a major route of SOCS3 turnover in a murine pro-B cell line (Ba/F3) [95]. Sasaki and co-workers generated an N-terminally truncated SOCS3 mutant that was resistant to ubiquitylation and turnover at the proteasome. Specifically, Lys6 was shown to be critical for the recognition and degradation of SOCS3 at the proteasome. Furthermore, a C-terminally truncated SOCS3 (lacking the SOCS box) that fails to bind components of the E3 ligase complex was also stabilised. The authors suggest that SOCS3 auto-ubiquitylation was responsible for the rapid turnover of this signalling molecule however the study failed to fully investigate the mechanism of SOCS3 ubiquitylation [95]. *In vitro* autoubiquitylation assays are relatively simple and assessing whether the SOCS box of the Lys6 mutant had the ability to interact with components of the E3 ligase complex would be informative. Finally, the authors did not consider the role of external E3 ligases that may regulate SOCS3 ubiquitylation and provide a therapeutic target for stabilising SOCS3.

1.3.9.2 Tyrosine phosphorylation regulates SOCS3 stability

Haan *et al* demonstrated that phosphorylation of SOCS3 at Tyr^{204} and Tyr^{221} within the C-terminal SOCS box region destabilised SOCS3 by targeting it for degradation via the proteasome [94]. In this study sodium pervanadate, a tyrosine phosphatase inhibitor, was employed to preserve the phosphorylation of SOCS3 at these two key Tyr residues. The authors demonstrated that activation of the receptor tyrosine kinase EGFR also triggered Tyr phosphorylation and down-regulation of SOCS3 to almost undetectable levels [94]. Conversely, the $SOCS3^{Y204F,Y221F}$mutant was resistant to tyrosine phosphorylation which correlated with an increase in SOCS3 stability. In addition to this, a cycloheximide chase assay revealed that in the presence of sodium pervanadate, the half-life of WT SOCS3 was reduced from 8 hrs to 4 hrs suggesting tyrosine phosphorylation played a key role in regulating the stability of SOCS3 [94]. Subsequent experiments confirmed JAK1 and JAK2 could also mediate the phosphorylation of SOCS3 *in vitro*. Following this, a decrease in SOCS3 expression was observed however this was rescued in the presence of a proteasome inhibitor. The key finding of this paper was that phosphorylation of SOCS3 at Y204 and Y221 correlated with an inability of the SOCS box to interact with Elongin C (a component of the E3 ligase machinery) [94]. Consequently, SOCS3 was degraded at the proteasome.

These data suggest that a therapeutic strategy to stabilise SOCS3 expression must ensure SOCS3 is still functional. As mentioned previously, SOCS3 provides a platform for the formation of the E3 ubiquitin ligase complex and targets substrates bound to the SH2 domain for proteasomal degradation (Figure1-11). The $SOCS3^{Y204F,Y221F}$mutant, though more stable than the WT, may not have the ability to target substrates for degradation (the authors failed to assess this) [94]. To date, 7 putative SOCS3 substrates have been identified (Table 1-2) however it is likely that many more substrates exist that are yet to be described.

In 2003, Haan *et al* used a COS-7 overexpression system to show that JAK1 or JAK2 catalysed the phosphorylation of SOCS3 [94]. The same group later reported that stimulation of mouse embryonic fibroblasts (MEFs), but not HEK293T cells, with IL6/s-IL6R and MG132 induced and stabilised the expression of endogenous SOCS3 [98]. Though SOCS3 tyrosine phosphorylation was observed, this did not correlate with the kinetics of JAK activation nor did it require the association of SOCS3 with the gp130R [98]. This subsequent study confirmed that in MEF cells this was a JAK independent post

translational modification predominantly mediated by Src itself or a related Src family kinase [98]. Collectively these data support the differential regulation of SOCS3 stability in different cell types. This also highlights that it may be more informative to assess the mechanism of endogenous SOCS3 turnover as opposed to the use of an overexpression system where possible.

1.3.9.3 Role of the SOCS3 PEST motif in determining stability

In 1986, Rogers and co-workers performed a literature search with the aim of identifying sequence similarities between eukaryotic proteins which possess relatively short half-lives (less than 120 mins) [99]. This seminal work identified a common feature known as the PEST motif: a sequence rich in pro (P), glu (E), ser (S) and thr (T) residues. A PEST motif is also found in SOCS3, located within the SH2 domain at position 129-162 as depicted in Figure1-7. Interestingly, pulse chase experiments have revealed that deletion of the PEST motif ($SOCS3_{\Delta PEST}$) enhanced protein stability when compared to WT SOCS3 [100]. The subsequent deletion of the N-terminus, PEST motif and SOCS box region ($^{22\text{-}185}SOCS3_{\Delta PEST}$) further enhanced the stability of SOCS3 [100]. Moreover, pharmacological inhibition of the proteasome specifically stabilised the expression of $SOCS3_{\Delta PEST}$ but not WT SOCS3 [100]. These data suggested that the proteasome was a major route of SOCS3 degradation in the absence of the PEST motif however full length WT SOCS3 was resistant to proteasome-mediated turnover and therefore must be degraded via an alternative route in HEK293T cells. Additionally, inhibition of caplain proteases and the lysosomal machinery had no obvious effect on WT SOCS3 stability in HEK293T cells and the authors failed to establish the mechanism of SOCS3 turnover in this cell system [100]. However, Haan *et al* previously confirmed that MG132-mediated proteasomal inhibition stabilised the expression of SOCS3 that was co-expressed with JAK1 in HEK293T cells [94]. As such, these data conflict with the Babon and co-workers observations [100].

1.3.9.4 Role of calpain proteases in determining SOCS3 stability

The calpain proteases comprise a family of 14 related proteins [101]. Calpain proteases are Ca^{2+}-dependent enzymes that rely on a nucleophilic Cys residue for proteolysis of target substrates [101]. The most well characterised members of this family are μ-calpain and m-calpain that require μM and mM Ca^{2+} concentrations respectively for catalytic activity [102]. In 2015, Miyazaki and colleagues demonstrated that SOCS3 was degraded *via* μ-

calpain proteolysis in human aortic endothelial cells (HAECs) [103]. The siRNA-mediated knockdown of endogenously expressed μ-calpain inhibitor calpastatin (CAST) resulted in a decrease in SOCS3 protein levels and a corresponding increase in STAT3 activation as measured by Tyr705 phosphorylation [103]. SOCS3 mRNA levels were unchanged confirming SOCS3 transcription was unaffected. Moreover, stimulation of the CAST-depleted HAECs with a calpain inhibitor (ALLM) restored SOCS3 protein levels and reduced STAT3 activation [103]. These data confirmed that the calpain protease system could play a role in SOCS3 degradation in this cell type. Calpain inhibitor therapies are currently being developed by several groups [104] with potential applications in cardiovascular disease [105], traumatic brain injuries [106, 107] and cancer [101, 108] amongst others. However, calpain inhibitor therapies have failed to progress beyond pre-clinical studies due to a lack of calpain isoform specificity [104, 109]. As such, a more targeted approach aimed at stabilising SOCS3 may be more productive.

More recently, the regulation of SOCS3 turnover was shown to involve both the calpain and proteasomal degradation pathways [84]. Initially, endogenous SOCS3 was induced via LPS stimulation in RAW264 macrophage cells. The addition of a calpain inhibitor (calpeptin) or proteasome inhibitor (epoxomicin) each prolonged the half-life of endogenous SOCS3 by 1 hr and 1.3 hrs respectively [97]. Interestingly, inhibition of both pathways produced a synergistic 10-fold increase in the half-life of SOCS3 to ~9 hrs. These data confirmed the importance of two distinct degradation pathways regulating SOCS3 turnover in a monocytic cell line, and suggest that the evolution of functional redundancy between calpain and proteasomal pathways ensures that the temporal and tight regulation of SOCS3 stability is maintained.

The same group have also utilised a modified, cell penetrable form of SOCS3 (CP-SOCS3) to show that SOCS3 dampened the inflammatory response in animal disease models [110]. CP-SOCS3 was modified to include a hydrophobic sequence that facilitated crossing of the plasma membrane phospholipid bilayer [110]. Subsequently, the CP-SOCS3 isoform was shown to exhibit an extended half-life of >6 hrs when compared to endogenous SOCS3 with a half-life of 0.7 hrs [110]. The group proposed that the inclusion of this hydrophobic sequence at the N-terminus of SOCS3 repressed proteolysis of SOCS3 via the PEST motif-calpain pathway, although this was not tested directly [110]. Interestingly, a follow up study in 2010 revealed that deletion of the C-terminal SOCS box region from CP-SOCS3 also increased the half-life of the protein by >40-fold and that this was attributable to a loss

of proteasomal degradation [97]. Mapping the preferred sites of Lys ubiquitylation may provide further insight into the disparity in SOCS3 stability described.

1.3.9.5 SOCS2 as a regulator of SOCS3 stability

In 2005, Tannahill et al demonstrated that SOCS2 played a role in targeting SOCS3 for proteasomal degradation in a suspension B cell line (Ba/F3s) [111]. Overexpression of SOCS2 in these cells reduced SOCS3 protein levels and following cytokine stimulation the ability of SOCS3 to negatively regulate JAK/STAT signalling was diminished. Interestingly, an intact SOCS box on SOCS2, allowing the formation of the ECS^{SOCS2} E3 ligase complex, was required for proteasomal degradation of SOCS3 [111].

1.4 Epigenetic modulation of SOCS3 expression in disease

Epigenetics describes a reversible change to the gene expression profile that is not a direct result of alterations to the DNA sequence [112]. Though epigenetic modifications provide an additional layer of regulation for gene expression, the aberrant epigenetic silencing of many genes is thought to play a major role in diseases such as cancer [112]. An emerging role for epigenetic regulation of SOCS3 expression has been documented in the literature.

1.4.1 SOCS3 promoter hyper-methylation in cancer

DNA methylation is an epigenetic modification in which a methyl group is added to the 5' of a cytosine base that is adjacent to a guanine base (CpG motif) [112]. Interestingly, hypermethylation of CpG islands within the promoter region of SOCS3 has been described in many cancer cell lines including lung cancer [113], breast cancer [113], hepatocellular carcinoma [114] and adenocarcinoma [115]. SOCS3 hypermethylation was also described in a patient with cholangiocarcinoma (CCA) [116]. Isomoto and co-workers employed demethylating compounds, to cleave the methyl groups from the SOCS3 promoter region in a CCA cell line [116]. This successfully restored the expression of a functional SOCS3 protein that exerted inhibition of STAT3 activation [116]. In the absence of SOCS3 negative regulation, prolonged IL6-mediated JAK/STAT signalling drives the expression of anti-apoptopic and mitogenic gene profiles which contribute to tumour progression. Conversely, epigenetic silencing of SOCS1 and 2 were shown to play a role in some ovarian and breast cancers where SOCS3 expression was unaffected [117].

1.4.2 SOCS3 promoter hyper-methylation in cardiovascular disease

Following myocardial infarction (MI) or transient ischaemic attack (TIA), the coronary artery may be narrowed therefore restricting blood flow to the heart. Percutaneous coronary intervention is a revascularisation procedure which may involve stent implant into the narrowed blood vessel (section 1.1.2). However, mechanical injury occurs during this procedure causing the release of pro-inflammatory and mitogenic factors including tumour necrosis factor α (TNFα) and insulin growth factor 1 (IGF1) respectively. Gupta *et al* previously showed that stimulation of porcine coronary artery smooth muscle cells (PCASMCs) with tumour TNFα or IGF1 alone upregulated the expression of SOCS3 [118]. Conversely, stimulation with both TNFα and IGF1 led to a decrease in SOCS3 expression. Similarly, Dhar *et al* confirmed this response in human CASMCs and revealed that hyper-methylation of the SOCS3 promoter occurred in the TNFα+IGF1 treatment group only [119]. The DNA methyltransferase 1 enzyme was also shown to be significantly upregulated in this group facilitating the covalent attachment of methyl groups to CpG islands in the SOCS3 promoter [119]. Silencing SOCS3 expression in this instance contributes to disease progression as loss of JAK/STAT control in vascular smooth muscle cells (VSMCs) may drive neointimal lesion formation and re-narrow the blood vessels.

1.4.3 Histone acetylation and deacetylation regulates transcription factor access to the SOCS3 promoter

Histone acetylation involves the addition of a negatively charged acetyl group to the lysine residue(s) of positively charged histone proteins [120]. This action is catalysed by histone acetytransferase (HAT) enzymes that neutralise the positive charge of the histone [120]. As such, the neutralised histones possess a reduced affinity for the negatively charged DNA and therefore promote the formation of euchromatin. Euchromatin is the gene-rich, open form of chromatin that facilitates access to the promoter region by the machinery required to drive transcription [121].

A study conducted in RAW264 monocytic cells described the role of epigenetic modifications in driving SOCS3 expression following LPS exposure [122]. Initially, euchromatin formation at the SOCS3 promoter was driven by the acetylation of histone 3

and 4. Subsequently, c-Fos, c-Jun and STAT3 transcription factors gained access to the SOCS3 promoter region and so inducing the expression of endogenous SOCS3 [122]. In the absence of histone acetylation, the SOCS3 promoter would be inaccessible to transcription factors and RNA polymerase II due to the dense packaging of histones and DNA (heterochromatin structure). Thus, the tight regulation of the chromatin structure is important for the maintenance of the JAK/STAT-SOCS3 negative feedback loop to avoid the detrimental effects of hyper-activation [122].

Conversely, histone deacetylase (HDAC) enzymes reverse the action of HATs by cleaving the acetyl group from histones and so promote the silencing of genes by limiting transcription factor access to the promoter region. As such, HDAC inhibitors promote the transcriptionally active euchromatin state and may provide a useful therapy in the treatment of some cancers. Curcumin is derived from turmeric and was recently shown to be a potent inhibitor of HDAC activity [123]. A study conducted in human leukaemia cells revealed that knockdown of HDAC8 or curcumin treatment correlated with increased histone 3/4 acetylation and was associated with an increase in SOCS1 and SOCS3 expression [123]. Moreover, primary cells derived from patient myeloproliferative tumours were cultured *in vitro* and treated with curcumin leading to the upregulation of SOCS3 expression by more than 2 fold in 67% of these patient tumour cell samples. Sodium Butyrate [124] and Trichostatin A [125] were also previously shown to act *via* HDAC8 inhibition however as curcumin is a naturally occurring anti-oxidant found in tumeric spice it may therefore provide a well-tolerated anti-cancer therapy in man [126].

1.5 Ubiquitylation

1.5.1 Ubiquitylation is an ATP dependent process involving three discrete enzymes

Ubiquitylation is a reversible post-translational modification (PTM) in which a ubiquitin moiety (8.5kDa) is covalently attached to a target Lys (K) residue on its substrate [127]. Ubiquitylation requires the sequential activity of three distinct enzymes referred to as the E1 (activating enzyme), E2 (conjugating enzyme) and an E3 (ligase enzyme) and has been reviewed recently [127]. Figure 1-12 illustrates the stepwise conjugation of ubiquitin to an acceptor Lys residue on target substrates. Initially, in the presence of ATP, a thioester bond is created between a cysteine residue (SH group exposed) located in the E1 active site and the C terminus of ubiquitin [127]. Following this, the ubiquitin moiety is transferred to a cysteine (thioester link) positioned in the active site of the E2 conjugating enzyme. The E3 ligase then interacts with the substrate and E2 conjugating enzyme forming an E3 ligase complex. The E3 then catalyses the direct, or indirect, transfer of the ubiquitin molecule from the E2 to the ε-amino group of the Lys acceptor in doing so creating a covalent isopeptide bond.

There are two E1 activating enzymes, 37 E2 conjugating enzymes and over 600 human E3 ligase enzymes [127]. The E3 ligase is the specificity determining factor for substrate recognition ensuring protein ubiquitylation is a highly selective and tightly regulated process. There are three main families of E3 ubiquitin ligases that catalyse the attachment of ubiquitin to Lys. The Really Interesting New Gene (RING) domain E3s contain a RING domain that interacts with the E2-ubiquitin moiety [128]. The E3 then catalyses the transfer of ubiquitin from the E2 active site directly to the substrate acceptor Lys. Within this family, the E3s have been further sub-divided based on their structure. For example the Cullin RING E3 ligases require the interaction of a Cullin scaffold protein in addition to an F box protein that recruits the substrate. In contrast, Homology to the E6AP C Terminus (HECT) class of E3s transfer ubiquitin from the Cys residue of the bound E2 to a cysteine residue on the E3 itself before catalysing ubiquitin conjugation to the target Lys [128]. HECT E3 activity therefore involves two stages that may be described as indirect ubiquitylation. The most recent family to be described in the literature were the RBR E3s which includes the Parkin E3 [128]. This class of E3s were initially thought to be a sub-class of the RING E3 family due to the presence of two distinct RING domain structures.

However, the RBR E3s contain a catalytic Cys residue that mediates the indirect transfect of ubiquitin to the substrates acceptor Lys i.e. functions similar to the HECT family.

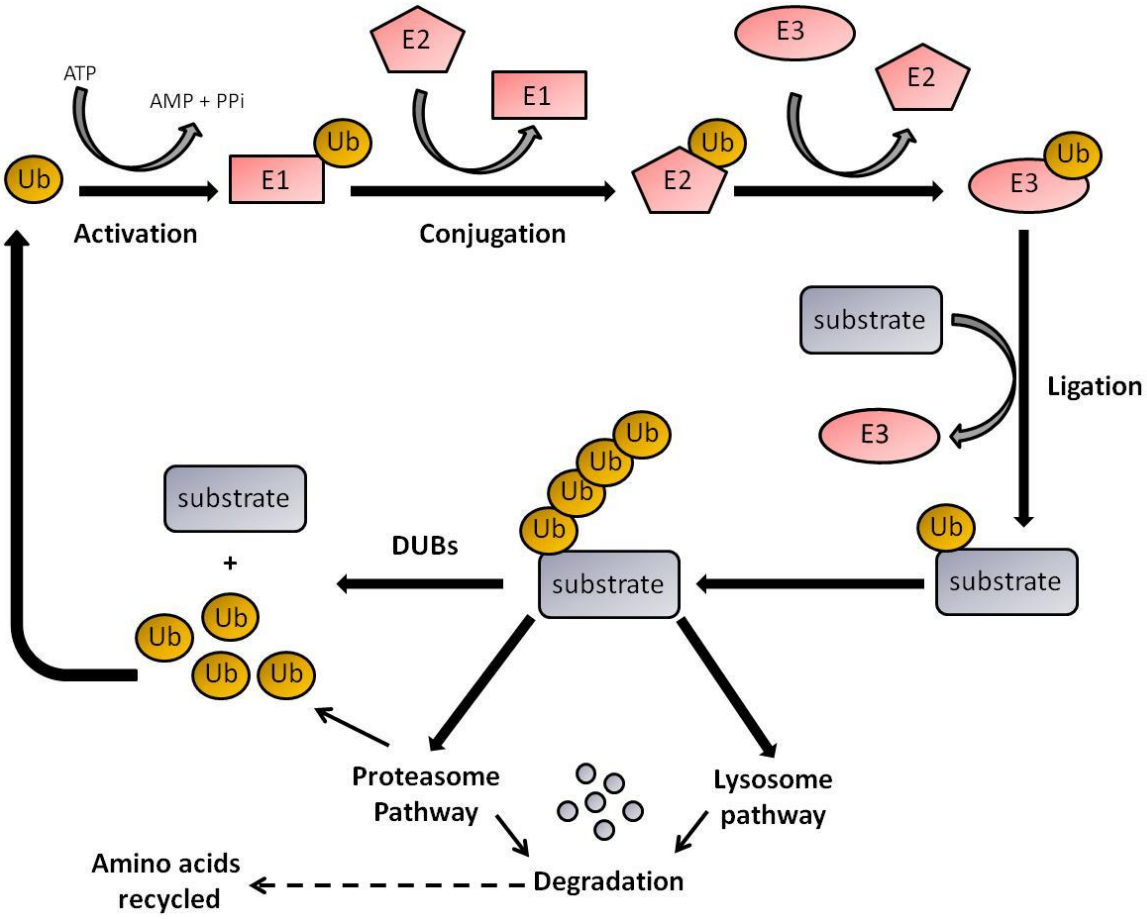

Figure 1-12 Ubiquitylation is a reversible modification that may regulate protein stability

Initially the E1 enzyme activates ubiquitin (Ub), in a ATP dependent manner, transferring the Ub moiety to a cysteine residue located within the E1 enzyme. Ub is then transferred to the conjugating E2 enzyme which interacts with its cognate E3 ligase partner. The E3 ligase is the specificity determining factor that interacts with the appropriate substrate. The E3 ligase then catalyses the conjugation of Ub to the target Lys residue on the interacting substrate. Depending on the linkage type, the ubiquitylated substrate may be targeted for proteasomal or lysosomal degradation and the amino acids are recycled for cellular processes. Alternatively, de-ubiquitylase (DUB) enzymes may cleave the ubiquitin chains from the substrate and so reverse the action of the E3 ligase. DUBs may therefore stabilise the expression of a protein that has otherwise been targeted for degradation. The Ub molecules cleaved by the proteasome or DUB action are then recycled and available for ubiquitylation of substrates once again. Figure adapted from [129] with permission.

1.5.1 Deubiquitylation of substrates

The human genome encodes around 100 deubiquitylase (DUB) enzymes that reverse the action of the E3 ubquitin ligases and may therefore promote substrate stabilisation or attenuate cell signalling events (Table 1-3) [130].

DUB family	Number of family members	Mechanism
Ubiquitin-Specific Proteases (USPs)	56	Cysteine protease
Ubiquitin C-Terminal Hydrolases (UCHs)	4	Cysteine protease
Ovarian Tumour Proteases (OTUs)	16	Cysteine protease
Machado–Joseph disease domain (Josephins)	4	Cysteine protease
Monocyte Chemotactic Protein-Induced Protein (MCPIPs)	7	Cysteine protease
JJAB1/MPN/MOV34 (JAMMs)	12	Zn^{2+} metalloprotease

Table 1-3: DUB families and the mechanism of catalysis

DUBs hydrolyse the isopeptide bond between the last two ubiquitin molecules in the chain and so progressively reduce polyubiquitin chain length. There are six DUB families (Table 1-3) described in the literature though DUB activity has not been confirmed for a small sub-set of predicted DUBs and the full complement of DUB substrates has not been elucidated. There are two mechanisms of DUB catalysis i) Cys proteases which involve a catalytic Cys residue in the active site and ii) Zn^{2+} metalloproteases that activate a water molecule to facilitate hydrolysis of the isopeptide bond [130]. A growing number of human diseases have been associated with the loss of DUB function, thereby reinforcing the importance of appropriately regulating ubiquitylation at the cellular level [131]. Singhal and co-workers provide a comprehensive review of DUB activity in human disease an example of which is the cylindromatosis (CYLD) protein [131]. CYLD is a known tumour suppressor that possesses DUB activity and is involved in the negative regulation of NF-κB signalling. Loss of CYLD activity was shown to play a role in the progression of skin cancer and highlights the significance of DUB activity in the body [131].

1.5.2 Ubiquitin chain arrangement

There are 3 general arrangements of substrate ubiquitylation including mono-ubiquitylation, multi-mono-ubiquitylation and poly-ubiquitylation (Figure 1-13). The ubiquitin chain conformation and linkage type determines the intracellular response to this modification.

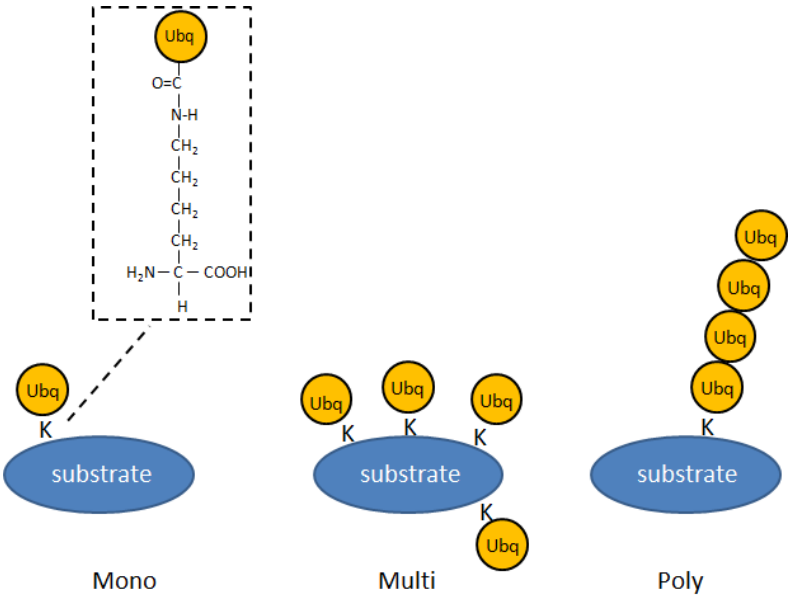

Figure 1-13: There are 3 main ubiquitylation arrangements: mono, multi-mono and poly
Monoubiquitylation describes an event in which a single ubiquitin molecule is covalently attached to one substrate lysine residue for example histone HB2 is modified at lys120 only [132]. Similarly, the epidermal growth factor receptor (EGFR) provides an example of mono-multi-ubiquitylation in which several K residues on EGFR are modified by a single ubiquitin molecule [133]. Moreover, ubiquitin possesses 7 internal K residues facilitating the formation of poly-ubiquitin chains at one or more lysine residues on the substrate surface. Figure modified from [127] with permission.

Ubiquitin is small 76 amino acid protein which possesses 7 internal lysine residues (K6, K11, K27, K29, K33, K48 and K63) and so facilitates the formation of poly-ubiquitin chains [127]. This involves the formation of an isopeptide bond between Gly76 of the last ubiquitin in the chain and the ε-amino-group of any of the seven Lys residues on the next ubiquitin extending the chain. To date, Lys48- and Lys63-linked chains have been best characterised.

1.5.3 Lys^{48} polyubiquitin chains target substrates for degradation at the 26S proteasome

In 1989, Chau and co-workers were the first to describe the degradation of a substrate that was conjugated specifically to Lys48-linked poly-ubiquitin chains [134]. It is now widely accepted that Lys48-linked chains target modified substrates for degradation, in an ATP dependent manner, at the 26S proteasome [127]. Expressed in both the nucleus and the cytoplasm, the 26S proteasome is a large (2000kDa) multi-subunit enzyme that contains two 19S regulatory subunits and a 20S catalytic subunit at the centre (Figure 1-14) [135].

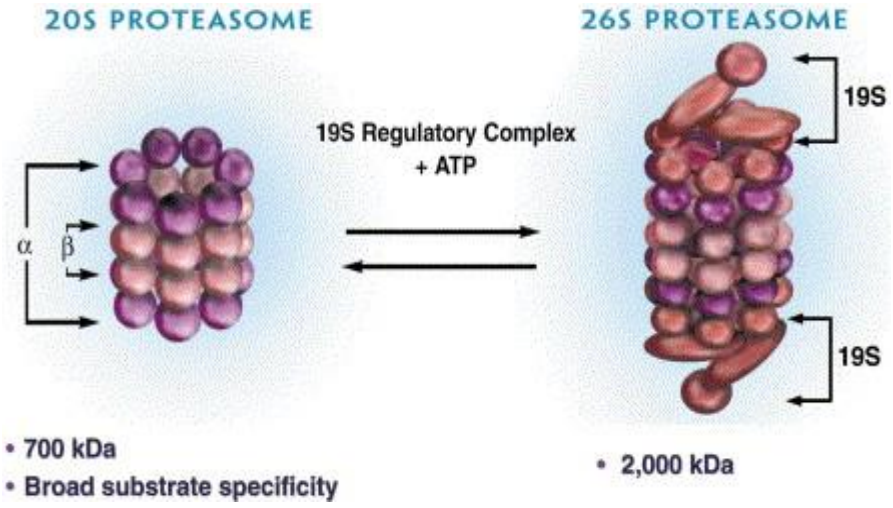

Figure 1-14: Assembly of the 26S proteasome

The 26S proteasome is involved in the selective degradation of proteins conjugated to lys48-linked polyubiquitin chain(s). Two 19S regulatory subunits sandwich a central 20S catalytic subunit and promote the degradation of substrates in the presence of ATP. Figure reproduced from [135] with permission.

The 19S regulatory domains initially recognise and bind to the poly-ubiquitin chain(s) conjugated to a protein substrate. The poly-ubiquitin chain is then removed and the substrate denatured to facilitate entry into the cylindrical 20S catalytic core. Finally, the protein substrate is digested into small, peptide fragments (3-25 amino acids) that can no longer form a functional protein conformation, and which are released back into the nucleus or cytosol. In the cytosol, proteolytic enzymes then rapidly cleave the peptide fragments to provide an additional source of amino acids for the translation of nascent proteins [136]. It has been reported that Lys48-linked chains required at least 4 ubiquitin molecules in order to target a substrate to the proteasome for degradation [137]. In this

way, protein stability within the cell can be tightly regulated at the 26S proteasome by this Lys48-linkage-specific modification. However, more recently the literature has described the 26S proteasomal degradation of a mono-ubiquitylated substrate known as paired box 3 protein (PAX3) [138]. Though this may be considered a rare event, it is likely that other mono-ubiquitylated substrates targeted for proteasomal degradation will emerge in the literature. It is also important to investigate the functional consequence of linkage specific ubiquitin modifications. One cannot assume an increase in Lys48-linked poly-ubiquitylation will translate to a decrease in protein stability.

More recently, the literature has suggested that substrates conjugated to non-Lys48 polyubiquitin chains can also undergo some level of digestion at the 26S proteasome. Xu *et al* stimulated yeast cells with a proteasome inhibitor (MG132) for 0-2 hours and assessed the abundance of polyubiquitin linkages *via* mass spectrometry [139]. With the exception of Lys63 polyubiquitin chains, proteasomal inhibition resulted in the accumulation of all polyubiquitin linkage types (K6, K11, K27, K29, K33 and K48). Though the largest increase in relative abundance was observed for Lys48 polyubiquitin chains, these data provided evidence to support a role for proteasome-mediated degradation of other linkage types in a eukaryotic system [139].

1.5.4 Lys63 polyubquitin chains: non-proteolytic or proteolytic

In contrast to Lys48-linked polyubiquitylation, Lys63-linked chains are generally associated with a non-proteolytic role within the cell including the regulation of NF-κB signalling [140], DNA damage repair [141] and immune responses within the cell [142]. It is argued that the structure of the Lys63-linked chains does not promote the recognition by or interaction with the 19S regulatory domain of the proteasome and therefore substrates are not targeted for degradation [143]. In addition, a study recently showed that Lys63-linked chains interact with a complex involving the Endosomal Sorting Complex Required for Transport (ESCRT0) which inhibits binding to the proteasome and therefore protein degradation [144]. In this study, Lys48 polyubiquitin chains were shown to associate with members of the Rad23 protein family which subsequently promotes binding to the proteasome [144].

While Lys63-linked chains may not promote degradation *via* the 26S proteasome, there is evidence to suggest they target proteins for lysosomal degradation, as exemplified by the DJ-1 protein [145]. Though its function remains unknown, mutation of the DJ-1 gene is associated with early onset Parkinson's Disease. Typically, misfolded isoforms of the DJ-1 protein are targeted for proteasomal degradation to avoid aggregation of the misfolded protein [145]. However, in the presence of a proteasome inhibitor (MG132) the E3 ligase Parkin was shown to catalyse Lys63-linked polyubiquitylation of misfolded DJ-1 targeting the protein for an endosomal compartment called an aggresome. DJ-1 was then targeted for the lysosomal degradation pathway. The authors proposed that loss of the E3 ligase Parkin would promote the accumulation of misfolded protein aggregates and result in protein-induced cellular dysfunction [145].

Additionally, a study conducted in 2013 described the conjugation of mixed Lys48-Lys63 polyubiquitin chains to the low density lipoprotein (LDL) receptor [146]. Interestingly, formation of this heterogenous ubiquitin chain was associated with both proteasome and lysosome-mediated degradation [146]. This may provide an example of functional redundancy to ensure the appropriate expression levels of a receptor that is involved in cholesterol metabolism and plays a role in diseases such as atherosclerosis [147].

A recent review summarised the existing literature on how Lys63-linked ubiquitylation could regulate the activation of and crosstalk between various signalling pathways by recruiting proteins that contain ubiquitin-binding domains (UBDs) [148]. The Toll like receptor 4 (TLR4) and IL-1 pathways provide an excellent example for the role of Lys63-linked ubiquitylation and in their review Chen *et al* proposed a working model for the activation of these pathways [148]. Following ligand activation, the adaptor protein MyD88 and Ser/Thr kinases IRAK1 and IRAK4 dock at the intracellular domain of the IL-1 or TLR4. An E3 ligase called TRAF6 is subsequently recruited and activated by the ser/thr kinases and an accessory protein TIFA. TRAF6 then catalysed the conjugation of Lys63-linked ubiquitin chains to itself (auto-ubiquitylation) and two additional signalling molecules IRAK1 and NEMO. Consequently, TAB2 and TAB3 kinases were recruited via an intrinsic ubiquitin binding domain resulting in the downstream activation of JNK and p38 MAPK pathways. Thus the authors propose a model whereby Lys63-polyubiquitin chains allow the signalling components involved in this the pathway to be in close enough proximity to drive the activation of the JNK and p38 downstream effectors [148].

1.5.5 The N-terminal α-amino group of a protein may be ubiquitylated

Interestingly, N-terminal ubiquitylation of substrates at non-Lys acceptor sites has been described [149]. A study conducted in 1998 revealed that N-terminal ubiquitylation of MyoD, a protein involved in muscle development, regulated its stability and that mutation of all potential Lys acceptors had no effect on MyoD turnover when the N-terminus of the protein was available [150]. However, the insertion of a MYC epitope- tag at the N-terminus of the protein appeared to inhibit proteasomal degradation [150]. Thus, investigating the ubiquitylation status of substrates is complex, may be context dependent, and it is possible that under different experimental conditions the pattern and preferential site(s) for ubiquitin conjugation may vary.

Within the field of cancer, pharmacological inhibitors targeting different effectors within the ubiquitin cascade (E1, E2, E3 or DUBs) have been developed [151]. However, similar to proteasome inhibitors, one of the major disadvantages of this strategy is the inability to selectively inhibit the ubiquitin-proteasome system (UPS) in tumour cells only [151].

1.5.6 Ubiquitin-like proteins (UBLs)

Ubiquitin-like proteins (UBLs) are so called due their structural arrangement involving the presence of the "β-grasp" ubiquitin fold [152]. Similar to ubiquitin, most UBLs require activation in order to modify a substrate and involve the sequential activity of specific enzyme cascades. Neddylation and SUMOylation represent two of the best characterised UBL modifications in the literature and Table 1-4 outlines the sequence similarity shared with ubiquitin [152].

Ubiquitin/Ubiquitin-like protein	Sequence identity with ubiquitin (%)	Role
Ubiquitin	100	Target substrate for degradation, DNA damage response, cell signalling.
NEDD8	58	Activation of cullin-RING E3 ubiquitin ligases
SUMO-1	14	Protein-protein interactions, subcellular localisation, compete for Lys with Ubiquitin
SUMO-2	13	
SUMO-3	13	

Table 1-4: The contrasting roles of ubiquitin-like proteins (UBLs) and their sequence homology to ubiquitin. Table adapted from [152].

1.5.6.1 SUMOylation

Similar to ubiquitylation, SUMOylation is a PTM catalysed by specific E1-E3 enzymes, in which an 11kDa small ubiquitin-like modifier (SUMO) group is covalently attached to an acceptor Lys on target proteins [153]. There are three isoforms of SUMO: SUMO-1, SUMO-2 and SUMO-3 however SUMO-1 does not participate in polySUMO chain formation [154]. In contrast to ubiquitylation, SUMOylation is more specific and requires the E2 SUMO-conjugating enzyme Ubc9 to recognise the consensus motif (Ψ-K-X-E/D where Ψ is any hydrophobic residue) on substrates[153]. SUMOylation confers a diverse range of functions on target proteins, including altering substrate activity, cellular localisation, protein-protein interaction profile or increasing substrate expression resulting from the blocking of ubiquitination [155].

SUMOylation was first observed in 1996 when investigators described a modified form of the RanGAP1 protein [156]. RanGAP1 associates with the nucleopore complex (NPC) that facilitates the import and export of proteins from the cytoplasm to the nucleus and *vice versa*. Unmodified RanGAP1 localised to the cytoplasm however following SUMOylation, and a 20kDa increase in molecular weight, the SUMO-RanGAP1 isoform was found to associate with the NPC [156]. This was the first evidence to suggest SUMOylation could promote protein-protein interactions and so alter the cellular localisation of a substrate. Accordingly, SUMOylation provides an important layer of regulation for protein stability and activity as evidenced by the contribution of SUMOylation to pathologies such as

Alzhiemer's disease [157], cancer [158], Huntington's disease [159] and more recently heart failure [160].

1.5.6.2 NEDDylation

NEDDylation is a PTM in which the neural precursor cell expressed developmentally downregulated protein 8 (NEDD8) UBL is covalently attached to a lysine acceptor on its substrate [161]. Similar to ubiquitylation and SUMOylation, NEDDylation is achieved through the sequential action of specific E1 activating, E2 conjugating and E3 ligase enzymes. NEDDylation of cullin is essential for the activation of cullin-RING E3 ubiquitin ligases and therefore provides an additional layer of regulation to the ubiquitin system [162, 163]. However Cys protease deNEDDylation enzymes have been described and therefore regulate the NEDDylation of status of substrates within the cell.

Inhibition of the NEDDylation process has been investigated as an anti-cancer therapy. In 2009, Soucy and co-workers characterised a pharmacological inhibitor of the E1 Neddylation Activation Enzyme (NAE) known as MLN4924 [164]. This small molecule inhibitor shared structural similarities to AMP and was shown to occupy the nucleotide binding domain of NEA. Accordingly, the ATP-dependent activation of NEDD8 by NEA is not possible thereby blocking the NEDDylation of substrates. Unlike the global proteasome inhibitor bortezomib, treatment of cells with MLN4924 *in vitro* stabilised the expression of a smaller collection of proteins that are targeted for proteasomal degradation *i.e.* substrates of the cullin-RING E3 ligase family [164]. Pre-clinical studies have suggested that MLN4924 induced apoptosis may be a useful tool for the treatment liver cancer [165], urothelial carcinoma [166] and NF-κB–dependent lymphomas [167]. Studies to investigate the role of NEDDylation for non-cullin-RING E3 ligase substrates are currently underway and may reveal an additional layer of regulation for cell signalling pathways [161].

1.5.7 Identifying putative sites of ubiquitylation

At present, no known consensus sequence for ubiquitylation has been described and therefore predicting sites of ubiquitylation can prove challenging. Protein conformation may also be a consideration when predicting sites of ubiquitylation, if the Lys acceptor is not exposed on the protein surface it is unlikely that the E3 ligase machinery could gain access. It is however possible to map PTMs such as ubiquitylation via liquid

chromatography mass spectrometery (LC-MS) analysis [168]. Previously, the isopeptide bond was formed between the C-terminal (Gly76) of ubiquitin and the ε-amino group of the target Lys [168]. Prior to LC-MS analysis, protein samples are digested with trypsin cleaving protein-protein interactions and creating shorter peptide fragments. However, as ubiquitin is cleaved from the Lys, a Glycine doublet (Gly^{75}-Gly^{76}) remains on the acceptor Lys. Identification of this Glycine doublet (2*57.02=~114 Da) on the digested peptide(s) facilitates the mapping of ubiquitylation sites [127]. More detailed analysis of substrate ubiquitylation can be achieved using the absolute quantification of ubiquitin (Ub-AQUA) method following trypsin digestion [169]. A set of isotope-labelled standard peptides are employed in order to measure the abundance of unbranched *versus* branched ubiquitin chains and therefore informs the investigators on ubiquitin chain arrangement [170]. Due to improved peptide standards that represent all ubiquitin-linkage types (K6, K11, K27, K29, K33, K48 and K63) it is also possible to determine the linkage type of polyubiquitin chains via this method [169].

1.6 SOCS3 in the vasculature

1.6.1 JAK/STAT signalling and NIH.

JAKs are critical modulators of proliferation in VSMCs [171]. Interestingly, in a rat model of carotid artery balloon injury, JAK2 and STAT3 were upregulated and constitutively activated (phosphorylated) in the injured blood vessel 7 days following surgery [172]. The investigators demonstrated that injured blood vessels stimulated with angiotensin II (AngII) *ex vivo* enhanced JAK2/STAT3 upregulation and promoted VSMC proliferation contributing to NIH [172]. This provides a rationale that SOCS3 mediated inhibition of JAK, in addition to the dampening of inflammatory infiltrate to the stented vessel, may attenuate restenosis and the prevalence of NIH.

1.6.2 SOCS3 and a role for endothelial barrier function?

At the vascular endothelium, IL6 acts as a pro-inflammatory cytokine [37, 173, 174] . The integrity of the vascular endothelium (VE) is key for the prevention of thrombosis in addition to providing a barrier to injury following PCI or vein graft procedures [20, 175]. SOCS3 functions as part of a negative feedback loop for signalling through the JAK/STAT

pathway at the IL6/gp130 receptor complex (Figure 1-6). However, following mechanical injury, the VE may switch to a 'dysfunctional' phenotype with a diminished contractile capacity, promoting a smouldering pro-inflammatory environment and increasing the risk of thrombus formation [176].

In primary endothelial cells derived from human vein (human umbilical vein endothelial cells; HUVEC) or arterial (human aortic endothelial cells; HAECs) tissue, SOCS3 has been shown to be induced *via* an alternative JAK-STAT-independent mechanism involving cyclic AMP (cAMP)[177]. Forskolin (Fsk) is an activator of adenylyl cyclase which catalyses the synthesis of the second messenger 3',5'-cyclic adenosine monophosphate or "cyclic AMP"(cAMP)[178]. Stimulation of human ECs with Fsk, resulted in a transient increase in intracellular stores of cAMP that was associated with an increase in SOCS3 expression and a decrease in IL6- and leptin-mediated activation of STAT3 [177]. Interestingly, this cAMP-mediated induction of SOCS3 required a protein known as EPAC-1 (exchange protein directly activated by cAMP-1). EPAC-1 is a guanine nucleotide exchange factor (GEF) involved in the activation of Rap1 and Rap2 small GTPases and whose activation is associated with improved endothelial barrier function [179]. As such, Sands and co-workers proposed a unique cAMP/Epac/SOCS3 pathway may be involved in maintaining the integrity of the vascular endothelium in addition reducing endothelial inflammation often associated with disease [177].

1.6.3 SOCS expression in atherosclerosis

As discussed previously in section 1.1.1, atherosclerosis is a chronic inflammatory disease often manifesting in the coronary artery and is a result of atheromatous plaque formation within the intimal layer of the blood vessel [6]. Comprised of a lipid core surrounded by infiltrating leukocytes, VSMC cells and an outer fibrous cap, this thickening process reduces the lumen diameter, impeding blood flow and therefore oxygen supply to the heart as seen in NIH (Figure 1-2).

The vulnerable shoulder region of the atherosclerotic plaque is located either side of the lipid core and is the site of rupture in ~66% of cases [180]. In 2009, Ortiz-Munoz and co-workers performed immunofluorescence visualisation of SOCS1 and SOCS3 in human atherosclerotic plaque tissue. This study revealed that both SOCS1 and SOCS3 were significantly upregulated in the shoulder region when compared to the fibrous cap

surrounding the plaque [181]. Of note, SOCS1 and SOCS3 co-localised with cell specific markers for VSMCs and macrophages indicating the increase in SOCS expression was cell specific. Additionally, overexpression of SOCS3 in VSMCs was shown to attenuate the proliferative effects of IL6, LDL and foetal calf serum (FCS) exposure *in vitro*. Conversely, a significant increase in VSMC proliferative capacity was observed in controls where SOCS3 was not overexpressed [181]. Collectively, these data suggested that SOCS3 may serve as a negative regulator for VSMC activation and therefore have a protective role against atherogenesis.

Mice in which the apolipoprotein E gene is deleted (*apoE*$^{-/-}$) display hypercholesterolaemia and spontaneously develop atherosclerosis on a normal chow diet [10]. As such, the *apoE*$^{-/-}$ strain provides a useful experimental model of atherosclerosis. Ortiz-Munoz and colleagues knocked down SOCS3 expression (siRNA delivery using PEI) in the vasculature of *apoE*$^{-/-}$ mice that were maintained on an atherogenic diet for 5 weeks [181]. This resulted in a significant reduction in SOCS3 protein expression in the aorta coupled with an increase in atherosclerotic lesion size when compared to control groups. Moreover, SOCS3 depletion was associated with an increase in VSMCs, macrophages and CD4^{+} T-lymphocytes present in the plaque, indicative of the contribution of SOCS3 in regulating the proliferation/migration of VSMCs and recruitment of pro-inflammatory cells. Based on these observations, stabilising SOCS3 expression in immune cells may suppress the leukocyte infiltration to sites of NIH as seen in murine atherosclerotic plaques where SOCS3 was overexpressed [181].

As mentioned previously, increased protein levels of both SOCS1 and SOCS3 were detected in VSMCs and macrophages located in the inflammatory shoulder region of human plaques [181]. Accordingly, the role of SOCS1 has also been investigated murine models of atherosclerosis [182, 183]. Gene delivery of SOCS1 reduced the size and enhanced the stability of atherosclerotic plaques in older mice [183]. The overexpression of SOCS1 in a macrophage cell line (RAW 264.7) *in vitro* promoted M2 macrophage polarisation which is associated with an anti-inflammatory role [183]. In addition, accelerated progression of atherosclerosis and an increase in M1 (pro-inflammatory) macrophages was observed in ApoE KO mice that were also deficient in SOCS1 [182]. Together these data provide the rational for athero-protective SOCS1 gene therapies which have an obvious effect on not only disease progression but the polarisation of infiltrating macrophages. However, caution must be warranted with gene therapies as overexpression

of SOCS3 in T cells, for example, reduced IL-17 production and enhanced the progression of atherosclerosis [184]. As such, the role of SOCS proteins appears to be cell type dependent with regards atherogenesis.

1.6.4 Reducing inflammatory infiltrate to the intimal layer reduced neointimal lesion growth

Following revascularisation procedures such as stenting, mechanical injury to the arterial wall triggers the progression of neointimal lesions and promotes re-narrowing of the modified vessel (section 1.1.2). Consequently, endothelial denudation may expose tissue factors (laminin, collagen, fibronectin and von Willebrand factor) to cells in the circulation and so promotes the adherence of platelets to the site of injury [20]. This then leads to the recruitment of leukocytes, which is mediated via the interaction of P-selectin, expressed on the platelet cell surface, and P-selectin glycoprotein ligand 1 (PSGL) on the leukocyte [185].

A study conducted by Phillips *et al* investigated the effects of blocking leukocyte recruitment in a murine model of NIH [186]. A wire filament was inserted into the carotid artery of *apoE*$^{-/-}$ mice inducing mechanical injury, endothelial denudation and promoting NIH. Monoclonal antibodies (mAbs) specific for either platelet adhesion molecule P-selectin or its leukocyte-localised ligand PSGL were then injected intraperitoneally in an attempt to physically block this cell-cell interaction. Strikingly, the neointimal lesion size was reduced by 50% and 80% in the 100 μg and 200 μg P-selectin mAb treatment groups respectively [186]. Similarly, the administration of 100 μg PSGL mAb reduced lesion size by 55% when compared to controls [186]. Notably, the macrophage content within the lesion was significantly reduced supporting the role of inflammatory cell infiltration in the progression of NIH.

However a subsequent review of this work raised concerns over mAb persistence in the circulation [185]. Re-endothelialisation of the denuded artery may be a slow process and continue 3-4 weeks following initial injury. Shah *et al* argued that if the mAb does not persist for the duration of re-endothelialisation, new platelets may be synthesised providing an additional supply of P-selectins and therefore facilitating leukocyte diapedesis (rolling along blood vessel wall before migration to the intimal layer) [185].

In addition, Resistin is a pro-inflammatory cytokine that can drive a STAT3-dependent increase in SOCS3 expression for up to 18 hrs following stimulation of human ECs *in vitro* [187]. Interestingly, knockdown of the SOCS3 gene in these cells was associated with a decrease in expression of cell adhesion molecules such as P-selectin. One concern over therapies that would promote stabilisation of SOCS3 to limit NIH or inflammatory disease is that if SOCS3 is upregulated in ECs, then P-selectin expression may be elevated promoting rolling adhesion of leukocytes (therefore a pro-inflammatory environment) and thrombus formation. However this was just one report in the literature therefore further investigation is required.

1.6.5 SOCS3 limits pathological angiogenesis

SOCS3 was recently shown to regulate pathological angiogenesis in various murine models of disease including retinopathy, lung carcinoma and skin melanomas [188]. In the retinopathy models, conditional knockout of SOCS3 specifically in vascular ECs revealed a significant increase in pathological retinal angiogenesis and therefore disease progression [188]. Interestingly, physiological angiogenesis and repair of the retinal blood vessel wall was unaffected by the loss of SOCS3 [188]. More recently, the Retinoic-acid-receptor–related orphan receptor alpha (RORα) was shown to drive pathological retinal angiogenesis [189]. RORα is a transcription factor and using chromatin immunoprecipitation (ChIP) was shown to bind the SOCS3 promoter region to effectively silence SOCS3 transcription. SOCS3 was shown to protect against this RORα–mediated retinopathy and dampen the associated pro-inflammatory response [189].

Similarly, in mice injected with melanoma or lung carcinoma cells, loss of SOCS3 in the vasculature was associated with an increase in neovascularisation, tumour size and therefore tumour aggression [188]. In a murine model of small cell lung cancer, adenoviral delivery of the SOCS3 gene was also shown to reduce tumour progression and the neovascularisation required to support tumour growth [190]. The protective role of SOCS3 involved inhibition of the AKT pathway specifically. This led to the downregulation of HIF1α, a subunit of the HIF1 transcription factor known to drive mitogenic gene profiles and angiogenesis that promote tumourigenesis [190]. Together these data indicate that SOCS3 has a specific role in limiting pathological angiogenesis. Hence it may be deduced that strategies designed to stabilise SOCS3 expression may have a therapeutic benefit in the context of pathological angiogenesis.

However, loss of SOCS3 in the vasculature promotes endothelial cell proliferation required for the sprouting of new vessels [188]. *In vitro*, knockdown of SOCS3 in human retinal ECs and mouse ECs was achieved using siRNA. Following this, cells were then stimulated with insulin growth factor -1 (IGF-1) and tumour necrosis factor-α (TNFα) driving a significant increase in proliferation which correlated with an increase in STAT3 activation [188]. In the context of SOCS3-mediated inhibition of NIH, the suppression of vessel re-endothelialisation would be detrimental and may promote thrombosis. As such, it would be advantageous for therapies that stabilise SOCS3 expression to selectively inhibit VSMC proliferation and migration.

1.7 Migration and proliferation of VSMCs

1.7.1 SOCS3 mediated inhibition of focal adhesion kinase 1 (FAK1) prevents cellular migration.

Integrin activation, through interaction with extracellular matrix (ECM) components or neighbouring cells, induces integrin clustering at the plasma membrane, formation of focal adhesions and recruitment of FAK1 [191]. Subsequently, Tyr phosphorylation and therefore activation of FAK1 initiates signal transduction pathways promoting cellular migration and proliferation. However, it was recently shown that SOCS3 interacts with P-Y379 on FAK1 thereby targeting it for proteasome-mediated degradation [93, 114]. This phospho-Tyr provides a docking site for Src-kinase and switches on the mitogen-activated protein kinase (MAPK) pathway (Figure 1-10). Activation of the MAPK pathway may also drive VSMC proliferation and is therefore a therapeutic target for NIH [192, 193]. Liu and co-workers stimulated 3T3 fibroblasts with platelet-derived growth factor (PDGF) and fibronectin (FN) activating the cell surface PDGFR and integrins respectively [93]. Interestingly, immunoprecipitation experiments revealed FAK1 and SOCS3 interacted exclusively following stimulation *in vitro*. Moreover, kinase assays confirmed this interaction inhibits FAK activity and targets both proteins to the proteasome *via* polyubiquitylation. Additionally, in a hepatocellular carcinoma cell line, SOCS3 methylation induced epigenetic silencing of the SOCS3 gene, therefore inhibition of FAK1 was lost, enhancing cell migration and proliferation, a key feature of cancer cells [114].

1.7.2 SOCS3-mediated downregulation of matrix metalloproteinases (MMPs) limits cell migration

To date, 23 members of the matrix metalloproteinase (MMP) family have been described [194]. The MMPs are a family of Zn^{2+}-dependent endopeptidases that digest specific components of the ECM. MMP-2 and MMP-9 are STAT3-responsive genes [195] that can degrade ECM and thereby facilitate cellular migration [196, 197]. Interestingly, *in situ* analyses of human melanomas have revealed that a reduction in SOCS3 expression was associated with upregulation of MMP-2 and MMP-9 in addition to poor patient outcome [198]. Expression of these MMPs facilitated cancer cell migration and tumour invasion. Moreover, loss of SOCS3 has been shown to enhance the proliferation, migration and invasive potential of hepatocellular carcinoma (HCC) cells [199]. siRNA-mediated knockdown of SOCS3 in a HCC cell line has been shown to result in the up-regulation of MMP-2/9 expression and increased cell proliferation, migration and invasion in a panel of *in vitro* assays [199]. A similar observation was made in an *in vivo* model of HCC whereby the loss of SOCS3 enhanced tumour progression [199]. Moreover, since treatment with a STAT3 inhibitor reduced tumour progression *in vivo*, the authors proposed that the JAK/STAT-SOCS3 negative feedback loop was key for HCC tumour suppression [199].

Similarly, SOCS3 may play a key role in limiting cell migration that contributes to other inflammatory pathologies. Gao and colleagues investigated the JAK inhibitor tofacitinib as a therapy for the chronic inflammatory disease psoriatic arthritis (PsA) [200]. Treatment of primary PsA synovial fibroblasts with tofacitinib *in vitro* resulted in a significant reduction in STAT3 activation and MMP-2/9 expression. Importantly, this reduction in MMP secretion was associated with a decrease in cellular migration which otherwise contributes to the disease progression [200].

More specific to the cardiovascular system, MMP-2 was shown to be constitutively expressed in VSMCs, though a further increase in expression may be driven by stressors such as arterial wall stretch [201]. Similarly, MMP-9, though not constitutively expressed, has been shown to be inducible in a rat carotid artery injury model [202]. MMPs are thought to degrade the basement membrane of VSMCs facilitating the “phenotypic switch” (discussed in section 1.7.3) required for migration during NIH lesion formation [203]. Southgate *et al* employed a pig model of NIH (autologous saphenous vein into carotid artery interposition grafting) to investigate the role of MMPs during neointimal thickening

[204]. Investigators revealed that MMP-2 and MMP-9 expression was elevated at 7 and 28 days post vein graft however these levels had returned to baseline at 168 days post graft. The authors noted that this expression profile coincided with the timeframe of neointimal thickening and the proliferation of VSMCs, suggesting that MMPs may provide a therapeutic target of interest for NIH [204]. Tissue inhibitors of metalloproteinases (TIMPs) are highly specific, endogenous inhibitors of MMPs and provide a candidate for gene therapy [203]. A study conducted by the Baker group revealed that overexpression of the TIMP3 gene could reduce NI lesion progression in a pig vein graft model [205]. Following the success of this investigation, the authors stated that they were seeking approval for adenovirus-TIMP3 clinical trials in man [205].

Furthermore, it has been reported that VSMC and macrophage secretion of MMPs promotes the hyper-degradation of ECM components in atherosclerotic lesions and contributes to plaque rupture [206]. As such, therapies that limit MMP-2/9 expression or activity may attenuate VSMC migration and vessel remodelling that contributes to NIH and atheromatous plaque rupture.

1.7.3 IL-6 signalling and cyclin D1 expression in VSMCs

Following vessel injury, the release of mitogenic growth factors and pro-inflammatory cytokines drives the VSMC phenotypic switch [207]. In a healthy blood vessel, VSMCs exist in the quiescent phase and function to maintain vascular tone [207]. Exogenous stimulation of VSMCs by mitogenic factors alters the gene expression profile resulting in a so-called “synthetic phenotype” which is characterised by the acquisition of capacities to proliferate and migrate (Figure 1-15).

IL-6 is a pro-inflammatory cytokine secreted by macrophages (innate immune system), T cells (adaptive immune system), VSMCs [208] and ECs [209]. Importantly, single nucleotide polymorphism (SNP) analysis of the IL-6R gene has revealed a subclass of variants associated with a higher circulating level of the cytokine ligand [210]. Moreover, this increase in plasma IL-6 was shown to correlate with an increased risk of developing CHD. IL-6 is thought to play a central role in driving VSMC migration following arterial vessel injury. In a study conducted by Liu and colleagues, SMCs derived from rat thoracic aortas were stimulated with the receptor tyrosine kinase ligand (PDGF-BB) *in vitro* [211]. This led to the induction of IL-6 expression and promoted SMC cell migration.

Interestingly, administration of an IL-6-neutralising antibody was able to suppress cell migration, thereby confirming a role for the cytokine in VSMC motility [211].

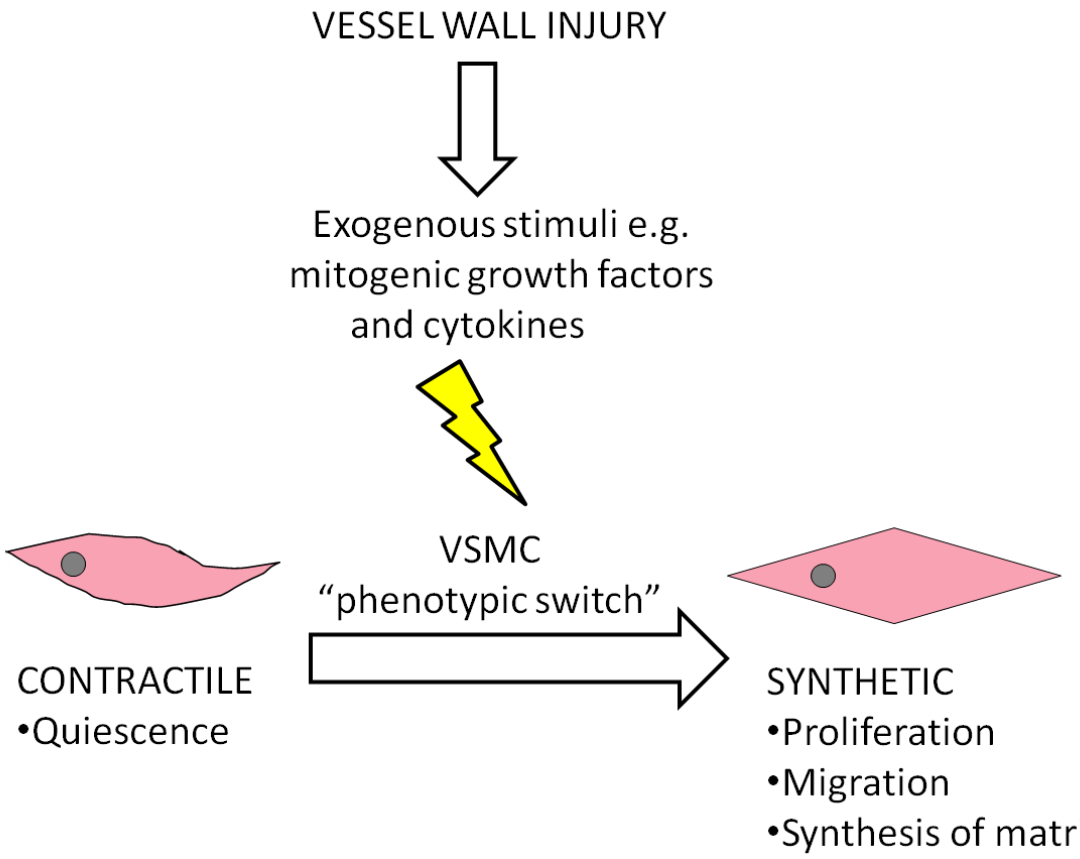

Figure 1-15: The VSMC phenotypic switch

VSMCs normally exist in the resting G_0 phase of the cell cycle and exhibit quiescence. This is referred to as the differentiated "contractile" phenotype. Following vessel wall injury, mitogenic growth factors and cytokines are secreted locally by both macrophage and VSMCs. This results in a switch to the synthetic phenotype permitting exit from the resting G_0 phase and cell proliferation and migration to the intimal layer of the blood vessel proceeds. It is this aberrant proliferation and migration that contributes to pathologies such as neointimal thickening following PCI procedures.

A subsequent study mirrored these findings, showing that *in vitro* stimulation of VSMCs with increasing concentrations of IL-6 produced a dose-dependent increase in cell migration [212]. Active gp130 recruits STAT3 and following STAT3 activation, dimerisation and translocation to the nucleus an increase in cyclin D1 expression was

observed. Cyclin D1 is associated with cell growth and proliferation by promoting entry to the S-phase of the cell cycle [213]. Interestingly, knockdown of cyclin D1 was shown to ablate VSMC motility and therefore confirmed as a causative gene in VSMC migration [212]. Moreover, an *in vivo* rat model of balloon injury to the carotid artery revealed this increase in STAT3 activation and cyclin D1 expression correlated with an increase in NIH lesion [212]. Conversely, adenovirus-mediated overexpression of dominant negative STAT3 or gp130 reduced cyclin D1 expression, SMC migration and importantly NIH lesion size [212].

More recently, the JAK-STAT3 pathway was shown to play a role in driving the contractile to synthetic phenotypic switch in VSMCs [214]. VEGF stimulation of VSMCs induced STAT3 activation and inhibited the expression of contractile gene profiles [214]. Furthermore, siRNA mediated knockdown of STAT3 suppressed this phenotypic switch and maintained a contractile VSMC population [214]. As such, the IL6-JAK-STAT3 pathway is a key regulator of VSMC activation and migration to the intimal region of the injured vessel wall. As described previously in section 1.3.1, SOCS3 is an important negative regulator of STAT3 signalling, and therefore enhancing SOCS3 stability may limit STAT3-driven VSMC proliferation and migration that is responsible, in part, for NIH and vessel stenosis.

1.7.4 SOCS3 induction in the vasculature and downregulation in neointimal lesions

Ortiz-Munoz *et al* have investigated the ability of SOCS3 to regulate JAK/STAT signalling in the vasculature [181]. This study reported that SOCS3 can be induced in VSMCs *via* stimulation with pro-inflammatory cytokines (IL6 and IFNγ), mitogenic growth factors such as IGF-1 and low density lipoproteins (LDLs) involved in the development of atherosclerotic plaques [181]. They also showed that SOCS3 overexpression *in vitro* could reduce the expression of pro-inflammatory molecules (Monocyte Chemoattractant Protein-1; MCP-1 and Intercellular Adhesion Molecule 1; ICAM-1) by VSMCs [181]. Moreover, immune complex (IgG bound to antigen) stimulation of the FcγR has also been shown to enhance SOCS3 expression in monocytes (precursor of macrophages), in SMCs lining the kidney vasculature (mesangial cells) [215] and mouse VSMCs [181]. Interestingly, in vascular endothelial cells, cAMP has been shown to promote SOCS3 induction through a guanine nucleotide exchange factor Epac-1 [177]. Collectively, these data suggest that

approaches to increase and/or stabilise SOCS3 expression in the vasculature has the potential to reduce the localised inflammation and VSMC proliferation responsible for driving NIH in the injured vessel.

A detailed characterisation of the nature of inflammatory response triggered by surgical procedures such as vein grafting, balloon angioplasty or stent implantation is currently lacking. However, one recent study revealed that SOCS3 expression was significantly reduced in a porcine model of NIH [118]. Yucatan mini-pigs were fed a high cholesterol diet over an 8 month period and at the 4 month time-point balloon angioplasty of the coronary artery was performed, thereby inducing a profound NIH [118]. Immunohistochemistry revealed a decrease in SOCS3 protein expression in the NIH lesion suggesting loss of this negative regulator promotes VSMC proliferation and migration to the expanding intimal layer [118].

More recently, Xiang and colleagues have employed a rat model of vein grafting (autologous jugular vein-to-carotid-artery) to investigate the role of SOCS3 in NIH [216]. 7 days post procedure, quantitative real-time PCR (qRTPCR) and immunoblot analysis of vein graft tissue confirmed both transcript (mRNA) and protein levels of inflammatory markers were significantly higher in the vein graft tissue compared to controls. Interestingly, activated STAT3 and SOCS3 were also elevated in the vein graft treatment group suggesting a role for the JAK/STAT3 pathway in vessel remodelling. Moreover, *in vitro* stimulation of VSMCs with the mitogenic growth factor PDGF-BB led to an increase in the expression of inflammatory markers including SOCS3 and STAT3 [216]. However, overexpression of SOCS3 (adenoviral delivery) resulted in a significant decrease in inflammatory markers expressed by the VSMCs following PDGF-BB stimulation. Collectively, these data support an anti-inflammatory role for SOCS3 in the vasculature.

In the same study, adenoviral delivery of SOCS3, prior to vein grafting *in vivo*, significantly reduced neointimal lesion size [216]. Moreover, histological staining of the vein tissue for proliferating cell nuclear antigen (PCNA), a marker of proliferation, confirmed VSMC proliferation was reduced in the SOCS3 treatment group compared to controls. Accordingly, these data suggest therapies to enhance SOCS3 expression in the injured vessel may dampen the pathological inflammatory response and expansion of neointimal lesions that contribute to re-stenosis.

1.8 Hypothesis

I hypothesise that stabilising the expression of SOCS3 in the vasculature will limit neointimal growth.

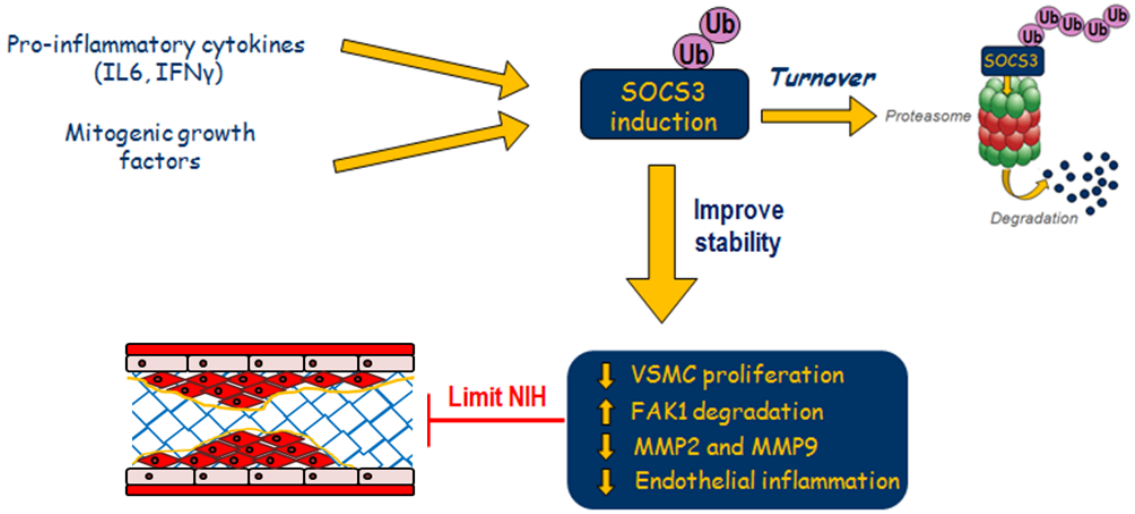

Figure 1-16: Hypothesis: stabilisation of SOCS3 expression by limiting turnover will limit neointimal growth

SOCS3 expression is induced upon stimulation by pro-inflammatory cytokines, such as IL6 and IFNγ, or mitogenic growth factors. However, SOCS3 has a short biological half life and is rapidly turned over at the proteasome. We hypothesise that stabilising SOCS3 expression will inhibit proliferation of VSMCs *via* inhibition of the JAK/STAT pathway. Additionally, SOCS3 would target FAK1 for degradation at the proteasome and thus block VSMC migration from the media to the intima which contributes to NIH. Finally, SOCS3 would reduce expression of STAT3 responsive genes MMP2 and MMP9 involved in the degradation of ECM and the promotion of cell migration. Ultimately, enhancing SOCS3 expression would limit NIH following PCI or CABG procedures.

1.9 Aims

There is an unmet clinical need for a therapy to reduce the incidence of NIH following CABG, balloon angioplasty and stent implant procedures. Currently available DESs, though effective at reducing VSMC proliferation and NIH, have an off-target effect of inhibiting re-endothelialisation of the injured vessel, thereby increasing the risk of further re-stenosis and thrombosis. The literature provides evidence in support of my hypothesis that strategies to stabilise the expression of SOCS3 in VSMC should limit NIH without interfering with re-endothelialisation of injured vessels. The aim of this PhD was to identify the mechanisms promoting the rapid turnover of SOCS3.

Key aims were:

1. To identify and investigate candidate residues as key regulators of SOCS3 turnover at the proteasome.

2. To develop a functional SOCS3 that is resistant to proteasomal degradation.

3. To develop a tool to screen an E3 ligase library, using an siARRAY, to sequentially knockdown all known E3 ligases in the presence of a SOCS3-luciferase fusion protein or endogenous SOCS3 in a high content imagine platform.

4. To identify external E3 ligase or deubiquitylase (DUB) enzymes controlling SOCS3 turnover and identify the sites of SOCS3 ubiquitylation via LC-MS-MS analysis.

5. To investigate SOCS3 protein expression within the various layers of a human blood vessel, specifically the human saphenous vein.

6. Conduct preliminary functional investigations to assess the effect of lentivirus-mediated SOCS3 overexpression on HSV SMC proliferation and migration *in vitro*.

2 Materials and Methods

2.1 Materials

Agilent Technologies, UK:

XL1-Blue Competent Cells (cat. no. 200249).

XL10-Gold Ultracompetent Cells (cat. no. 200315)

QuikChange Lightening Site Directed Mutagenesis kit (cat. no. 210518)

Applied Biosystems

1x TaqMan® Universal Master Mix II no UNG (cat. no. 4440040)

Bio-Rad Laboratories Ltd, UK:

Precision Plus Protein™ Kaleidoscope™ Standards (cat. no. 161-0375)

Carestream Health, UK:

Medical X-ray Blue/MXBE Film (cat. no. 7710783)

Cyagen, USA:

Customised Lys-less lentivirus cDNA vector

Fischer Scientific, UK:

Opti-MEM® I Reduced Serum Media (cat. no. 11058021)

Laemmli Sample Buffer (Bio-Rad Laboratories, 161-0737)

NuPAGE® Sample Reducing Agent (cat. no. NP0004)

NuPAGE® Novex® 10% Bis-Tris protein gel (cat. no. NP0301BOX)

NuPAGE® MOPS SDS Running Buffer (20X) (cat. no.NP0001)

GeneArt Gene Synthesis service produced the customised Lys-less cDNA insert

GE Healthcare Life Sciences, UK:

Amersham™ Protran™0.2 μm pore Nitrocellulose Membrane (cat. no. 10600001)

Invitrogen™, UK:

Colloidal Blue staining kit (cat. no. LC6025)

Merck Biosciences, UK:

MG-132 (cat. no. 474790)

Forskolin (cat. no. 344270)

Perkin-Elmer Life Sciences, UK:

Enhanced chemiluminescence (ECL) reagents (cat. no. NEL 104)

Promega, USA:

Wizard® Plus SV minipreps (cat. no. A1330)

6 x Blue/Orange Loading Dye (cat. no. G1881)

1kb DNA ladder (cat. no. G5711)

100bp DNA ladder (cat. no. G2101)

Dual-Luciferase® Reporter Assay System (cat. no. E1910)

PromoCell, Germany:

Smooth Muscle Cell Basal Medium 2 (Promocell, C-22262)

Smooth Muscle Cell Medium 2 SupplementMix (Promocell, C-39267)

Qiagen, UK:

Endofree plasmid Maxi kit (cat. no. 12362)

Polyfect Transfection reagent (Qiagen, 301105)

Roche Applied Science, UK:

Complete, EDTA-free protease inhibitor cocktail tablets (cat. no. 11836170001)

Sigma-Aldrich, UK:

Greiner CELLSTAR® white flat bottom 96 well plate (cat. no. 655083)

Dulbecco's Modified Eagle's Medium (DMEM) (cat. no. D6046)

Foetal bovine serum (FBS) (cat. no. F9665)

L-glutamine (cat. no. G7513)

Penicillin-Streptomycin solution (cat. no. P0781)

Dublecco’s Phosphate Buffered Saline (cat. no. D8537)

1x Trypsin-EDTA solution (cat. no. T3924)

Endothelial Cell Growth Medium (EBM-2) supplemented with EGM™-2 Bulletkit (Lonza

Trypsin-EDTA solution (cat. no. 4299)
Ampicillin (cat. no. A9393)
Kanamycin (cat. no. K1377)
Goat serum (cat. no. 9023)
Donkey serum (cat. no. 9663)
Paraformaldehyde (cat. no. 158127)
Anti-FLAG M2 affinity gel (cat. no. A2220)
Emetine (cat. no. E2375)
Protein G-Sepharose 4B Fast Flow (cat. no. P3296)
Sterile filtered cell culture water (cat. no. W3500)
Tween – 20 (cat. no. P5927)
30% (w/v) acrylamide/0.8% (w/v) bis-acrylamide (cat. no. A3699)
Anti-mouse IgG (peroxidase-conjugated) (cat. no. A4416)
Anti-rabbit IgG (peroxidase-conjugated) (cat. no. A6154)
Anti-Goat IgG (peroxidase-conjugated) (cat. no. A5420)
Soybean trypsin inhibitor (cat. no. T9003)
Benzamidine (cat. no. 12072)
Bovine serum albumin (cat. no. A7030)
N, N, N',N'-tetramethylethylenediamine (TEMED) (cat. no. T9281)
Phenylmethylsulphonyl fluoride (PMSF) (cat. no. P7626)
Puromycin (cat. no. P8833)

VWR International Ltd, UK:

Corning® 6 well flat bottomed cell culture plate (cat. no. 734-1599)
Corning® 60mm cell culture dish (cat. no. 734-1699)
Corning® 100mm cell culture dish (cat. no. 734-1815)

Cell lines:

WT (SOCS3+/+) and SOCS3-/- MEFs [88] provided by Prof. Akihiko Yoshimura (Kyushu University, Japan) were available as liquid nitrogen-frozen stocks.

Human endothelial angiosarcoma (AS-M.5) [217] provided by Dr Vera Krump-Konvalinkova V (Johannes Gutenberg University, Germany).

2.2 Methods

2.2.1 Cell Culture

All cells were maintained in T150 cm flasks at 37°C in 95% (v/v) air/5% (v/v) CO_2 in a humidified cell culture incubator and passaged at ~80-85% confluency.

2.2.1.1 Culture of HEK293 and murine embryonic fibroblasts(MEFs)

Human embryonic kidney (HEK) 293 cells, HEK 293 cells stably expressing SV40 large T antigen (HEK293T), and mouse embryonic fibroblasts (MEFs) were maintained in Dulbecco's Modified Eagle's Medium (DMEM) (Sigma®, D6046) supplemented with 10% (v/v) foetal bovine serum (FBS) (Sigma®, F9665), 1mM (v/v) L-glutamine (Sigma®, G7513) and 50U/ml (v/v) Penicillin-Streptomycin solution (Sigma®, P0781).Passage of cells was performed by washing a T150 cm flask with 2 mls tissue culture grade Dublecco's Phosphate Buffered Saline (PBS) followed by incubation with 2 mls 1xTrypsin-EDTA solution (Sigma®, T3924) for 3-4 mins at 37°C to allow detachment from the flask surface. Trypsinisation was inactivated by the addition of 8 mls fresh media and cells were pelleted by centrifugation (200g, 5 mins at room temperature). Supernatant was removed and the cell pellet was gently re-suspended in the appropriate volume of fresh media. Cells were split 1 in 20 into fresh T150 cm flasks at each passage.

2.2.1.2 Culture of AS-M.5.5, HSVEC and HUVECs

Human endothelial angiosarcoma (AS-M.5) [217], human saphenous vein endothelial cells (HSVECs) and human umbilical vein endothelial cells (HUVEC) were maintained in Endothelial Cell Growth Medium (EBM-2) supplemented with EGM^{TM}-2 Bulletkit (Lonza). Passage of cells was performed as above except 2 ml of Trypsin-EDTA solution (Sigma®, 4299) was used for cell detachment. AS-M.5 cells were split 1 in 20 and HSVEC/HUVECs were split 1 in 6 per passage. HSVEC and HUVEC cultures were not used beyond passage 5 and morphological differentiation was monitored routinely.

2.2.2 Culture of HSVSMCs

Human saphenous vein smooth muscle cells (HSVSMCs)[218] were maintained in Smooth Muscle Cell Basal Medium 2 (Promocell, C-22262) with manufacturer-provided

supplement mix (Promocell, C-39267) plus 10% (v/v) FBS (Sigma®, F9665) (to give a final total FBS concentration of 15% (v/v) FBS), 1mM (v/v) L-glutamine (Sigma®, G7513) and 50U/ml (v/v) Penicillin-Streptomycin solution (Sigma®, P0781). HSVSMCs were cultured in T75cm flasks (37°C; 5% CO2) and split 1 in 2 per passage. HSVSMC cultures were used at passage 3-4 in experiments and morphological differentiation was monitored routinely.

2.2.2.1 Coating of plastic ware with poly-D-lysine for HEK293 cells

HEK293 cells are a useful overexpression system however following transfection and washing procedures were fragile and detached from uncoated plastic ware. As such, prior to the plating of HEK293 cells in 6 well plates, 6 cm or 10 cm dishes, plastic ware was coated in 2 ml poly-D-lysine. Excess poly-D-lysine was removed *via* pipette and plates were allowed to air dry for 1 hour at room temperature before seeding cells.

2.2.3 Cloning of cDNA constructs in *E.coli*

2.2.3.1 Transformation of competent *E. coli*

cDNA plasmids containing the gene of interest were first propagated by transforming competent XL1-Blue *E.coli* (Agilent Technologies, 200249). Initially, 1.5 ml microcentrifuge tubes were chilled on ice prior to the addition of 45µl *E. coli* XL1 Blue suspension and 50-100ng DNA. Samples were then gently swirled and incubated on ice for 20 mins before heat-shock transformation (1.5 min, 42°C water bath). Samples were then placed on ice for 2 mins prior to the addition of 455µl pre-warmed (37°C) Luria Bertani (LB) broth (1% (w/v) tryptone, 0.5% (w/v) yeast extract, 1% (w/v) sodium chloride, pH 7.5). Cultures were then agitated (180rpm, 37°C) for 45 mins. Following this, 100 µl of the culture was spread onto dry LB-agar (LB broth with 1.5% (w/v) MP-agar) plates supplemented with 50 µg/ml ampicillin for antibiotic resistance selection. Plates were then incubated at 37°C overnight. *E.coli* containing the plasmid of interest expressed an ampicillin resistance gene and therefore replicated overnight to form single colonies. Subsequently, plates were removed from the incubator and stored at 4°C for a maximum of 2 weeks until required.

2.2.3.2 Transformation of ultracompetent *E.coli* for ligations.

*E. coli*XL10-Gold Ultracompetent Cells (Agilent Technologies, 200315) were transformed and plated onto dry LB-agar plates as above with the exception that heat-shock was performed for 30 seconds in a 42°C water bath.

2.2.3.3 Glycerol stock preparation

Single colonies were picked from LB agar plates, using a P200 sterile pipette tip, and used to inoculate 5 ml LB broth supplemented with 50 μg/ml ampicillin (Amp) or kanamycin (Kan) where specified. Initial 5 ml cultures were agitated (180 rpm 37°C) overnight until turbid. 1 ml of the overnight culture was then mixed with 0.4 ml 50% (v/v) glycerol in a sterile cryovial by pipetting gently up and down 5 times. Glycerol stocks were then rapidly frozen by immersion in dry ice before storage at -80°C freezer.

2.2.4 DNA plasmid isolation, quantification and visualisation

2.2.4.1 Small scale: Wizard® Plus SV Miniprep

Single colony-derived glycerol stocks were used to generate starter cultures. Initially a P200 sterile pipette tip was used to scrape a sample from the glycerol stock and inoculate 5 ml LB broth (Amp or Kan) at the concentration described in section 2.2.3.3. The starter culture was then agitated overnight (180 rpm, 37°C) to facilitate bacterial replication. DNA was purified from turbid 5 ml starter cultures using the Wizard® Plus SV miniprep kit (Promega, A1330). All centrifugation and incubation steps were carried out at room temperature. The bacterial pellet was harvested via centrifugation (5 min, 10,000 x g) and the supernatant removed. The resultant pellet was then resuspended in 250 μl of Cell Resuspension Solution (50 mM Tris-HCl, pH 7.5, 10 mM EDTA, 100 μg/ml RNase A) by vortexing and transferred to sterile 1.5 ml microfuge tubes. Lysis was performed via the addition of 250 μl Cell Lysis Solution (0.2 M NaOH, 1% (w/v) SDS) and inverting 4-6 times prior to incubating for 5 min ensuring partial clearing of the sample. Subsequently, 10 μl of Alkaline Protease was added to the sample, inverting 4-6 times, and incubating for 5 min to inactivate endonucleases released during bacterial lysis which may cut the DNA construct of interest. The lysis reaction was then inactivated by adding 350 μl of Neutralisation Solution (4.09 M guanidine hydrochloride, 0.759 M potassium acetate, 2.12 M glacial acetic acid, pH 4.2) and mixed by inversion. The neutralised lysate was then

transferred to spin columns within a 2 ml collection tube for centrifugation (14,000 x g, 1 min). The flow through was removed from the collection tube and 750 µl Column Wash Solution (60% (v/v) ethanol, 60 mM potassium acetate, 8.3 mM Tris-HCl (pH 7.5), 0.04 mM EDTA (pH 8.0) added to the spin column prior to further centrifugation (14,000 x g, 1 min). This step was repeated using 250 µl Column Wash Solution and centrifugation (14,000 x g, 2 min). The spin column was then transferred to a sterile 1.5 ml microfuge tube and elution of the DNA plasmid was performed by the addition of 50 µl nuclease free water, incubating for 1 min, and centrifugation (14,000 x g, 1 min). DNA was then stored at -20°C until required.

2.2.4.2 Large scale: EndoFree Plasmid Maxiprep

Larger DNA stocks were generated by initially growing 5 ml starter cultures for 8 hours (180 rpm, 37°C) as described above. This was then transferred to a glass conical flask containing 250 ml LB broth supplemented with Amp or Kan (section 2.2.3.3) overnight (180 rpm, 37°C). The DNA was then purified using the EndoFree Plasmid Maxi Kit (Qiagen, 12362) as per manufacturer's instruction. The bacterial pellet was harvested *via* centrifugation (15 min, 6,000 x g, 4°C) and the supernatant removed. The resultant pellet was then resuspended in 10 ml of Buffer P1 (50 mM Tris-HCl (pH 8.0), 10 mM EDTA, 100 µg/ml RNase A, Lyse blue reagent 1:1000) by vortexing and transferred to sterile 1.5 ml microfuge tubes. Lysis was performed via the addition of 10 ml buffer P2 (0.2 M NaOH, 1% (w/v) SDS) and homogenised by vigorously inverting 4-6 times prior to incubating for 5 min at room temperature. Successful lysis was indicated by the mixture turning blue. Neutralisation of cell lysis was performed via the addition of 10 ml of chilled buffer P3 (3.0 M potassium acetate, pH 5.5) and mixing by inversion 4-6 times.

The neutralised lysate was then transferred to a QIAfilter Cartidge with screw cap nozzle and incubated for 10 mins at room temperature. The screw cap nozzle was then removed and a plunger gently inserted into the cartridge in doing so filtering the lysate into a 50 ml collection tube. Following this, endotoxins removal was facilitated by addition of 2.5 ml buffer ER (composition not available) to the filtered lysate and incubated on ice for 30 min. A Qiagen-tip 500 was placed in a test tube rack within plastic tray for collection of wash buffers. The tip was then equilibrated with 10 ml buffer QBT (750 mM NaCl, 50 mM MOPS (pH 7.0), 15% (v/v) isopropanol, 0.15% (v/v) Triton® X-100). When buffer QBT has run through the tip, the filtered lysate was applied and allowed to enter the resin by gravity flow. The tip was then washed with 2x30 ml Buffer QC (1.0 M NaCl, 50 mM

MOPS (pH 7.0), 15% (v/v) isopropanol). Finally the DNA was eluted with 15 ml Buffer QN (1.6 M NaCl, 50 mM MOPS (pH 7.0), 15% (v/v) isopropanol) and collected in a 30 ml NalgeneTM, Oak Ridge High-Speed Polycarbonate Centrifuge tube. The DNA was then precipitated by adding 10.5 ml isopropanol, mixed by inversion and pelleted by centrifugation (30 min, 15,000 x g, 4°C). The supernatant was discarded and the white/clear pellet washed with 5 ml endotoxin-free 70% (v/v) ethanol and a final centrifugation (10 min, 15,000 x g, 4°C) performed. Supernatant was discarded, and the DNA pellet was allowed to air dry for 10 min before gentle re-suspension in TE buffer (10 mM Tris-Cl (pH 8.0), 1 mM EDTA) and transfer to a 1.5 ml microfuge tube for storage at -20°C.

2.2.4.3 Quantification of plasmid DNA concentration

DNA concentration was determined using a NanoDropTM 2000 spectrophotometer (ThermoScientifc). This system measures the absorbance of UV light at defined wavelengths. Both RNA and DNA absorb UV light at 260nm. Conversely, protein absorbs UV light at 280nm therefore the 260/280nm ratio should be ~1.8 for DNA. A 260/280 nm ratio notably lower than 1.8 may suggest protein contamination in the sample. The 260/230 nm ratio indicates salt or chemical contaminants in the sample as molecules such as EDTA absorb UV light at 230nm. A 260/230 nm ratio ~2.0-2.2 was considered acceptable.

2.2.4.4 DNA gel electrophoresis

Gel electrophoresis allows the visualisation of DNA (such as plasmids or PCR products) according to size. DNA has an overall negative charge and so during electrophoresis migrates through the agarose gel matrix toward a positive electrode (anode). Agarose gels were prepared by dissolving 1-2% (w/v) agarose in 1 x Tris-Acetate-EDTA (TAE) buffer (0.04 M Tris – Acetate, 0.001 M EDTA) using a microwave. Upon cooling, 10 µl ethidium bromide, which intercalates with DNA, was added to the molten gel before pouring. Once the gel had set, DNA samples were prepared in 6 x Blue/Orange Loading Dye (Promega, G1881) at a ratio of 1:10 dye to DNA. To facilitate molecular sizing, a 1kb (Promega, G5711) and 100bp (Promega, G2101) DNA ladder was prepared (1:5 ratio of dye to DNA) and run on each gel. Electrophoresis was performed at 80 V for >1hr and the fractionated DNA visualised by UV trans-illumination and image capture using a Bio-Rad Laboratories Gel Doc System.

2.2.5 SOCS3 mutagenesis

2.2.5.1 SOCS3 truncation mutants

In order to map the essential regions for SOCS3 ubiquitination in cells we received progressive human SOCS3 truncation mutants from Professor Fred Schaper of the University of Magdeburg and have been described previously [219]. Each mutant was cloned into a PCMV-2-FLAG vector and possessed an N-terminal FLAG tag [219]. Schematic presented in Figure 2-1: Schematic of the SOCS3 protein

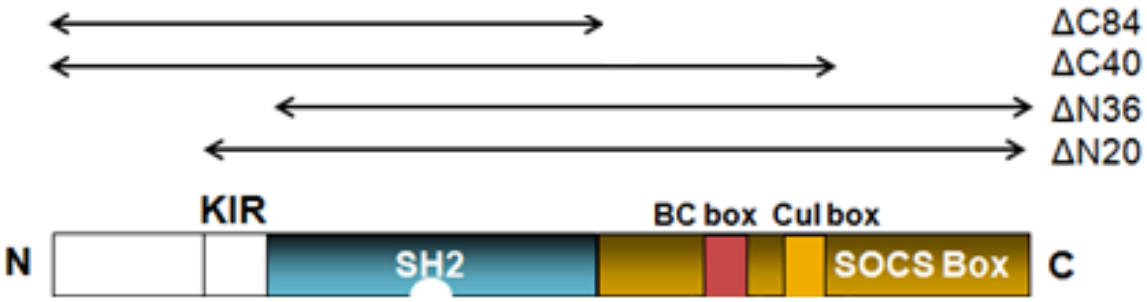

Figure 2-1: Schematic of the SOCS3 protein

The region of the SOCS3 molecule covered by the N terminal and C terminal truncations are illustrated via the arrows. ΔC84 denotes deletion of the C terminal 84 amino acid residues; ΔC40 denotes deletion of the C terminal 40 amino acid residues; ΔN36 denotes deletion of the N terminal 36 amino acid residues and ΔN20 denotes deletion of the N terminal 20 amino acid residues. The structural domains of SOCS3 include the kinase inhibitory region (KIR); Src Homology 2 (SH2) domain and the SOCS box which provides the platform for the E3 ligase machinery. Within the SOCS box is the BC box where Elongin B and C interact and the Cul box where Cullin interacts. Elongin B, Elongin C and Cullin are components of the E3 ligase machinery required for ubiquitylation of substrates.

2.2.5.2 Site-directed PCR mutagenesis

To investigate the role of individual amino acid residues on SOCS3 stability, mutagenesis was performed in which a codon was mutated resulting in an alternative amino acid being incorporated during protein translation. To facilitate this, the QuikChange Lightening Site Directed Mutagenesis kit (Agilent®, #210518) was used. Mutagenic primers were designed manually with the following properties: site of mutation in the centre of the primer, 25-45 nucleotides in length, G/C clamp at the 3'end, 40-60% G/C content and melting temperature (Tm) >78°C according to the manufacturers calculation:

Tm (C°) = 81.5 + 0.41(%GC) (675/N) - % mismatch

N = nucleotide length of primer

% mismatch = the % of bases in the primer that will not base pair with the WT cDNA template

The reverse mutagenic primer used was the reverse compliment of the forward mutagenic primer. The thermocycling protocol was as follows (Table 2-1: PCR mutagenesis thermocycling protocol:

Number of cycles	**Temp (C°)**	**Duration**	**Function**
1	95	2 min	Denaturing
18	95 60 68	20 sec 10 sec 2 min 30 sec (30 secs per kb plasmid)	Denaturing Annealing Elongation
1	68	5 min	Final elongation
1	4	-	Store until use

Table 2-1: PCR mutagenesis thermocycling protocol

*Dpn*I digestion of the parental WT template strand was then performed *via* the addition of 2 µl *Dpn*I enzyme to the amplicon mix and incubated at 37°C for 5 min. Finally, 10 µl of the PCR mix was used to transform XL10-Gold Ultracompetent Cells as described in section 2.2.3.2. Single colonies were isolated from ampicillin-innoculated agar plates and DNA amplified via maxi-prep (section 2.2.4.2). To ensure that no additional mutations were incorporated, the sequence was verified *via* DNA sequencing (Dundee Sequencing and Services^{TM}) and the predicted amino acid sequence verified using an online tool (http://web.expasy.org/translate).

SOCS3 mutant	DNA mutation 5'-3' sense	Forward primer 5'-3' sense	Reverse primer 5'-3' anti-sense
K6Q	AAG→CAG	GTCACCCA**CAG**CCAGTTTCCC GCCGCC	GGCGGCGGGAAAGTGG**CTG**TG GGTGAC
K173R	AAG→AGG	GGCGAG**AGG**ATTCCGCTGGT ACTGAAC	GTTCAGTACCAGCGGAAT**CCT** CTCGCC

Table 2-2: Mutagenic primers used for PCR mutagenesis of K6Q and K173R SOCS3

2.2.5.3 Generation of a Lys-less human SOCS3

In order to synthesise a more stable isoform of SOCS3 we hypothesised that mutation of all 10 Lys residues, within the SOCS3 open reading frame, to non-ubiquitinatable Arg should block proteasomal degradation and therefore enhance SOCS3 stability. The sequence containing a C-terminally Flag epitope-tagged human SOCS3 open reading frame in which each Lys was mutated to Arg at positions 6, 23, 28, 40, 85, 91, 122, 173, 195 and 206) was generated by GeneArt® and subcloned into a pcDNA3.1 mammalian expression vector. A summary of the WT and mutant SOCS3 constructs used are shown in Table 2-3:

SOCS3 variant	Species	Vector backbone	Epitope tag
WT	Mouse	pcDNA3.1	c-terminal FLAG
K6Q	Mouse	pcDNA3.1	c-terminal FLAG
L189A	Mouse	pcDNA3.1	c-terminal FLAG
WT	Human	pCMV-FLAG-5a	c-terminal FLAG
K173R	Human	pCMV-FLAG-5a	c-terminal FLAG
Lys-less (GeneArt)	Human	pCMV-FLAG-5a	c-terminal FLAG
ΔN20	Human	pCMV-2-FLAG	n-terminal FLAG
ΔN36	Human	pCMV-2-FLAG	n-terminal FLAG
ΔC40	Human	pCMV-2-FLAG	n-terminal FLAG
ΔC84	Human	pCMV-2-FLAG	n-terminal FLAG

Table 2-3: SOCS3 construct description

2.2.6 Transfection of cDNA

DNA is negatively charged molecule and combined with the large size of this molecule DNA cannot diffuse across the plasma membrane of cells. As such, we employed the Polyfect Transfection reagent (Qiagen, 301105) to facilitate the efficient delivery of DNA into the cell. Using this method, branched dendrimers form a spherical structure to encapsulate the DNA molecule. The dendrimer-DNA capsule possesses a net positive charge which facilitates interaction with negatively charged glycoprotein receptors on the plasma membrane surface. The DNA is then delivered across the phospholipid bilayer *via* the endocytosis of the dendrimer capsule. Table 2-4 summarises the optimised parameters based on the manufacturer's recommendation:

Dish	**Cell density**	**DNA (µg)**	**OptiMEM® (Life Technologies) (µl)**	**Polyfect reagent (µl)**	**Medium to add to cells (ml)**	**Medium to add to complexes (ml)**
6 well plate	$8x10^5$	2	100	20	1.5	0.6
6cm dish	$13x10^5$	5	150	40	3	1
10cm dish	$26x10^5$	8	300	80	7	1

Table 2-4: Optimal conditions for DNA transfection with polyfect reagent

2.2.7 Cell protein analysis *via* immunoblotting

2.2.7.1 Cell harvesting

Initially, six well dishes of cells were placed on ice and medium was removed. Cell monolayers were then washed with 400 µl ice cold PBS per well to remove residual media and any pharmacological treatments. After removal, cells were harvested *via* the addition of 100 µl radioimmunoprecipitation assay (RIPA) buffer (50 mM sodium HEPES [pH 7.5], 150 mM sodium chloride, 5 mM EDTA, 10 mM sodium fluoride, 10 mM sodium phosphate, 1% (v/v) Triton X-100, 0.5% (w/v) sodium deoxycholate, 0.1% (w/v) sodium

dodecyl sulphate (SDS), 0.1 mM phenylmethylsulphonyl fluoride, 10 μg/ml soybean trypsin inhibitor, 10 μg/ml benzamidine, and EDTA-free complete protease inhibitor mix) and scraping with a plastic cell scraper. The sample was then transferred to a 1.5 ml microfuge tube and placed on a rotating wheel (20 rpm, 4°C, 30 mins) to facilitate cell lysis and solubilisation. Samples were then centrifuged (21,000 x g, 4°C, 15 mins) to remove detergent-insoluble cell debris and the supernatant transferred to a fresh 1.5 ml microfuge tube for storage at -20°C until required.

2.2.7.2 The bicinchoninic acid (BCA) protein assay

The BCA assay is a sensitive and rapid method for the quantification of protein concentration in detergent extracts [220]. This is particularly useful for immunoblot analysis as it allows equal protein loading per lane on the gel. The assay relies on the reduction of Cu^{2+} (present in BCA reagent B) to Cu^{+} by proteins in the sample. The Cu^{+} then reacts with the BCA reagent A to form a purple colour (green→purple colour change). There is a linear correlation between the intensity of purple colour and protein concentration therefore the absorbance at ~562 nm is measured by a spectrophotometer to quantify this.

The BCA assay was performed in clear, 96 well, flat-bottomed plates with standards and samples performed in duplicate. Standard curves were prepared using 0-2 mg/ml BSA in the appropriate sample buffer (RIPA /NDB/co-IP buffer). The sample was diluted 1 in 5 (2 μl sample + 8 μl buffer) to which 200 μl of the BCA reagent mix was added. The BCA reagents were prepared in a 20 ml universal at a ratio of 9.8 ml reagent A (1% (w/v) 4,4 dicarboxy-2,2 biquinoline, disodium salt, 2% (w/v) sodium carbonate, 0.16%(w/v) sodium potassium tartate, 0.4% (w/v) sodium hydroxide, 0.95% (w/v) sodium bicarbonate, pH 11.25) to 0.2 ml reagent B (4% (w/v) copper sulphate) prior to addition to the plate. The plate was left at room temperature for approximately 15 mins or until a graded green→ purple colour change was observed across the standards. The plate was read at 492 nm using the POLARstar OPTIMA microplate reader and the mean absorbance calculated. Absorbance at 492 nm was selected as this was the closest filter to 560 nm available on our microplate reader. A % covariance <5 was deemed acceptable for each duplicate standard/sample.

2.2.7.3 Sodium dodecyl sulphate polyacrylamide gel electrophoresis (SDS-PAGE) and Immunoblotting

Detergent-soluble whole cells lysates were prepared for SDS-PAGE in 30 µl 50:50 sample:sample buffer ((50 mM Tris (pH 6.8), 10% (v/v) glycerol, 12% (w/v) SDS, 0.0001 % (w/v) bromophenol blue, 1 mM DTT). Using the BioRad Mini-PROTEAN® cell system, samples were fractionated *via* SDS-PAGE on 7-12% (w/v) poly-acrylamide gels in running buffer (27.4 mM Tris, 0.19 M glycine, 0.1 % (w/v) SDS) at a constant voltage of 150V. Protein markers (Bio-Rad, Precision Plus Protein™ Kaleidoscope™ Standards, #161-0375, range 15-250 kDa) prepared in sample buffer were run in parallel to facilitate estimation of the relative molecular mass of immunoreactive bands. Electrophoretic transfer onto nitrocellulose blotting membrane (0.2 µm pore size, Amersham™ Protran™, 10600001) was then performed using a Mini PROTEAN® Tetra Cell (Bio-Rad) transfer system. The transfer was performed in transfer buffer (24.7 mM Tris, 0.19 M glycine in 20% (v/v) methanol) at a current of 400mA for 45 mins. For proteins with an estimated molecular mass >100kDa the transfer duration was increased to 60 min and proteins >250kDa for 100 min.

2.2.7.4 Blocking nitrocellulose membrane and incubation with primary antibody

The membrane blocked with 5% (w/v) dried milk powder (Marvel) in Tris-buffered saline + Tween 20 (TBS/T: 20 mM Tris-HCl, pH 7.5, 150 mM NaCl, 2 mM $CaCl_2$, 0.05% (v/v) Tween 20) for 1hr at room temperature or overnight at 4°C to reduce non-specific antibody reactivity. Following this, membranes were incubated in a sealed bag with 2 ml of the appropriate primary antibody (Table 2-5) diluted in milk-TBS/T, or 5% (w/v) BSA-TBS/T for phosphor-specific antibodies, and agitated overnight at 4°C.

2.2.7.5 Incubation with secondary antibodies and immunoblot visualisation

Membranes were then washed in TBS/T (3x10 mins) at room temperature by agitating on a shaker (150 rpm). Following the last wash, the nitrocellulose was incubated for 1hour at room temperature with the appropriate horseradish peroxidise (HRP)-conjugated secondary antibody or protein G (Molecular Probes®) (Table 2-6) diluted in milk-TBS/T before a final set of washes with TBS/T (3x10 mins). Protein bands were then visualised using a chemiluminescence method in which 2 ml of ECL reagent (Western Lightening® Plus

ECL, Perkin Elmer, NEL104001EA) was added to each membrane for 1 min with gentle agitation. Residual ECL substrate was removed *via* gentle dabbing on tissue paper and immunoreactive bands were visualised following exposure to Medical X-ray Blue/MXBE Film (Carestream Health, 7710783)and development using a X-OMAT 2000 processor (Kodak).

2.2.7.6 Stripping of membranes

The nitrocellulose membrane was incubated in stripping buffer (0.15 M NaCl, 0.1 M Glycine, pH 2.6) for 30 mins at room temperature with shaking. The membrane was then washed in TBS/T (3 x 5 mins) and blocked in 5% (w/v) dried milk before incubation with primary antibody as described in section 2.2.7.4.

2.2.7.7 Gel components

10% resolving gel: 3.4 ml (v/v) dH_20, 2.5 ml (v/v) Buffer 1 (1.5 M Tris, pH 8.8, 0.4% (w/v) SDS), 0.65 ml (v/v) 50% (v/v) glycerol, 0.032 ml (v/v) ammonium persulphate (APS, 0.3 mg/ml), 0.008 ml (v/v) TEMED, 3.3 ml 30% (w/v) acrylamide/bis-acrylamide.

The percentage of the resolving gel was altered by adjusting the volumes of distilled deionised water (dH_20) and acrylamide/bis-acrylamide as follows:

8% resolving gel: 4.07 ml dH_20, 2.64 ml 30% (w/v) acrylamide/bis-acrylamide

12% resolving gel: 2.74 ml dH_20, 3.96 ml 30% (w/v) acrylamide/bis-acrylamide

Stacking gel: 3.4ml (v/v) dH_20, 1.34 ml (v/v) Buffer 2 (0.5 M Tris-HCl, pH 6.8, 0.4% (w/v) SDS), 0.054 ml (v/v) ammonium persulphate (APS, 0.3 mg/ml), 0.007 ml (v/v) TEMED, 0.63 ml 30% (w/v) acrylamide/bis-acrylamide (37.5:1)

Primary Antibody	Manufacturer	Catalogue number	Species raised in	Dilution	Prepared in
HA (YPYDVPDYA)	Sigma-Aldrich	SAB4300603-100UG	Rabbit	1:1000	5% (w/v) dried milk
Myc (9E10, EQKLISEEDL)	In house	N/A-	Mouse	1:1000	5% (w/v) dried milk
FLAG (DYDDDDK)	Sigma-Aldrich	F3165	Mouse	1:1000	5% (w/v) dried milk
SOCS3	In house	Bleed 4827	Rabbit	1:1000	5% (w/v) dried milk
SOCS3	Abcam	ab16030	Rabbit	1:200-1:1000	5% (w/v) dried milk
SOCS3	Santa Cruz Biotechnology	sc-7009	Goat	1:200-1:1000	5% (w/v) dried milk
GFP	In house	N/A-	Sheep	1:2000	5% (w/v) dried milk
Ubiquitin (P4D1)	Santa Cruz Biotechnology	sc-8017	Mouse	1:1000	5% (w/v) dried milk
Ubiquitin (linkage-specific K63)	Abcam	ab179434	Rabbit	1:1000	5% (w/v) dried milk
HectD1	Proteintech Group	20605-1-AP	Rabbit	1:500	5% (w/v) dried milk
USP15	MRC-PPU reagents	DU 19772	Sheep	1:1000	5% (w/v) dried milk

Table 2-5: Primary antibodies used for immunoblotting and immunofluorescence studies.*(Continued overleaf)*

GAPDH	Abcam	Ab8245	Mouse	1:20,000	5% (w/v) dried milk
Phospho-STAT3 (Tyr705)	Cell Signaling	9131	Rabbit	1:500	5% (w/v) BSA
STAT3	Cell Signaling	9132	Mouse	1:1000	5% (w/v) dried milk
JAK2	Abcam	ab37226	Mouse	1:1000	5% (w/v) dried milk
Phospho-JAK2 (Tyr1007/1008)	Cell Signaling	3771	Rabbit	1:1000	5% (w/v) BSA

Table 2-5: Primary antibodies used for immunoblotting and immunofluorescence studies.

Secondary antibody	**Conjugant**	**Manufacturer**	**Catalogue number**	**Species raised in**	**Dilution**
Rabbit	HRP	Sigma-Aldrich	A6154	Goat	1:1000
Mouse	HRP	Sigma-Aldrich	A4416	Goat	1:1000
Non-antibody reagents					
Protein G	HRP	Millipore	18-161	N/A-	1:200

Table 2-6: Secondary antibodies and non-antibody reagents used for immunoblot visualisation

2.2.7.8 Densitometry

Where appropriate, densitometry analysis of immunoblot data was performed on non-saturating films using Totallab v2.0 (Phoretix) by normalising the expression of the protein of interest expression to glyceraldehyde 3-phosphate dehydrogenase (GAPDH) (N=3). These data were then plotted as a % of the relevant control group (set at 100%).

2.2.8 Immunoprecipitation

Immunoprecipitation (IP) describes the isolation of a protein of interest by incubating a detergent-soluble extract with a specific primary antibody raised against the target protein antigen. IP is a useful method to determine whether 2 or more proteins interact either directly or indirectly within a protein complex at the time of cell harvest and under various experimental conditions. Moreover, under denaturing conditions, IP can be used to determine the ubiquitylation status of a target protein. Importantly, the type of IP dictated which lysis buffer was used. Denaturing IP to investigate the ubiquitylation status of SOCS3 mutants

Denaturing IP conditions were used to assess the ubiquitylation status of SOCS3. HEK293 cells were seeded in 6cm dishes on day 1 (section 2.2.2.1) and co-transfected on day 2 (section 2.2.6) with 2 μg/well Ubiquitin-HA (Ub-HA) ± 2μg /well WT or mutant SOCS3-FLAG (ΔN20, ΔN36, ΔC40, ΔC84 truncation/K6Q/L189A/K173R/Lys-less) as described in Table 2-3. On day 4, cells were treated with MG132 (6 μM, 2 hrs) prior to placing on ice, removal of medium and washing with ice-cold PBS. Cells were lysed by the addition of 100 μl/well denaturing IP buffer (DNB; 50 mM sodium-HEPES, pH 7.5, 100 mM sodium chloride, 1 mM *N*-ethylmaleimide, 2% (w/v) SDS, 0.1 mM phenylmethylsulphonyl fluoride, 10 μg/ml soybean trypsin inhibitor, 10 μg/ml benzamidine, and EDTA-free complete protease inhibitor mix). This ensured that SOCS3 ubiquitylation was specifically detected and not the ubiquitylation of any interacting protein. In addition, the DNB, containing NEM, inactivated de-ubiquitylating enzymes (DUBs) [221] which remain active in non-denaturing cell lysis buffers and may therefore reduce the ubiquitylation of target proteins following cell harvest. The sample was briefly vortexed and warmed to 95°C on a heat block before probe sonication (10seconds, 40% amplitude with a 2mm diameter tip, Vibra-Cell – Sonics & Materials, Inc., VCX130) to homogenise. The sample was then diluted 1 in 2 with non-denaturing buffer (NDB; 50 mM NaHEPES pH7.5, 100 mM NaCl, 1 mM *N*-ethylmaleimide, 1.1% (v/v) Triton-X-100, 0.55% (w/v) sodium

deoxycholate + EDTA-free complete protease inhibitor mix) and centrifuged (21,000 x g, 4°C, 15 mins) to remove insoluble cell debris. Following protein quantification, 500 μg protein was equalised to a total volume of 1 ml with NDB buffer and added to 30 μl 50% (v/v) anti-FLAG-coated Sepharose bead slurry (Sigma®). Samples were rotated overnight (15rpm, 4°C) to facilitate antibody reactivity with the antigen. Samples were then centrifuged (300 x g, 4°C, 1min) and washed 3 times in 1 ml NDB buffer centrifuging (300 x g, 4°C, 1min) in between each wash. Supernatant was removed and the bead pellet re-suspended in 30 μl 12% (w/v) SDS buffer + 1mM dithiothreitol (DTT). Samples were then placed on a 95°C heatblock (5 min) to promote elution of protein from the beads prior to SDS-PAGE. All IP samples were loaded onto the SDS-PAGE gel (section 2.2.7.3) using a Hamilton® syringe to ensure no beads were transferred which may block the poly-acrylamide gel pores.

Finally, immunoblotting was performed probing for HA epitope-tagged ubiquitin (anti-HA antibody H6908), FLAG tagged SOCS3 (anti-FLAG antibody F3165) and GAPDH (section 2.2.7.4).

2.2.8.1 Co-Immunoprecipitation (co-IP) of SOCS3-interacting proteins.

Co-IP is a less stringent than a denaturing IP and was used to investigate whether two or more proteins interact either directly or indirectly as part of a protein complex in detergent-soluble cell extracts.

On day 1, HEK293 cells were initially plated in 6 cm dishes (section 2.2.2.1) and co-transfected (section 2.2.6) on day 2 with 1 μg/well Elongin B, 1 μg/well Elongin C ±2μg/well WT or mutant (ΔC84/L189A/Lys-less) SOCS3 as described in Table 2-3. On day 4, cells were treated with MG132 (6 μM, 2 hrs) prior to harvesting in co-IP buffer (50 mM sodium HEPES (pH7.4), 150 mM sodium chloride, 5 mM EDTA (pH8.0), 1% (v/v) Triton X-100, 10% (v/v) glycerol, 0.1 mM phenylmethylsulphonyl fluoride, 10 μg/ml soybean trypsin inhibitor, 10 μg/ml benzamidine, and EDTA-free complete protease inhibitor mix). Following protein quantification by BCA assay (section 2.2.7.2), samples were equalised for protein content (500 μg) and co-IP buffer was added to a final volume of 1 ml. Sample was then added to either 30 μl 50% (v/v) protein G-Sepharose bead slurry (in co-IP buffer)with 15μl peptide affinity-purified anti-SOCS3 antibody (in-house, 4827) or 30 μl 50% (v/v) anti-FLAG-coated Sepharose bead slurry (in co-IP buffer, Sigma®). Samples were rotated overnight (15 rpm, 4°C) to facilitate antibody reactivity with the

antigen. Samples were then centrifuged (300 x g, 4°C, 1min) and washed 3 times in 1 ml co-IP buffer, centrifuging (300 x g, 4°C, 1min) in between each wash. The supernatant was removed completely and the bead pellet re-suspended in 30 µl 12% (w/v) SDS buffer + 1mM dithiothreitol (DTT). Samples were then placed on a 95°C heatblock (5 min) to promote elution of protein from the beads prior to removal with a Hamilton® syringe for loading onto SDS-PAGE gels. Finally, immunoblotting was performed probing for myc epitope-tagged Elongin B and C (anti-myc antibody 9E10), FLAG tagged SOCS3 (anti-FLAG antibody F3165) and GAPDH (section 2.2.7.4).

2.2.9 Emetine chase to investigate the stability of WT vs. mutant SOCS3

SOCS3 KO MEFs seeded in 10 cm dishes (section 2.2.1.1) were transfected (section 2.2.6) with 8 µg/dish FLAG-tagged human WT SOCS3, FLAG-tagged mouse WT SOCS3 or mutant (K6Q/K173R/Lys-less) SOCS3 (Table 2-3). The next day, cells were trypsinised and split into 7 wells of two 6 well plates (section 2.2.1.1). The following day, cells were treated with protein synthesis inhibitor Emetine (100 µM) for up to 8 hrs.

A positive control in which cells were treated with Emetine (100 µM) and MG132 (6 µM) was included. MG132 acts as a proteasome inhibitor therefore stabilising SOCS3 expression in the presence of Emetine. Comparing the 8 hr Emetine only vs. 8 hr Emetine + MG132 treatment group allows us to confirm whether the Emetine treatment was effective at inhibiting protein synthesis in each experiment. Non-transfected cells were also included to provide a negative control for SOCS3 immunoreactivity. Following Emetine treatment, cells were harvested in RIPA buffer and analysed for SOCS3 and GAPDH expression by SDS-PAGE and immunoblotting (section 2.2.7.3-2.2.7.5, Table 2.4)

2.2.10 Optimising the sensitivity of the Epo/Gp130 chimeric receptor (Epo/Gp130R) assay to measure SOCS3 functionality

HEK293 cells were co-transfected with 2 µg WT/mutant (*Y759F*) Epo/Gp130 chimeric receptor or JAK1 cDNA (section 2.2.6). Prior to harvesting, cells were serum starved (3 hrs, 37°C, 5%CO_2) and treated with ±50-500 ng/ml erythropoietin (Epo), 30,000 units interferon-α (IFNα) or vehicle only (PBS) for 15 min (37°C, 5%CO_2). The stimulation was then terminated by removal of the media and addition of 400 µl ice cold PBS. Cells

were harvested in RIPA buffer and analysed for phosphorylated STAT3 and total STAT3 expression by SDS-PAGE and immunoblotting (section 2.2.7.3-2.2.7.5, Table 2.4).

2.2.11 The identification of an E3 ubiquitin ligases and DUBs controlling SOCS3 turnover: the development of a SOCS3-luciferase fusion protein as a tool to screen an E3 ligase siRNA library

2.2.11.1 Investigating the proteasome as a major route of SOCS3 turnover in AS-M human endothelial cells

AS-M and MEF cells were stimulated with±50 μM Forskolin (Fsk) and ±6 μM MG132 (5 hrs, 37°C, 5% CO_2).The stimulation was then terminated by removal of the media and addition of 400 μl ice cold PBS. Cells were harvested in RIPA buffer and analysed for SOCS3 and GAPDH expression by SDS-PAGE and immunoblotting (section 2.2.7.3-2.2.7.5, Table 2.4).

2.2.11.2 The identification of a cell system to be used in an E3 ligase siRNA library screen

MEF or AS-M.5 cells in 6 well plates were treated with or without forskolin (Fsk; 50 μM) with or without MG132 (6 μM) before harvesting in RIPA lysis buffer and analysis of SOCS3 and GAPDH expression by SDS-PAGE and immunoblotting (section 2.2.7.3-2.2.7.5, Table 2.4).

2.2.11.3 Generation of a SOCS3-Firefly Luciferase fusion protein

The cytomegalovirus (CMV) promoter fused to the mouse SOCS3 open reading frame (accession number O35718) was amplified *via* polymerase chain reaction (PCR). The primers used were as follows: forward primer: GGGGGAGAATCTAGACGTTACATAACTTACGGTAAATG (*Xba*I site underlined), rev primer: AAAAGGAGACTCGAGGATAAGTGGAGCATCATACTG (*Xho*I site underlined)) using *Pfu* DNA polymerase as per manufacturer's instructions (Promega). The template used was an existing construct (pcDNA3.1/mouse FLAG-SOCS3, Table 2-3) previously generated in the Palmer lab. PCR products were resolved by gel electrophoresis (80V; 1.5hr) on a 1% (w/v) agarose gel. The predicted size of the CMV-SOCS3 amplicon was ~1200bp. The predicted CMV-SOCS3 1200bp amplicon was excised from the gel

using a sterile blade. To purify the DNA from the gel a QIAquick Gel Extraction Kit (Qiagen, 28704) was used. The now purified PCR product was subsequently digested with *Xho*I and *Xba*I (2units/enzyme) as per the manufacturer's instructions (Promega). The digested products were then resolved by agarose gel electrophoresis as above and bands were excised and purified as per the manufacturer's instruction (QIAquick gel extraction kit; Qiagen).

The *Xho*I-*Xba*I digested PCR product and similarly digested p-lenti-MCS vector (Pierce™ LentiLuc Packaging kit) were ligated at molar ratios of 1:3, 1:6 and 1:9 vector:insert with T4 DNA ligase as per the manufacturer's instructions (Promega, M1801). The ligation product (p-lenti-CMV-SOCS3-Luc) was then used to transform XL10-Gold Ultracompetent E.coli (Agilent Technologies) that were subsequently plated onto dry LB-agar plates (Amp) as described in section 2.2.3.2. Colonies were then picked and the cDNA construct was purified using Wizard® Plus SV minipreps (Promega) as described in section 2.2.4.1. We then screened for successfully ligated p-lenti-CMV-SOCS3-Luc by digesting with *Xho*I-*Xba*I and resolving the products on a 1% (w/v) agarose gel. The presence of a 1200bp fragment, representing CMV-SOCS3, indicated ligation was successful. The ligated constructs were then sequenced in its entirety to confirm that no erroneous mutations had been introduced (Dundee DNA Sequencing & Services).

2.2.11.4 Luciferase assay

In order to assess the enzymatic activity of the luciferase component of the SOCS3-Luc fusion protein, luciferase assays were performed on whole cell lysates using a luciferase assay kit as per the manufacturer's instructions (Dual-Luciferase® Reporter Assay System, Promega, E1910). Briefly, HEK293 cells were transfected with either p-lenti-SOCS3-Luc or a p-lenti control construct (section 2.2.6). 48 hrs post transfection, cells were harvested in the lysis buffer provided with the kit. Lysates were subject to two rapid freeze-thaw cycles on dry ice to ensure complete cell lysis. Increasing volumes of sample 0-40 µl were plated in triplicate into white, flat bottomed 96 well plates prior to the addition of 100 µl luciferase assay reagent (LAR). The luminescence signal was quantified immediately using the POLARstar OPTIMA microplate reader (BMG Labtech).Generation of SOCS3-Luc lentivirus particles.

2.2.11.5 Generation of a SOCS3-Luc lenti virus

Lentivirus (LV) particles expressing SOCS3-Luc under a CMV promoter were generated *via* triple transfection of 12x T150cm flasks of HEK293T cells as described previously [218, 222]. Each flask was transfected with 50 μg p-lenti-SOCS3-Luc, 17.5 μg envelope plasmid (pMD.G2, which encodes the envelope of vesicular stomatitis virus; VSVg) [222] and 32.5 μg integrase packaging plasmid (pCMV delta R8.74) [223] using 3 μl polyethylenimine (PEI) transfection reagent in 10 ml OptiMEM. Flasks were incubated for 6 hrs (37°C, 5% CO_2) before replacing the OpitMEM with 20 ml fresh growth media and returning the cell culture incubator. Media containing the virus particles (20 ml/flask) was removed 48 hrs post infection, filter sterilised (using a 0.22 μm filter unit attached to a vacuum pump, Millipore, SCGPU05RE) and stored at 4°C overnight. To each T150 cm cell flask, a further 20 ml of fresh media was gently pipetted into one corner of the flask, to avoid cell detachment, before returning to the cell culture incubator overnight. Spent media was then removed, filter sterilised as above and pooled with the 48 hr media for storage at 4°C until concentration of the virus that day.

A mouse WT SOCS3 and human Lys-less SOCS3 lentivirus was also generated as above using lentivirus plasmids synthesised by Cyagen Biosciences Inc.

2.2.11.6 Concentration of the lentivirus particles

Virus particles were concentrated using an ultracentrifuge. Initially, ~18 ml media containing LV particles was loaded into open top 14x95 mm Ultra-Clear™ tubes (Beckman Coulter Ltd). Subsequently, virus particles were concentrated via 6 x 1 hr 7 min ultracentrifugation cycles at 4°C (SW40 rotor, 90353 × g; 23,000 rpm; acceleration maximum; break 9; Beckman Optima™ L-80 XP) decanting the supernatant in between centrifugation cycles avoiding disruption of the invisible virus particle pellet. The final pellet was re-suspended in 100 μl OptiMEM and incubated for 20 min on ice. Virus samples were then aliquoted (10 μl) into 0.5 ml microfuge tubes and stored at -80°C. Virus samples were used once and were not subjected to multiple rounds of freeze-thawing.

2.2.11.7 Measuring virus particle titre

Virus titres were measured via the TaqMan® quantitative real time PCR (qPCR) method quantifying the incorporation of LV into a host cell genome as described previously [224].

Primer/probe sets targeted at the late reverse transcriptase gene were employed as follows: 100 nM LRT-P probe, 5'(FAM)-CAGTGGCGCCCGAACAGGGA-(TAMRA)3'; 300 nM forward primer MH531 5'-TGTGTGCCCGTCTGTTGTGT-3' and 300 nM reverse primer MH532 5'-GAGTCCTGCGTCGAGAGAGC-3' (Applied Biosystems).

On day 1, HEK239T cells were seeded at a density of $5x10^4$ cells/well in 12 well plates and returned to the incubator overnight to facilitate cell adhesion. On day 2, cells were infected with virus particles (titration of stock 10^{-2} – 10^{-6}) and returned to the incubator. 72hrs post infection, cells were harvested in 200 µl PBS and the DNA was extracted as per manufacturer's instruction (Qiagen, QiaAMP DNA mini kit).

For qPCR, 250ng DNA of each sample was loaded into 384 well plates. In conjunction with this, a standard curve of the expression plasmid used to make the virus (p-lenti-CMV-SOCS3-Luc) was performed ($1x10^{13}$-10^4 plasmid copies) on the same plate. Samples were performed in triplicate with a non-template control included to confirm there was no reagent contamination. To each sample, 1x Mastermix (TaqMan® Universal Master Mix II no UNG, Applied Biosystems, 4440040) was added in addition to the late reverse transcriptase primer/probe sets described above to a final volume of 12.5 µl. PCR amplification was performed as follows:

50°C – 2 min

95°C- 10 min

95°C – 15 sec
60°C – 1 min
} 40 cycles

The copy number of the virus particles was then calculated by reading off the standard curve.

2.2.11.8 Generation of AS-M.5 clonal cell lines stably expressing SOCS3-Luc

The SOCS3-Luc LV particles co-expressed a puromycin resistance gene to allow for selection of cell lines that have stably incorporated the LV genome. Preliminary so-called

"kill curve" experiments determined that a puromycin concentration of 2 μg/ml was sufficient to kill parental AS-M.5. cells within 2 days (image not shown).

AS-M.5cells were grown to 40% confluency in 10 cm dishes and infected with SOCS3-Luc LV particles (2 IFU/cell) the following day. On day 3, growth medium was replaced and, 48hrs post infection, cells were trypsinised (section 2.2.7.1). The resulting cell pellet was re-suspended in media supplemented with 2 μg/ml puromycin and serial dilutions of the re-suspended mix were plated in 10 cm dishes in puromycin-containing selection medium. Cultures were maintained for up to 14 days, replenishing media every 48hrs, until single puromycin-resistant clones could be picked for expansion. Initially, clones were expanded in 24 well plates, and upon reaching confluence were plated into duplicate 6 well plates. One set of 6 well plates were used for screening for SOCS3-Luc-expressing clones by treatment with or without MG132 (6 μM, 2 hrs) and harvesting for luciferase assay (section 2.2.11.4). The assay window (AW) for each clone was calculated as: (mean luminescent signal with MG132) - (the mean luminescent signal without MG132). Clones were identified by a single letter of the alphabet A-P.

To increase the AW of the AS-M.5 SOCS3-Luc clone E, cells were treated with or without Emetine (100 μM) and with or without MG132 (6 μM) over a 7 hr time course. Lysates were harvested for luciferase assay (section 2.2.11.4) and the AW between each treatment group time point was calculated as above.

2.2.12 Immunofluorescence visualisation of SOCS3 in MEFs and HUVECs as a method for screening an E3 ligase siRNA library.

WT MEFs, SOCS3 knockout MEFs or HUVECs were plated on glass coverslips in 6 well plates and grown to 60% confluence. Following stimulation with either 10 μM Fsk + 6 μM MG132 or vehicle (DMSO) only for 5hrs, cells were washed with PBS (2x1 ml) before fixation with 3% (w/v) paraformaldehyde (PFA), prepared in PBS, on ice (15 min). PFA was then removed and replaced with 2 ml methanol on ice (10 min). Further PBS washes were performed (3x1 ml) before permeabilisation on ice for 10 mins with 2 ml PBS, 0.1% (v/v) Triton-X-100. Subsequently, a further 3x1 ml PBS washes were performed to remove residual detergent. Coverslips were then incubated with blocking solution (PBS containing 0.1% (v/v) Triton-X-100 and 3% (v/v) donkey serum) for 1hr at room temperature. Primary antibodies were prepared in blocking solution as follows: WT and SOCS3 KO MEFs were incubated with 0-2 μg/ml rabbit anti-SOCS3 (ab16030), HUVECs were

incubated with 2 μg/ml goat anti SOCS3 (sc-7009) or 1 μg/ml rabbit anti-SOCS3 (ab16030) and negative controls were incubated with 3% (v/v) donkey serum. Coverslips were then placed in a humidifying chamber (2hrs, 4°C) before washing with PBS (3x1 ml) and incubation with Alexa Fluor® 488 donkey anti-rabbit IgG secondary antibody (diluted in PBS containing 0.1% (v/v) Triton-X-100) in the dark (humidifying chamber, 1hr, 4°C). Subsequently, coverslips were washed in PBS (3x1 ml) before nuclear staining with DAPI (LifeTechnologies, D1306) as per manufacturer's instruction. Additional 3x1 ml PBS washes were performed before mounting onto glass slides (Thermo Scientific Shandon™ Immuno-Mount™). Immunolocalisation of SOCS3 was then visualised under oil immersion using a 63x objective fitted to a Zeiss LSM Pascal Exciter confocal imaging system. Representative images are shown. WT and SOCS3 KO MEF lysates were also prepared in parallel by harvesting cells in RIPA lysis buffer and immunoblotting for SOCS3 (ab16030) and GAPDH (ab9484) (section 2.2.7.3-2.2.7.5).

2.2.13 Reversed-phase liquid chromatography tandem mass spectrometry (LC-MS) screen to identify E3 ligase/DUB enzymes interacting with SOCS3.

2.2.13.1 IP of SOCS3 for LC-MS-MS analysis

HEK293 cells seeded in four 10cm dishes (section 2.2.1.1) were transfected with 10 μg/dish FLAG-tagged pcDNA3.1 murine WT SOCS3 (two plates) or 10 μg pcDNA3.1 only as a negative control (two plates) using Polyfect as described in section 2.2.6. The next day, cells were harvested in a modified co-IP lysis buffer (50 mM Na HEPES pH7.4, 150 mM NaCl, 0.5 M EDTA (pH8.0), 1% (v/v) Triton-X-100, 10% (v/v) glycerol, 0.1 mM PMSF, 1 mM sodium orthovanadate, 6 μM MG132, 10 μg/μl benzamidine, 10 μg/μl soybean trypsin inhibitor, EDTA-free complete protease inhibitor mix) with the SOCS3 transfected samples pooled together and the pcDNA3.1 transfected samples pooled together.

Following protein quantification (section 2.2.7.2), samples equalised for protein content (15 mg) and volume (3 ml) were loaded into 15 ml Falcon™ tubes and pre-cleared of non-specific binding proteins by incubating each sample with 60 μl of a 50:50 protein G Sepharose bead slurry (Generon, PC-G25). A further 8.5 mls lysis buffer was added to each tube and samples were rotated for 30 mins (12rpm, 4°C) prior to gentle centrifugation (5 min, 300 x g, 4°C). The supernatant was then transferred to a fresh 15 ml Falcon™ tube containing 240 μl of a 50% (v/v) anti-FLAG M2 affinity gel bead slurry. Samples were

rotated for 3 hrs (12rpm, 4°C) before further centrifugation (5 mins, 300 x g, 4°C). The supernatant was discarded, beads were re-suspended in 1 ml co-IP lysis buffer and transferred to 1.5 ml microfuge tubes for centrifugation (1 min, 300 x g, 4°C). The beads were then washed 3x1 ml in lysis buffer with centrifugation (1 min, 300 x g, 4°C) between washes. Finally, samples were eluted from the beads via the addition of 35µl 2x Laemmli Sample Buffer (Bio-Rad Laborotories, 161-0737) plus 10 µl NuPAGE® Sample Reducing Agent (Novex, NP0004®). Samples were the placed on a heat block (5 min, 95°C) and the eluate transferred to a fresh microfuge tube via Hamilton® syringe for storage at -80°C until required.

2.2.13.2 SDS-PAGE and in-gel protein visualisation.

All procedures were conducted in a laminar flow hood to minimise keratin contamination which may reduce the quality of LC-MS data.

Samples were initially resolved *via* SDS-PAGE on a NuPAGE® Novex® 10% Bis-Tris protein gel with NuPAGE® MOPS SDS Running Buffer (x20) at a constant 150V for 1.5hrs. The gel was disassembled and protein visualised using a Colloidal Blue staining kit (LC6025, Invitrogen™). This kit is based on the Coomassie Brilliant Blue stain [225] where under acidic buffer conditions, the Coomassie dye interacts with the hydrophobic (water repelling) or basic amino acid residues that form the protein structure. Briefly, the gel was incubated with the colloidal blue stain for 30 mins at room temperature before de-staining with distilled deionised water for 1 hr.

2.2.13.3 Band excision and trypsin digestion.

Following protein band visualisation, gel slices (8 per lane) were excised and de-stained and extracted from the acrylamide gel before digestion. Briefly, proteins were reduced with 50 µl 10 mM DTT at 60°C for 30 mins followed by alkylation with 50 µl 50 mM iodoacetamide, in the dark, at room temperature for 30 mins. Subsequently, the solvent was removed and the samples were washed with 50% (v/v) acetonitrile (ACN)/50 mM ammonium bicarbonate (AMBIC) and dried using a SpeedVac. In-gel trypsin digestion was performed *via* the addition of 20 µl 0.05 µg/ml sequencing grade trypsin in 50 mM AMBIC overnight at 30°C. Digests were then extracted *via* the addition of a 50% (v/v) ACN/2.5% (v/v) formic acid solution for 20 mins at room temperature prior to drying

using a SpeedVac. Finally, the dried peptides were re-dissolved in a 5% (v/v) ACN/0.25% (v/v) formic acid solution and stored at -20°C until required.

2.2.13.4 LC-MS-MS analysis.

The LC-MS-MS run and analysis was performed by Dr David Sumpton (Beatson Institute). Reversed-phase liquid chromatography tandem mass spectrometry analysis was performed on a LTQ-Orbitrap Velos coupled to a Proxeon Easy-LC. The peptide mixtures were loaded onto a C18 guard column (1.9 µm; 0.1 × 20 mm) and separated on a C18 in-house packed emitter (1.9 µm; 0.075 × 150 mm) over a 60 min linear gradient. The Orbitrap was set to analyse the survey scans (m/z 350-1600) at 60000 resolution and the top 10 ions in each duty cycle were selected for MS/MS in the LTQ linear ion trap. The data were searched against the Swiss-Prot *Mus musculus* database (50807 entries) using Mascot v2.4.1 software (Matrix Science Ltd.) [226]. All Mascot result files were then loaded into Scaffold v4.3.4 proteomic software [227]. The data were combined with the previous experiments raw files (n=2) and searched against the same database using MaxQuant (v1.4.1.6) for both protein identification and label free quantitation [228, 229]. MaxQuant software is free to download at www.maxquant.org. The MaxQuant ID information was then pooled with the Mascot results in the same Scaffold analysis.

To confirm the endogenous site(s) of ubiquitylation on SOCS3, the LC-MS/MS data were searched for a glycine-glycine signature at each individual lysine. The presence of this signature confirmed ubiquitylation had occurred at this site [230] and this was determined by a +114 mass shift from unmodified lysine.

2.2.14 Investigating SOCS3 in the vasculature

2.2.14.1 Immunolocalisation of SOCS3 in HSV tissue.

Surplus HSV tissue was derived from 3 individual patients (281A, 304A, 306D) undergoing CABG procedures. The tissue was fixed in 10% (v/v) formalin and paraffin embedded by Mrs Nicola Britton (Institute of Cardiovascular and Medical Sciences, University of Glasgow). Paraffin-embedded tissue was then sectioned to provide slices that were 4µm thick using a Leica Finese 325 microtome (Fisher Scientific). Tissue was mounted onto glass slides by floating the tissue sections in a 37°C water bath and allowing

the wax to gently melt. Following this, slides were heated in a 60°C oven (3hrs) and transferred to a 40°C oven overnight to ensure adherence of tissue to the glass slides.

Initially, paraffin was removed by washing sections in Histoclear (2 x 5 min) followed by re-hydration of tissue through a gradient of ethanol troughs (100% → 90% → 70% (v/v)) for 5 mins each. A final wash in distilled deionised water was performed (minimum of 6 mins) to avoid drying out prior to an antigen retrieval step. Antigen was retrieved by incubating slides with citrate buffer (8 mM trisodium citrate, 2 mM citric acid, pH 6.0) and heating in a microwave for 20 min topping up with buffer if boiled over. Slides were then allowed to cool for a further 30 min to allow the antigen to fold correctly. Slides were then rinsed under running cold tap water before quenching of endogenous peroxidase activity by incubation with 3% (v/v) H_20_2 in methanol (20 min) followed by washing in PBS + 0.1% (v/v) Triton-X 100 (2 x 5 min). Blocking was achieved by incubating sections with 20% goat serum (diluted in TBS/T) for 1 hr in a humidifying chamber to minimise non-specific binding. Blocking solution was removed by gently dabbing the edge of the slide on tissue paper. Rabbit anti-SOCS3 (ab16030) or rabbit IgG control primary antibody was prepared in 2% goat serum (diluted in TBS/T) at a concentration of 0.01 mg/ml or 0.005 mg/ml and incubated with the appropriate sections (4°C, overnight) in a humidifying chamber. The following day, sections were washed in PBS + 0.1% (v/v) Tween20 solution (3 x 5 min) to remove residual primary antibody. Following this, the biotinylated goat anti-rabbit (Ba-100) secondary antibody, provided with the Vectastain® ABC universal kit (PK-6200), was prepared in 2% goat serum (diluted in TBS/T) at a concentration of 1:300 and incubated with sections for 30 min at room temperature. Sections were then washed in PBS + 0.1% Tween20 (3 x 5 min) and incubated with ABC reagent (30 min, room temperature). Sections were washed twice in PBS before addition of the pre-prepared 3,3'-diaminobenzidine (DAB) substrate (DAB substrate kit, Vector labs SK-400) for 1-5 min. Staining time was determined by microscopic evaluation of development on the SOCS3 primary antibody (0.01 mg/ml) slide. Finally the reaction was quenched by immersing sections in running tap water (5 min). Nuclei were then counterstained with haematoxylin (1 min) and immersed in running tap water (5 min) before dehydration of the sections in an ethanol gradient (70% → 90% → 100% (v/v)) for 6 mins each with a final wash in histoclear (6 min). Slides were mounted using Histomount (National Diagnostics) and allowed to dry in a fume hood for 24hrs. Finally, tissue images were taken on the Olympus BX41 microscope at x4 and x10 objectives and analysed using the QCapture Pro 6.0 Software. Representative data were shown.

2.2.14.2 Optimising the infection efficiency of the Sffv-GFP LV in HSVECs.

HSVEC and HSVSMCs are primary human cell cultures may prove challenging to transfect, as such the efficiency of LV infection and gene expression was assessed in surplus HSVECs. HSVECs were plated in 6 cm dishes ($5x10^5$ cells/dish) and infected with 0-20IFU/cell GFP LV the following day. 48 hrs post infection, GFP expression was visualised using the Axiovert 40 CFL (Carl Zeiss Microscopy, LLC) fluorescent microscope and Carl 4.0 software. The infection efficiency was calculated as the proportion of cells expressing GFP in a given area. Samples were then harvested in RIPA lysis buffer for SDS-PAGE and immunoblotting for GFP (in-house) and GAPDH (Ab8245) (section 2.2.7.3-2.2.7.5).

2.2.14.3 Proliferation assay

BrdU cell proliferation assays (Roche) were employed to assess HSVSMC proliferation following SOCS3-Luc or GFP LV infection (as per the manufacturer's instructions). Briefly, SMCs were seeded in white 96 well, flat bottomed plates ($1x10^3$ cells/well). The following day, cells were serum starved for 72hrs before returning to 15% (v/v) FBS SMC media and infection with 0-20IFU/cell SOCS3-Luc or control GFP viruses (48hrs). 31hrs post infection BrdU label was added to each well and cells were returned to the incubator for 17hrs. Each well was then fixed and BrdU incorporation measured by measuring absorbance at 450nm using a plate reader (POLARstar OPTIMA).

2.2.14.4 Migration assay

The *in vitro* scratch assay previously described by Liang and colleagues [231] was employed to measure cellular migration following SOCS3 overxpression on SMCs. HSVSMCs were seeded at $1x10^9$ cells/well in 6 well plates and grown to 100% confluence. Cells were then serum starved for 72 hrs (MEM, 0.2% (v/v) FBS, 1 mM (v/v) L-glutamine, 50 U/ml (v/v) Penicillin-Streptomycin solution to induce cell quiescence. Subsequently, 3 scratches/well were made with a P200 tip followed by a PBS (1 ml) wash to remove detached cells. Reference marks (2 vertical scratches on the plastic plate) were made to specify which area of the scratch to image and cells were returned to 15% (v/v) FBS SMC media or fresh 0.2% (v/v) FBS media as above. At this point, cells were infected with SOCS3-Luc or GFP virus particles (0-10IFU/cell) and scratch wounds were imaged at 0 and 24hr time-points with representative images shown.

2.2.14.5 Statistical analysis

Results were expressed as the mean ± standard error of the mean (SEM) representing error bars. The statistical significance between treatment groups was assessed using an unpaired, two-tail t-test or one way ANOVA with *Bonferroni* correction as stated. A P-value <0.05 was deemed significant.

3 Investigating the regulation of SOCS3 stability

3.1 Introduction

The role of SOCS3 as a negative regulator of JAK/STAT signalling has now been well characterised however little is known about the regulation of SOCS3 turnover specifically. Multiple routes of SOCS3 degradation exist though the contribution of each may be dependent on the cell type under investigation. For example, calpain protease-mediated degradation of SOCS3 was recently described in the literature [103]. In addition, phosphorylation has previously been shown to destabilise SOCS3 levels by promoting proteasomal turnover [94]. Deletion of the PEST motif within SOCS3 was also reported to stabilise SOCS3 levels [100]. SOCS3 has previously been shown to be polyubiquitylated and consequently targeted for degradation at the proteasome. For this reason, SOCS3 has a relatively short biological half-life that varies from 40-120 mins depending on the cell type [97]. Sasaki *et al* generated an N terminal truncation mutant of SOCS3 and found that deletion of 11 residues at the N terminus or mutation of Lysine 6 (Lys6) specifically enhanced the stability of the protein in Ba/F3 cells (murine pro-B cell line) [95]. As such Lys6 is thought to be the master regulator of SOCS3 stability however the precise mechanism of SOCS3 turnover remains unclear. Interestingly, studies in which the C-terminal SOCS box was deleted showed that SOCS3 failed to bind other components of the E3 ligase complex and that this also enhanced the stability of SOCS3 [95]. Accordingly, the group proposed that SOCS3 was autoubiquitylated as opposed to an external E3 ligase catalysing this post-translation modification of SOCS3.

3.1.1 Aims

Though Lys6 has been reported to be a key regulator of SOCS3 stability [95] no other group has reproduced this finding nor has any follow up study been published in the literature. As such, the mechanism of SOCS3 turnover remains controversial. In this study the identification of key lysine residues involved in targeting SOCS3 for proteasomal degradation was performed. In addition, we assessed whether SOCS3 has the ability to autoubiquitylate and regulate its' own turnover. Furthermore, we characterised a Lysine-less SOCS3 mutant and compared its stability with WT SOCS3 via Emetine chase experiments. Finally we adapted the existing Epo/Gp130R assay to measure Lys-less SOCS3 function and determine whether mutagenesis affected the ability of SOCS3 to inhibit JAK/STAT signalling.

3.2 Results

3.2.1 Identification of key lysine residues involved in SOCS3 ubiquitylation

Previously, it had been shown that Lysine 6 (K6) was an important regulator of SOCS3 turnover in Ba/F3 cells (murine pro-B cell line) [95]. To investigate the role of K6 further, we generated a FLAG epitope-tagged *K6Q* SOCS3 mutant and expressed the construct in HEK293 cells in parallel with a similarly FLAG epitope-tagged wild type (WT) SOCS3 and HA epitope-tagged ubiquitin (Figure 3-1). Immunoprecipitation of the WT vs. *K6Q* SOCS3 mutant with anti-FLAG conjugated Sepharose beads and blotting for HA tagged ubiquitin was performed. Discrete stepwise increases in immunoreactivity (from ~37 kDa to >250 kDa) were detected for WT SOCS3 consistent with polyubiquitylation (Figure 3-1). *K6Q* mutated SOCS3 was polyubiquitylated similar to WT SOCS3 (Figure 3-1 B), and densitometry analysis confirmed that mutation of K6 had no effect on SOCS3 ubiquitylation (Figure 3-1 C). Both WT and the K6Q mutated SOCS3 were insensitive to proteasome inhibition (MG132 treatment) suggesting the proteasome was not the major route of SOCS3 degradation in HEK293 cells (Figure 3-1 B-C).

3.2.2 Emetine treatment to assess the role of Lys6 on SOCS3 protein stability

Though the *K6Q* SOCS3 mutant was still ubiquitylated in HEK293 cells (Figure 3-1), it was important to confirm that this mutant was degraded at the proteasome and that loss of K6 did not alter the stability of SOCS3. To establish the role of K6 in controlling SOCS3 stability, we expressed FLAG-tagged WT or *K6Q* SOCS3 in SOCS3 KO MEF cells. Use of the SOCS3 KO cell line ensured only that we measured the stability of the transfected SOCS3 construct only and not endogenous SOCS3. The cells were stimulated with a protein synthesis inhibitor, Emetine, for the indicated time points (0-8 hrs). A positive control in which cells were treated with Emetine plus MG132 was included to confirm the proteasome was the major route of degradation. Immunoblotting for FLAG-tagged SOCS3 confirmed that turnover of the K6Q mutant was comparable to the WT SOCS3 turnover (Figure 3-2 A-B). Both WT and K6Q SOCS3 protein levels decreased gradually over time and was no longer detected following 8 hrs Emetine treatment (Figure 3-2 A and B). There was no statistically significant change in stability ($P>0.05$) between WT and *K6Q* SOCS3 (Figure 3-2 C). From these data, we concluded that the proteasome was a major route of SOCS3 degradation in a mouse fibroblast cell line and that Lys 6 was not a key regulator of SOCS3 stability.

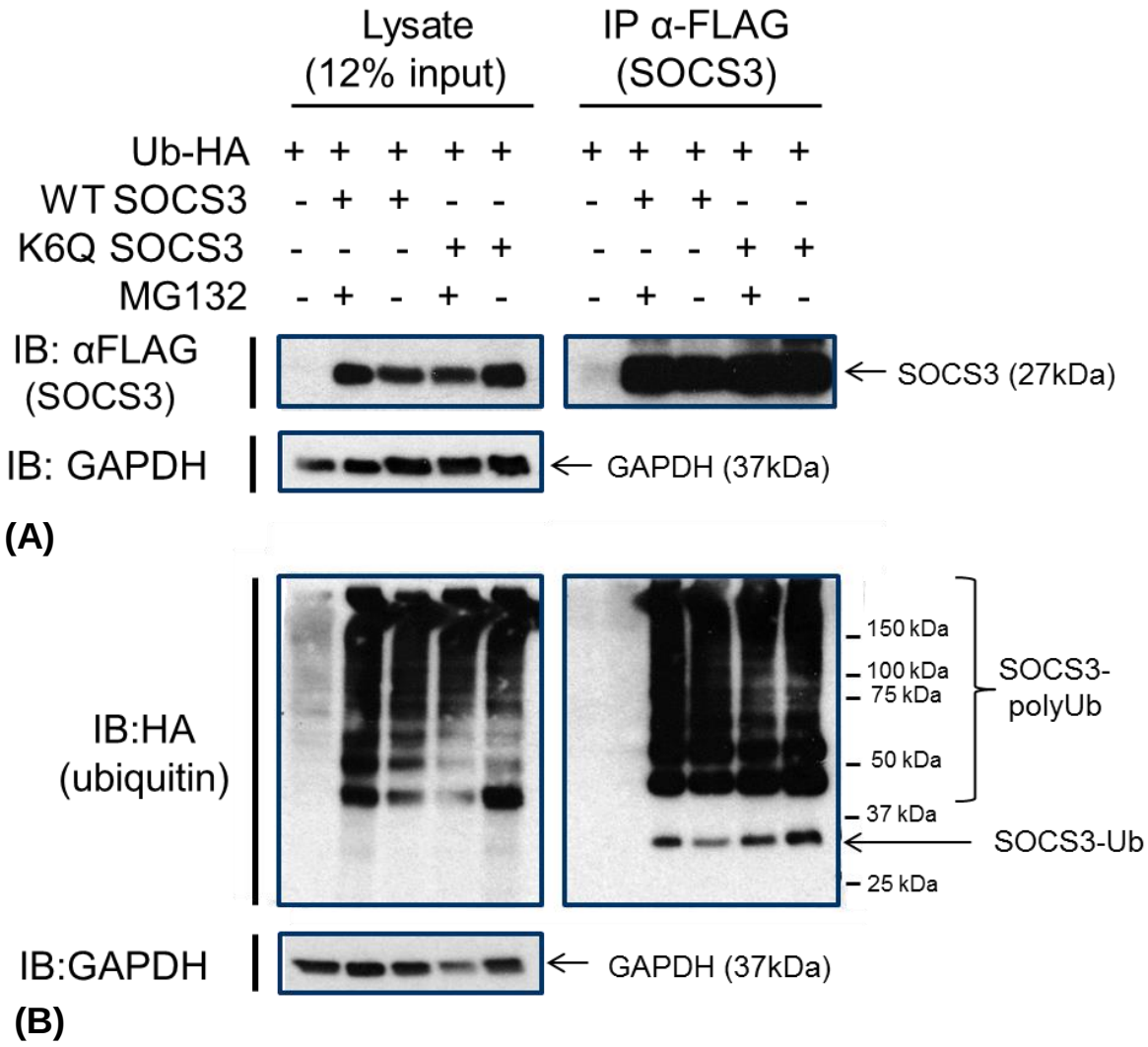

Figure 3-1: SOCS3 *K6Q* mutant was subject to poly-ubiquitylation *(continued overleaf)…*

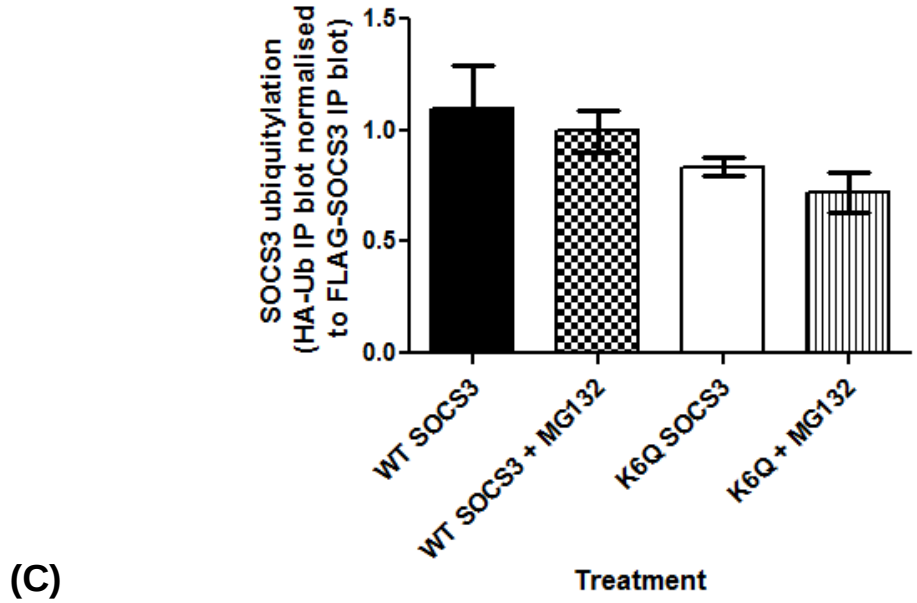

Figure 3-1: SOCS3 K6Q mutant was subject to poly-ubiquitylation

HEK293 cells were transiently transfected with 2μg FLAG tagged WT or K6Q SOCS3 and HA tagged Ubiquitin (Ub-HA). SOCS3 was then immunoprecipitated from lysates with anti-FLAG coated Sepharose beads. IP samples (500 μg) were split over two gels (250 μg/gel) alongside 30 μg whole cell lysate. Samples were resolved by SDS-PAGE and transferred to nitrocellulose membrane for western blotting. (A) Mouse anti-FLAG (1:1000) was used in western blotting with protein G-HRP (1:1000) for band visualisation. (B) Rabbit anti-HA (1:1000) with anti-rabbit IgG-HRP (1:1000) secondary antibody. Membranes were then stripped and were probed with mouse anti- GAPDH (1:20,000) and anti-mouse IgG-HRP to provide a loading control. The upper bands represented poly-ubiquitination chains. (C) Densitometry analysis was performed using Total lab by normalising SOCS3 polyubiquitylation (Ub-HA blot) to the amount of SOCS3 present in the FLAG-SOCS3 IP blot. The data were presented as mean ± SEM. One-way ANOVA with Bonferroni correction was performed using GraphPad software where $P < 0.05$ was deemed significant. (C) There was no significant difference in the ubiquitylation status of WT and K6Q mutated SOCS3 in the presence or absence of MG132 suggesting that in HEK239 cells Lys 6 is not the only site of ubiquitylation. The experiment was repeated to N=3 and representative data shown.

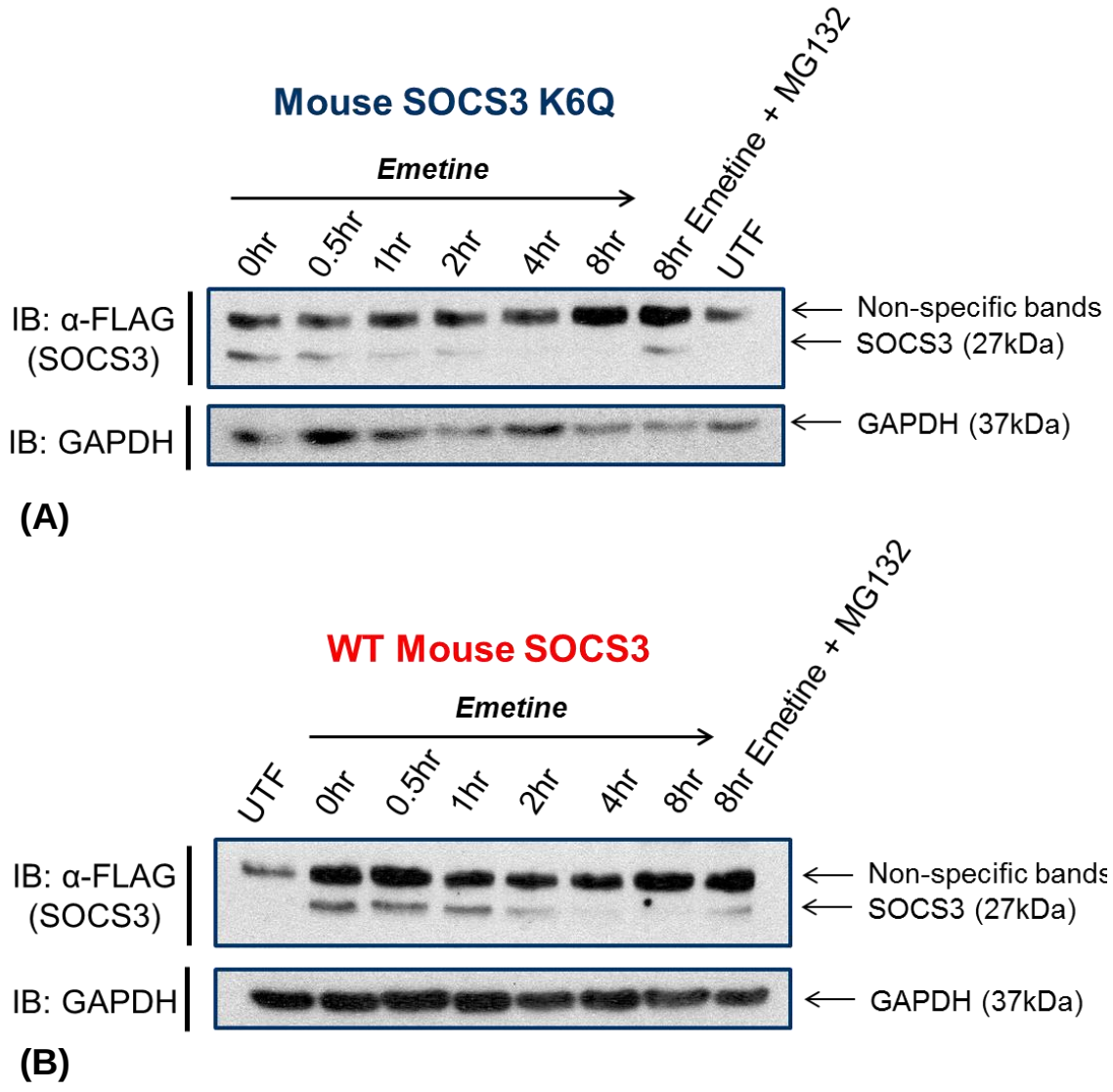

Figure 3-2: SOCS3 K6Q mutant was not more stable than WT SOCS3 *(Continued overleaf)*

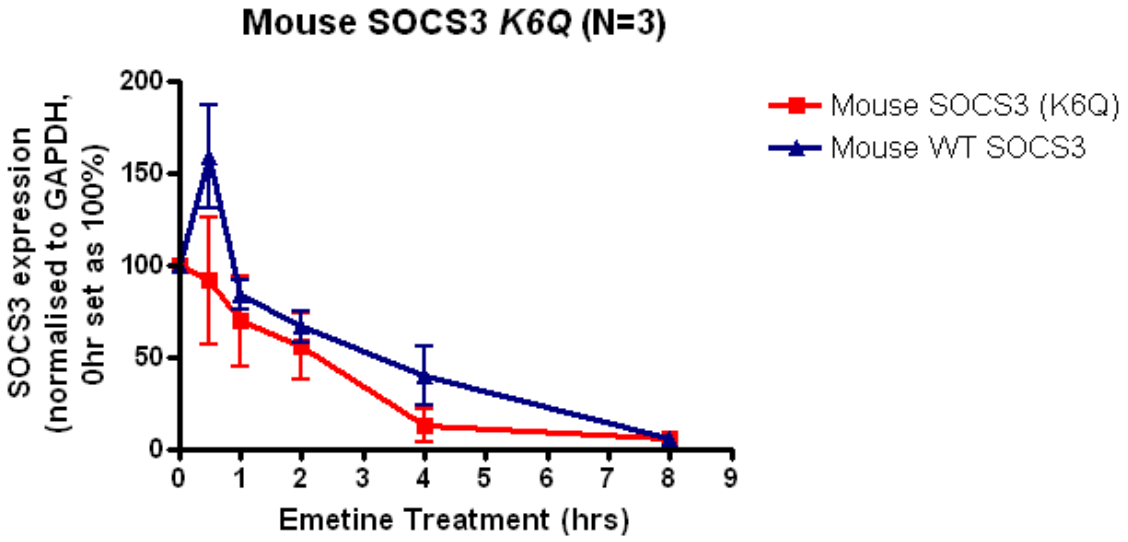

(C)

Figure 3-2: SOCS3 K6Q mutant was not more stable than WT SOCS3.

HEK293 cells were seeded in 10 cm dishes and transfected with 10µg FLAG tagged WT human SOCS3 or K6Q mutant the following day. 24 hrs post transfection, cells were trypsinised and split into 7 wells of 2 x 6 well plates. 48 hrs post transfection, cells were then stimulated with ± Emetine (100 µM) and ± MG132 (6 µM) for the indicated time (0-8 hrs). UTF denotes untransfected. (A-B) Whole cell lysates were resolved via SDS-PAGE and immunoblot analysis performed with anti-FLAG and anti- GAPDH. Representative image shown (N=3). (C) Densitometry analysis was performed using Total lab by normalising SOCS3 expression to GAPDH. The data were presented as mean ± SEM % SOCS3 remaining where the 0 hr time point was set to 100%. Student's t-test (2-tailed, un-paired) was performed at each time point where $P<0.05$ was deemed significant. The *K6Q* SOCS3 mutant was not significantly more stable than WT SOCS3.

3.2.3 Mapping the site of SOCS3 ubiquitylation

Having eliminated a role for Lys6 in controlling SOCS3 ubiquitylation in HEK293 cells, we tested a range of N- and C-terminal truncation mutants of SOCS3 in an attempt to identify key Lys residues involved in SOCS3 ubiquitylation. A panel of FLAG tagged SOCS3 truncation mutants were expressed in HEK293 cells and immunoprecipitated using anti-FLAG beads (Figure 3-3). Immunoblotting for HA-tagged ubiquitin confirmed that poly-ubiquitin chains were visible in whole cell lysates and IP samples for WT, *ΔN20*, *ΔN36* and *ΔC40* SOCS3 (Figure 3-3).However, the *ΔC84* SOCS3 truncation revealed no poly-ubiquitin chains and was comparable to the HA-ubiquitin only control (Figure 3-3). From these data, we concluded that the region of SOCS3 spanning aa142-185 was essential to observe ubiquitylation of SOCS3.

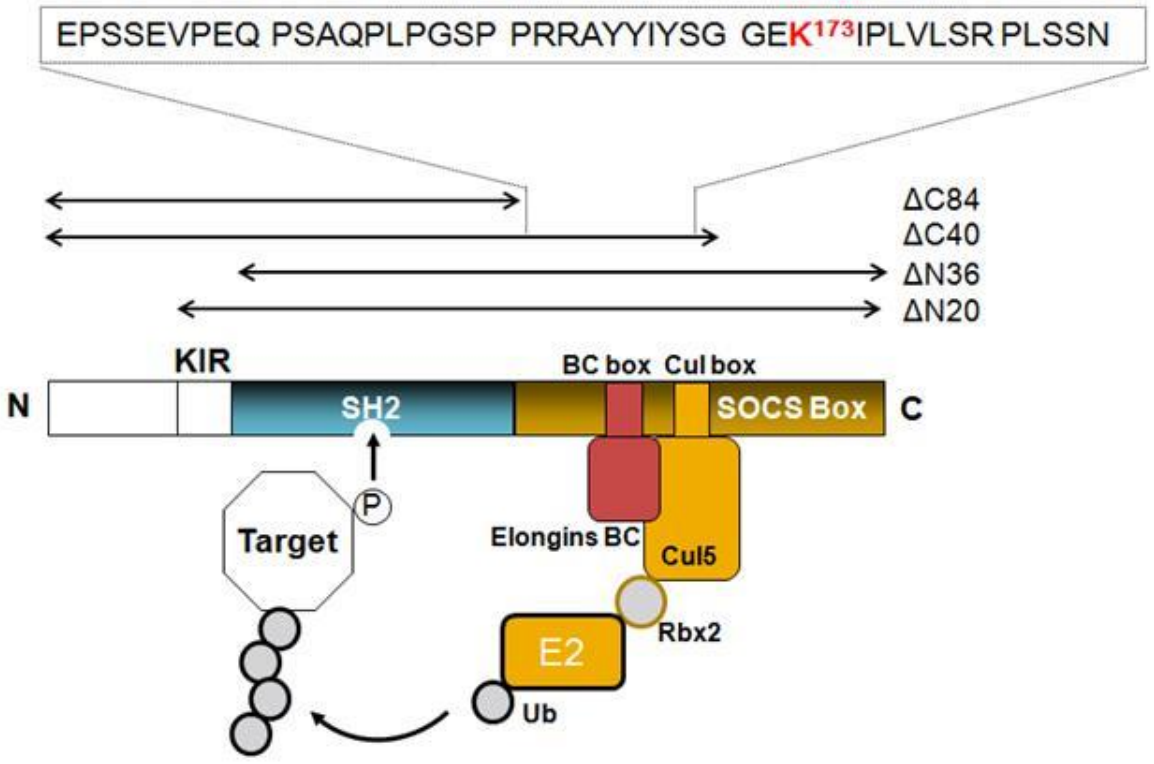

(A)

Figure 3-3: Identification of a C-terminal, 44 amino acid, region required for SOCS3 ubiquitylation

(Continued overleaf)…

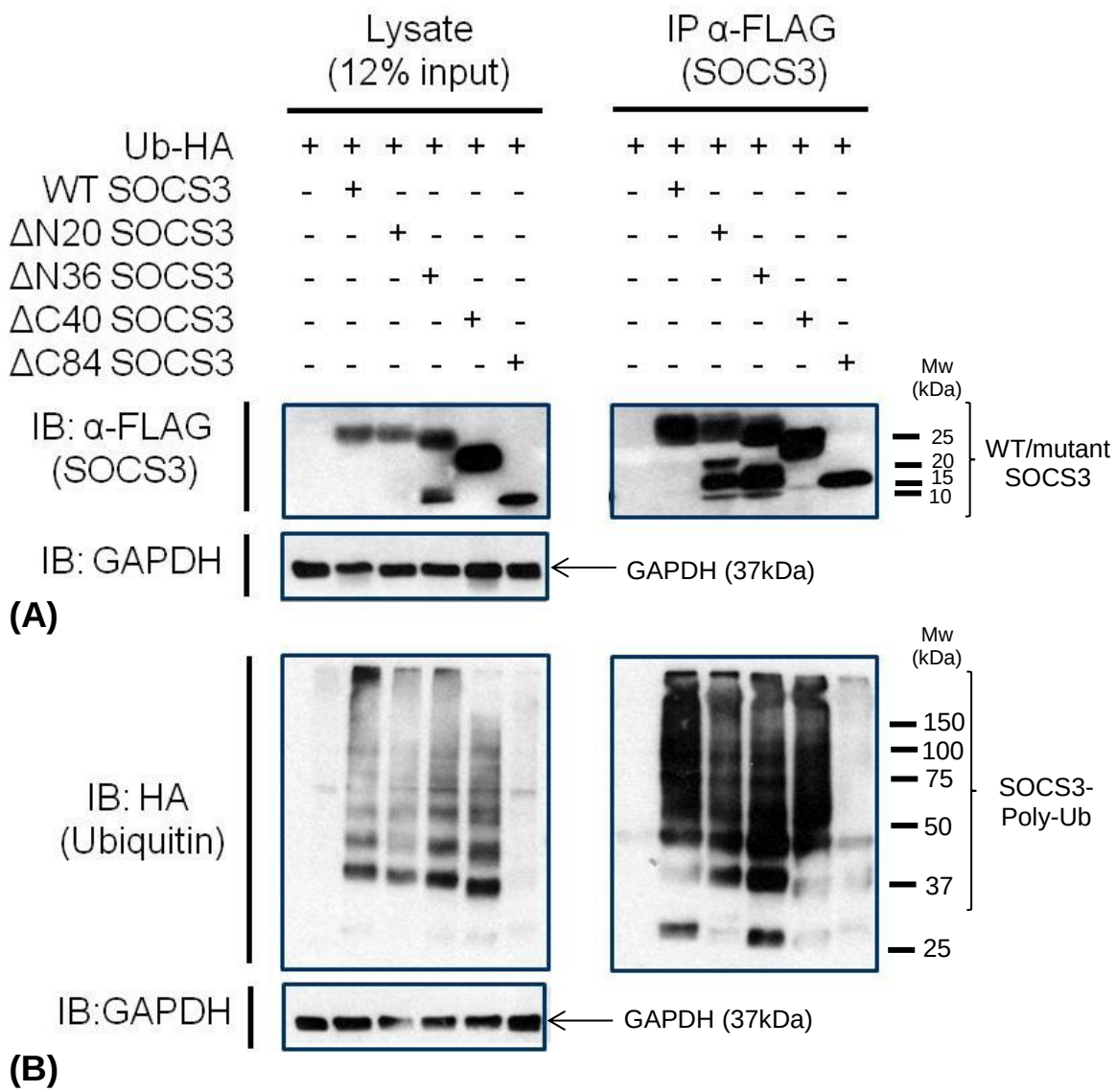

Figure 3-3: Identification of a C-terminal, 44 amino acid, region required for SOCS3 ubiquitylation

(A) Schematic showing WT SOCS3 and truncation mutant structure. The 44 amino acid peptide sequence present in *ΔC40* but not *ΔC84* is shown and the single lysine[173] present highlighted. (B) and (C) HEK293 cells were transiently transfected with 2μg FLAG tagged WT or truncated (*ΔN20, ΔN36, ΔC40, ΔC84*) SOCS3 and HA tagged Ubiquitin (Ub-HA). SOCS3 was then immunoprecipitated from lysates with anti-FLAG coated Sepharose beads. IP samples (500 μg) were split over two gels (250 μg/gel) alongside 30 μg whole cell lysate. Samples were resolved by SDS-PAGE and transferred to nitrocellulose membrane for western blotting. (B) Immunoblotting of whole cell lysates and IP SOCS3 (αFLAG) with mouse anti-FLAG (1:1000) and protein G-HRP (1:1000) to detect FLAG tagged SOCS3. (C) Immunoblotting of whole cell lysates and IP SOCS3 with rabbit anti-HA (1:1000) with anti-rabbit IgG-HRP (1:1000) secondary antibody to detect HA tagged ubiquitin. Membranes were then stripped and probed with mouse anti-GAPDH (1:20,000) and anti-mouse IgG-HRP to provide a loading control. Molecular weights (Mw) in kDa are shown. The upper bands in (C) represented poly-ubiquitin chains. Deletion of 84 residues in the C-terminus of SOCS3 (*ΔC84*) resulted in a loss of ubiquitination and identified an important 44 amino acid region of SOCS3 involved in ubiquitination. The experiment was repeated to N=3 and representative data shown.

3.2.4 Investigating the potential for SOCS3 to auto-ubiquitylate

Auto-ubiquitylation of SOCS3 would require the formation of an E3 ligase complex at the C-terminal SOCS box involving Elongin B and C (components of the E3 ligase machinery). Previously, alanine scanning identified a conserved Leucine residue (Leu189) within the SOCS3 SOCS box that was required for Elongin B and C to interact [232]. As such, the Palmer lab generated an *L189A* mutation in the C-terminal BC box of SOCS3 (Jamie Williams, University of Glasgow). To examine whether the *L189A* SOCS3 mutant could interact with Elongin B and Elongin C we co-expressed MYC-tagged Elongin B and C in the presence of FLAG-tagged WT vs. *L189A* SOCS3 in HEK293 cells. Immunoprecipitation of the WT vs. *L189A* SOCS3 mutant using anti-FLAG beads and immunoblotting for MYC tagged Elongin B and C revealed that the *L189A* mutant could not interact with the Elongins in contrast to WT SOCS3 (Figure 3-4). These data were consistent with Babon and co-workers original work that revealed Leu189 was required for Elongin interaction. Moreover, to further examine whether SOCS3 was auto-ubiquitylated, we co-expressed FLAG-tagged WT or *L189A* SOCS3 with HA-tagged ubiquitin in HEK293 cells (Figure 3-5). Immunoprecipitation of SOCS3 using anti-FLAG beads and immunoblotting for HA-tagged ubiquitin revealed that the *L189A* SOCS3 mutant was ubiquitylated similar to the WT (Figure 3-5). The *ΔC84* SOCS3 truncation was included as a negative control for no ubiquitylation and was again comparable to the HA ubiquitin only lane (Figure 3-5 B). The L189A mutant failed to interact with Elongin B and C (Figure 3-4) but otherwise contained all the necessary Lys residues intact for ubiquitylation to proceed (Figure 3-5 B). Densitometry analysis confirmed that L189A mutated SOCS3 was polyubiquitylated similar to WT SOCS3 ($P > 0.05$) (Figure 3-5 C). Together these data suggested that SOCS3 was not auto-ubiquitylated and that an external E3 ligase may regulate the ubiquitylation of SOCS3. Additionally, to assess whether the loss of ΔC84 SOCS3 mutant ubiquitylation (Figure 3-3) was due to an inability to bind components of the E3 ligase machinery, a co-IP of Elongin B and C with ΔC84 SOCS3 was performed in parallel to the WT and L189A SOCS3 mutant as above (Figure 3-4). Similar to the L189A SOCS3 mutant, the ΔC84 SOCS3 mutant was unable to interact with Elongin B and C in HEK293 cells (Figure 3-4). Though ΔC84 SOCS3 could no longer interact with the Elongins, the fact that the ΔC40 SOCS3 mutant was ubiquitylated despite the deletion of the SOCS box (aa186-225) suggested that formation of the E3 ligase complex on SOCS3 was not required for ubiquitylation and therefore SOCS3 was not auto-ubiquitylated.

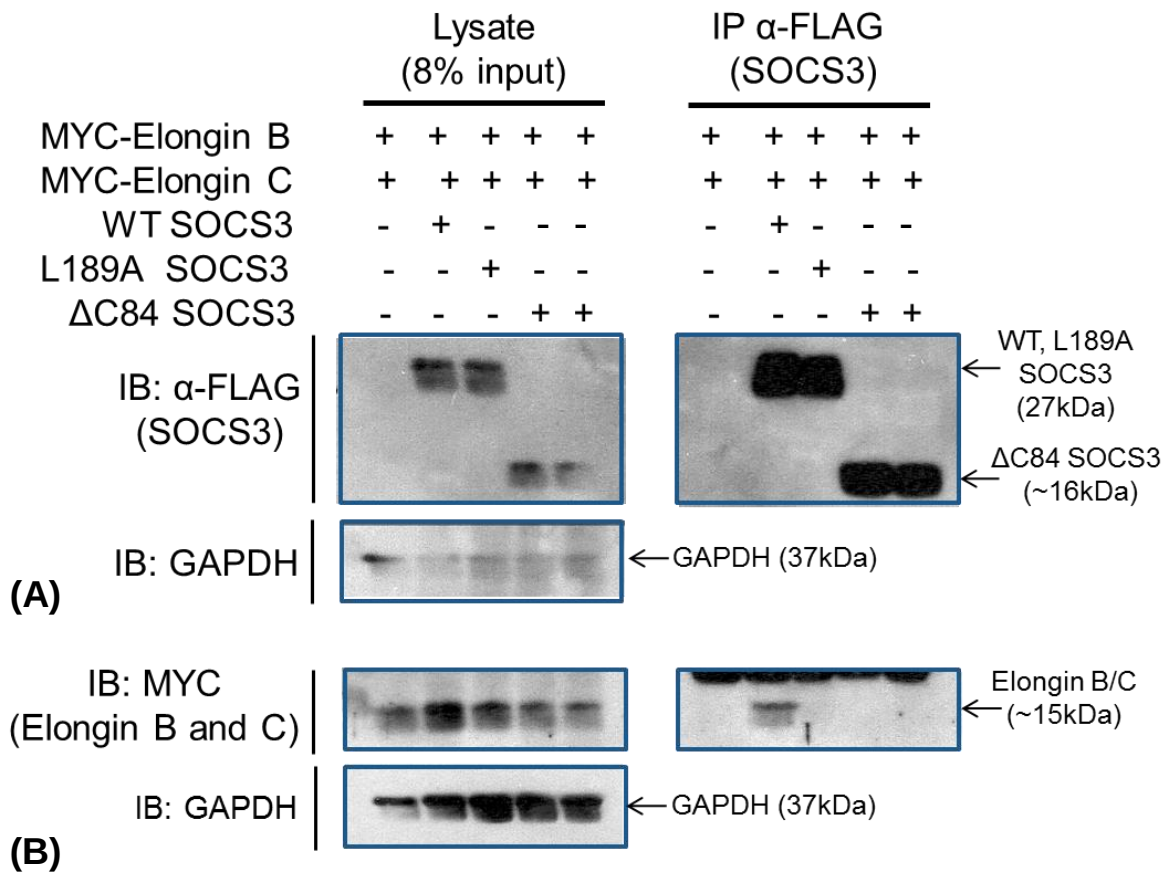

Figure 3-4: Effect of the L189A point mutation and ΔC84 truncation on SOCS3 ubiquitylation

HEK cells were transiently transfected with 2µg FLAG tagged WT or mutant (L189A, ΔC84) SOCS3 and MYC tagged Elongin B and Elongin C. SOCS3 was then immunoprecipitated from lysates with anti-FLAG coated Sepharose beads. IP samples (500 µg) were split over two gels (250 µg/gel) alongside 20 µg whole cell lysate. Samples were resolved by SDS-PAGE and transferred to nitrocellulose membrane for western blotting. (A) Immunoblotting of whole cell lysates and IP SOCS3 (αFLAG) with mouse anti-FLAG (1:1000) and protein G-HRP (1:1000) to detect FLAG tagged SOCS3. (B) Immunoblotting of whole cell lysates and IP SOCS3 with mouse anti-MYC (1:1000) with anti-mouse IgG-HRP (1:1000) secondary antibody to detect MYC tagged Elongin B and C. Membranes were then stripped and probed with mouse anti-GAPDH (1:20,000) and anti-mouse IgG-HRP to provide a loading control. WT SOCS3 interacted with Elongin B and C in contrast to the L189A and ΔC84 mutants which could no longer interact with the MYC tagged Elongin B and C. The experiment was repeated to N=3 and representative data shown.

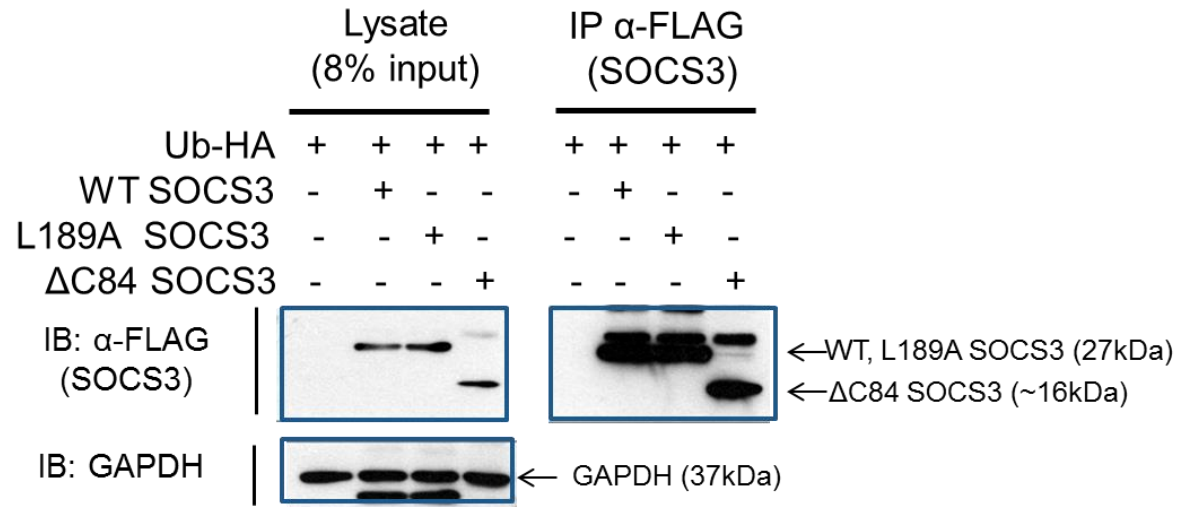

(A)

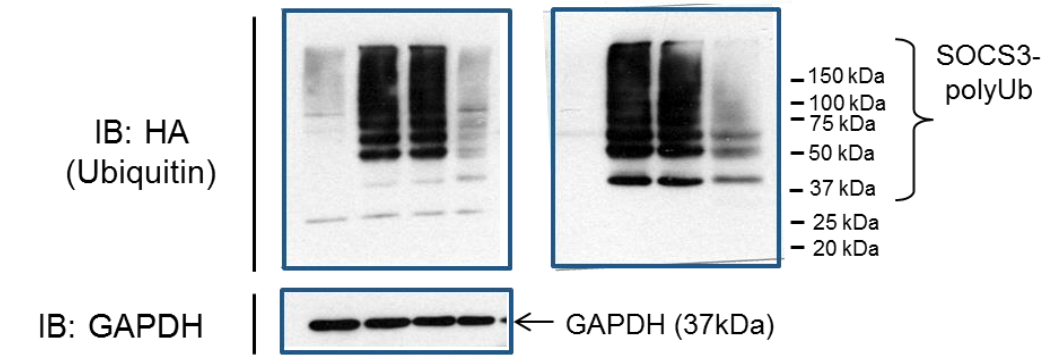

(B)

Figure 3-5: The SOCS3 (L189A) SOCS box mutant was ubiquitylated in contrast to the ΔC84 mutant

(Continued overleaf)…

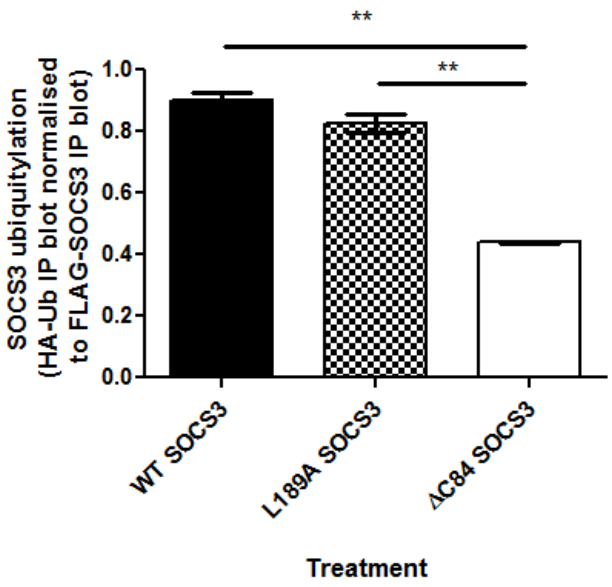

(C)

Figure 3-5: The SOCS3 (L189A) SOCS box mutant was ubiquitylated in contrast to the ΔC84 mutant HEK293 cells were transiently transfected with 2µg FLAG tagged WT or mutant (L189A, ΔC84)SOCS3 and HA tagged Ubiquitin (Ub-HA). SOCS3 was then immunoprecipitated from lysates with anti-FLAG coated Sepharose beads. IP samples (500 µg) were split over two gels (250 µg/gel) alongside 20 µg whole cell lysate. Samples were resolved by SDS-PAGE and transferred to nitrocellulose membrane for western blotting. (A) Immunoblotting of whole cell lysates and IP SOCS3 (αFLAG) with mouse anti-FLAG (1:1000) and protein G-HRP (1:1000) to detect FLAG tagged SOCS3. (B) Immunoblotting of whole cell lysates and IP SOCS3 with rabbit anti-HA (1:1000) with anti-rabbit IgG-HRP (1:1000) secondary antibody to detect HA tagged ubiquitin. Membranes were then stripped and probed with mouse anti-GAPDH (1:20,000) and anti-mouse IgG-HRP to provide a loading control. The upper bands in (B) represented poly-ubiquitin chains. (C) Densitometry analysis was performed using Total lab by normalising SOCS3 polyubiquitylation (Ub-HA blot) to the amount of SOCS3 present in the FLAG-SOCS3 IP blot. The data were presented as mean ± SEM. One-way ANOVA with Bonferroni correction was performed using GraphPad software where $P < 0.05$ was deemed significant. ** $P < 0.001$ (C) There was a significant decrease in ΔC84 SOCS3 polyubiquitylation ($P < 0.001$) when compared to WT and L189A SOCS3. The experiment was repeated to N=3 and representative data shown.

3.2.5 Investigating whether Lys173 is a key site of SOCS3 ubiquitylation

Having isolated a C-terminal region of SOCS3 (aa142-185) that was required for ubiquitylation (Figure 3-3), sequence analysis identified only one potential ubiquitylation site (Lys173) within this region. To determine whether Lys173 (K173) was a key site for SOCS3 ubiquitylation, and therefore turnover, we generated a FLAG-tagged *K173R* SOCS3 mutant and co-expressed the construct with HA-tagged ubiquitin in HEK293 cells in parallel with WT SOCS3 as described in Figure 3-1. Immunoprecipitation of the WT vs. *K173R* SOCS3 mutant with anti-FLAG beads and immunoblotting for HA tagged ubiquitin confirmed both were poly-ubiquitylated as shown by the immunoreactive laddering consistent with the addition of ubiquitin chains (Figure 3-6 B). Negative controls for ubiquitylation were provided by the *ΔC84* SOCS3 truncation and the HA-ubiquitin only lanes which revealed no poly-ubiquitin chains (Figure 3-6 B). Densitometry analysis revealed that there was a significant reduction in K173R SOCS3 ubiquitylation when compared to WT SOCS3 (Figure 3-6 C). We concluded that K173 may provide a key site of ubiquitylation for SOCS3 and therefore regulate its turnover.

3.2.6 Emetine treatment to assess the role of Lys173 on SOCS3 protein stability

Though a significant decrease in the ubiquitylation of the *K173R* SOCS3 mutant was observed (Figure 3-6 C), it was important to assess if this mutant was still turned over at the proteasome and whether loss of K173 altered the stability of SOCS3. To establish the role of K173 in controlling SOCS3 stability, we expressed FLAG-tagged WT or *K173R* SOCS3 in SOCS3 KO MEFs. The cells were stimulated with a protein synthesis inhibitor, Emetine, for the indicated time points (0-8 hrs). A positive control in which cells were treated with Emetine plus MG132 was included to confirm the proteasome was the major route of degradation. Immunoblotting for FLAG-tagged SOCS3 confirmed that turnover of the *K173R* mutant was comparable to the WT SOCS3 turnover (Figure 3-7 A-B). Both WT and *K173R* SOCS3 expression decreased gradually over time and expression was abolished following 8 hrs Emetine treatment (Figure 3-7 A and B). With the exception of the 2 hr time point, there was no statistically significant change in stability ($P>0.05$) between WT and *K173R* SOCS3 (Figure 3-7 C). From these data, we concluded that Lys 173 was not a key regulator of SOCS3 stability in a mouse fibroblast cell line.

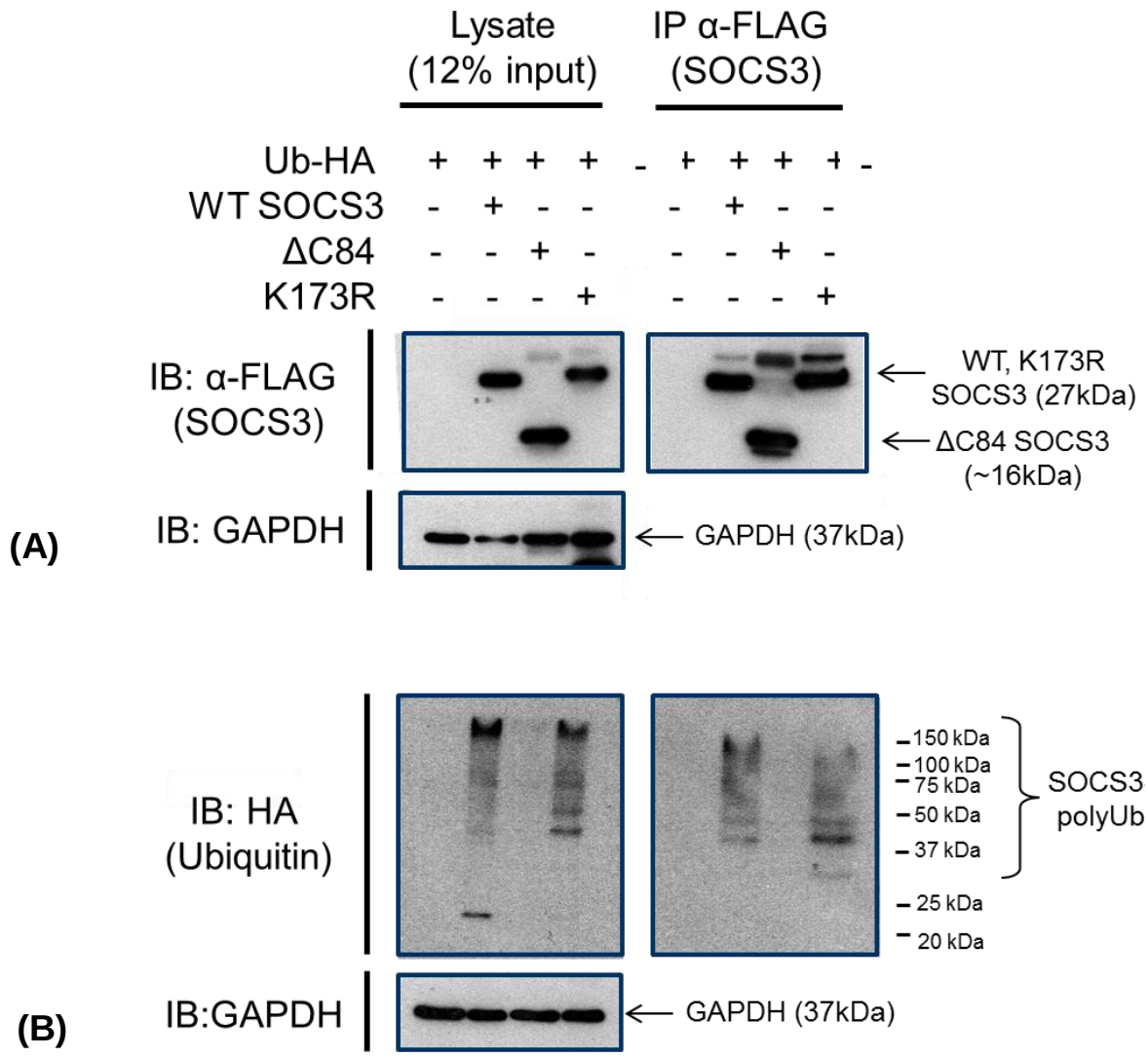

Figure 3-6: SOCS3 K173R mutant was subject to poly-ubiquitylation *(Continued overleaf)…*

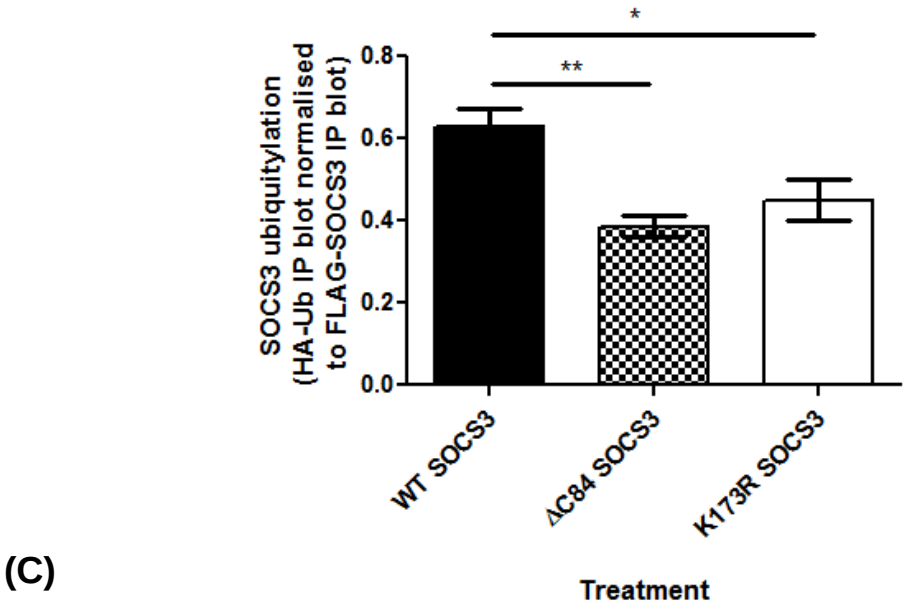

(C)

Figure 3-6: SOCS3 K173R mutant was subject to poly-ubiquitylation

HEK293 cells were transiently transfected with 2µg FLAG tagged WT, or K173R SOCS3 and HA tagged Ubiquitin (Ub-HA). SOCS3 was then immunoprecipitated from lysates with anti-FLAG coated Sepharose beads. Lysates (30 µg) and IP samples (500 µg) were resolved by SDS-PAGE and transferred to nitrocellulose membrane. (A) Rabbit anti-SOCS3 (1:1000) was used in western blotting with anti-rabbit IgG-HRP (1:1000) secondary antibody. (B) Membranes were then stripped and probed with rabbit anti-HA (1:1000) with anti-rabbit IgG-HRP (1:1000) secondary antibody. After a final strip membranes were probed with mouse anti- GAPDH (1:20,000) and anti-mouse IgG-HRP to provide a loading control. The upper bands in (B) represented poly-ubiquitination chains. (C) Densitometry analysis was performed using Total lab by normalising SOCS3 polyubiquitylation (Ub-HA blot) to the amount of SOCS3 present in the FLAG-SOCS3 IP blot. The data were presented as mean ± SEM. One-way ANOVA with Bonferroni correction was performed using GraphPad software where $P < 0.05$ was deemed significant. * $p<0.05$ and ** $p<0.001$ (C) There was a significant decrease in K173R SOCS3 polyubiquitylation when compared to WT SOCS3 ($P < 0.05$). There was also a significant reduction in ΔC84 ubiquitylation when compared to WT SOCS3 ($p< 0.001$). These data suggested that Lys 173 was a key site of SOCS3 polyubiquitylation in HEK293 cells. The experiment was repeated to N=4 and representative data shown.

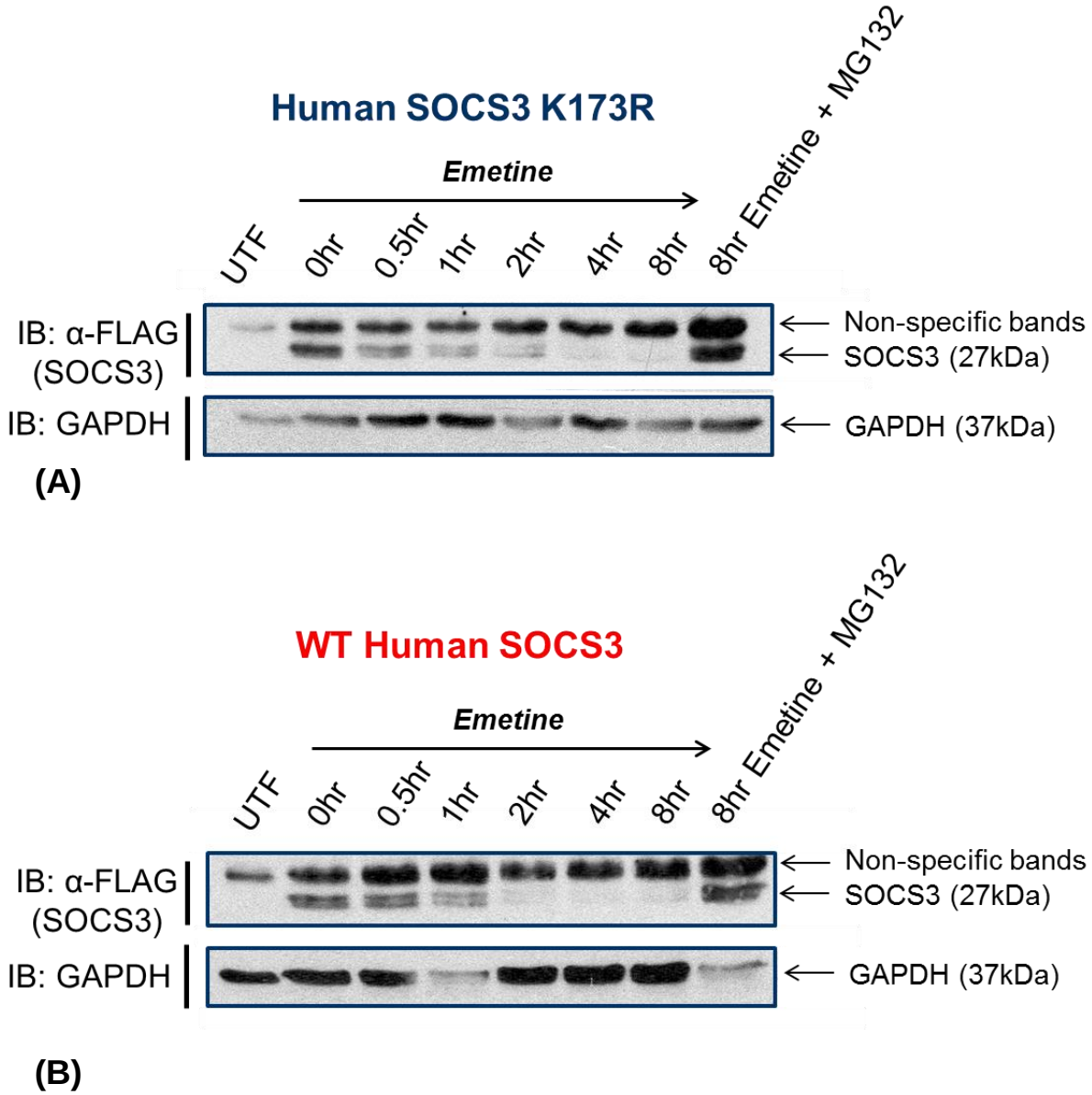

Figure 3-7: K173R SOCS3 mutant was not more stable than the WT SOCS3 *(Continued overleaf).*

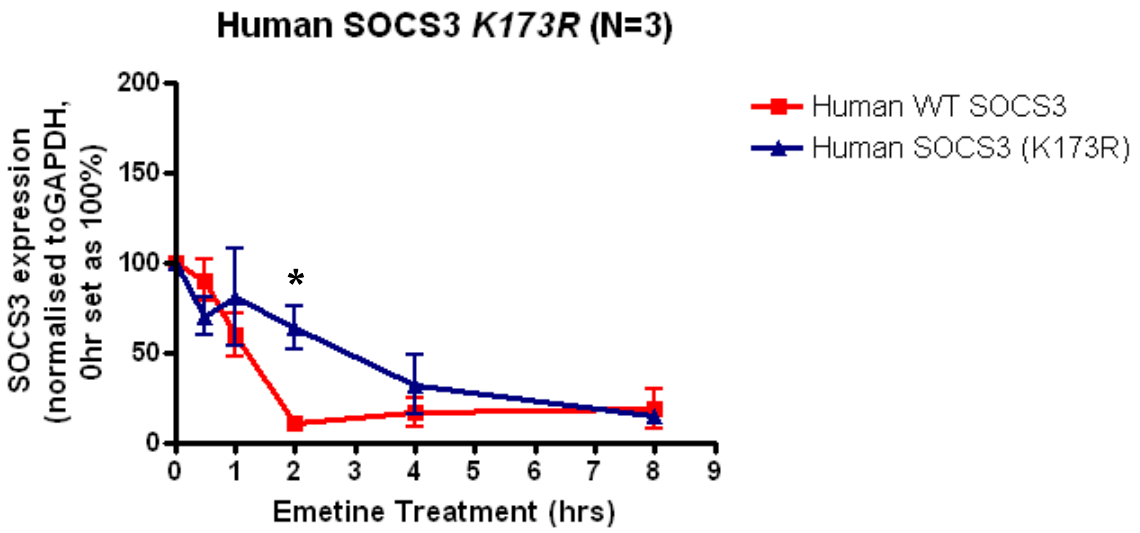

(C)

Figure 3-7: K173R SOCS3 mutant was not more stable than the WT SOCS3 8 hrs post emetine treatment

HEK293 cells were seeded in 10 cm dishes and transfected with 10µg FLAG tagged WT human SOCS3 or K173R mutant the following day. 24 hrs post transfection, cells were trypsinised and split into 7 wells of 2 x 6 well plates. 48 hrs post transfection, cells were then stimulated with ±Emetine (100 µM) ±MG132 (6 µM) for the indicated time (0-8 hrs). (A-B) Whole cell lysates were resolved via SDS-PAGE and immunoblot analysis performed with anti-FLAG and anti- GAPDH. Representative image shown (N=3). (C) Densitometry analysis was performed using Total lab by normalising SOCS3 expression to GAPDH. The data were presented as mean ± SEM % SOCS3 remaining where the 0 hr time point was set to 100%. Student's t-test (2-tailed, un-paired) was performed at each time point where $P<0.05$ was deemed significant. The *K173R* SOCS3 was significantly more stable than WT SOCS3 at the 2 hr time point only.

3.2.7 Mapping the sites of SOCS3 ubiquitylation via LC-MS-MS

The issue of redundancy proved challenging to assign the sites of ubiquitylation via SOCS3 mutagenesis. Thus to identify putative acceptor Lys residues of ubiquitin on SOCS3 LC-MS-MS analysis was employed. FLAG tagged WT SOCS3 or pcDNA3.1 was overexpressed in HEK293 cells and a co-IP of SOCS3 was performed using anti-FLAG beads. The SOCS3 or pcDNA3.1 control eluate was subsequently prepared for LC-MS-MS analysis at the Beatson Institute (Dr David Sumpton). To identify putative sites of ubiquitylation on SOCS3 the LC-MS-MS data were searched for the presence of a Gly-Gly doublet (+114 Da mass shift) through Mascot and MaxQuant software. Table 3-1 summarises the peptide fragments containing the ubiquitylated lysine residues and the position of these modified sites (K^{23}, K^{28}, K^{40}, K^{85}, K^{91}, K^{173}, K^{195} and K^{206}). A mass shift of +114 Da was identified at K^{23} by the MaxQuant analysis only and similarly K^{91} was identified by the Mascot analysis only (Table 3-1). K^{40} was identified as ubiquitylated by both software packages however the scores were relatively low (Table 3-1).

The schematic in Figure 3-8 A illustrated the location of the lysine ubiquitylation sites as defined by the LC-MS-MS data in Table. K^{23} and K^{28} were located in the KIR domain, K^{40}, K^{85}, K^{91} and K^{173} in the SH2 domain and finally K^{195} andK^{206} were located in the c-terminal SOCS box region (Figure 3-8 A). Figure 3-8 B outlined the process by which ubiquitin was cleaved following trypsin digestion, leaving the Gly-Gly doublet which is identified as a +114 Da mass shift. Figure 3-8 C shows an example MS/MS spectrum of the peptide AYYIYSGGEKIPLVLSR that was ubiquitylated on Lys173 of SOCS3. The mass shift of +114 Da (below y8, blue and below b10, red) was computed by comparing the mass of each lysine against an unmodified lysine (data not shown). The LC-MS-MS analysis did not identify Lys6 as a key site of ubiquitylation on SOCS3 (Figure 3-8) and was consistent with previous investigations that showed the *K6Q* SOCS3 mutant was not resistant to ubiquitylation in HEK293 cells (Figure 3-1). These data confirmed that no single Lys residue was ubiquitylated and therefore regulates SOCS3 stability in HEK293 cells (Figure 3-8). Functional redundancy exists for the attachment of ubiquitin to target Lys residues on SOCS3 (Figure 3-8).

Lysine site	Peptide ID Sequence	Mascot Ion score	MaxQuant P-score	Start position	Stop position
K^{23}	(R)LkTFSSKSEYQLVVNAVR(K)	-	112.24	22	39
K^{28}	(R)LKTFSSkSEYQLVVNAVR(K)	63.09	154.69	22	39
K^{28}	(K)TFSSkSEYQLVVNAVR(K)	62.53	193.31	24	39
K^{40}	(R)kLQESGFYWSAVTGGEANLLLSAEPAGTFLIR(D)	34.28	73.361	40	71
K^{85}	(R)HFFTLSVkTQSGTK(N)	69.19	153.14	78	91
K^{91}	(R)HFFTLSVKTQSGTkNLR(I)	36.39	-	78	94
K^{173}	(K)RAYYIYSGGEkIPLVLSR(P)	54.7	130.27	163	180
K^{173}	(R)AYYIYSGGEkIPLVLSR(P)	58.87	148.36	164	180
K^{195}	(R)kTVNGHLDSYEK(V)	60.98	186.51	195	206
K^{206}	(K)TVNGHLDSYEkVTQLPGPIR(E)	46.6	84.249	196	215

Table 3-1: Identifying putative sites of ubiquitylation on murine SOCS3

Scaffold 4.3.4 summarised the Lys-ε-Gly-Gly modifications identified using both Mascot and MaxQuant software. Sites identified by the peptides marked in pink should be viewed with caution; these were identified either by only one search engine or a low score or both. The peptide identifications marked in yellow appear to be of high quality and correspond to Lys173. Start and stop position denotes the location of the peptide fragment within the SOCS3 protein i.e. position along the 225 amino acid protein sequence. 8 putative sites of ubiquitylation (K^{23}, K^{28}, K^{40}, K^{85}, K^{91}, K^{173}, $K^{195}$and K^{206}) were identified though Lys173 provided the most reliable data suggesting ubiquitylation.

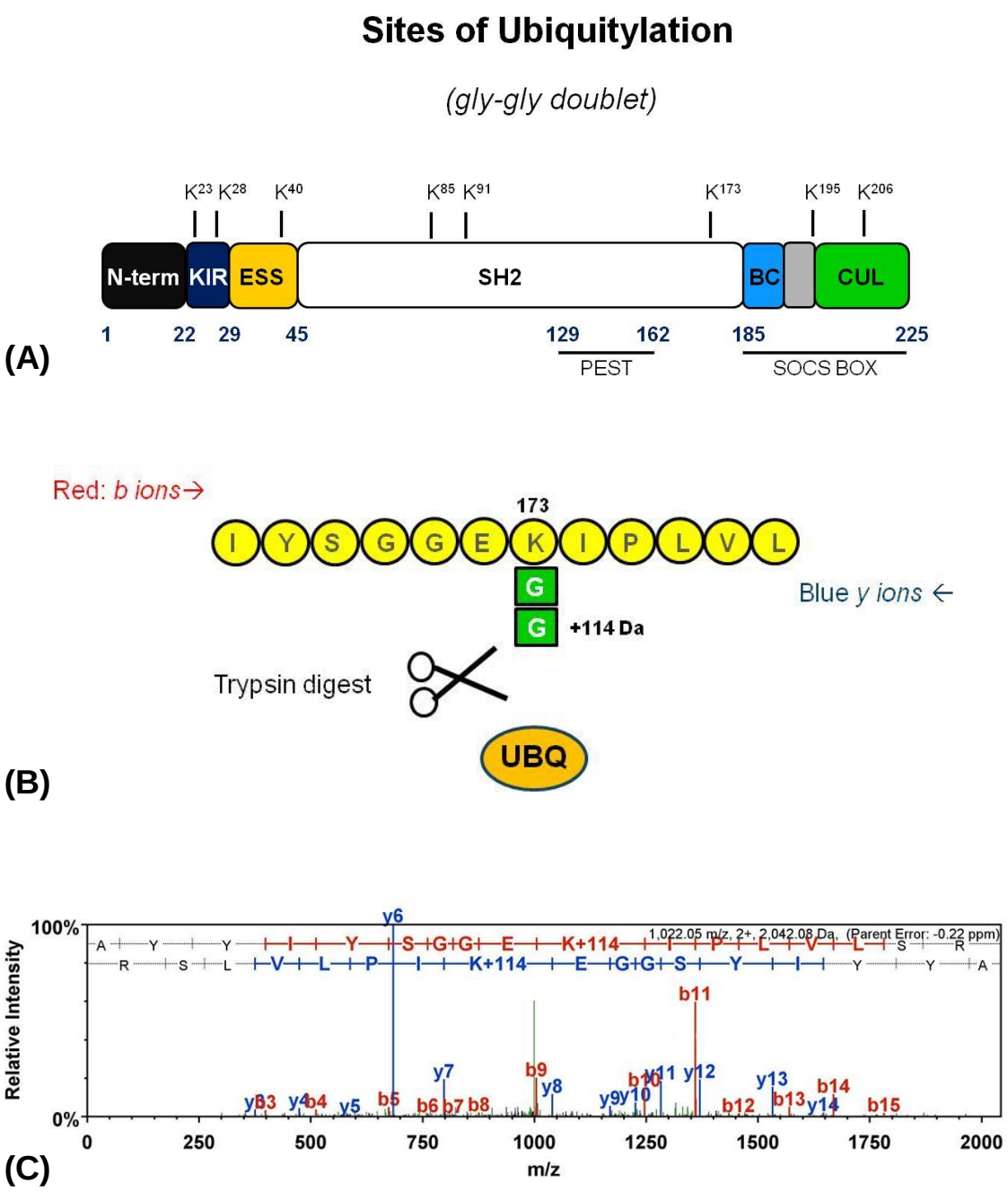

Figure 3-8: The identification of ubiquitylation sites on murine SOCS3

The LC-MS/MS data were searched for a glycine-glycine signature at each individual lysine (K) to identify specific sites of ubiquitin modification. (A) Schematic depicting the sites of ubiquitylation on SOCS3 identified. (B) Following trypsin digestion, ubiquitin is cleaved leaving a Gly-Gly doublet with a mass shift of + 114 Da. The MS/MS analyser reads the peptide fragment from left to right (red) and right to left (blue). (C) Example MS/MS spectrum of peptide AYYIYSGGEKIPLVLSR ubiquitylated on Lys173 of SOCS3. Following trypsin digestion the remnant signature (Lys-ε-Gly-Gly) remains at the site of ubiquitylation as the poly-ubiquitin chain is cleaved. The result is a mass shift of +114 Da compared to the other unmodified Lys residues. Charged peptide fragments retained within the MS analyser are denoted b if charge retained on N terminus (red) and y if charge retained on C terminus (blue) of the fragment. m/z denotes the mass:charge ratio. A mass shift of +114 Da was observed at Lys173 on this peptide indicating ubiquitylation. Figure in (A) adapted from [49].

3.2.8 Characterisation of a Lysine-less SOCS3 mutant

3.2.8.1 Investigating the ubiquitylation status of a Lysine-less SOCS3 mutant

Poly-ubiquitylation of a target Lysine residue(s) marks a protein for degradation at the 26S proteasome. LC-MS-MS analysis confirmed that functional redundancy exists for the attachment of ubiquitin to target Lys residues on SOCS3 (Figure 3-8). As such, we hypothesised that mutation of all 10 Lys residues (Lys → Arg) to generate a so-called "Lys-less" SOCS3 would provide a SOCS3 mutant that was resistant to ubiquitylation and proteasomal degradation while potentially maintaining functionality in terms of its capacity to inhibit JAK-STAT signalling. The Lys-less SOCS3 construct contained a FLAG-tagged SOCS3 open reading frame (ORF) in which all 10 Lys residues were mutated to Arg, an amino acid which has the same positive charge as Lys at physiological pH but which cannot be ubiquitylated.

To determine the ubiquitylation status of the Lys-less SOCS3 we co-expressed HA tagged ubiquitin in the presence or absence of FLAG tagged WT or Lys-less SOCS3 in HEK293 cells. Immunoprecipitation of SOCS3 with anti-FLAG beads and immunoblotting for HA-tagged ubiquitin revealed that Lys-less SOCS3 was not ubiquitylated in contrast to the WT SOCS3 that was ubiquitylated (Figure 3-9 B). The negative control for ubiquitylation (HA-tagged ubiquitin only) showed no ubiquitylation on the HA-ubiquitin immunoblot and was comparable to the Lys-less SOCS3 IP (Figure 3-9 B). Densitometry analysis confirmed there was a significant reduction in Lys-less SOCS3 ubiquitylation when compared to the WT SOCS3 (Figure 3-9 C). These data were not due to a lack of Lys-less SOCS3 expression as it was detectable at comparable levels to WT in the lysates and the Flag IP (Figure 3-9 A). We therefore concluded that mutation of all 10 Lys residues within SOCS3 produced a Lys-less SOCS3 mutant that was resistant to ubiquitylation.

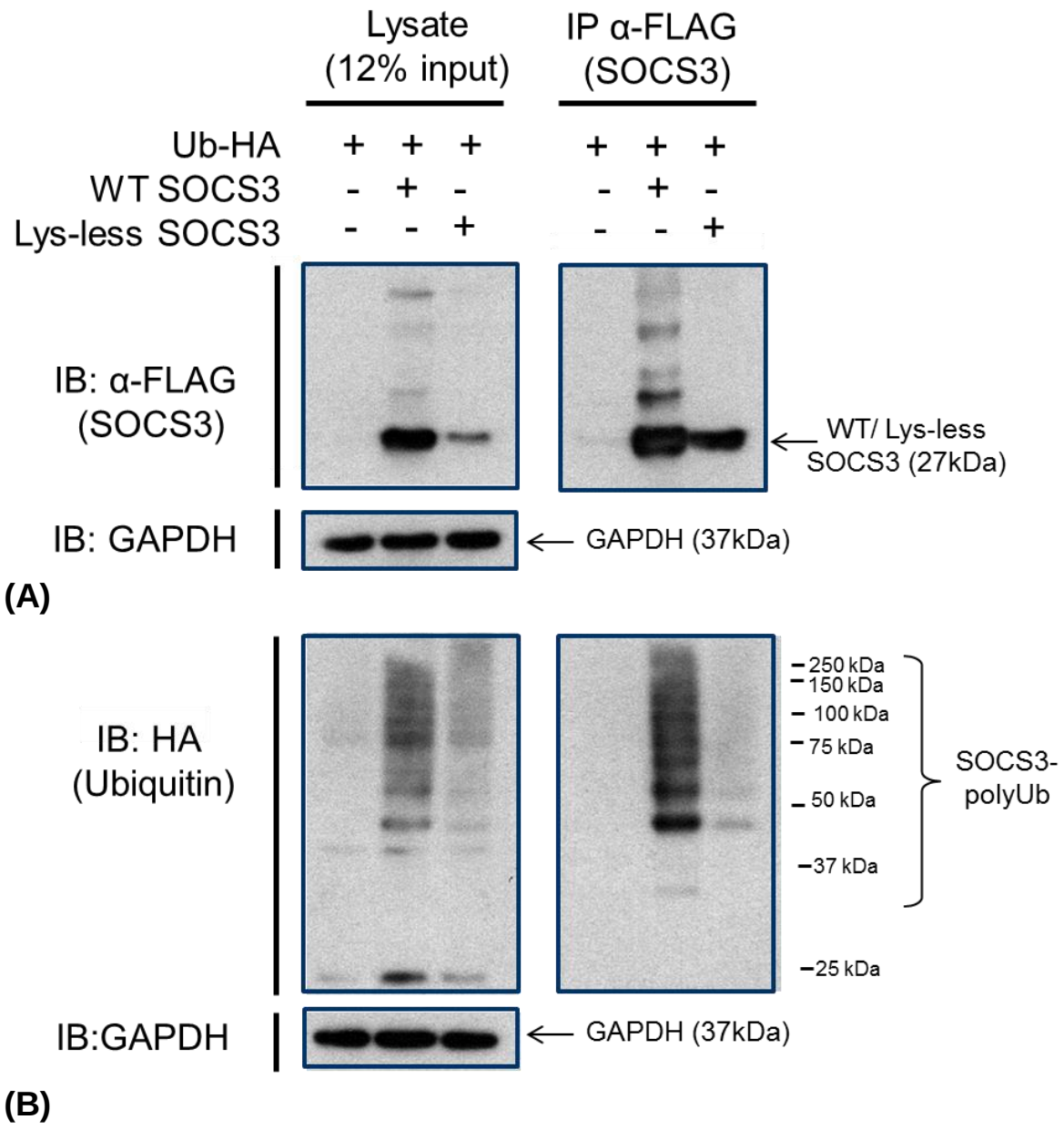

Figure 3-9: Assessing the ubiquitylation status of Lys-less SOCS3 *(Continued overleaf)…*

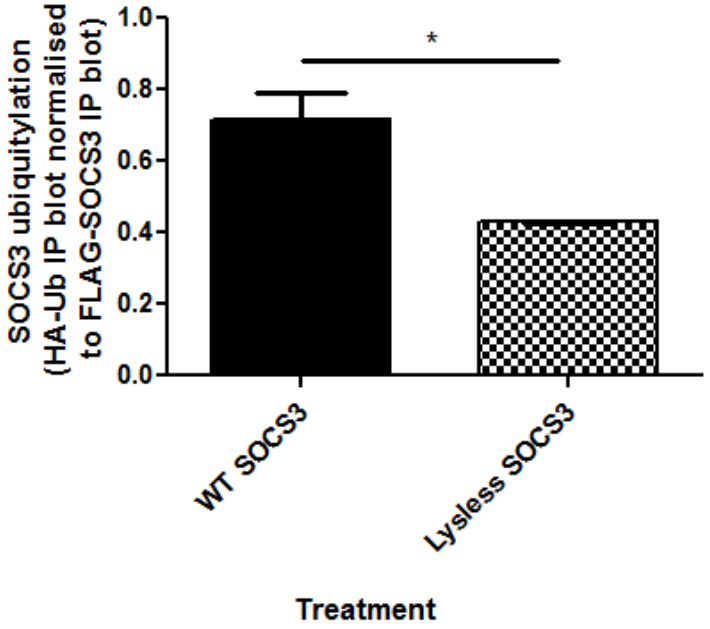

(C)

Figure 3-9: Assessing the ubiquitylation status of Lys-less SOCS3

HEK293 cells were transiently transfected with 2µg HA tagged Ubiquitin (HA-Ub); 2µg FLAG tagged WT or Lys-less SOCS3. SOCS3 was then immunoprecipitated from lysates with anti-FLAG coated Sepharose beads. IP samples (500 µg) were split over two gels (250 µg/gel) alongside 30 µg whole cell lysate. Samples were resolved via SDS-PAGE and transferred to nitrocellulose membrane for western blotting. (A) Immunoblotting of whole cell lysates and IP SOCS3 (αFLAG) with mouse anti-FLAG (1:1000) and protein G-HRP (1:1000) to detect FLAG tagged SOCS3. (B) Immunoblotting of whole cell lysates and IP SOCS3 with rabbit anti-HA (1:1000) with anti-rabbit IgG-HRP (1:1000) secondary antibody to detect HA tagged ubiquitin. Membranes were then stripped and probed with mouse anti-GAPDH (1:20,000) and anti-mouse IgG-HRP to provide a loading control. (C) Densitometry analysis was performed using Total lab by normalising SOCS3 polyubiquitylation (Ub-HA blot) to the amount of SOCS3 present in the FLAG-SOCS3 IP blot. The data were presented as mean ± SEM. Student's t-test (2-tailed, un-paired) was performed using GraphPad software where $P < 0.05$ was deemed significant. * $P < 0.05$. (C) There was a significant reduction in Lys-less SOCS3 polyubquitylation when compared to WT SOCS3 ($P < 0.05$). The experiment was repeated to N=3 and representative data shown.

3.2.8.2 Emetine treatment to the compare the stability of WT and Lys-less SOCS3

Having confirmed the Lys-less SOCS3 mutant was resistant to ubiquitylation (Figure3-9), we hypothesised that this would reduce the proteins turnover at the proteasome and therefore enhance its stability. To test this hypothesis we expressed FLAG-tagged WT or Lys-less SOCS3 in SOCS3 KO MEF cells (Figure 3-10). The cells were stimulated with a protein synthesis inhibitor, Emetine, for the indicated time points (0-8 hrs). A positive control in which cells were treated with Emetine plus MG132 was included to confirm the proteasome was the major route of degradation. Immunoblotting for FLAG-tagged SOCS3 confirmed that Emetine treatment did not lead to the downregulation of Lys-less SOCS3 protein expression in contrast to the WT SOCS3 (Figure 3-10 A-B). The Lys-less SOCS3 mutant was significantly ($P<0.05$) more stable than WT SOCS3 at the 4 and 8 hr time points (Figure 3-10 C). From these data, we concluded that loss of all 10 Lys residues within SOCS3 blocked its turnover at the proteasome and therefore significantly enhanced its stability in SOCS3 KO MEFs.

3.2.9 Functional assessment of the Lys-less SOCS3 mutant

We examined the functionality of Lys-less SOCS3 via 2 criteria i) the ability to interact with components of the E3 ligase machinery and ii) the ability to inhibit JAK/STAT signalling. First, we examined its capacity to bind the other components required to make a functional E3 ligase complex, i.e. Elongin B and Elongin C [48]. MYC tagged Elongin B and C was co-expressed with or without WT, Lys-less or *L189A* SOCS3 in HEK293 cells. Immunoprecipitation of SOCS3 with anti-FLAG beads and immunoblotting for MYC tagged Elongin B and C was then performed. The *L189A* SOCS3 mutant was previously shown not to interact with the Elongins (Figure 3-4) and was therefore included as a negative control for this experiment (Figure 3-11). In contrast to the L189A mutant, WT and Lys-less SOCS3 could both interact equivalently with the Elongins (Figure 3-11). From these data we concluded that the Lys-less SOCS3 mutant could form an E3 ligase complex at the C-terminal SOCS box, a requirement for SOCS3-mediated substrate degradation [47].

Future functional studies will involve LV mediated SOCS3 overexpression in primary vascular cells that may be difficult to transfect. Thus a Lys-less and WT SOCS3 LV was generated. To confirm the LV SOCS3 ORF was in frame and expressed well, HEK293

cells were infected with two different batches of FLAG-tagged Lys-less LV particles (Figure 3-12 A). Immunoblotting for FLAG-tagged SOCS3 confirmed that both batches (A-B) of the Lys-less SOCS3 LV expressed well in HEK293 cells at the expected molecular weight ~27kDa (Figure 3-12 A). Similarly, HEK293 cells were infected with increasing volumes of FLAG-tagged WT SOCS3 LV (Figure 3-12 B). Immunoblotting for FLAG-tagged SOCS3 confirmed that the WT SOCS3 LV expressed well in HEK293 cells at the expected molecular weight ~27kDa and that increasing the volume of virus infected (20-40 µl) was associated with an increase in SOCS expression (Figure 3-12 B). These data confirmed that the Lys-less and WT SOCS3 LV particles express well however virus titres must be calculated prior to use for future investigations.

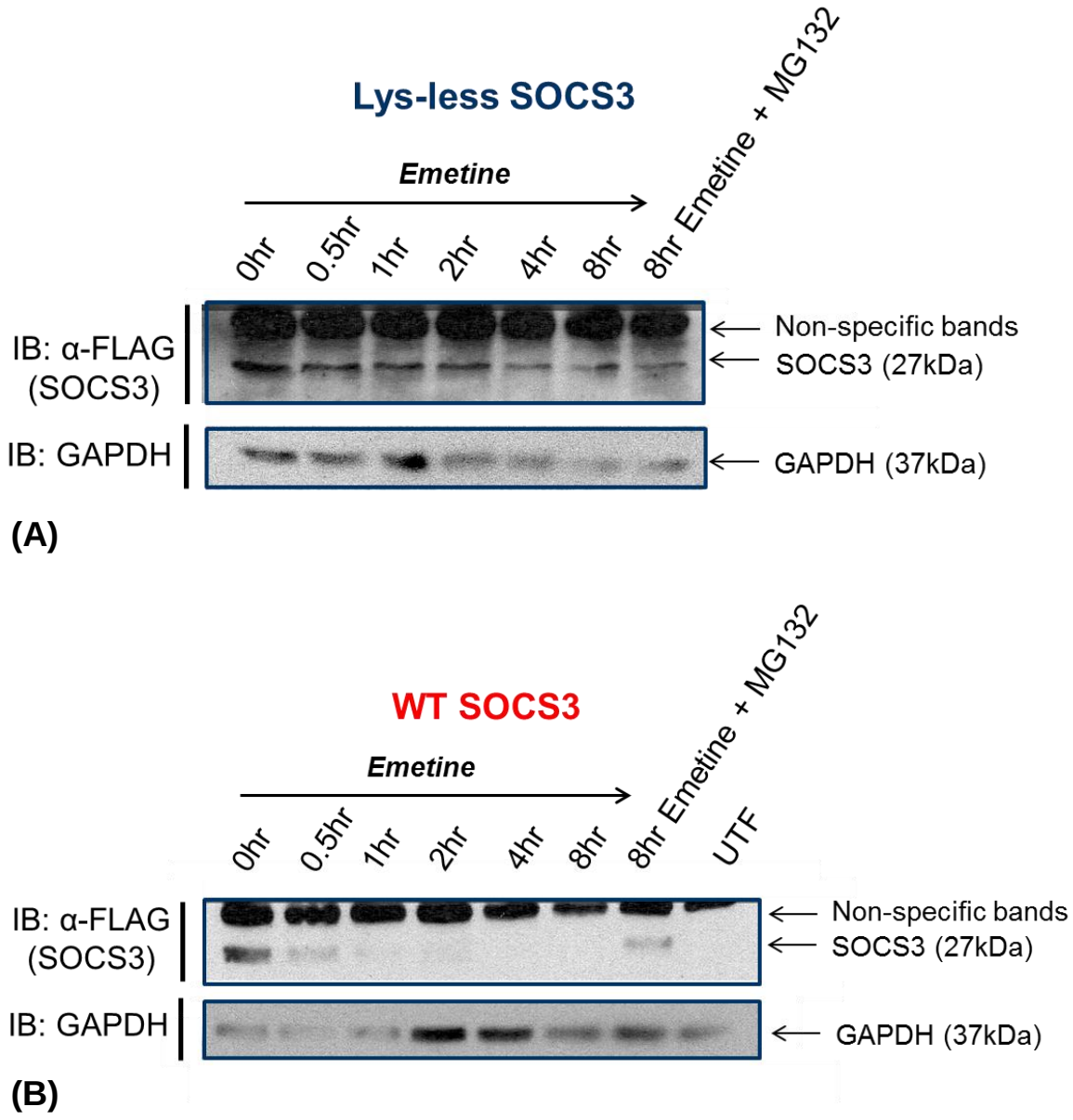

Figure 3-10: Lys-less human SOCS3 was more stable than WT SOCS3. *(Continued overleaf…)*

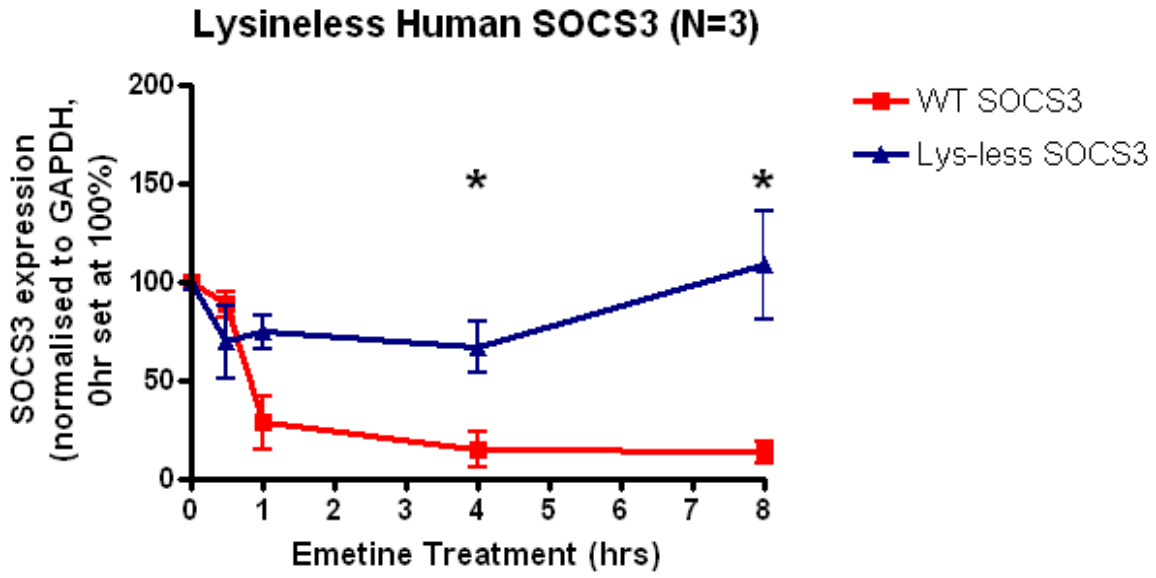

(C)

Figure 3-10: Lys-less human SOCS3 was more stable than WT SOCS3.

HEK293 cells were seeded in 10cm^2 dishes and transfected with 10µg FLAG tagged WT human SOCS3 or Lys-less mutant the following day. 24 hrs post transfection, cells were trypsinised and split into 7 wells of 2 x 6 well plates. 48hrs post transfection, cells were then stimulated with ±Emetine (100 µM) and ±MG132 (6 µM) for the indicated time (0-8hrs). (A-B) Whole cell lysates were resolved via SDS-PAGE and immunoblot analysis performed with anti-FLAG and anti- GAPDH. Representative image shown (N=3). (C) Densitometry analysis was performed using Total lab by normalising SOCS3 expression to GAPDH. The data were presented as mean ± SEM % SOCS3 remaining where the 0 hr time point was set to 100%. Student's t-test (2-tailed, un-paired) was performed at each time point where * $P < 0.05$ was deemed significant. The 2 hr time point (outlier) was removed for illustration. The Lys-less SOCS3 mutant was significantly more stable than WT SOCS3 at the 4hr and 8hr time points.

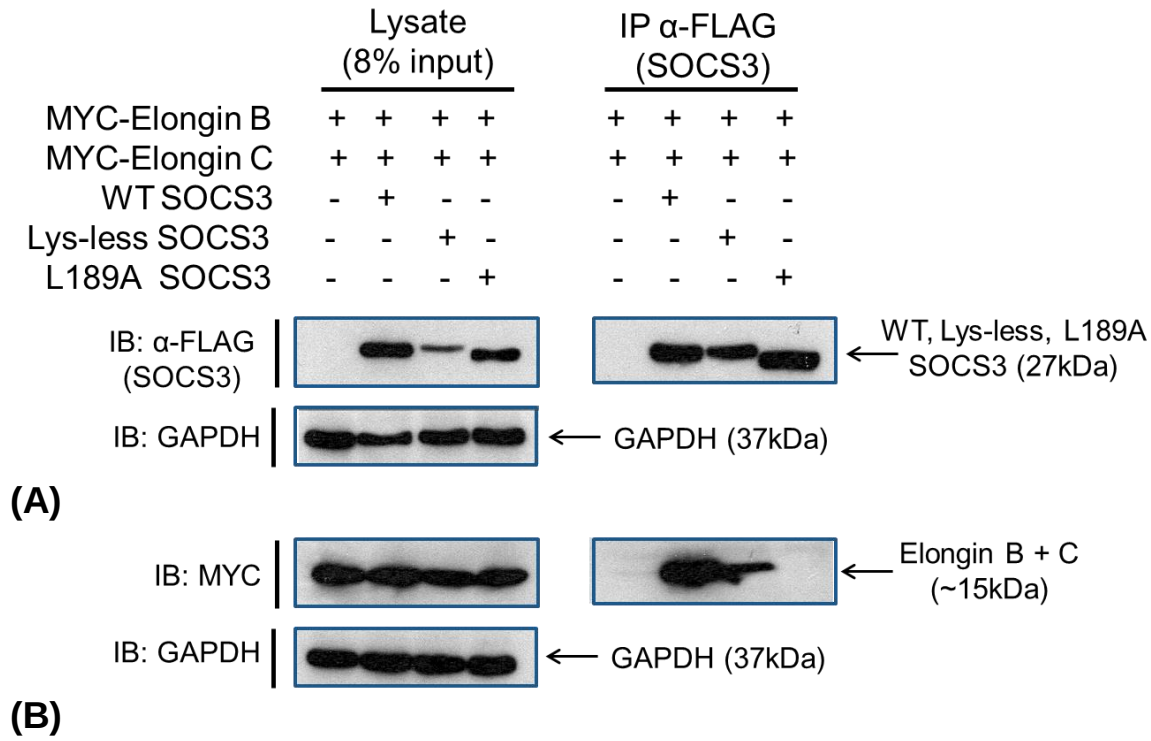

Figure 3-11: Lys-less SOCS3 interacts with components of the E3 ligase machinery.

HEK293 cells were transiently transfected with 2 µg FLAG tagged WT or mutant (L189A, lys-less) SOCS3 and MYC tagged Elongin B and Elongin C. SOCS3 was then immunoprecipitated from lysates with anti-FLAG coated Sepharose beads. IP samples (500 µg) were split over two gels (250 µg/gel) alongside 30 µg whole cell lysate. Samples were resolved by SDS-PAGE and transferred to nitrocellulose membrane for western blotting. (A) Immunoblotting of whole cell lysates and IP SOCS3 (αFLAG) with mouse anti-FLAG (1:1000) and protein G-HRP (1:1000) to detect FLAG tagged SOCS3. (B) Immunoblotting of whole cell lysates and IP SOCS3 with mouse anti-MYC (1:1000) with anti-mouse IgG-HRP (1:1000) secondary antibody to detect MYC tagged Elongin B and C. Membranes were then stripped and probed with mouse anti-GAPDH (1:20,000) and anti-mouse IgG-HRP to provide a loading control. WT and Lys-less SOCS3 interacted with Elongin B and C in contrast to the L189A mutant which could no longer interact with the MYC tagged Elongin B and C. The experiment was repeated to N=3 and representative data shown.

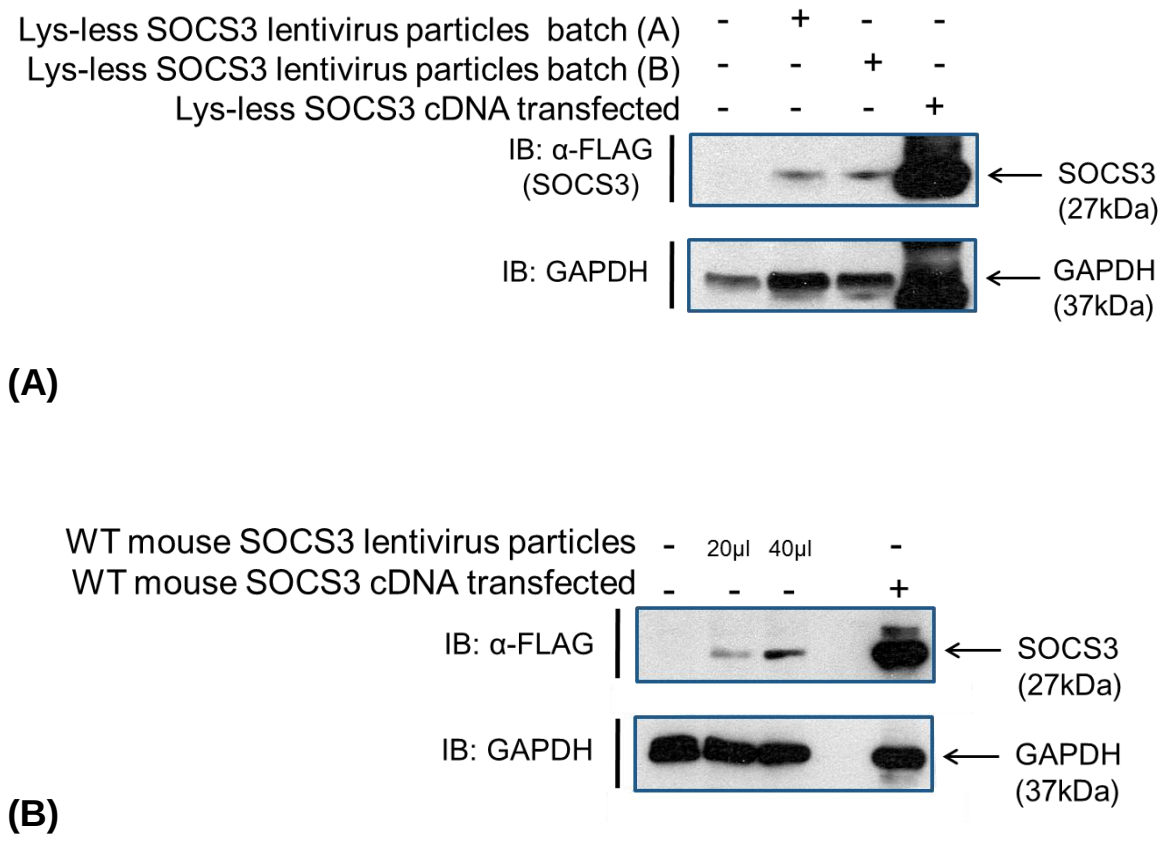

Figure 3-12: Generation of a WT SOCS3 and Lys-less LV

HEK293 cells were infected with 20 µl Lys-less human SOCS3 LV particles (batch A or B) or transfected with or without 4 µg Lys-less human SOCS3 LV cDNA construct for 48 hrs. (B) HEK293 cells were infected with 20-40 µl WT mouse SOCS3 LV particles or transfected with or without 4 µg WT mouse SOCS3 LV construct for 48 hrs. Prior to harvesting, cells were treated with 6 µM MG132 for 2 hours and cell lysates were then prepared for immunoblotting with mouse anti-FLAG (1:1000) and IgG-HRP. Membranes were then stripped and probed with mouse anti-GAPDH (1:20,000) and IgG-HRP to provide a loading control. The Lys-less and WT SOCS3 LV expressed well in HEK293 cells at the expected molecular weight ~27kDa.

3.2.10 Developing a method to assess SOCS3 function

3.2.10.1 Optimising the sensitivity of the Epo/Gp130 chimeric receptor (Epo/Gp130R) assay to measure SOCS3 functionality

The Epo/Gp130R chimera is composed of the extracellular ligand binding domain of the EpoR fused to the trans-membrane and cytoplasmic/signalling domain of the Gp130R as described previously [58]. To assess the function of SOCS3, we optimised the existing Epo/Gp130R assay described by Schmitz *et al*. [58]. Briefly, overexpression of the chimeric receptor and stimulation with Epo led to the induction of a Gp130R response within the cell [58]. As such, measuring the ability of SOCS3 to inhibit STAT3 activation (P-STAT3 at Y705) would provide a readout of SOCS3 activity. Immunoblot analysis using a phospho-specific STAT3 (Y705) antibody was used to confirm the status of STAT3 activation.

Optimisation of the Epo stimulation was initially performed by expressing the Epo/Gp130R in HEK293 cells and stimulating with Epo (50-500 ng/ml) for 15 mins prior to harvesting (Figure 3-13 A). Immunoblotting for P-STAT3(Y705) and total STAT3 confirmed Epo treatment induced STAT3 phosphorylation at 50-500 ng/ml in contrast to vehicle treatment groups which failed to induce P-STAT3 (Figure 3-13A). As a positive control for P-STAT3 immunoblotting, a JAK1 construct was expressed in HEK293 cells and stimulated with 30,000 units IFNα leading to the induction of P-STAT3 (Figure 3-13A).

To investigate the minimum concentration of WT SOCS3 required to inhibit P-STAT3, WT or mutant (*Y759F*) Epo/Gp130R was co-expressed with FLAG tagged WT SOCS3 (0-2 μg) in HEK293 cells (Figure 3-13 B-G). At 2 μg SOCS3, complete inhibition of P-STAT3 was observed (Figure 3-13). Titration of SOCS3 down to 0.005 μg, also demonstrated complete inhibition of P-STAT3 (1:400 ratio of SOCS3 to receptor) (Figure 3-13 D-E). This decrease in P-STAT3 expression was statistically significant ($P<0.05$) over the concentration range 0.005-0.05 μg SOCS3 (Figure 3-13 F). However, these data varied between experimental repeats and therefore reproducibility of N numbers was an issue (Figure 3-13B-G).

To assess whether the Lys-less SOCS3 mutant could inhibit STAT3 Y705 phosphorylation at the chimeric receptor we co-expressed 2 μg Epo/GP130 ± 2 μg FLAG tagged WT or Lys-less SOCS3 in HEK293 cells (ratio of 1:1 receptor to SOCS3) (Figure 3-14). Immunoblotting for STAT3 Y705 phosphorylation revealed a band in the Epo/GP130R + Epo lane only (Figure 3-14A). In the presence of WT or Lys-less SOCS3 STAT3 Y705 phosphorylation was not detected though faint bands were observed in the untransfected (UTF) lanes. Densitometry analysis confirmed that following Epo stimulation, the presence of WT and Lys-less SOCS3 led to a significant ($P<0.001$) decrease in STAT3 Y705 phosphorylation compared to the maximum stimulation (Epo/Gp130R + Epo only) (Figure 3-14B).

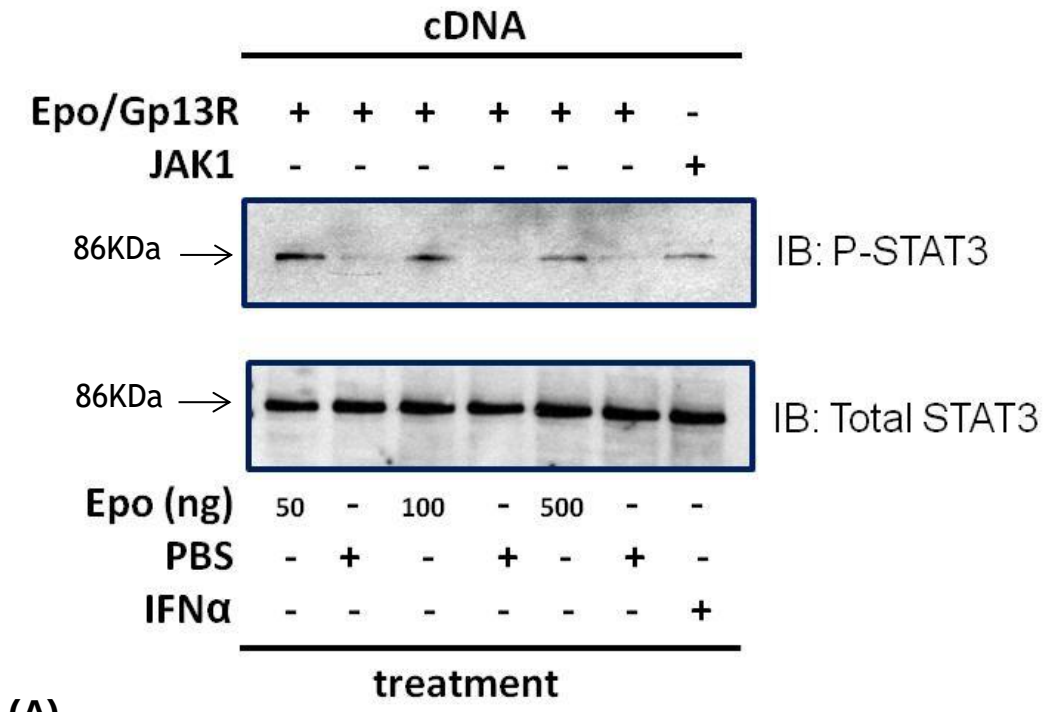

(A)

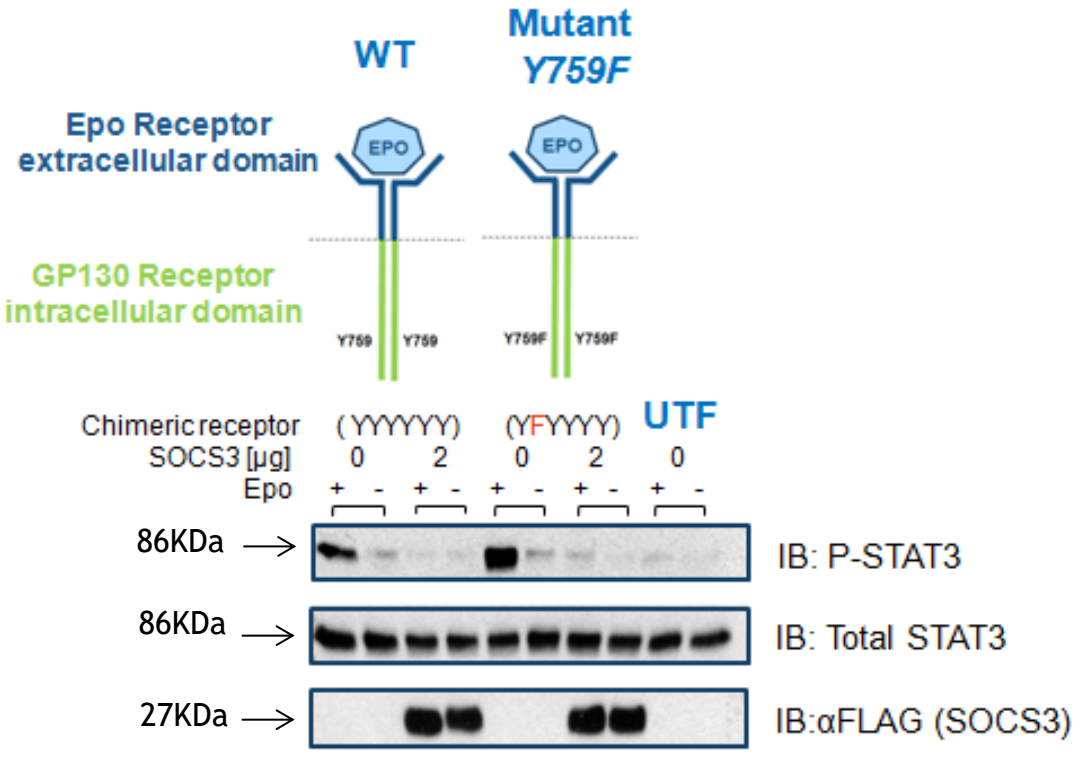

(B)

Figure 3-13: SOCS3 mediated inhibition of STAT3 phosphorylation at the Epo/Gp130R chimera*(Continued overleaf)*

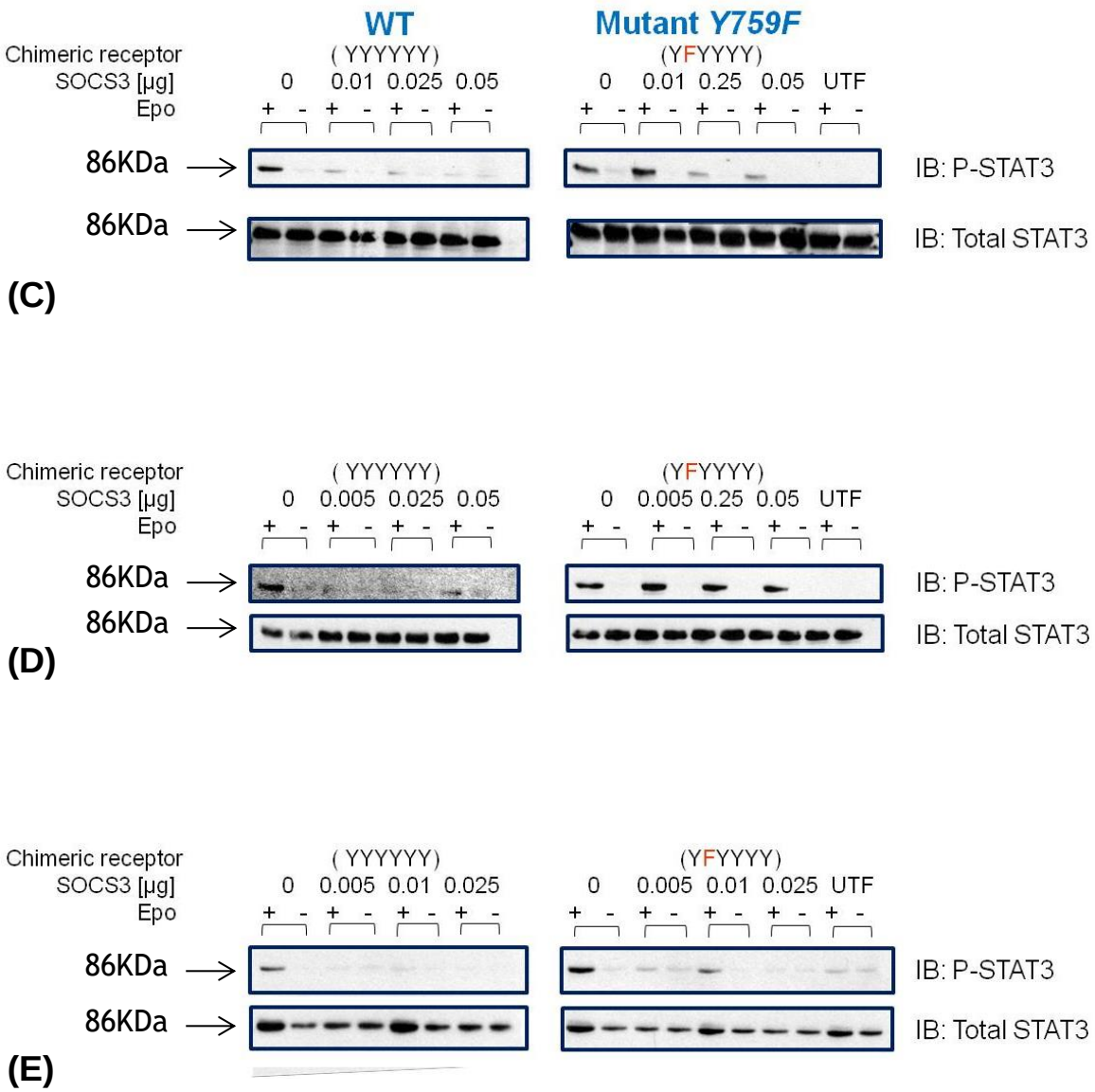

Figure 3.13: SOCS3 mediated inhibition of STAT3 phosphorylation at the Epo/Gp130R chimera

(Continued overleaf)…

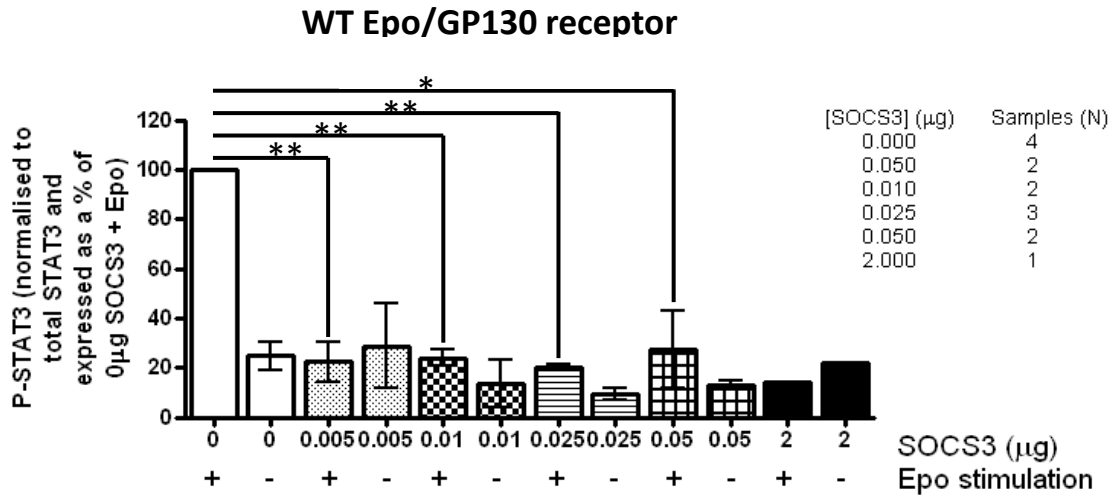

(F)

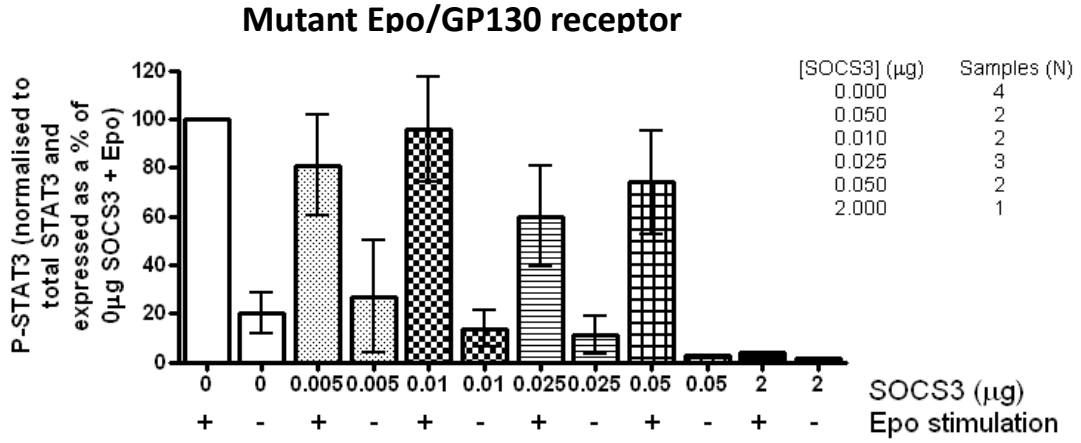

(G)

Figure 3-13: SOCS3 mediated inhibition of STAT3 phosphorylation at the Epo/Gp130R chimera.

(A) HEK293 cells were co-transfected with 2 µg WT/mutant (*Y759F*) Epo/Gp130 chimeric receptor or JAK1 cDNA. Prior to harvesting, cells were serum starved (3hrs, 37°C, 5%CO_2) and treated with ±50-500 ng/ml Epo, 30,000 units interferon-α (IFNα) or vehicle only (PBS) (15 min, 37°C, 5%CO_2). Cell lysates (30 µg) were resolved by SDS-PAGE and transferred to nitrocellulose membrane. Mouse anti-P-STAT3 (1:1000) and rabbit anti-total STAT3 (1:1000) was used in western blotting. 50 ng/ml EPO was sufficient to stimulate STAT3 phosphorylation. Data shown were N=1. (B-E) HEK293 cells were co-transfected with 2 µg WT or mutant (*Y759F*) Epo/Gp130 chimeric receptor ±0-2 µg WT SOCS3. Prior to harvesting, cells were serum starved (2 hrs, 37°C, 5%CO_2) and treated with 50 ng/ml Epo + or PBS (-) (15 min, 37°C, 5%CO_2). Cell lysates (30 µg) were resolved by SDS-PAGE and transferred to nitrocellulose membrane. Mouse anti-P-STAT3 (1:1000), rabbit anti-total STAT3 (1:1000) and mouse anti-FLAG (1:1000) was used in western blotting where stated. (F-G) Densitometry analysis was performed using Total Lab software. P-STAT3 expression was normalised to total STAT3 and expressed as a % of the maximum (0 µg SOCS3 + Epo set at 100%). Each concentration of SOCS3 analysed was performed at N=1-4 as indicated in figure (F-G). Student's T-test (2-tailed, un-paired) was performed for each SOCS3 concentration vs. 0 µg SOCS3 + Epo where N numbers permitted. $P<0.05$ (*) and $P<0.01$ (**) was deemed significant (Excel). 0.005 µg SOCS3 was sufficient to inhibit STAT3 phosphorylation in the presence of WT Epo/Gp130R + Epo however the inherent variability of this assay meant that N numbers could not be completed to N=3 for each SOCS3 concentration.

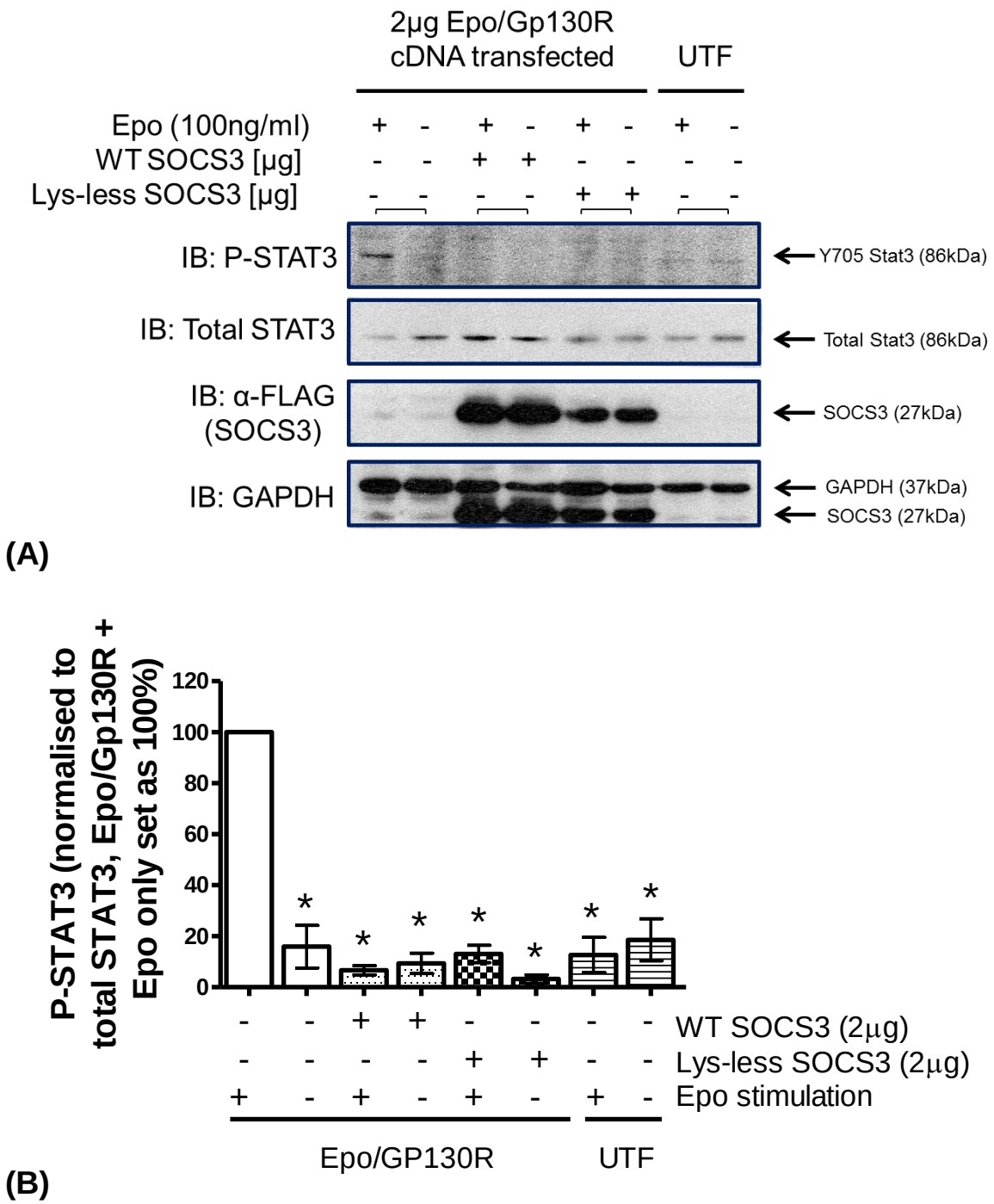

Figure 3-14: Lysine-less SOCS3 mediated inhibition of STAT3 phosphorylation at the Epo/Gp130R chimera.

HEK cells were co-transfected with 2 µg WT Epo/Gp130 chimeric receptor ±2 µg WT or Lys-less SOCS3. Prior to harvesting, cells were serum starved (2 hrs, 37°C, 5%CO2) and treated with 100 ng/ml Epo + or PBS (-) (15 min, 37°C, 5%CO2). Cell lysates (30 µg) were resolved by SDS-PAGE and transferred to nitrocellulose membrane. Mouse anti-P-STAT3 (1:1000), rabbit anti-total STAT3 (1:1000) and mouse anti-FLAG (1:1000) was used in western blotting where stated. Experiments were repeated to N=3 and a representative immunoblot shown. (B) Densitometry analysis was performed using Total Lab software. Y705 P-STAT3 expression was normalised to total STAT3. The data shown represent the mean ± SEM % of the maximum STAT3 Y705 phosphorylation (0 µg SOCS3 + Epo set at 100%) of three independent experiments. One-way ANOVA was performed using InStat GraphPad software (* $P < 0.001$) with Bonferroni correction. 2 µg WT or Lys-less SOCS3 was significantly reduced STAT3 Y705 phosphorylation at the Epo/Gp130R.

3.3 Discussion

The aim of this chapter was to understand the mechanism of SOCS3 degradation, at the proteasome, and in doing so identifying key points of regulation that when modified may enhance SOCS3 stability.

Sasaki *et al* previously generated an N-terminal truncation mutant of SOCS3 and found that mutation of Lys6 (K6) specifically or N-terminal truncation (*ΔN11*) enhanced the stability of the protein in Ba/F3 cells (murine pro-B cell line) [95]. In addition, the group found that a major route of SOCS3 turnover was the 26S proteasome as MG132 proteasomal inhibition enhanced SOCS3 stability. To investigate this further, we generated a SOCS3 *K6Q* mutant and showed that loss of K6 did not affect the ubiquitylation status of SOCS3 (Figure 3-1). Moreover loss of this residue did not stabilise SOCS3 following proteasome inhibition in HEK293 cells (Figure 3-1) contradicting the existing literature in the Ba/F3 cell line. However, Sasaki noted that this may be a cell specific response which may explain the conflicting results [95]. Consistent with the existing literature [100], we have shown that inhibition of the proteasome had no obvious effect on SOCS3 stability suggesting the proteasome is not a major route for SOCS3 degradation in HEK293 cells (Figure 3-1). To our knowledge since publication by Sasaki *et al* 2003, initial reports of K6 regulation of SOCS3 stability have not been followed up or characterised in detail. Therefore, this suggests that control of SOCS3 stability and targeting for degradation may be cell type specific. A suspension pro B cell line may not be the most appropriate model of SOCS3 regulation in the vasculature.

In order to map the essential regions for SOCS3 ubiquitylation, in HEK293 cells, we assessed the ubiquitylation status of progressive SOCS3 truncation mutants. The key finding of this experiment was the identification of a ubiquitin resistant SOCS3 mutant (ΔC84) despite the presence of upstream lysine residues (Figure 3-3). Conversely, loss of the C-terminal 40 residues did not affect the ubiquitylation status of SOCS3. This led us to identify a 44 amino acid region (aa142-185) in the C-terminal domain of SOCS3 that is required for SOCS3 ubiquitylation to proceed in HEK293 cells (Figure 3-3). These data suggested that either the machinery required for catalysing ubiquitylation may no longer assemble or that preferential K residues within the 44 amino acid region were no longer available. In contrast to phosphorylation and sumoylation, there is no consensus sequence for ubiquitination therefore predicting Lys residues that may be sites of ubiquitylation using bioinformatic tools was not possible [233].

The SOCS box is located at the C-terminus of the SOCS3 protein and contains binding sites for components of the E3 ligase machinery to bind. The SOCS box provides a platform for the sequential assembly of the E3 ligase complex in which Elongin B and C must first dock at the SOCS box [48]. Failure of the Elongins to interact at this site means Cul5 and Rbx1 can no longer bind and the E3 ligase complex cannot assemble. As a result, SOCS3 substrates, bound by the SH2 domain, can no longer be ubiquitylated and targeted for the proteasome.

It has been argued that SOCS3 auto-ubiquitylation was responsible for the rapid turnover of this signalling molecule [95]. Sasaki and colleagues generated a C-terminal truncation mutant, in which the SOCS box was removed; therefore components of the E3 ligase complex (Elongin B and C) could not interact. The authors showed that the C-terminal truncation mutant and the K6Q mutant were significantly more stable than WT SOCS3 in the Ba/F3 cell line suggesting that this provided evidence for SOCS3 auto-ubiquitylation. However, we hypothesised that one or more external E3 ligases may be involved in regulating the protein turnover.

Babon and co-workers previously demonstrated that the conserved Leu189 on SOCS3 was required for Elongin B and C interaction however the ubiquitylation status of this mutant was never investigated [100]. In order to test whether SOCS3 auto-ubiquitylates itself or is targeted by an external E3 ligase(s), the Palmer lab generated an L189A SOCS box mutant. The L189A SOCS3 mutant was poly-ubiquitylated and was comparable to the WT SOCS3 (Figure 3-5). The absence of ubiquitin chains on ΔC84 SOCS3 confirmed that the poly-ubiquitylation observed was not an artefact of SOCS3 expression and that it was a specific, post-translational modification of the L189A and WT SOCS3 protein. Subsequently, we demonstrated that the L189A and ΔC84 (SOCS box deleted) mutation on SOCS3 disrupted the interaction with Elongin B and C (Figure 3-4). However, WT SOCS3 was able to bind the Elongins confirming Leucine189 (L189) was required for this interaction and therefore the formation of the E3 ligase complex on SOCS3. If the L189A mutant were not ubiquitylated this would suggest an auto-ubiquitylation event by SOCS3 as upstream and downstream Lys acceptors were still available. However, our data confirmed that despite an inability to bind the Elongins (Figure 3-4) the L189A mutant was ubiquitylated (Figure 3-5). Furthermore, the ΔC40 SOCS3 truncation mutant was shown to be ubiquitylated despite the deletion of the SOCS box (aa186-225) (Figure 3-3). Together these data suggested that formation of the E3 ligase complex at the SOCS box was not essential for

SOCS3 ubiquitylation and that the 44aa region identified between the ΔC40 and ΔC84 mutants controls sensitivity to ubiquitylation by a separate E3 ligase.

Within this 44 amino acid region identified in the truncation studies (Figure 3-3) human SOCS3 contains one single lysine at position 173 (K173) (accession number O14543). To assess whether this residue was a key point of regulation for SOCS3 stability we first generated the K173R SOCS3 mutant and tested its ubiquitylation status (Figure 3-6). Densitometry analysis revealed that mutation of K173 significantly reduced the polyubiquitylation status of SOCS3 (Figure 3-6 C) however this mutation was shown to stabilise SOCS3 expression 2 hrs post emetine treatment only (Figure 3.7). It would be advantageous for a SOCS3 therapy to possess enhanced stability over a longer period of time (i.e. beyond 2 hrs) to maximise the inhibition of VSMC proliferation and migration. As such, these data suggest Lys173 is not a master regulator of SOCS3 turnover (Figure 3.7) and it is likely that functional redundancy exists within the ubiquitin proteasome system (UPS). In the absence of a preferred lysine, upstream/downstream lysine residues may provide a site for ubiquitin conjugation due to the lack of consensus sequence requirement. Similarly, Lys acceptor functional redundancy was observed by King and co-workers whilst characterising the ubiquitylation of cyclin B [234]. Functional redundancy may be advantageous for the maintenance of appropriate protein levels as many disease states can be attributed to the accumulation of misfolded proteins including Altzheimer's, Huntington's and Parkinson's disease [235]. Interestingly, mitochondrial dysfunction may play a role in the pathogenesis of Parkinson's disease [236]. An E3 ligase called Parkin is recruited to and ubiquitylates the dysfunctional mitochondrial outer membrane and consequently targets it for autophagy and lysomsomal degradation. Importantly, mutation of the Parkin gene (PARK2) has been associated with the early development of Parkinson's disease [237]. In this disease setting, the evolution of more than one external E3 ligase regulating the ubiquitylation of dysfunctional mitochondria may be advantageous.

Initial mutagenesis studies failed to identify key sites of ubiquitylation responsible for targeting SOCS3 to the proteasome (Figure 3-1– 3.7). To identify putative sites of ubiquitylation on SOCS3 the LC-MS-MS data were searched for the presence of a Gly-Gly doublet (+114 Da mass shift). 8 distinct sites of ubiquitylation (K^{23}, K^{28}, K^{40}, K^{85}, K^{91}, K^{173}, K^{195} and K^{206}) were identified though Lys173 provided the most reliable data as highlighted in yellow (Table 3-1). Of note, the +114 Da mass shift was identified at K^{23} and K^{91} by one software analysis package only (MaxQuant and Mascot respectively)

warranting caution when interpreting these data (Table 3-1). Importantly, a site of modification identified by both software packages enhanced the reliability of a true positive hit. Similarly, though K^{40} was identified as ubiquitylated by both software packages, the scores were relatively low again warranting caution when interpreting these data (Table 3-1). Lys173 was previously identified as a preferred site of ubiquitylation in the truncation studies (Figure 3-3) and via LC-MS-MS (Table 3-1, Figure 3-8) however loss of this residue failed to significantly influence SOCS3 stability (Figure 3-7). Together, these data confirmed that functional redundancy governs SOCS3 ubiquitylation i.e. when the preferred lysine is not available, upstream/downstream targets were ubiquitylated.

One of the disadvantages associated with using LC-MS-MS analysis to map the ubiquitylation sites on SOCS3 was that ubiquitylation could not be discriminated from a different post translational modification called neddylation. Neddylation describes the conjugation of a small protein (NEDD8) to the target lysine. During LC-MS-MS sample preparation, trypsin digestion cleaves the NEDD8 group leaving a Gly-Gly doublet (mass shift +114 Da) at the modified lysine which is the signature also used to recognise a ubiquitylation event. However, in 2011 Kim *et al* published a study which suggested that ubiquitylation was responsible for ~75% of Gly-Gly motifs detected on trypsin digested peptide fragments [238]. The authors, treated cells with a ubiquitin cleaving enzyme (ubiquitin-specific-protease 2; USP2cc) before performing a di-glycine enrichment technique using an anti–K-ε-GG antibody (reviewed by [230]) and MS analysis of cell extract peptide fragments. Immunoblot analysis confirmed that ubiquitylation was abolished in the presence of the USP2cc enzyme and that the number of peptide fragments modified by the di-glycine motif was reduced by 75% compared to cell extracts that were not treated with USP2cc.

Similarly, ISG15ylation is a post translational modification in which a ubiquitin like group (Interferon-Stimulated Gene 15; ISG15 [239]) is conjugated to a lysine residue and following protein trypsin digestion the di-glycine signature (K-ε-GG) is left intact. However, immunoblotting in other cell types confirmed this PTM occurs following interferon (IFN)-α/β stimulation only [127]. The present study (Table 3-1) was conducted in HEK293 cells in the absence of IFN-α/β and therefore excluded the possibility that the K-ε-GG signature identified on SOCS3 (Table 3-1) was due to ISG15ylation.

A final consideration when interpreting the LC-MS-MS data (Table 3-1) is that it was not possible to confirm whether mono, multi-mono or poly (Lys^{48} vs. Lys^{63})-ubiquitin chains were conjugated at each of the 8 ubiquitylation sites identified on SOCS3. The pattern of ubiquitylation and linkage of the poly-ubiquitin chain(s) will determine the cell response to this PTM such as protein degradation at the proteasome (Lys^{48}) or the induction of a signalling cascade (Lys^{63}) [127].

To discriminate between Lys^{48} and Lys^{63} linked chains the overexpression of mutant ubiquitin constructs may be of use [240]. Mutation of internal Lys residues on ubiquitin (Lys→Arg; K48R or K63R) impedes the assembly of poly-ubiquitin chains at the substrate ubiquitin acceptor site. Mono-ubiquitylation may proceed and immunoblot analysis would reveal an 8.5kDa band shift for the protein of interest as opposed to the stepwise laddering that represents poly-ubiquitin chains [240]. The use of a K63R mutant ubiquitin was previously used in a yeast study to investigate the role of Lys^{63} linked ubiquitin chains in regulating DNA repair pathways [241]. Alternatively, Kaiser *et al* described a method in which purification of the protein of interest is followed by MS analysis using different mass:charge (m/z) windows [240]. Each m/z window corresponds to one of the various ubiquitin chain linkage types (K6, 11, 27, 29, 33, 48, 63). The sequential analysis of the spectra allows the user to deduce which linkage type was present at the Lys acceptor site [240]. More recently, the use of a "middle-down MS" technique to determine whether poly-ubiquitin chains were linear or branched structures was described [242]. Middle-down MS employs a less stringent trypsin digestion stage allowing the discrimination of linear chains (single Gly-Gly motif on Ub-1-74 detected) and branched chains (two Gly-Gly motifs on Ub1-74 detected) [242].

3.3.1 Enhancing the stability of SOCS3

We hypothesised that the beneficial effects of SOCS3 on VSMC proliferation, migration and vascular inflammation responsible for the development of NIH are compromised by its ubiquitylation and rapid turnover by the proteasome. As such, strategies that stabilise SOCS3 levels by inhibiting its ubiquitylation have the potential to enhance its beneficial effects. Failure to identify a single lysine residue controlling SOCS3 ubiquitylation (Figure 3-1 - 3-7) led to the generation of a Lys-less SOCS3 construct which was shown to be resistant to ubquitylation in HEK293 cells (Figure 3-9). Importantly, loss of all 10 lysine residues on human SOCS3 (Lys-less) did not disrupt the interaction with Elongin B and C

and therefore the formation of the E3 ligase complex (Figure 3-11). To confirm whether a loss of ubiquitylation resulted in an increase in protein stability, we performed Emetine chase assays over an 8 hour time period. Mutation of Lys6 to Gln (*K6Q*) had no effect on murine SOCS3 stability with complete protein degradation observed after 8 hours protein synthesis inhibition (Figure 3-2). Mutation of Lys173 to Arg (*K173R*) enhanced the stability of SOCS3 at the 2 hr time point only. However, at following 8 hrs emetine treatment the band for SOCS3 was no longer visible on the immunoblot suggesting complete degradation (Figure 3-7). It would be advantageous for a SOCS3 therapy to be significantly more stable than endogenous SOCS3 over a longer period of time. Interestingly, the stability of the human Lys-less SOCS3 protein was significantly greater than the WT SOCS3 (Figure 3-10). This enhanced stability was associated with a loss of ubiquitylation (Figure 3-9) suggesting ubiquitylation plays a key role in controlling proteasomal turnover of SOCS3 in MEF cells.

A more stable SOCS3 molecule may provide a useful candidate for gene therapy. With the advent of drug eluting stents the more stable Lys-less SOCS3 molecule could be delivered locally and so avoids the complication of raising SOCS3 expression globally. Alternatively CABG procedures are amenable to *ex vivo* adenovirus mediated gene therapies where the saphenous vein conduit for example may be incubated with the virus prior to grafting [21]. For example, in 2011, a phase 2 clinical trial used the adeno-associated virus type 1 vector to successfully deliver the Sarcoplasmic Reticulum Ca^{2+}-ATPase (SERCA) via intra-coronary infusion in patients with heart failure [243].

Additionally, the adenovirus mediated delivery of SOCS3 was shown to be protective in mouse models of rheumatoid arthritis (RA) [244]. Shouda and co-workers described the hyper-activation of STAT3 in the synovial tissue of patients with RA specifically. In attempt to control the deleterious effects of STAT3 hyper-activation, the investigators injected adenovirus particles expressing SOCS3 into the ankle joint of mice with RA. These data confirmed that the localised overexpression of SOCS3 significantly reduced the disease pathology. We therefore hypothesise that the use of a more stable SOCS3 isoform such as Lys-less SOCS3 would pro-long and potentially enhance the beneficial effects of this therapy in RA models of disease.

3.3.2 Assessing the functionality of SOCS3 mutants

It was essential that mutagenesis of SOCS3, to enhance its stability, did not impair the function of SOCS3 as an inhibitor of the JAK/STAT pathway. As such, a strategy for measuring SOCS3 activity was devised by adapting the existing Epo/Gp130R assay [58]. The Epo/Gp130R chimera is composed of the extracellular domain of the erythropoietin receptor fused to the trans-membrane and intracellular domain of the glycoprotein-130 receptor as described previously [58]. Schmitz *et al* previously demonstrated inhibition of STAT3 phosphorylation (P-STAT-3), by SOCS3, at this transiently expressed receptor in COS-7 cells [58]. We therefore selected this system as a measure of SOCS3 activity in HEK293 cells. Stimulation with Epo induces a gp130R response at the chimeric receptors only as HEK293 cells do not express an endogenous EpoR. Accordingly, the population of cells which failed to take up the Epo/Gp130R cDNA construct during transfection did not influence the P-STAT3 end point measure i.e. we can measure a response in transfected cells only. The optimisation of this assay involved identifying the minimum concentration of WT SOCS3 that was sufficient to inhibit STAT3 activation i.e. the ratio of receptor to SOCS3. Initially, a 1:1 ratio of receptor to SOCS3 (2 μg) effectively blocked the activation of STAT-3 at the WT Epo/Gp130R (Figure 3-13 B). As such, a titration of SOCS3 was performed with 0.005-0.05 μg effectively reducing the activation of STAT-3 (Figure 3-13C-E).

Importantly, the Epo/Gp130R mutation (*Y759F*) prevents SOCS3 docking at the intracellular domain of gp130R. It was expected this mutation would block SOCS3 mediated inhibition of the JAKs responsible, in turn, for STAT3 phosphorylation. However, SOCS3 appeared to have a partial effect on STAT3 activation at the Y759F mutant receptor at a receptor to SOCS3 ratio of 1:1 (Figure 3-13B). Interestingly, at lower concentrations of SOCS3 this inhibition appeared to be lost (Figure 3-13 C-E). One possible explanation may be that at higher SOCS3 concentrations (e.g. 2 μg, Figure 3-13 B) SOCS3 directly interacts with and inhibits JAK activity through its KIR domain. Typically, the gp130 docking site (*Y759)* promotes this inhibition by bringing SOCS3 into close proximity with JAK [57] thought this is not essential [70]. Schmitz described this observation as a "receptor independent mechanism" [58].

However, these data at lower concentrations of SOCS3 were not reproducible and completion of each SOCS3 concentration to three experimental repeats (N=3) was not possible as reflected in the densitometry analysis (Figure 3-13 F-G) where statistical

significance was tested only when sample N≥2. Though SOCS3 significantly reduced STAT3 activation at the WT receptor (Figure 3-13 F) the variability of these data rendered the assay unsuitable as a measure of SOCS3 function over the lower SOCS3 concentration range. We were able to obtain reproducible SOCS3-mediated inhibition at high concentrations of SOCS3 however this likely reflected gp130-dependent and gp130-independent (direct JAK inhibition) aspects of its functionality (Figure 3-13B). Thus, the Epo/Gp130R assay provided a robust indicator of SOCS3 function at a 1:1 ratio of receptor to SOCS3 (Figure 3-13B).

Similar to WT SOCS3, the Lys-less SOCS3 mutant significantly inhibited STAT3 activation at the chimeric receptor (1:1 ratio) following Epo stimulation (Figure 3-14). The Lys-less SOCS3 mutant was previously shown to interact with Elongin B and C (components of the E3 ligase machinery) (Figure 3-11) suggesting that mutagenesis induced conformational change to the protein structure did not impede SOCS3 function. Moreover, the ability of Lys-less SOCS3 to inhibit STAT3 activation in the Epo/Gp130R assay (Figure 3-14) provided further evidence that SOCS3 mutagenesis was not detrimental to protein function. Lys-less SOCS3 may therefore provide a useful tool for therapeutic strategies that aim to control the hyperactivation of the IL6-mediated JAK/STAT pathway.

Overall, this chapter has provided evidence that SOCS3 is not auto-ubiquitylated contrary to the existing literature [95]. We propose that one or more external E3 ligases may be involved in regulating SOCS3 protein turnover. Moreover, we have mapped 8 putative sites of SOCS3 ubiquitylation and generated a more stable Lys-less SOCS3 mutant. Mutation of all 10 lysine residues along the SOCS3 molecule did not impair its ability to interact with components of the E3 ligase machinery or inhibit STAT3 activation in the Epo/Gp130R assay. Accordingly, the functional Lys-less SOCS3 mutant may be a more potent inhibitor of SMC proliferation in NIH though this remains to be tested.

3.3.3 Limitations of the study

In this chapter it was demonstrated that the proteasome was not a major route of SOCS3 degradation in HEK293 cells, a finding which was also reported by Babon and co-workers [100]. A cell system in which endogenous SOCS3 expression could be induced and where the proteasome is a major route of SOCS3 degradation would be a more suitable model.

One possibility would be the WT and SOCS3 KO MEFs used for the imaging experiments in chapter 4, although these also have the limitation of being a non-vascular cell type.

Several experiments in chapter 3 used the transfection of plasmid cDNA as a method of overexpressing a gene of interest in the cell. One of the major limitations of this method is that transfection efficiency, and therefore copy number, will vary between cells. The transfection efficiency will also vary depending on the size of the plasmid. It may be argued that changes in ubiquitylation status were attributed to variation in transfection efficiency and thus plasmid copy number between cell populations. I employed PolyFect Transfection reagent, which relies on the formation of a dendrimer-DNA capsule, to facilitate efficient delivery of DNA across the cell membrane (section 2.2.6). However incubation of cells with this transfection reagent >24 hrs or at high concentrations was cytotoxic therefore it was important to optimise the transfection protocol for each cell type based on the manufacturers recommendations (data not shown).

Furthermore, HEK293 cells may be regarded as a synthetic overexpression system. I selected this immortalised cell line as the efficiency of plasmid expression in primary vascular cells, using standard transfection reactions, is often substantially lower versus HEK293 cells. It would be informative to assess the ubiquitylation of SOCS3 in primary vascular cells (endothelial and smooth muscle) which have a high transfection efficacy. Alternatively, virus particles could be employed as a method of stable overexpression of the gene of interest.

Emetine chase time course experiments were conducted to investigate the effect of mutagenesis on SOCS3 stability (Figure 3-2, 3-7 and 3-10). Data analysis involved normalising WT/mutant SOCS3 protein levels to the housekeeping gene GAPDH that was used as a loading control. Three independent experimental repeats were performed and the data were presented as a percentage of the maximum i.e. vehicle/time point 0. However, using this method, it is possible that during statistical analysis the significance is affected by low errors and may therefore increase the likeliness of a type I error. Moreover, to combat the issue of variation in transfection efficiency we transfected a 10 cm dish of SOCS3 KO MEFs, trypsinised this cell population and seeded the transfected MEFs in 6 wells plates for emetine chase. One of the drawbacks of this procedure was that the transfected cells did not proliferate as well in the 6 well plates and so the protein concentration of whole cell lysates was low. It may therefore be argued that the emetine chase immunoblot data is difficult to interpret due to low protein expression (Figure 3-2, 3-

7 and 3-10). As with the HEK293 system, it would be informative to assess the kinetics of SOCS3 turnover in primary vascular cells that would be the target of a SOCS3 stabilising therapy.

4 The identification of novel SOCS3 interactors: E3 ligase and DUB enzymes controlling SOCS3 turnover

4.1 Introduction

Ubiquitylation is a reversible PTM of a lysine acceptor that requires the sequential activity of three distinct enzymes referred to as the E1 (activating enzyme), E2 (conjugating enzyme) and an E3 (ligase enzyme) [127] (section 1.5). The E3 ligase is the specificity determining factor for substrate recognition of which three families have been described including the Really Interesting New Gene (RING) domain, Homology to the E6AP C Terminus (HECT) and RING-between-RING (RBR) E3s [128]. Polyubiquitin chains may be linkage specific with Lys48 modifications targeting substrates for proteasomal degradation and Lys63 modifications regulating signalling events or targeting substrates for lysosomal degradation. Importantly, deubiquitylase (DUB) enzymes may reverse the action of E3 ubquitin ligases and can therefore promote substrate stabilisation or attenuate cell signalling events.

Previously, Sasaki and colleagues reported that SOCS3 must auto-ubiquitylate and regulate its' own turnover at the proteasome [95]. However, data generated in this thesis challenges this hypothesis and supports the role of an external E3 ligase to catalyse SOCS3 ubiquitylation. The C-terminal SOCS box binds adaptor proteins Elongin B and C. Subsequently, this provides a platform for the formation of an E3 ligase complex (involving Cul5 and Rbx2) which catalyses the ubiquitylation of substrates bound by the SOCS3 SH2 domain (section 1.3.8). In chapter 3 of this thesis, SOCS3 containing a single amino acid substitution (Leu189Ala, L189A) within the C-terminal "BC box" was incapable of binding the Elongin proteins required for E3 ligase activity (Figure 3-4) and was ubiquitylated to a similar extent as WT SOCS3 (Figure 3-5). Therefore the ubiquitylation and stability of SOCS3 must be controlled by one or more separate E3 ubiquitin ligases.

Previously, a cell-based ubiquitylation assay was used to successfully screen for inhibitors of the MDM2-MDMx E3 ligase that regulates p53 stability [245]. In the resting cell, p53 levels are maintained at a relatively low level through the action of MDM2. However,

following mutagenesis, p53 levels must increase to inhibit cell cycle progression. To achieve this, MDM2 auto-ubiquitylates and therefore targets itself for proteasomal degradation. Inhibitors of the MDM2 E3 ligase would enhance p53 stability and may therefore provide a useful therapy for cancer. The overexpression of an MDM2-luciferase fusion protein in HEK293T cells allowed the investigators to measure changes in MDM2 expression (and therefore stability) using a luminometer [245]. A decrease in luminescent signal indicated MDM2 ubiquitylation and proteasomal degradation. Therefore in the presence of an MDM2-MDMx inhibitor the MDM2-luciferase fusion protein would be stabilised. We sought to adapt this assay to identify E3 ligases controlling SOCS3 turnover using a commercially available siRNA library (si-ARRAY) for over 300 known E3 ligases.

4.1.1 Aims

In this chapter, the development of a SOCS3-luciferase and immunofluorescence based assay to screen an E3 ligase si-ARRAY was investigated. In addition, LC-MS-MS analysis of a SOCS3 co-immunoprecipitate was performed to identify E3 ligase or DUB enzymes that interact with SOCS3 and potentially regulate its turnover at the proteasome. Functional validation of an E3 ligase (HectD1) and a DUB (USP15) identified in the LC-MS-MS screen was performed. Finally, the role of Cullin-RING-Ligases (CRLs) was determined by assessing SOCS3 ubiquitylation status in the presence of a neddylation inhibitor.

4.2 Results

4.2.1 The proteasome is a major route of SOCS3 degradation in a human endothelial cell line.

Several studies have demonstrated that SOCS3 is rapidly turned over either by the proteasome [94-96] or via a calpain-dependent process [103]. However, it is likely that the mechanism of SOCS3 turnover is cell type dependent as a study conducted in HEK293T cells demonstrated that pharmacological inhibition of the proteasomal, calpain or lysosomal pathways did not enhance the stability of SOCS3 [100]. To determine the contribution of the proteasome to SOCS3 degradation in the cell lines used in our study, MEFs and ASM.5 cells were stimulated with ±Fsk ±MG132 for 5 hrs. Immunoblotting for SOCS3 revealed that, in both cell types, SOCS3 levels appeared to be increased in the Fsk+MG132 vs Fsk or MG132 alone treatment groups (Figure 4-1). Densitometry analysis of the AS-M and MEF immunoblot confirmed this was a significant increase in SOCS3 levels ($P<0.001$) in the Fsk + MG132 treatment group by ~4fold (Figure 4-1B-C). In contrast, either Fsk or MG132 treatment alone resulted in a slight increase in SOCS3 levels ($P>0.05$) (Figure 4-1B-C).

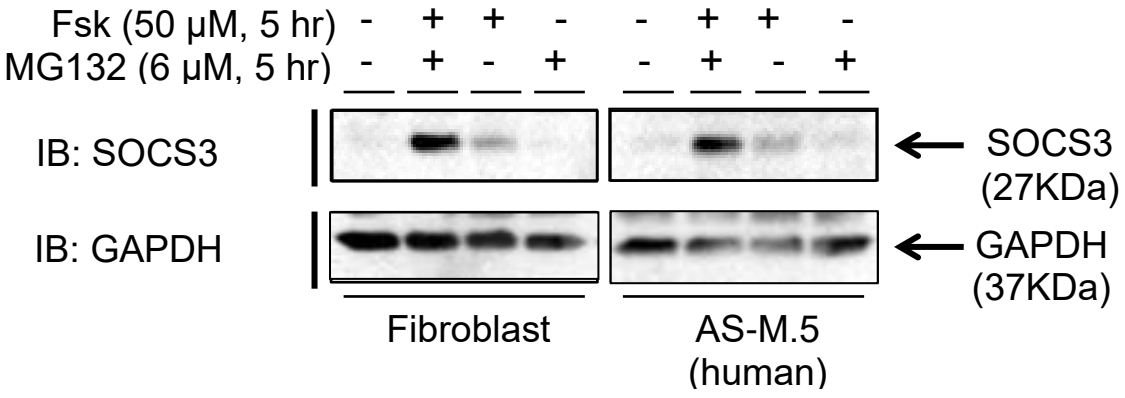

(A)

Figure 4-1: The proteasome is a major route of SOCS3 turnover in AS-M human endothelial cells.

(Continued overleaf)

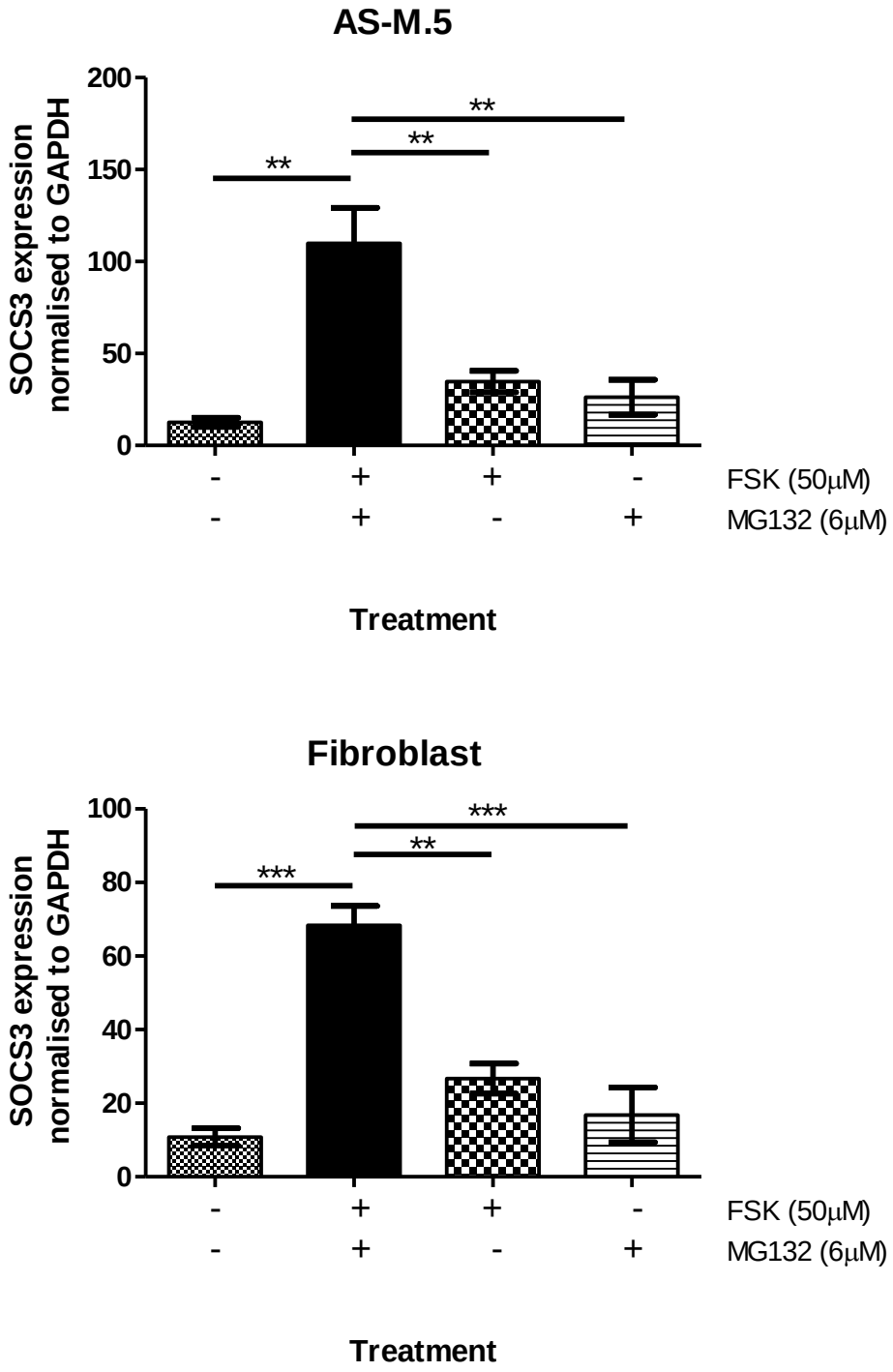

Figure 4-1: The proteasome is a major route of SOCS3 turnover in AS-M human endothelial cells.
(A) AS-M and MEF cells were treated ±50 μM Forskolin (Fsk) and ±6 μM MG132 (5 hrs, 37°C, 5% CO_2) before harvesting in RIPA lysis buffer. Immunoblotting of cell lysates for SOCS3 revealed an accumulation of SOCS3 in the +Fsk,+MG132 group and to a lesser extent the +Fsk,-Mg132 group The experiment was repeated to N=3 and representative immunoblot shown. (B-C) Densitometry analysis of the immunoblots were performed (N=3). The mean data with SEM error bars were plotted and statistical significance tested using a one-way ANOVA with Bonferroni correction (GraphPadPrism, ** $P < 0.01$), *** $P < 0.001$). cAMP-induced SOCS3 accumulation was significantly greater in the presence of MG132 in both AS-M and MEF cell lines ($P < 0.01$).

4.2.2 Generation and characterisation of a SOCS3-Luciferase fusion protein for a luciferase assay based screen

Previously, a screen to identify small molecule inhibitors of the Mdm2 E3 ligase were identified using a luciferase cell based assay [245]. Mdm2 is an E3 ligase that auto-ubiquitylates itself and the tumour suppressor p53. Herman *et al*, generated an Mdm2-luciferase fusion protein as a reporter of Mdm2 stability. Subsequently they performed a high throughput screen of small molecules to determine which compounds correlated with an increased luminescent signal i.e. Mdm2-Luciferase expression [245].

Our screening strategy was to generate a stable AS-M cell line expressing a SOCS3-Luciferase fusion protein for use in an si-ARRAY to screen for E3 ligases that control SOCS3 turnover. Knockdown of the E3 ligase controlling SOCS3 turnover would result in an increase in SOCS3-Luciferase stability and therefore luminescent signal.

To confirm the SOCS3-Luciferase fusion protein was in frame, expression in a mammalian cell line was investigated (Figure 4-2). HEK293 cells were transfected with WT SOCS3 or SOCS3-Luc and immunoblotting for SOCS3 revealed a prominent band at ~27KDa in the WT lane vs ~86KDa band in the SOCS3-Luc lanes (Figure 4-2A). In contrast, immunoblotting of lysates with a luciferase antibody revealed an 86KDa band in the SOCS-luc lanes only (Figure 4-2). These data were consistent with the predicted molecular weight of luciferase ~59KDa accounting for the larger SOCS3-Luc size observed (Figure 4-2).

To examine whether the SOCS3-Luc fusion protein was ubiquitylated, the co-expression of WT SOCS3 or SOCS3-Luciferase with HA tagged ubiquitin (HA-Ub) was performed in HEK293 cells (Figure 4-3). IP of SOCS3, under denaturing conditions, and immunoblotting for SOCS3 revealed WT SOCS3 was expressed at a molecular weight of ~27KDa in contrast to the SOCS3-Luc construct which was detected at a higher molecular weight ~86KDa (Figure 4-3A). Similarly, the HA immunoblot of IP samples revealed SOCS3-Luc poly-ubiquitin chains were present at a higher molecular weight than WT SOCS3 (Figure 4-3 B). Collectively these data confirmed that SOCS3-Luc fusion protein was in frame and can be functionally expressed in a mammalian cell.

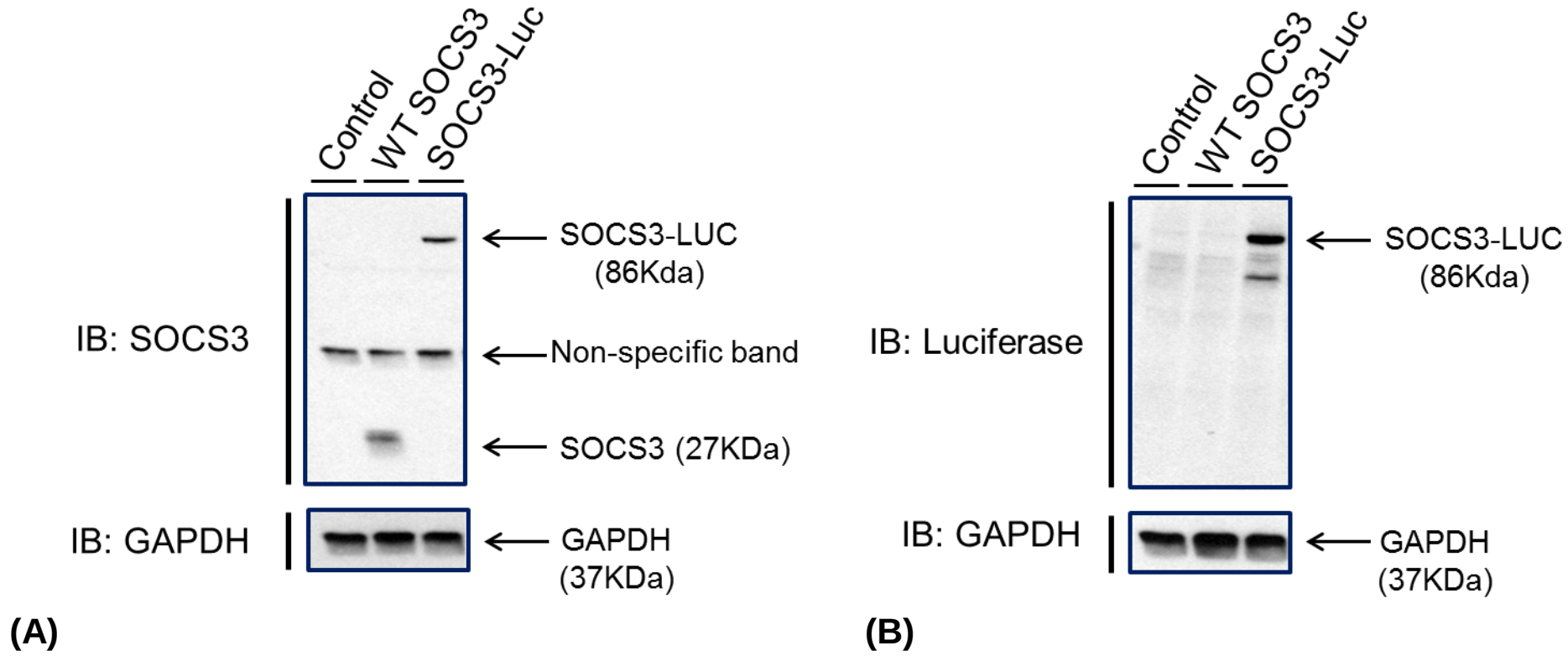

Figure 4-2: Detection of the SOCS3-Luciferase fusion protein by western blotting.

HEK293 cells were transiently transfected with 2 µg FLAG tagged WT (lane 2), 2 µg SOCS3-Luciferase (lane3) or untransfected (lane1). Lysates (30 µg) were resolved by SDS-PAGE and transferred to nitrocellulose membrane. (A) Rabbit anti-SOCS3 (1:1000) was used in western blotting with anti-rabbit IgG-HRP (1:1000) secondary antibody. (B) Mouse anti-luciferase (1:150) was used to visualise luciferase tagged SOCS3. Membranes were then stripped and probed with mouse anti- GAPDH (1:20,000) and anti-mouse IgG-HRP to provide a loading control. The experiment was repeated to N=3 and representative immunoblot shown. SOCS3-LUC was detected only in lane 3 at the expected molecular weight ~86KDa confirming expression in a mammalian cell line under the CMV promoter (A-B).

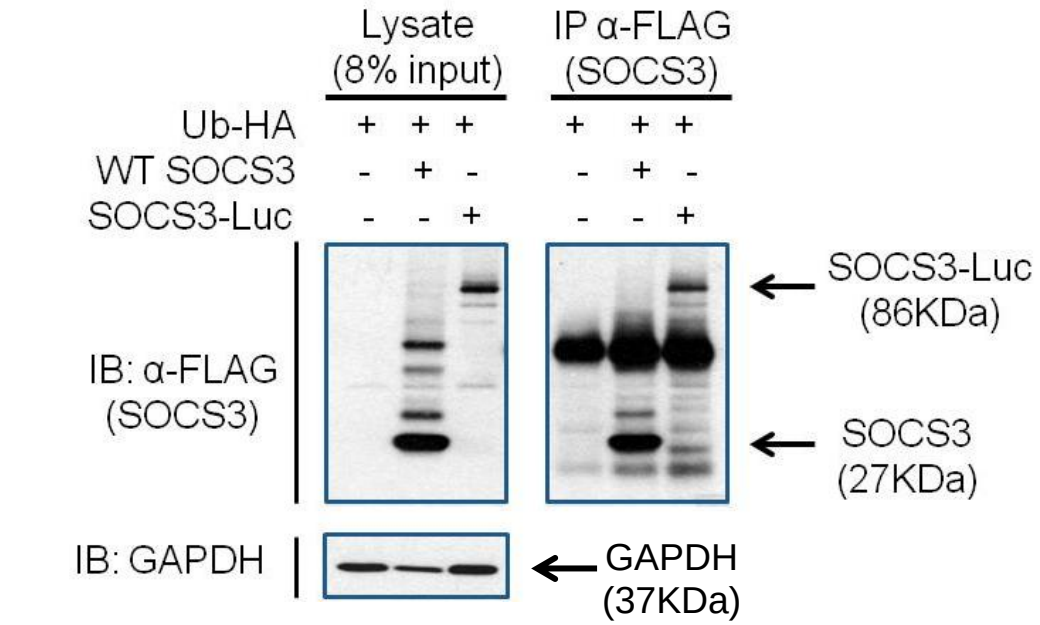

(A)

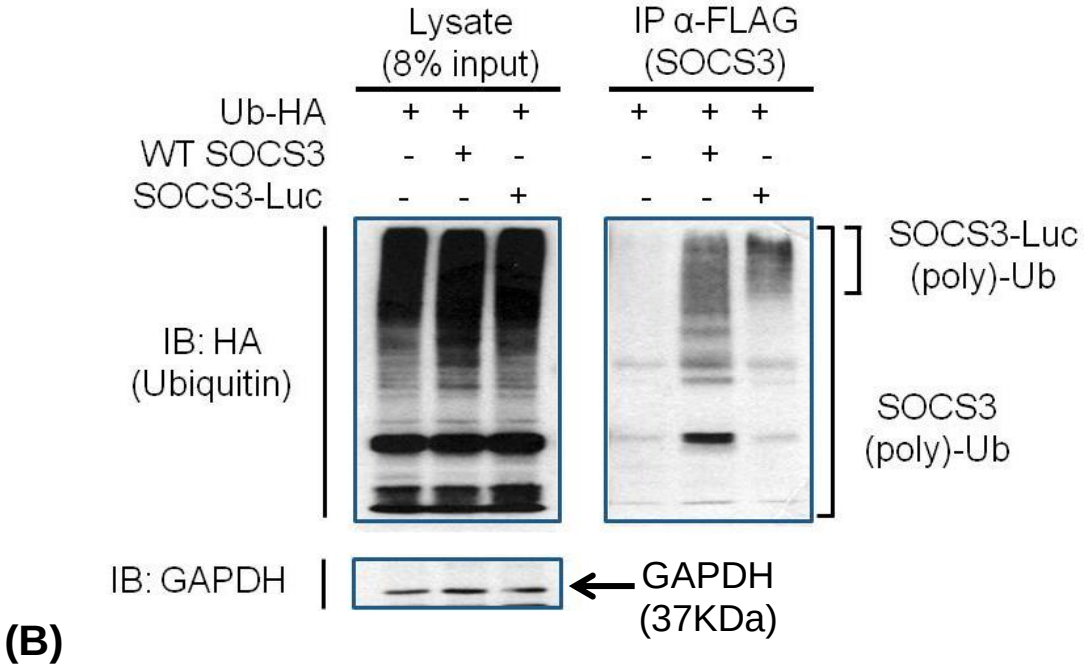

(B)

Figure 4-3: The SOCS3-Luciferase fusion protein was expressed and ubiquitylated in HEK293 cells. HEK293 cells were transiently transfected with 2 µg HA tagged Ubiquitin ± 2 µg WT SOCS3-FLAG or 2 µg SOCS3-Luciferase. Lysates (20 µg) were resolved by SDS-PAGE and transferred to nitrocellulose membrane. (A) Immunoblotting of whole cell lysates and IP SOCS3 with rabbit anti-SOCS3 (1:1000) and anti-rabbit IgG-HRP (1:1000) secondary antibody. (B) Rabbit anti-HA (1:1000) and anti-rabbit IgG-HRP (1:1000) secondary antibody to detect HA tagged ubiquitin. The upper bands in (B) represented poly-ubiquitin chains. Membranes were then stripped and probed with mouse anti-GAPDH (1:20,000) and anti-mouse IgG-HRP to provide a loading control. The experiment was repeated to N=3 and representative immunoblot shown. SOCS3-Luciferase fusion protein was expressed at a higher molecular weight (86KDa) than WT SOCS3 (27KDa) (A). Similarly, the poly-ubiquitin chains on SOCS3 luciferase were observed at a higher molecular weight than the WT SOCS3 molecule (B).

4.2.3 Generation of a lenti virus (LV) expressing the SOCS-Luc fusion protein

Screening an E3 ligase si-ARRAY using a luciferase cell based assay required the generation of a stable cell line expressing SOCS3-Luc. LV vectors incorporate the gene of interest into the host cell genome of both proliferating and non-proliferating cells and therefore facilitate the generation of stable cell lines [246]. When generating a stable cell line it was important not to infect AS-M cells with too many LV particles. Very high levels of SOCS3-Luc protein expression may impair the ability of the luciferase assay to detect the effect of proteasome inhibition or identify an E3 ligase controlling SOCS3 turnover in the si-ARRAY.

Initially we assessed the linearity of the luciferase assay by infecting AS-M cells with SOCS3-Luc LV (10IFU/cell). Cells were treated ±MG132 for 2 hrs prior to harvesting for the luciferase assay and these data were plotted as a line graph to assess the linearity of the assay (Figure 4-4). Increasing the volume of lysate sample correlated with an increasing luminescent signal up to 240,000 RLU (Figure 4-4).

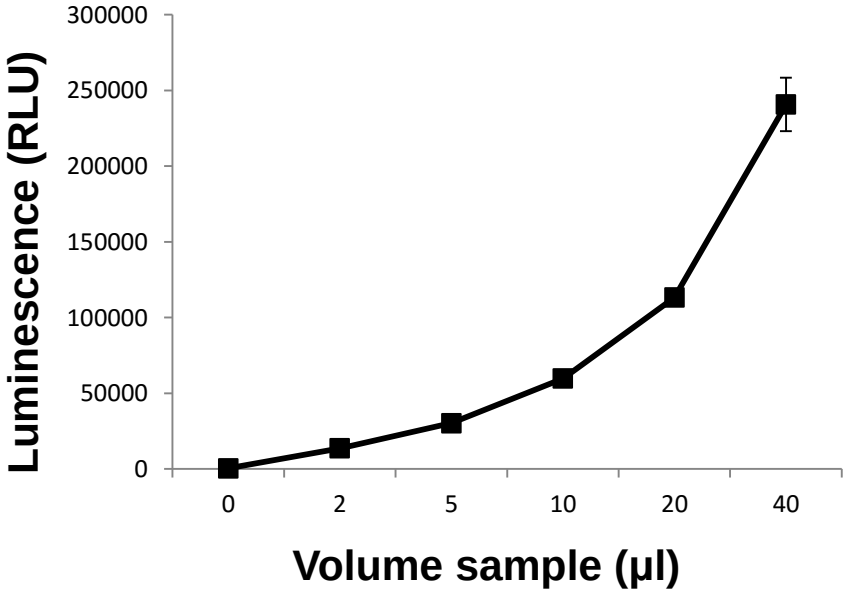

Figure 4-4: Quantification of the SOCS3-Luciferase luminescent signal.

AS-M.5 cells stably expressing SOCS3-Luciferase were treated with MG132 (6 µM, 2 hrs) and lysates were prepared for luciferase assay. Increasing volumes of sample (0-40 µl) were tested (in technical triplicates) and these data presented as mean luminescent signal ±SEM. Luminescent signal increased with increasing volume of sample from 0-240,000 relative luminescent units (RLU).

In addition, we investigated the effect of MG132 on increasing concentrations of SOCS3-Luc LV in AS-M cells. Initially, AS-M cells were infected with 0-10IFU/cell LV (48 hrs) ±MG132 for 2 hrs prior to harvesting lysates for immunoblot analysis of SOCS3-Luc expression and endogenous ubiquitin (Figure 4-5). Immunoblotting with the luciferase antibody revealed an 86kDa SOCS3-Luc band in cells infected with 10IFU/cell of LV particles (Figure 4-5 A). Immunoblot analysis with the SOCS3 primary antibody revealed an 86kDa SOCS3-Luc band in the 2, 5 and 10 IFU/cell LV infected cells (Figure 4-5 B). Immunoblots for endogenous ubiquitin revealed darker poly-ubiquitin chain smears in the MG132 treated lanes (Figure 4-5 A-B). Densitometry analysis of the SOCS3 primary antibody immunoblots showed that MG132 treatment significantly increased SOCS3-Luc expression at the 5IFU/cell concentration only ($P < 0.001$).

4.2.4 Screening stable AS-M SOCS3-Luc single clones for MG132 sensitivity

Stable AS-M cells expressing SOCS3-Luc were isolated using puromycin (2 mg/ml) resistance selection. Single clones were isolated and expanded treating ± MG132 for 2 hrs before harvesting for luciferase assay (Figure 4-6). The AW was calculated as the difference between the mean luminescent signal of clone with MG132 and without MG132. A larger AW was advantageous as in a screening environment there should be no overlap between positive and negative controls in order to correctly identify the E3 ligase from the si-ARRAY (improved sensitivity). AS-M clone E presented the largest AW of 2.12 when treated with MG132 therefore this clone was taken forward (Figure 4-6). An independent repeat of clone E returned an AW of 1.2 which was lower than the original 2.12 observed (Figure 4-6).

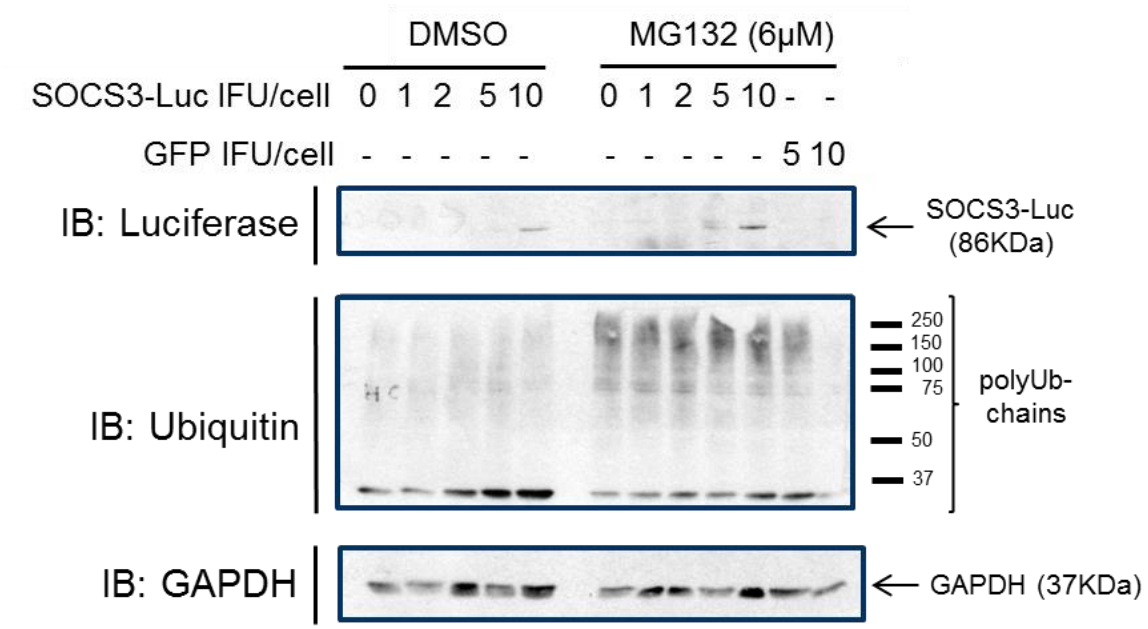

(A)

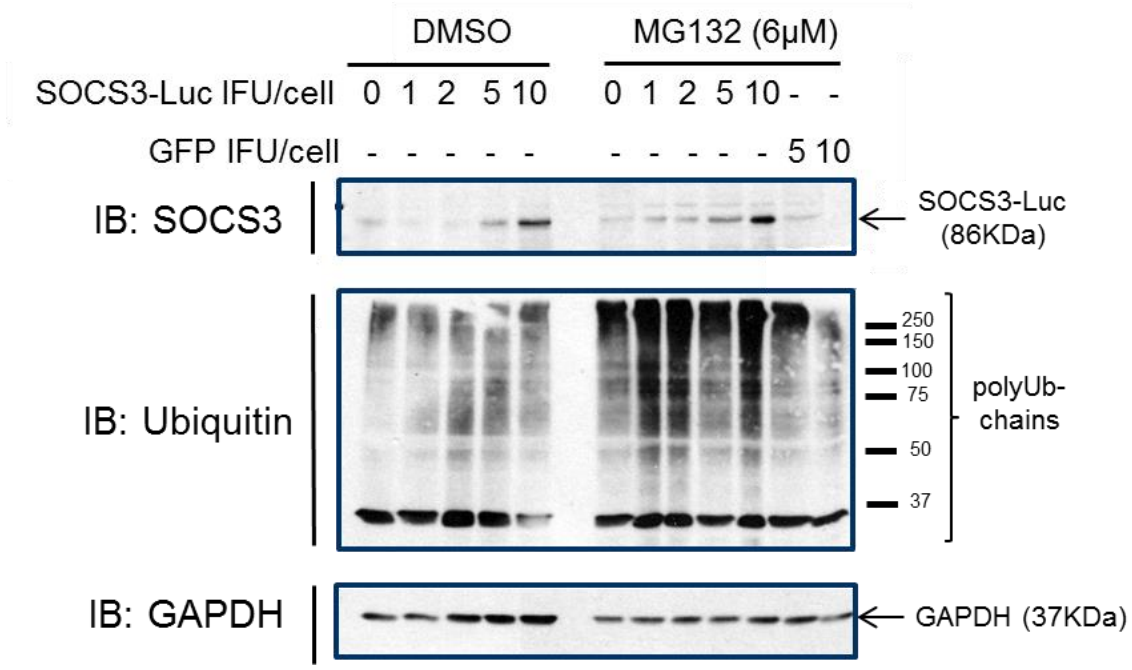

(B)

Figure 4-5: The effect of MG132 on increasing concentrations of SOCS3-Luciferase virus in AS-M cells. *(Continued overleaf)…*

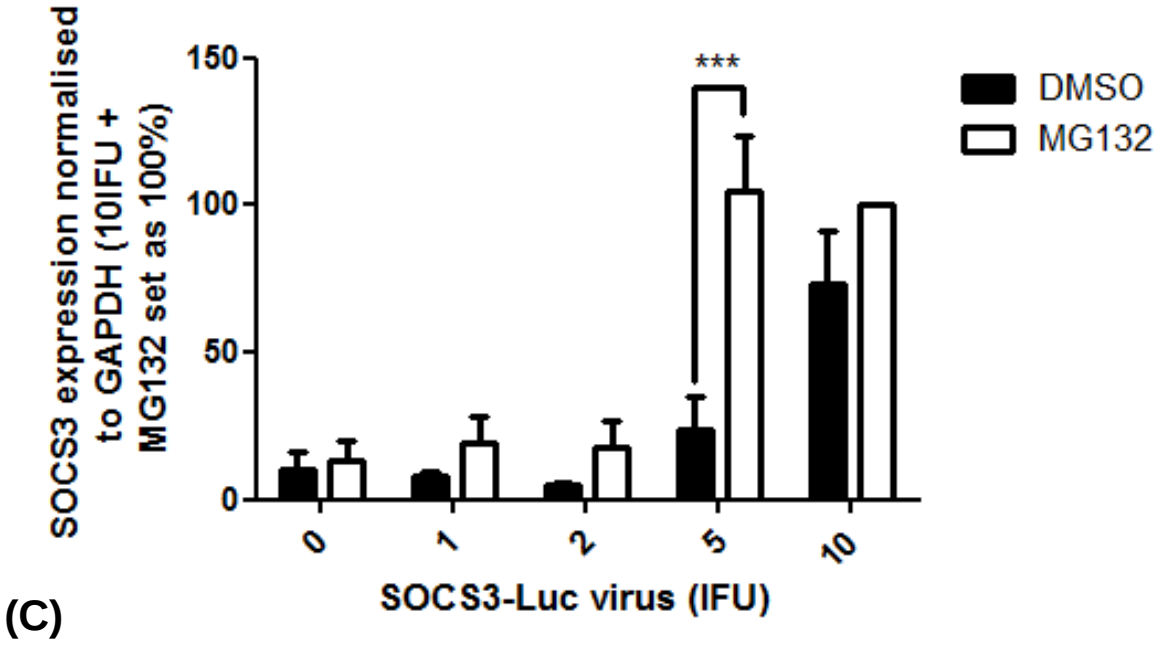

Figure 4-5: The effect of MG132 on increasing concentrations of SOCS3-Luciferase virus in AS-M cells.

AS-M cells were infected with increasing concentrations of SOCS3-Luciferase lentivirus (0-10IFU/cell) for 48 hours. Following this, cells were treated with ±6 μM MG132 for 2 hours and cell lysates were then prepared for immunoblotting with (A) mouse anti-luciferase (1:150) and mouse anti-ubiquitin (1:400) or (B) rabbit anti-SOCS3 (1:1000) and mouse anti-ubiquitin (1:400). Membranes were then stripped and probed with mouse anti-GAPDH (1:20,000) and anti-mouse IgG-HRP to provide a loading control. The experiment was repeated to N=3 and representative immunoblots shown. (C) Quantification of SOCS3-Luc expression was determined by densitometry analysis (TotalLab software) of the SOCS3 immunoblots. SOCS3 expression was normalised to GAPDH and expressed as a % of the maximum (10IFU + MG132 set at 100%). Data shown represent the mean SOCS3 expression ±SEM from three independent experiments. Statistical significance was tested using a one-way ANOVA with Bonferroni correction (GraphPadPrism, ***$P < 0.001$). SOCS3-Luc expression appeared to increase with increasing concentration of virus (IFU) (A-B). At MOI 5, MG132 treatment significantly increased the expression of SOCS3-Luciferase ($P < 0.001$) (C).

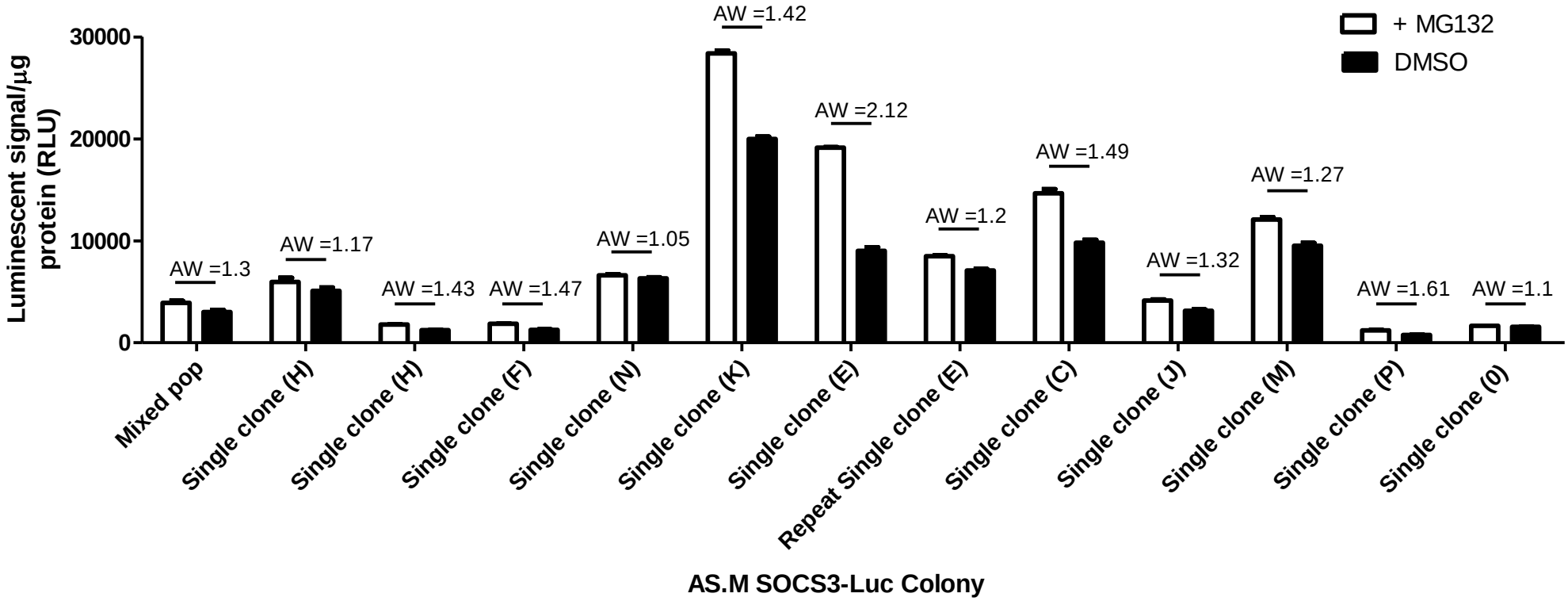

Figure 4-6: Luciferase screening: single colonies of AS-M.5 cells which demonstrated stable expression of the SOCS3-Luciferase fusion construct.

AS-M.5 cells were infected with a SOCS3-Luciferase lentivirus (MOI 1) and cells stably expressing the construct were selected for by supplementing growth media with puromycin antibiotic. Cells were then grown in 10 cm dishes until single colonies were observed. Single colonies were expanded and plated in 6 cm dishes on day 1. On day 2 cells were treated with MG132 (6 µM) or DMSO for 2hrs and harvested for luciferase assay. Luciferase assay samples were performed in technical triplicates and data were presented as the mean luminescent signal/ µg protein with SEM error. The assay window (AW) was calculated as follows: mean luminescent signal with MG132 treatment – mean luminescent signal without MG132 treatment. Clone E revealed the largest assay window (2.12) in contrast to the remaining clones which possessed an assay window <2.

4.2.5 A strategy for increasing the luciferase AW with Emetine and MG132 treatment

To determine whether the inhibition of protein synthesis + proteasome inhibition would increase the AW of SOCS3-Luc clone E, Emetine/MG132 time course experiments were conducted (0-7hrs) and lysates were prepared for luciferase assay (Figure 4-7). Figure 4-7 (A-C) represents three independent experiments. MG132 and Emetine treatment alone showed a trend toward decreasing luminescent signal over time (Figure 4-7). Similarly, Emetine + MG132 treatment groups revealed a trend of decreasing luminescent signal over time as expected. However, when the AW was calculated for each time point (mean signal in Emetine alone group – mean signal in Emetine + MG132) the assay window was not increased beyond 2.12 as observed in Figure 4-6. Moreover the AW calculated for each treatment group varied markedly between independent experiments (Figure 4-6A, B and C). Thus, the luciferase cell based assay was not taken forward, as a tool to screen the si-ARRAY, due to variability of these data and low AW.

4.2.6 An alternative si-ARRAY screening approach: immunofluorescence of endogenous SOCS3 for a high content biology screen

Due to the inherent variability of the luciferase assay data and limited size of the AW, an alternative screening approach was tested. Previously, we demonstrated that the major route of endogenous SOCS3 turnover was via the proteasome in AS-M.5 human endothelial cells (Figure 4-1). As such, immunofluorescence visualisation of endogenous SOCS3 was investigated as a tool to screen the E3 ligase si-ARRAY. Essentially, siRNA mediated knockdown of the E3 ligase would increase SOCS3 stability and therefore the intensity of the immunofluorescent signal.

We conducted a small scale immunofluorescence visualisation of SOCS3 in WT and SOCS3 KO MEFs using confocal microscopy (Figure 4-8). The Abcam 16030 SOCS3 primary antibody was titrated from 0-2 μg/ml however SOCS3 expression appeared unchanged in the control (vehicle only) when compared to Fsk + MG132 treated cells at various gain settings (Figure 4-8 A). Moreover, SOCS3 expression was detected in SOCS3 KO MEFs (Figure 4-8 A). In parallel to immunofluorescence experiments, lysates were prepared and immunoblotting for SOCS3 confirmed that stimulation with fsk induced endogenous SOCS3 expression and MG132 inhibited proteasome mediated degradation

(Figure 4-8 B). SOCS3 was detected (~27KDa) in the WT MEFs treated with Fsk + MG132 only (Figure 4-8 B). An intense band was observed in all lanes at ~25KDa (Figure 4-8 B). This smaller band represented non-specific interaction of the SOCS3 Abcam primary antibody which may explain the aberrant immunofluorescence results. Similar results were obtained using the SC-7009 and in-house SOCS3 antibodies (data not shown).

To investigate whether this was a cell specific problem with the SOCS3 primary antibodies, a 5 hr Fsk/MG132 time course was performed in HUVECs and immunofluorescent visualisation of SOCS3 was performed using the Abcam (Ab16030) (Figure 4-9 A) or SantaCruz (SC-7009) (Figure 4-9B) SOCS3 primary antibody. Immunofluorescent images revealed that stimulation with or without Fsk or MG132 had no obvious effect on SOCS3 expression in HUVECs (Figure 4-9 A-B). Cell lysates were prepared in parallel and immunoblotting for SOCS3 confirmed that Fsk induced endogenous SOCS3 expression and MG132 inhibited proteasome mediated degradation in HUVECs (Figure 4-9C-D). However, the Ab16030 (Figure 4-9 C) and in-house (Figure 4-9 D) SOCS3 primary antibodies revealed non-specific bands at ~25kDa and ~39kDa respectively. These data confirmed Fsk and MG132 were active therefore the aberrant immunofluorescence data must be attributed to non-specific immunoreactivity of the SOCS3 antibodies tested. Consequently, an siRNA screening approach was not progressed and alternative methods to identify an E3 ligase(s) controlling SOCS3 turnover were investigated.

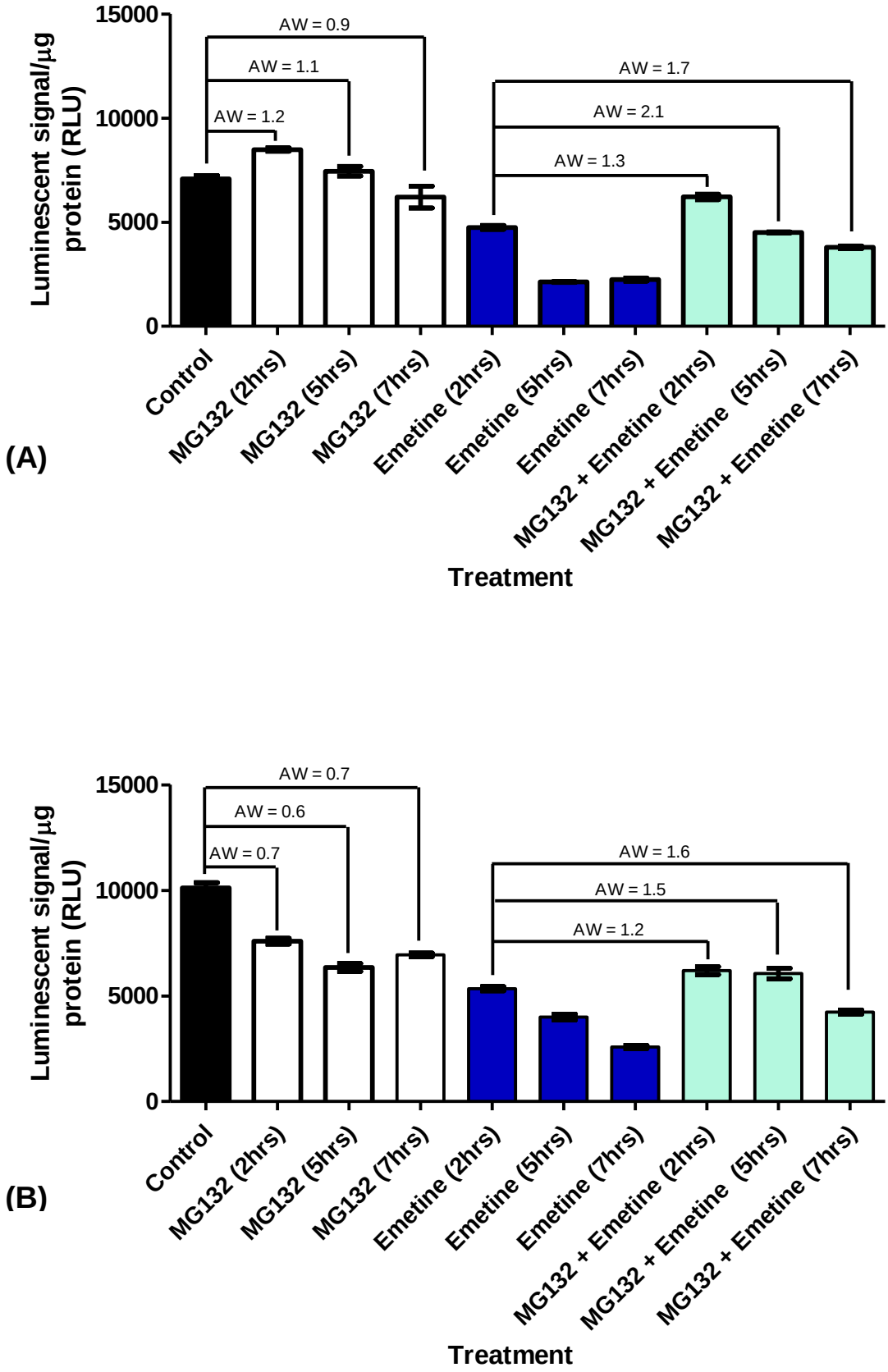

Figure 4-7: Luciferase assay: MG132 and Emetine time course in AS-M.5 cells stably expressing the SOCS3-Luciferase fusion construct *(Continued overleaf)…*

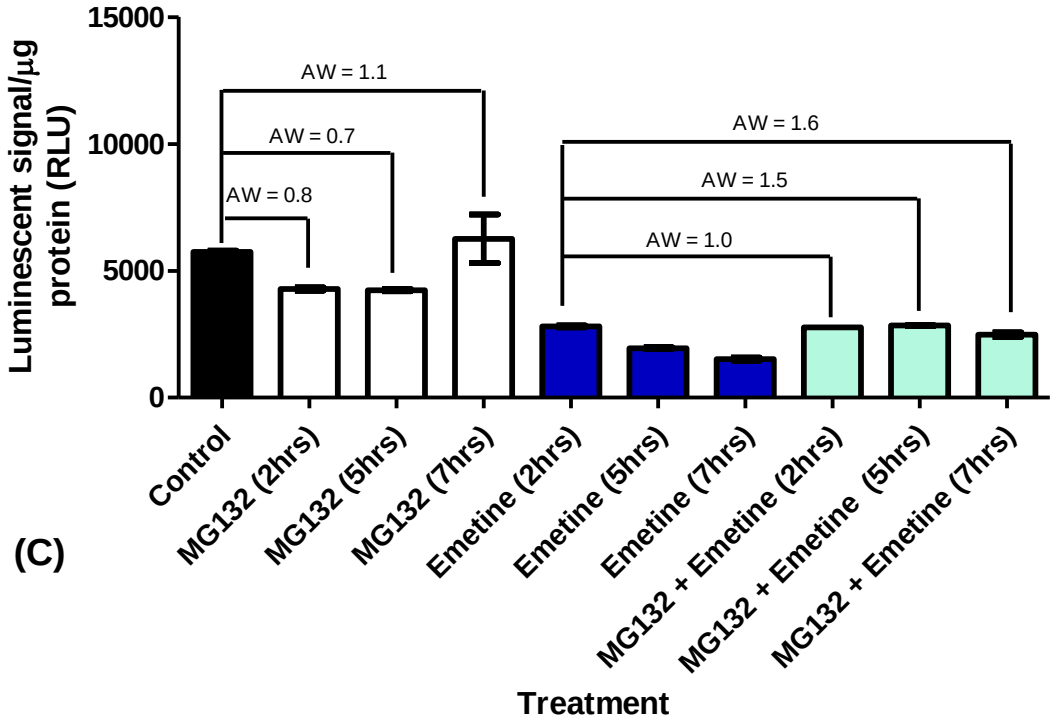

Figure 4-7: Luciferase assay: MG132 and Emetine time course in AS-M.5 cells stably expressing the SOCS3-Luciferase fusion construct

AS-M.5 cells stably expressing SOCS3-Luc were selected for by supplementing growth media with puromycin antibiotic. Cells were then grown until single colonies were observed. Clone E of the AS-M stable cells were seeded in 6 well plates and treated ± MG132 (6 µM) ± Emetine (100 µM) or vehicle only (control) for 2hrs, 5hrs and 7hrs. Cells were then harvested and luciferase assay performed (technical triplicates). The data were plotted as the mean luminescent signal/ µg protein with SEM error bars. (A) data from N=1, (B) data from N=2, (C) data from N=3. The assay window (AW) was calculated as follows: mean luminescent signal with MG132 treatment – mean luminescent signal without MG132 treatment. The inherent variability of the luciferase assay was observed between experimental repeats (A-C). Though MG132 + Emetine treatment appeared to increase the assay window the variability of the data limited progression to a luciferase based siRNA screening platform to identify the SOCS3 E3 ligase (A-C).

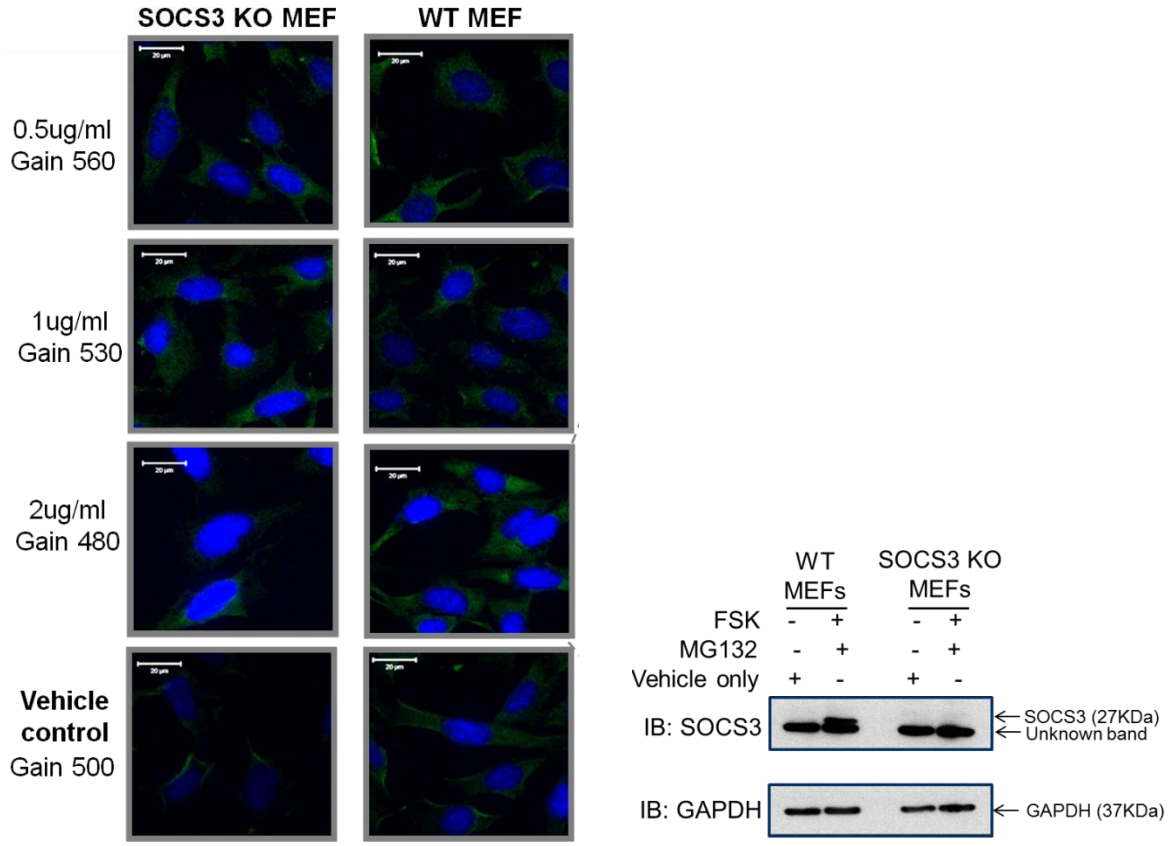

Figure 4-8: Immunofluorescence visualisation of SOCS3 in MEFs.

WT and SOCS3 knockout (KO) MEF cells were grown on glass coverslips and stimulated with ±Fsk (10 μM) and MG132 (6 μM) or vehicle (DMSO) only for 5 hrs. (A) Cells were then fixed in paraformaldehyde, permeabilised in 0.1% Triton X-100, blocked in rabbit serum and stained with a rabbit anti-SOCS3 primary antibody (Ab16030) over a concentration range of 0.5-2 μg/ml for 16 hrs at 4°C. Incubation with donkey anti-rabbit secondary antibody (AlexaFlour 488) (2 hrs, 4°C) was followed by DAPI nuclear staining and coverslips were mounted on glass slides for visualisation with the confocal microscope. (B) Whole cell lysates were prepared in parallel for immunoblotting with SOCS3 and GAPDH. The SOCS3 primary antibody revealed non-specific binding in the SOCS3 knockout MEF cells (A). Western blot analysis confirmed the absence of SOCS3 in the KO MEFs however SOCS3 was induced and stabilised in the WT MEF population (B). A prominent non-specific band was observed at ~23KDa on the SOCS3 immunoblots (B). The experiment was repeated to N=2 and representative images and immunoblots shown.

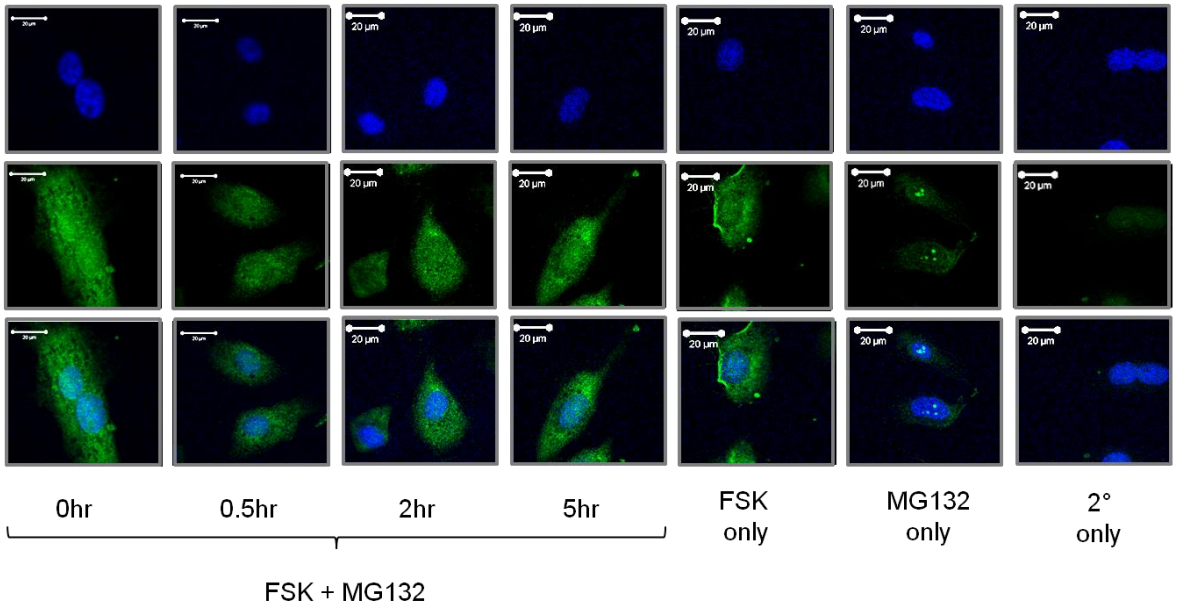

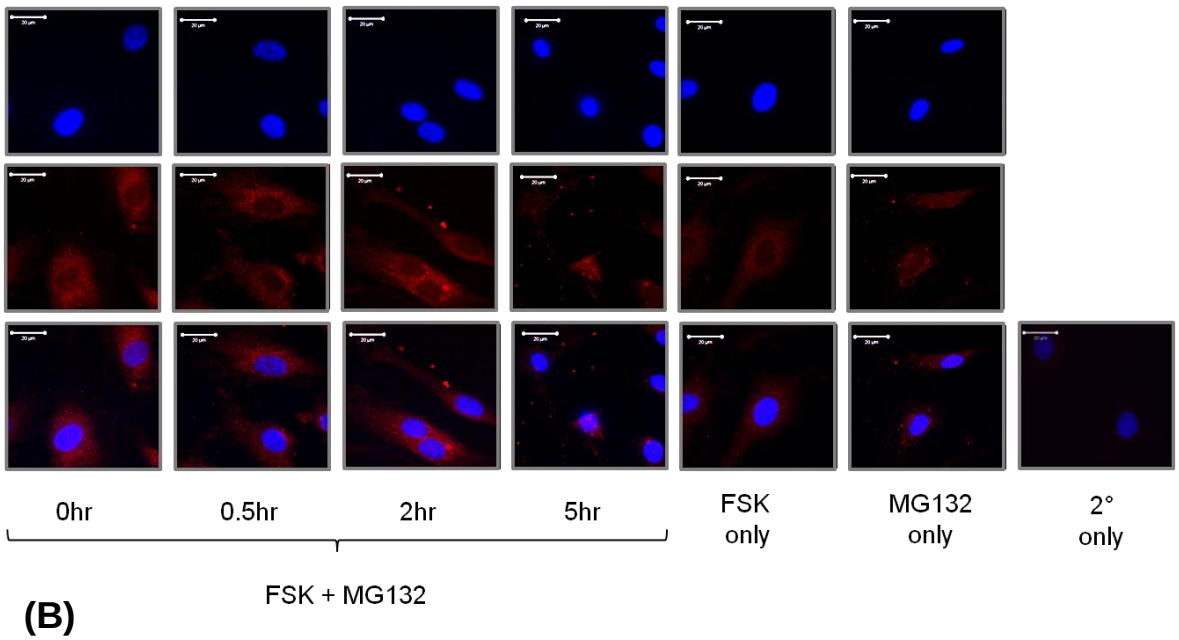

Figure 4-9: Immunofluorescence visualisation of SOCS3 in HUVECs *(Continued overleaf)***…**

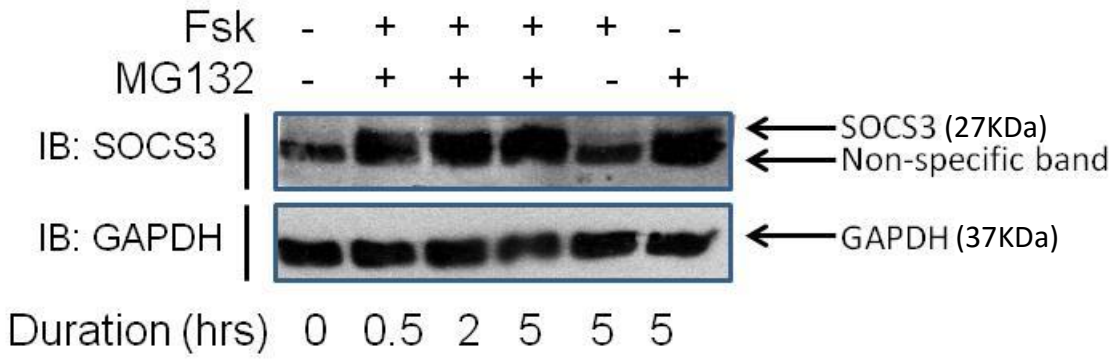

(C)

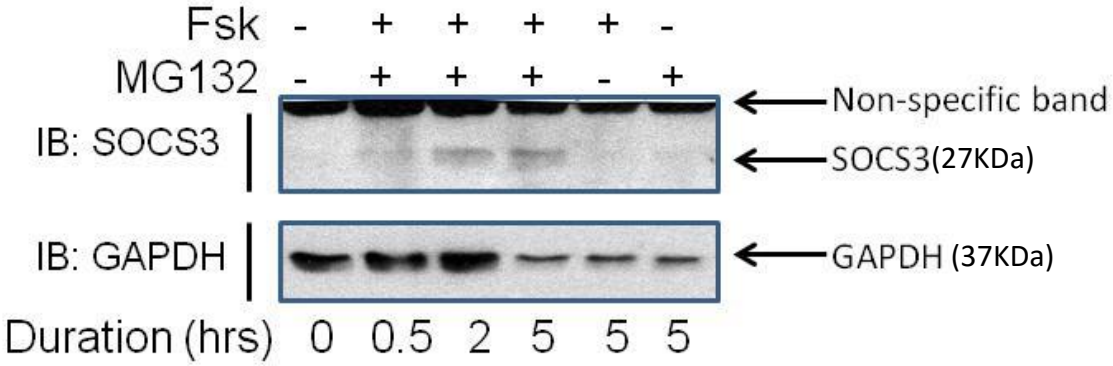

(D)

Figure 4-9: Immunofluorescence visualisation of SOCS3 in HUVECs

HUVECs were grown on glass coverslips and stimulated with ±Fsk (10 µM) ± MG132 (6 µM) or vehicle (DMSO) for 0-5 hrs. (A-B) Cells were then fixed in paraformaldehyde, permeabilised in 0.1% Triton X-100, blocked in rabbit or goat serum and stained with 1 µg/ml rabbit anti-SOCS3 primary antibody (Ab16030) (A) or 2 µg/ml goat anti-SOCS3 (SC-7009) (B) for 16 hrs at 4°C. Incubation with donkey anti-rabbit (AlexaFlour® 488) or donkey anti-goat (AlexaFlour® 594) secondary antibody (2 hrs, 4°C) was followed by DAPI nuclear staining and coverslips were mounted on glass slides for visualisation with the confocal microscope. (C-D) Whole cell lysates were prepared in parallel for immunoblotting with SOCS3 ab16030 (C) or In-house (D) primary antibodies. Immunoblotting for GAPDH was performed as a loading control. (A-B) Immunofluorescence did not reveal a change in SOCS3 expression over the 5 hr Fsk/MG132 time course suggesting non-specific binding of the Ab16030 and SC-7009 primary antibodies (A and B respectively). (C-D) Immunoblot analysis of lysates confirmed the FSK and MG132 stimulation worked. SOCS3 expression was maximal at 5 hrs Fsk + MG132 treatment (C-D). However, non-specific bands were visible at ~25 kDa (below SOCS3) or at ~39kDa (above SOCS3) for the Ab16030 and in-house SOCS3 antibodies respectively. The experiment was repeated to N=2 and representative images and immunoblots shown.

4.2.7 The identification of SOCS3 interacting E3 ligase or DUB enzymes via LC-MS-MS

To identify potential E3 ligase and DUB enzymes that control proteasome-mediated SOCS3 turnover we used LC-MS-MS and subsequent bioinformatics analysis to identify proteins that co-immunoprecipitated with SOCS3. FLAG tagged WT SOCS3 was overexpressed in HEK293 cells and a co-IP of SOCS3 was performed using anti-FLAG beads. The co-IP sample was resolved via SDS-PAGE and protein was visualised using Coomassie stain (Figure 4-10). An intense black band (~25kDa) was observed in both the pcDNA3.1 and WT SOCS3 lane representing the light chain fragment of the anti-FLAG IP antibody (Figure 4-10). SOCS3 was visible at ~27kDa in the WT SOCS3 lane however this band was absent in the pcDNA3.1 control lane (Figure 4-10). Bands superior to this, and unique to the SOCS3 lane, may represent interacting proteins. The co-IP was more efficient in experimental repeat 2 (N=2) as the number and intensity of the bands visualised above 27kDa in the SOCS3 lane was greater than that of experimental repeat 1 (N=1) (Figure 4-10).

Following protein visualisation, the pcDNA3.1 and WT SOCS3 samples were excised from the gel and prepared for reversed-phase liquid chromatography tandem mass spectrometry analysis (performed by Dr David Sumpton, Beatson Institute). These data for experimental repeat 1 (N=1) and 2 (N=2) were analysed through MaxQuant (v1.4.1.6) and Mascot (v2.4.1) separately before being pooled and loaded into the Scaffold (v4.3.4) software for viewing (Figure 4-11). At a protein threshold of 95%, 713 proteins were identified as unique to the SOCS3 co-IP sample (Figure 4-11). These data were manually filtered by searching for gene name containing the word “ubiquitin” (Figure 4-11). 17 E3 ligase/ubiquitin related genes were identified in addition to 4 DUBs (Table 4-1). UBR2, HECTD1 and HERC2 were the most abundant E3 ligases identified by the screen with an abundance score ≥28. The detection of interacting proteins in the N=2 results indicated that the co-IP was more efficient for this experimental repeat as suggested by the Coomasie stain (Figure 4-10). For example, the E3 ligase KCMF1 had an abundance score of 28 in the N=2 data set however this protein was not detected in the N=1 MS-MS data set (abundance score of 0) (Table 4-1). Similarly, the USP9x, USP15 and USP11 DUBs had an abundance score of ≥25 in the N=2 data set however this score was <4 in the N=1 data set (Table 4-1).

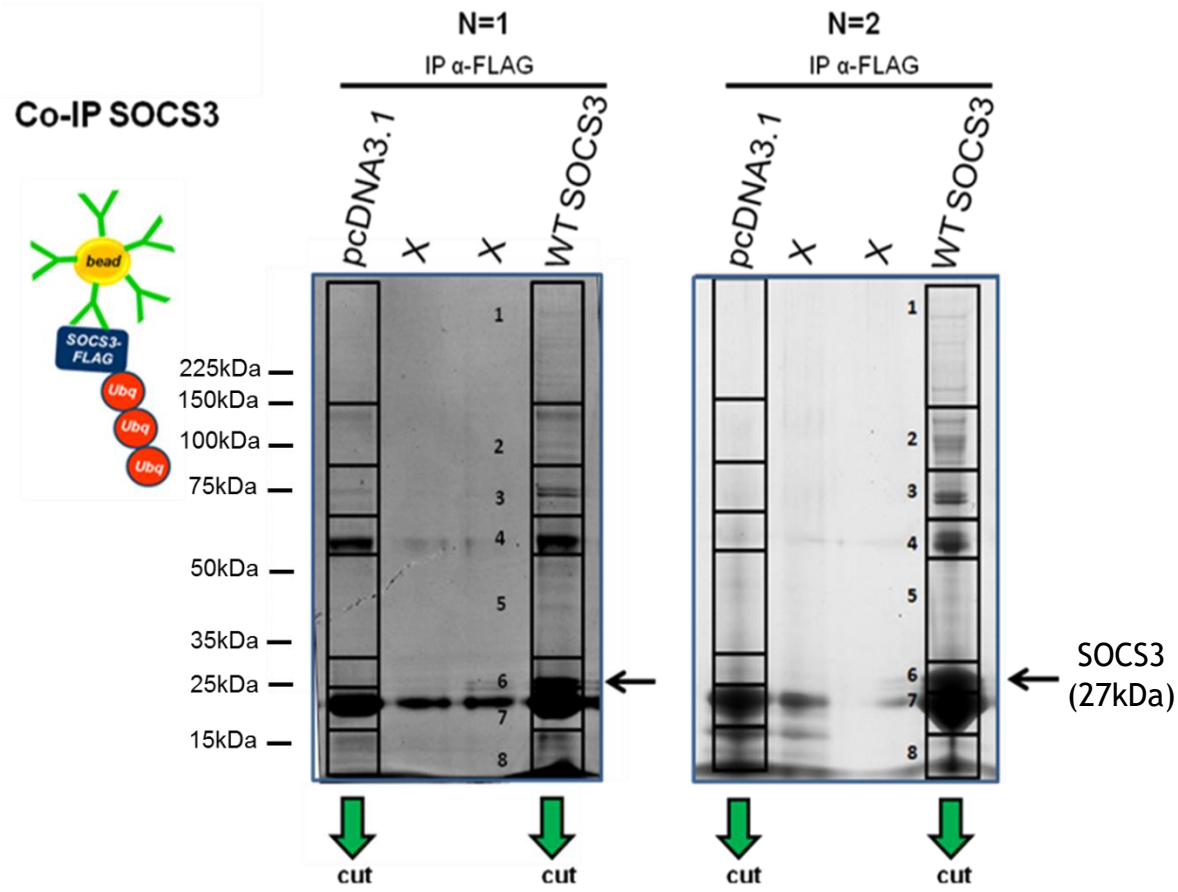

Figure 4-10: Co-Immunoprecipitation of SOCS3-FLAG in HEK293 cells for Mass Spectrometry.
HEK293 cells were transiently transfected with 10 μg FLAG tagged WT SOCS3 or pcDNA3.1. SOCS3 was then immunoprecipitated from whole cell lysates with anti-FLAG coated Sepharose beads. (A) IP samples (10 mg) were resolved by SDS-PAGE and Coomasie stain was performed. The intense black band at ~25KDa represents light chain fragments of the IP antibody. SOCS3 was visible at ~27KDa in the SOCS3 sample (black arrow) and absent in the pcDNA3.1 control lane. Superior bands unique to the SOCS3 lane may represent interacting proteins at the time of cell harvesting. Each band was excised from the gel, de-stained and subject to trypsination. Following a series of extractions and dehydration, the dried peptides were re-suspended in 5% (v/v) ACN/0.25% (v/v) formic acid solution and stored at -20°C until LC-MS/MS analysis. These data were collated from two experimental repeats.

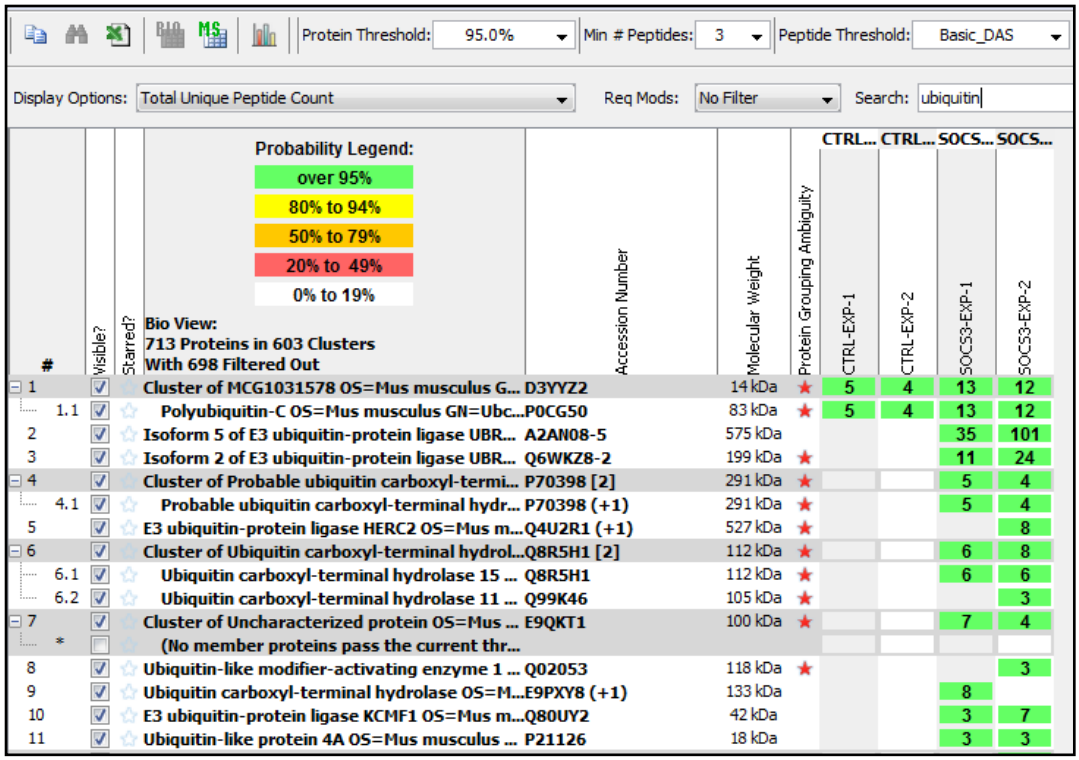

Figure 4-11: LC-MS-MS data analysis using Mascot v2.4.1 and Scaffold 4.3.4 software to identify potential SOCS3 interacting proteins

The SOCS3 or control co-IP samples were prepared for LC-MS-MS analysis as described in section 2.2.13. EXP-1 and EXP-2 denotes results from experimental repeat 1 and 2 respectively. Reversed-phase liquid chromatography tandem mass spectrometry was performed on a LTQ-Orbitrap Velos coupled to a Proxeon Easy-LC by Dr David Sumpton at The Beatson Institute, Glasgow. These data were searched against the Swiss-Prot *Mus musculus* database (50807 entries) using Mascot v2.4.1 software. The data were combined with the previous experiments raw files (n=2) and searched against the same database using MaxQuant (v1.4.1.6) for both protein identification and label free quantitation. The MaxQuant ID information was then pooled with the Mascot results and loaded into the Scaffold 4.3.4 proteome software package for viewing. The probability threshold was set at 95% increasing the likeliness of correct protein identification in the LC-MS sample. These data were searched for protein name containing the word “ubiquitin” and this list was manually filtered for E3 ligase and DUB enzymes.

E3 ubiquitin protein ligases

Protein Accession Number	Protein names	Gene names	Unique peptides	Sequence coverage (%)	Mol. weight (kDa)	EXP 1 abundance	EXP 2 abundance
Q6WKZ8	E3 ubiquitin-protein ligase UBR2	Ubr2	21	14.20	199.20	32.11	33.95
Q69ZR2	E3 ubiquitin-protein ligase HECTD1	Hectd1	16	7.30	289.23	29.28	30.82
Q4U2R1	E3 ubiquitin-protein ligase HERC2	Herc2	8	2.10	523.38	28.30	29.07
O08759	Ubiquitin-protein ligase E3A	Ube3a	7	10.00	99.82	27.98	27.38
O70481	E3 ubiquitin-protein ligase UBR1	Ubr1	2	1.60	200.24	27.10	0.00
O35445	E3 ubiquitin-protein ligase RNF5	Rnf5	2	9.40	19.84	26.79	0.00
Q80TP3	E3 ubiquitin-protein ligase UBR5	Ubr5	59	24.10	308.96	8.43	10.40
A2AN08	E3 ubiquitin-protein ligase UBR4	Ubr4	96	19.60	570.29	7.34	35.61
A2AFQ0	E3 ubiquitin-protein ligase HUWE1	Huwe1	57	17.60	482.63	6.14	33.52
E9PUJ6	Probable E3 ubiquitin-protein ligase MYCBP2	Mycbp2	19	5.80	517.36	3.90	30.69
Q80UY2	E3 ubiquitin-protein ligase KCMF1	Kcmf1	8	24.10	41.79	0.00	28.09
Q3U487	E3 ubiquitin-protein ligase HECTD3	Hectd3	3	4.20	97.35	0.00	27.06
Q91YL2	E3 ubiquitin-protein ligase RNF126	Rnf126	2	7.00	34.08	0.00	26.25

Table 4-1: Ubiquitin related proteins identified as possible SOCS3 interactors via mass spectrometry *(Continued overleaf)*

Q80U95	Ubiquitin-protein ligase E3C	Ube3c	3	3.20	123.97	0.00	26.20
Q8CH72	E3 ubiquitin-protein ligase TRIM32	Trim32	3	6.10	72.06	0.00	25.76
Q3U1J4	DNA damage-binding protein 1	Ddb1	45	39.7	126.85	2.96	2.35
O88738	Baculoviral IAP repeat-containing protein 6	Birc6	44	10.8	529.41	4.07	33.69
Deubiquitylases							
Q4FE56	Ubiquitin carboxyl-terminal hydrolase 9x	Usp9x	5	2.70	290.21	3.55	28.57
Q8R5H1	Ubiquitin carboxyl-terminal hydrolase 15	Usp15	7	9.40	112.32	0.60	26.98
Q99K46	Ubiquitin carboxyl-terminal hydrolase 11	Usp11	2	3.40	105.38	0.00	25.03
Q6A4J8	Ubiquitin carboxyl-terminal hydrolase 7	Usp7	8	8.50	127.99	2.03	0.00

Table4-1: Ubiquitin related proteins identified as possible SOCS3 interactors via mass spectrometry

Protein list generated in Mascot v2.4.1 and MaxQuant v1.4.1.6 software and loaded into the Scaffold 4.3.4 proteome software package. The EXP1 log2 1-SOCS3/ 1-Control and The EXP1 log2 2-SOCS3/ 2-Control indicate the abundance of the peptide fragments in identified in the MS/MS data. These data were normalised to the abundance of the peptide identified in the control sample and logged (log2). The greater the abundance of a peptide, the more likely the protein is a SOCS3 interactor. EXP1 and EXP2 denotes experimental repeat 1 and 2 respectively. These data were searched for protein name containing the word “ubiquitin” and this list was manually filtered for E3 ligase and DUB enzymes. 17 E3 ligase related proteins were identified in addition to 4 deubiquitylase related proteins.

4.2.8 Immunoblot validation of SOCS3 interacting proteins

To validate the interaction of SOCS3 with various targets identified in the LC-MS-MS screen (Table 4-1), we co-expressed FLAG tagged WT SOCS3 with a construct expressing the target of interest and performed a co-IP of SOCS3 using anti-FLAG beads (Figure 4-12 – 4-15 and Figure 4-18). Immunoblotting for the target of interest, and SOCS3, was performed to confirm this interaction was not an artefact of the LC-MS-MS analysis which could not be repeated to N=3 due to the associated cost.

Following immunoblot analysis, HA-tagged DDB1 was detected in the whole cell lysate at ~127kDa however this band was absent in the IP lane containing SOCS3 and DDB1 (Figure 4-12). Similarly, immunoblot analysis revealed GFP-tagged USP9x was expressed in the whole cell lysate at ~130kDa however this band was absent in the IP lane, containing SOCS3 and GFP-USP9x (Figure 4-13). These data confirmed that both DDB1 and USP9x were not *bona fide* SOCS3 interactors as suggested by the LC-MS-MS screen (Table 4-1).

Investigating whether UBR5 interacted with SOCS3 was not possible as the HA-tagged UBR5 construct did not express in HEK293 cells (Figure 4-14). A positive control for the HA primary antibody was included (HA-ubiquitylated SOCS3 lysate) confirming the primary antibody was immunoreactive with HA tag antigen (Figure 4-14). Due to time constraints on the project constructs which failed to express in HEK293 cells were not investigated further.

4.2.9 HectD1 was identified as a potential E3 ligase for SOCS3

HectD1 is a lys63(K^{63})-specific E3 ubiquitin ligase that was recently shown to ubiquitylate the adenomatous polyposis coli (APC) protein and so promote the negative regulation of Wnt signalling [247]. HectD1 was identified as a novel SOCS3 interactor in our LC-MS-MS screen (Table 4-1). Accordingly, validation of this interaction via co-IP of FLAG tagged SOCS3 with HectD1 using anti-FLAG beads was performed. Immunoblotting for HectD1 revealed that HectD1 was expressed in the whole cell lysate at ~290kDa (Figure 4-15). The presence of a 290kDa band in the IP lane containing SOCS3 and HectD1 confirmed this was a *bona fide* interaction (Figure 4-15).

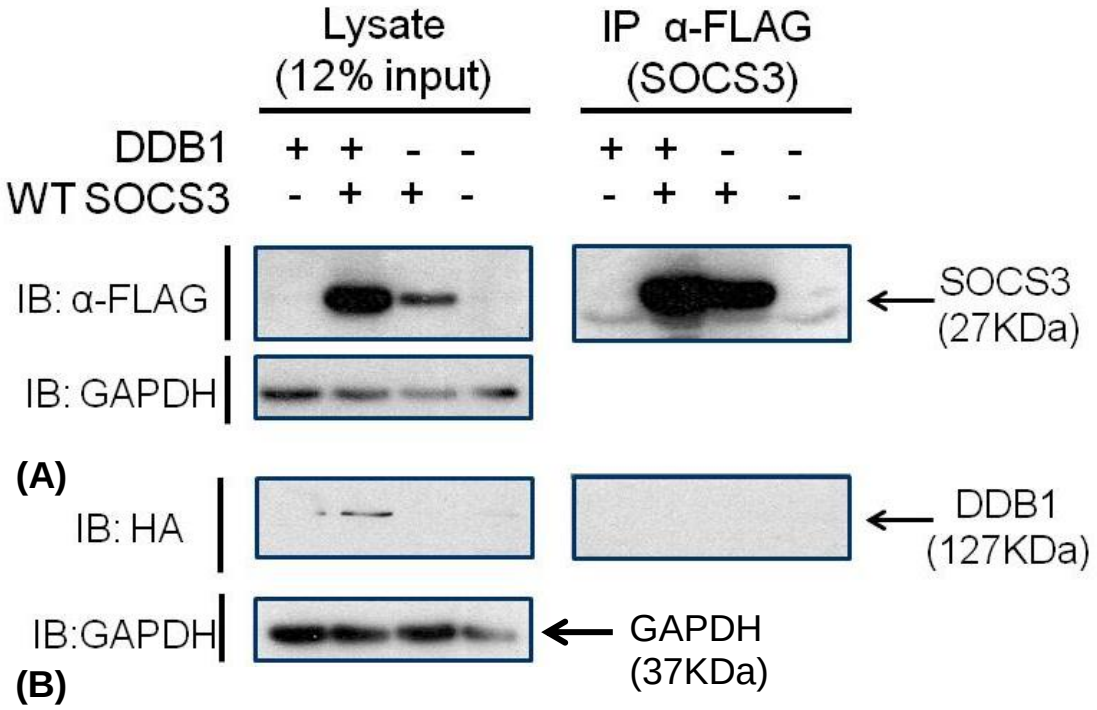

Figure 4-12: DDB1 did not interact with SOCS3 in HEK293 cells

HEK293 cells were transiently transfected with 2 µg FLAG tagged WT SOCS3 and HA tagged (DNA damage-binding protein 1 (DDB1). 48 hrs post transfection cells were treated with MG132 for 2 hrs (37°C, 5% $C0_2$) prior to harvesting in co-IP buffer. SOCS3 was then co-immunoprecipitated from lysates with anti-FLAG coated Sepharose beads. IP samples (500 µg) were split over two gels (250 µg/gel) alongside 30 µg whole cell lysate. Samples were resolved by SDS-PAGE and transferred to nitrocellulose membrane for western blotting. (A) Immunoblotting of whole cell lysates and IP SOCS3 (αFLAG) with mouse anti-FLAG (1:1000) and protein G-HRP (1:1000) to detect FLAG tagged SOCS3. (B) Immunoblotting of whole cell lysates and IP SOCS3 with rabbit anti-HA (1:1000) with anti-rabbit IgG-HRP (1:1000) secondary antibody to detect HA tagged DDB1. Membranes were then stripped and probed with mouse anti-GAPDH (1:20,000) and anti-mouse IgG-HRP to provide a loading control. WT SOCS3 did not interact with DDB1 (B). The experiment was performed to N=1.

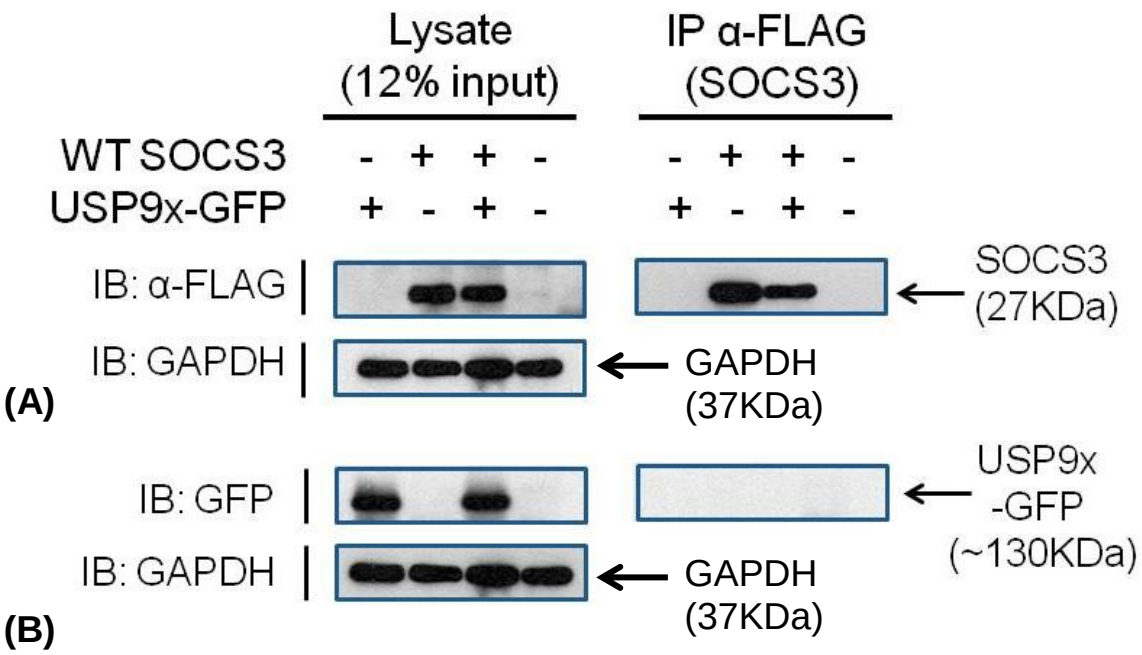

Figure 4-13: USP9x-GFP did not interact with SOCS3 in HEK293 cells

HEK293 cells were transiently transfected with 2 μg FLAG tagged WT SOCS3 and GFP tagged USP9x. 48 hrs post transfection cells were treated with MG132 for 2 hrs (37°C, 5% $C0_2$) prior to harvesting in co-IP buffer. SOCS3 was then co-immunoprecipitated from lysates with anti-FLAG coated Sepharose beads. IP samples (500 μg) were split over two gels (250 μg/gel) alongside 30 μg whole cell lysate. Samples were resolved by SDS-PAGE and transferred to nitrocellulose membrane for western blotting. (A) Immunoblotting of whole cell lysates and IP SOCS3 (αFLAG) with mouse anti-FLAG (1:1000) and protein G-HRP (1:1000) to detect FLAG tagged SOCS3. (B) Immunoblotting of whole cell lysates and IP SOCS3 with sheep anti-GFP (1:1000) with protein G-HRP (1:1000) to detect GFP tagged USP9x. Membranes were then stripped and probed with mouse anti-GAPDH (1:20,000) and anti-mouse IgG-HRP to provide a loading control. WT SOCS3 did not interact with USP9x-GFP (B). The experiment was performed to N=1.

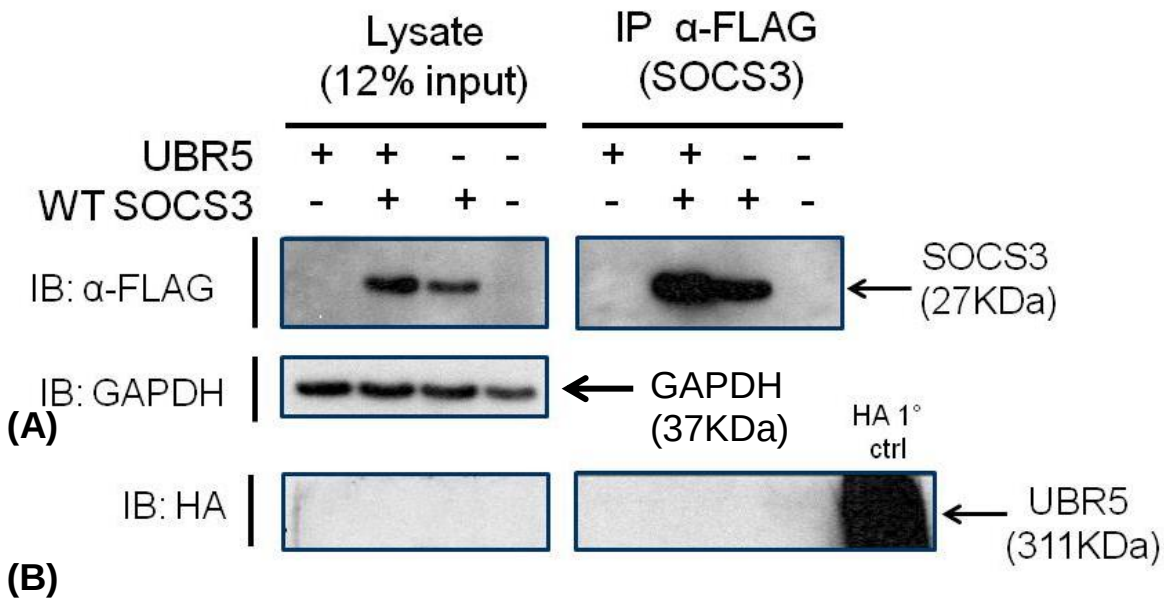

Figure 4-14: UBR5 did not interact with SOCS3 in HEK293 cells

HEK293 cells were transiently transfected with 2μg FLAG tagged WT SOCS3 and HA tagged UBR5. 48 hrs post transfection cells were treated with MG132 for 2 hrs (37°C, 5% $C0_2$) prior to harvesting in co-IP buffer. SOCS3 was then co-immunoprecipitated from lysates with anti-FLAG coated Sepharose beads. IP samples (500 μg) were split over two gels (250 μg/gel) alongside 30 μg whole cell lysate. Samples were resolved by SDS-PAGE and transferred to nitrocellulose membrane for western blotting. (A) Immunoblotting of whole cell lysates and IP SOCS3 (αFLAG) with mouse anti-FLAG (1:1000) and protein G-HRP (1:1000) to detect FLAG tagged SOCS3. (B) Immunoblotting of whole cell lysates and IP SOCS3 with rabbit anti-HA (1:1000) with anti-rabbit IgG-HRP (1:1000) secondary antibody to detect HA tagged UBR5. Membranes were then stripped and probed with mouse anti-GAPDH (1:20,000) and anti-mouse IgG-HRP to provide a loading control. WT SOCS3 did not interact with UBR5. The experiment was performed to N=1.

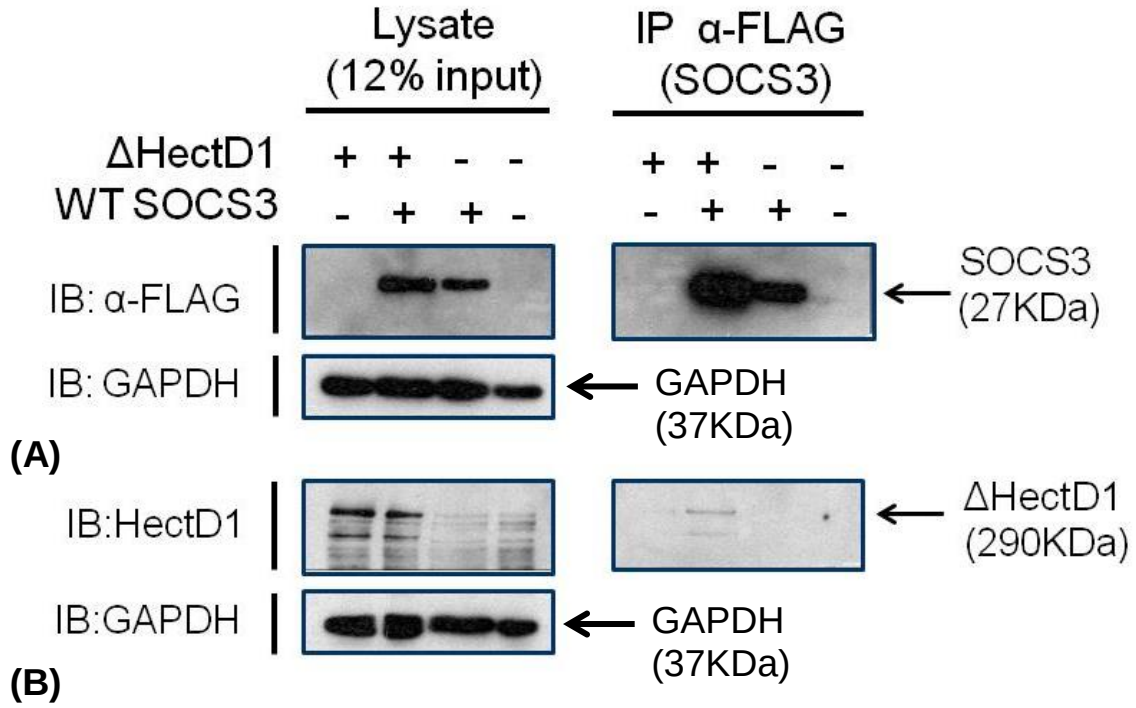

Figure 4-15: SOCS3 interacts with HectD1 in HEK293 cells

HEK293 cells were transiently transfected with 2 μg FLAG tagged WT SOCS3 and HA tagged mutant HectD1 ($cys^{2579}gly$). 48 hrs post transfection cells were treated with MG132 for 2 hrs (37°C, 5% $C0_2$) prior to harvesting in co-IP buffer. SOCS3 was then co-immunoprecipitated from lysates with anti-FLAG coated Sepharose beads. IP samples (500 μg) were split over two gels (250 μg/gel) alongside 30 μg whole cell lysate. Samples were resolved by SDS-PAGE and transferred to nitrocellulose membrane for western blotting. (A) Immunoblotting of whole cell lysates and IP SOCS3 (αFLAG) with mouse anti-FLAG (1:1000) and protein G-HRP (1:1000) to detect FLAG tagged SOCS3. (B) Immunoblotting of whole cell lysates and IP SOCS3 with rabbit anti-HectD1 (1:1000) with protein G-HRP (1:1000) secondary antibody to detect HectD1. Membranes were then stripped and probed with mouse anti-GAPDH (1:20,000) and anti-mouse IgG-HRP to provide a loading control. WT SOCS3 interacts with HectD1 ($cys^{2579}gly$). The experiment was repeated to N=3 and representative immunoblot shown.

In order to map the sites(s) of interaction between HectD1 and SOCS3 we assessed progressive SOCS3 truncation mutants. A panel of FLAG tagged SOCS3 truncation

mutants were co-expressed with HectD1, in HEK293 cells, and immunoprecipitated using anti-FLAG beads (Figure 4-16). Immunoblotting for HectD1 revealed that WT SOCS3 in addition to the SOCS3 truncation mutants (ΔC84, ΔC40, and ΔN36) interacted with HectD1 (Figure 4-16). The ΔN20 SOCS3 truncation mutant showed a faint band for HectD1 following co-IP suggesting a very weak interaction.

Moreover, to investigate whether HectD1 increased SOCS3 ubiquitylation, FLAG tagged SOCS3 was expressed in HEK293 cells in the presence of WT or catalytically inactive HectD1 (cys^{2579}→gly). $Cysteine^{2579}$ is located in the active site of HectD1 and is required for HectD1 enzyme activity therefore the cys^{2579}→gly mutant was catalytically inactive [248]. A denaturing IP was performed and immunoblotting for HA tagged ubiquitin revealed a slight increase in the poly-ubiquitylation of SOCS3 in the presence of WT HectD1 when compared to mutant HectD1 (Figure 4-17 B) however densitometry analysis confirmed that this was no a significant increase in SOCS3 ubiquitylation (Figure 4-17 C). Together these data suggested that HectD1 may not be a major regulator of SOCS3 ubiquitylation in HEK293 cells. The literature described HectD1 has as a K^{63}-specific E3 ligase therefore immunoblot analysis using a K^{63}-specific ubiquitin antibody was performed. Similarly, immunoblotting for K^{63}-linked ubiquitin showed a slight increase in the poly-ubiquitylation of SOCS3 in the presence of WT HectD1 when compared to mutant HectD1 (Figure 4-17 A).

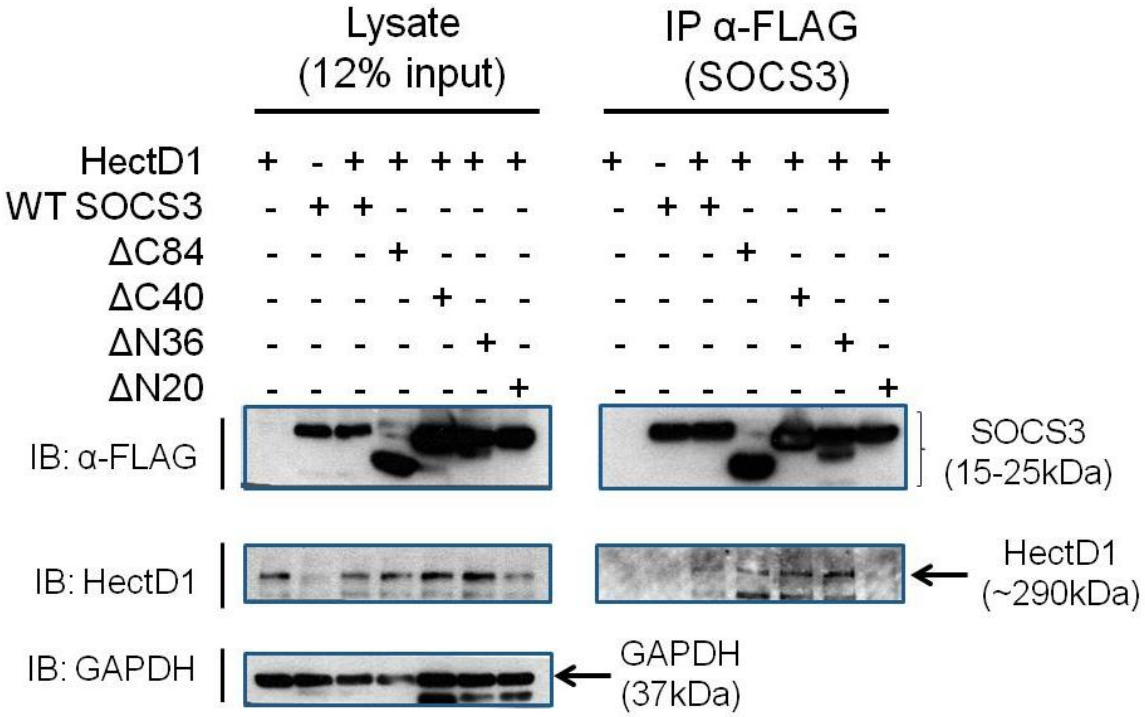

Figure 4-16: Mapping the interaction of HectD1 and SOCS3

HEK293 cells were transiently transfected with 1 µg FLAG tagged WT or mutant(ΔC84, ΔC40, ΔN36, ΔN20) SOCS3 and HA taggedHectD1. 48hrs post transfection cells were treated with MG132 for 2 hrs (37°C, 5% $C0_2$) prior to harvesting in co-IP buffer. SOCS3 was then co-immunoprecipitated from lysates with anti-FLAG coated Sepharose beads. IP samples (500 µg) were split over two gels (250 µg/gel) alongside 30 µg whole cell lysate. Samples were resolved by SDS-PAGE and transferred to nitrocellulose membrane for western blotting. (A) Immunoblotting of whole cell lysates and IP for SOCS3 (αFLAG) with mouse anti-FLAG (1:1000) and protein G-HRP (1:1000) to detect FLAG tagged SOCS3. (B) Immunoblotting of whole cell lysates and IP with rabbit anti-HectD1 (1:1000) with protein G-HRP (1:1000) to detect HectD1. Membranes were then stripped and probed with mouse anti-GAPDH (1:20,000) and anti-mouse IgG-HRP to provide a loading control. WT, ΔC84, ΔC40 and ΔN36 SOCS3 interacted well with HectD1 in contrast to the ΔN20 SOCS3 truncation mutant which revealed a very faint band for HectD1 in the co-IP lane. Loss of the n-terminal 20 residues of SOCS3 appeared to reduce the ability of SOCS3 to interact with HectD1. The experiment was repeated to N=3 and representative immunoblot shown.

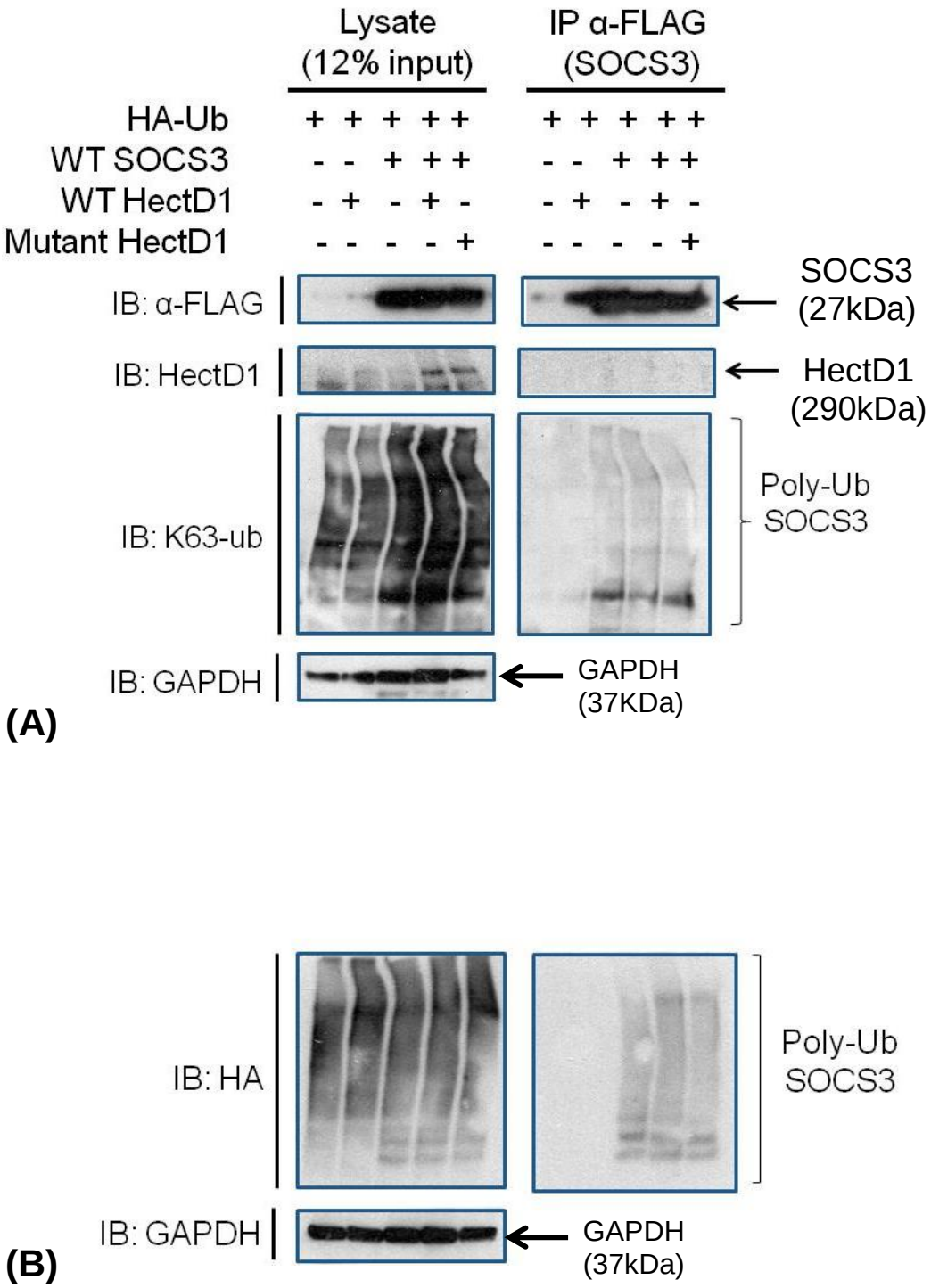

Figure 4-17: Investigating the effect of HectD1 on SOCS3 ubiquitylation *(Continued overleaf)…*

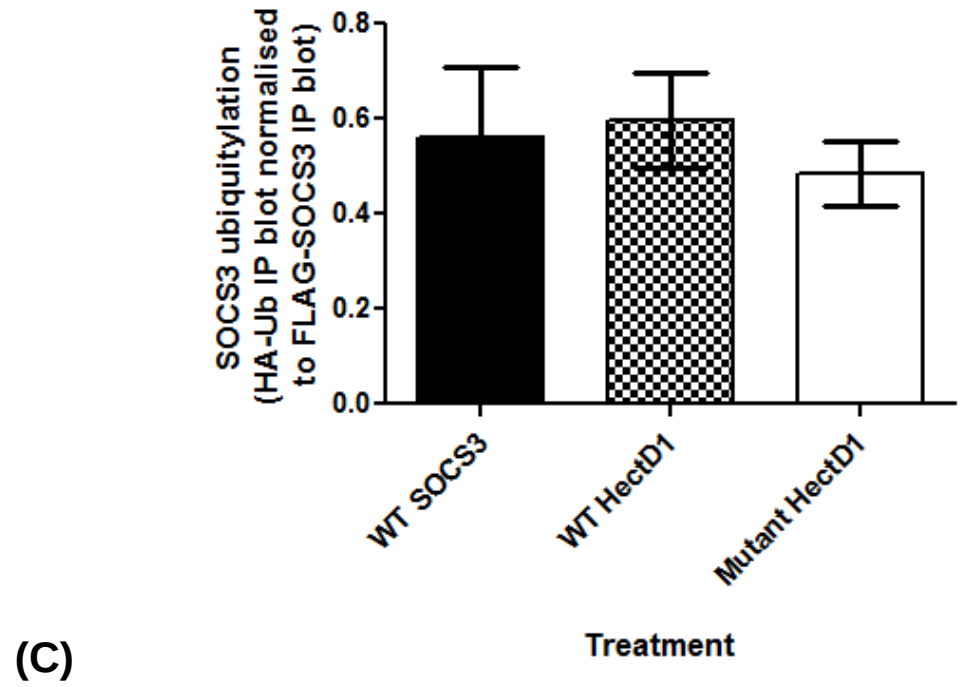

(C)

Figure 4-17: Investigating the effect of HectD1 on SOCS3 ubiquitylation

HEK293 cells were transiently transfected with 2 µg HA tagged ubiquitin (HA-Ub), 1 µg FLAG tagged WT SOCS3 and 3 µg WT HectD1 or mutant HectD1 ($cys^{2579}gly$). 48 hrs post transfection cells were treated with MG132 for 2 hrs (37°C, 5% $C0_2$) prior to harvesting in denaturing IP buffer. SOCS3 was then immunoprecipitated from lysates, under denaturing conditions, with anti-FLAG coated Sepharose beads. IP samples (500 µg) were split over two gels (250 µg/gel) alongside 30 µg whole cell lysate. Samples were resolved by SDS-PAGE and transferred to nitrocellulose membrane for western blotting. (A) Immunoblotting of whole cell lysates and IP SOCS3 (αFLAG) with mouse anti-FLAG (1:1000) to detected FLAG tagged SOCS3. The membrane was stripped and sequentially re-probed with rabbit anti-HectD1 (1:1000), rabbit anti-K-63 linked ubiquitin and mouse anti-GAPDH (1:20,000). (B) Immunoblotting of whole cell lysates and IP SOCS3 with rabbit anti-HA (1:1000) to detect HA tagged ubiquitin. Membranes were then stripped and re-probed with mouse anti-GAPDH (1:20,000). (A-B) Immunoblot visualisation was achieved using protein G-HRP (1:250) and enhanced chemiluminescence. (C) Densitometry analysis was performed using Total lab by normalising SOCS3 polyubiquitylation (Ub-HA blot) to the amount of SOCS3 present in the FLAG-SOCS3 IP blot. The data were presented as mean ± SEM. One-way ANOVA with Bonferroni correction was performed using GraphPad software where $P < 0.05$ was deemed significant. (C) WT HectD1 overexpression led to a slight increase in SOCS3 poly-ubiquitylation compared to the mutant HectD1 however this was not significant ($P > 0.05$) and suggests that HectD1 is not a major regulator of SOCS3 ubiquitylation. The experiment was repeated to N=3 and representative immunoblot shown.

4.2.10 USP15 was identified as a potential DUB for SOCS3

USP15 was identified as a novel SOCS3 interactor in our LC-MS-MS screen (Table 4-1). Accordingly, validation of this interaction via co-IP of FLAG tagged SOCS3 with USP15 using FLAG tagged beads was performed. Immunoblotting for USP15 demonstrated that USP15 was expressed in the whole cell lysate at ~112kDa (Figure 4-18). The presence of a 112kDa band in the IP lane containing SOCS3 and USP15 confirmed this was a *bona fide* interaction (Figure 4-18).

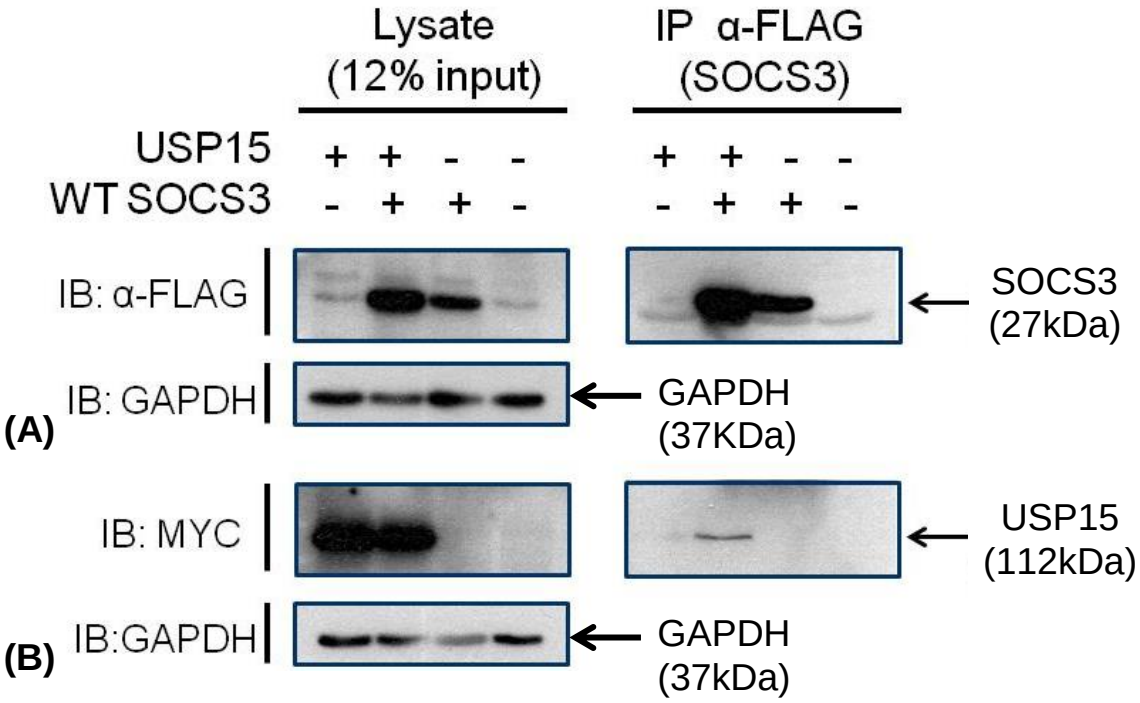

Figure 4-18: SOCS3 interacts with USP15 in HEK293 cells

HEK293 cells were transiently transfected with 2 µg FLAG tagged WT SOCS3 and MYC tagged USP15. 48hrs post transfection cells were treated with MG132 for 2 hrs (37°C, 5% $C0_2$) prior to harvesting in co-IP buffer. SOCS3 was then co-immunoprecipitated from lysates with anti-FLAG coated Sepharose beads. IP samples (500 µg) were split over two gels (250 µg/gel) alongside 30 µg whole cell lysate. Samples were resolved by SDS-PAGE and transferred to nitrocellulose membrane for western blotting. (A) Immunoblotting of whole cell lysates and IP SOCS3 (αFLAG) with mouse anti-FLAG (1:1000) and protein G-HRP (1:1000) to detect FLAG tagged SOCS3. (B) Immunoblotting of whole cell lysates and IP SOCS3 with mouse anti-MYC (1:1000) with protein G-HRP (1:1000) secondary antibody to detect MYC tagged USP15. Membranes were then stripped and probed with mouse anti-GAPDH (1:20,000) and anti-mouse IgG-HRP to provide a loading control. WT SOCS3 interacts with USP15. The experiment was repeated to N=3 and representative immunoblot shown.

In order to map the sites(s) of interaction between USP15 and SOCS3 we co-expressed a panel of FLAG tagged SOCS3 truncation mutants with USP15, in HEK293 cells, and immunoprecipitated SOCS3 using anti-FLAG beads (Figure 4-19). Immunoblotting for USP15 revealed that WT and ΔN36 SOCS3 had the strongest interaction with USP15. A faint band for USP15 was detected in the ΔN20 SOCS3 co-IP lane however no interaction was observed with the ΔC40 or ΔC84 SOCS3 truncation mutants (Figure 4-19).

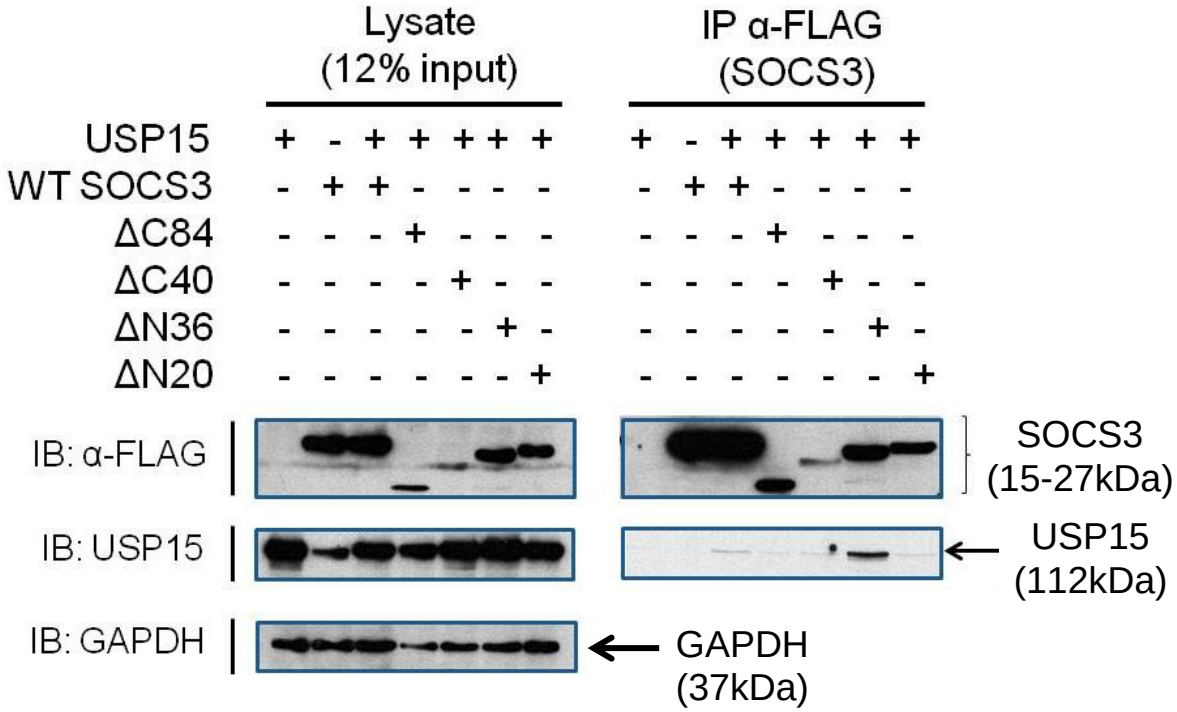

Figure 4-19: WT and ΔN36 SOCS3 co-immunoprecipitated with USP15

HEK293 cells were transiently transfected with 1 μg FLAG tagged WT or mutant(ΔC84, ΔC40, ΔN36, ΔN20)SOCS3 and MYC taggedUSP15. 48hrs post transfection cells were treated with MG132 for 2 hrs (37°C, 5% $C0_2$) prior to harvesting in co-IP buffer. SOCS3 was then co-immunoprecipitated from lysates with anti-FLAG coated Sepharose beads. IP samples (500 μg) were split over two gels (250 μg/gel) alongside 30 μg whole cell lysate. Samples were resolved by SDS-PAGE and transferred to nitrocellulose membrane for western blotting. (A) Immunoblotting of whole cell lysates and IP for SOCS3 (αFLAG) with mouse anti-FLAG (1:1000) and protein G-HRP (1:1000) to detect FLAG tagged SOCS3. (B) Immunoblotting of whole cell lysates and IP with sheep anti- USP15 (1:1000) with protein G-HRP (1:1000) to detect USP15. Membranes were then stripped and probed with mouse anti-GAPDH (1:20,000) and anti-mouse IgG-HRP to provide a loading control. WT and ΔN36 SOCS3 interacted with USP15. A faint band for USP15 was detected in the ΔN20 SOCS3 co-IP however ΔC84 and ΔC40 truncation mutants could no longer interact with USP15. The experiment was repeated to N=3 and representative immunoblot shown.

Moreover, to investigate whether USP15 reduced SOCS3 ubiquitylation, FLAG tagged SOCS3 was expressed in HEK293 cells in the presence of WT or catalytically inactive USP15 (C269S). A denaturing IP was performed and immunoblotting for HA tagged ubiquitin revealed a slight decrease in the poly-ubiquitylation of SOCS3 in the presence of WT USP15 only (Figure 4-20). However densitometry analysis confirmed that WT USP15 did not significantly reduce the ubiquitylation of SOCS3 in the HEK293 cell system (Figure 4-20 C).

4.2.11 The cullin-RING E3 ligase family do not control SOCS3 ubiquitylation

The cullin protein family require activation in order to form part of an E3 ligase complex. This is achieved via neddylation which describes the addition of a NEDD8 (neural precursor cell expressed developmentally downregulated protein 8) group [162, 163]. To examine whether the E3 ligase(s) controlling SOCS3 ubiquitylation require member(s) of the cullin protein family (cullin-RING ligases; CRLs), a neddylation inhibitor (MLN4924) was employed. HEK293 cells were transfected with 1 μg HA tagged ubiquitin ± 1 μg FLAG tagged WT SOCS3 (Figure 4-21). Cells were then treated with vehicle or a titration of MLN4924 for 24 hrs and MG132 for 2 hrs before harvesting. IP of SOCS3, under denaturing conditions, and immunoblotting for HA tagged ubiquitin revealed that MLN4924 treatment (1.2-4.8 μM) had a minimal effect on SOCS3 ubiquitylation (Figure 4-21B). It is possible that the laddering of the ubiquitin chains appears to move down slightly with increasing concentration of the inhibitor however densitometry analysis confirmed there was no significant change in SOCS3 ubiquitylation in the presence of MLN4924 (Figure 4-21C). As a control for MLN4924 activity, immunoblotting of lysates for p27 confirmed that in the presence of MLN4924, but not vehicle only, p27 expression was detected (Figure 4-21D).

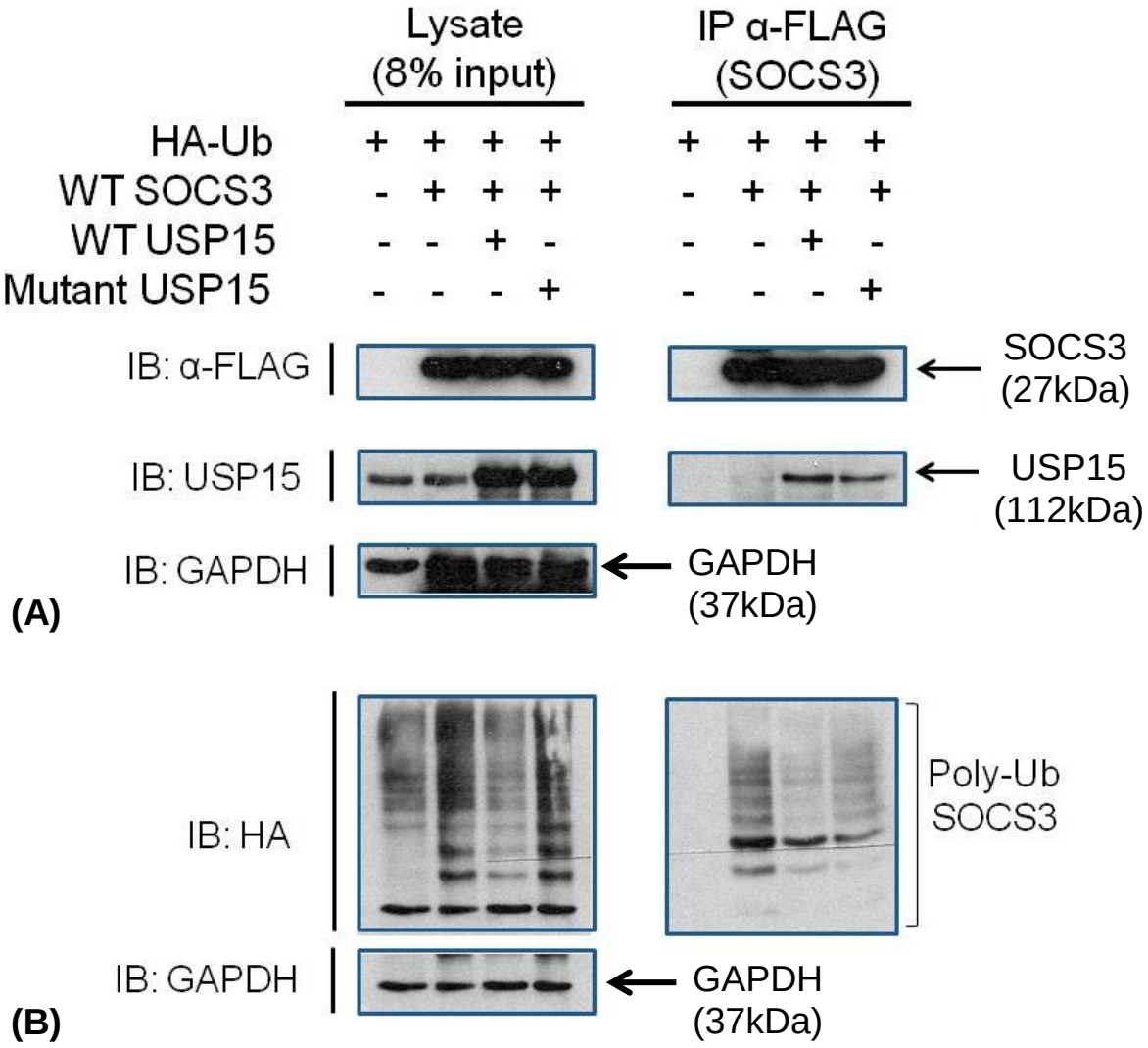

Figure 4-20: Investigating the effect of USP15 on SOCS3 ubiquitylation *(Continued overleaf)…*

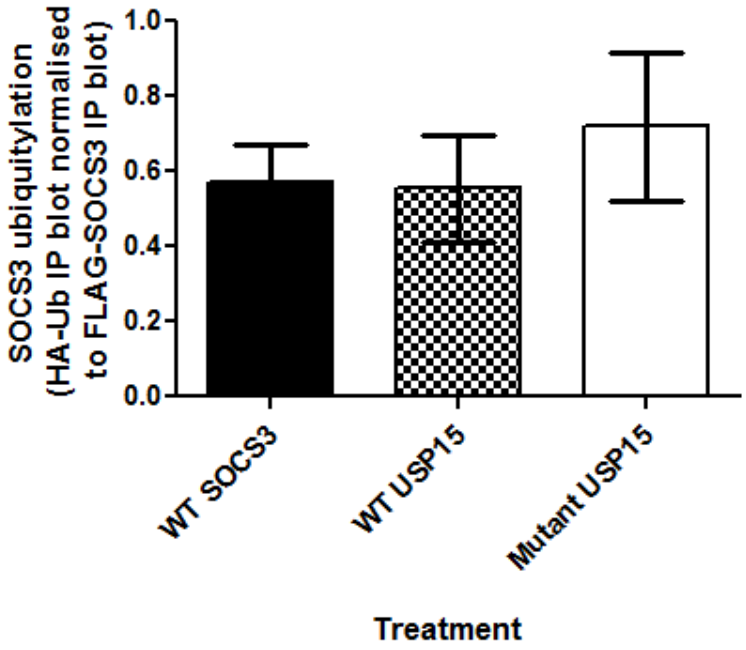

(C)

Figure 4-20: Investigating the effect of USP15 on SOCS3 ubiquitylation

HEK293 cells were transiently transfected with 2 µg HA tagged ubiquitin (HA-Ub), 1 µg FLAG tagged WT SOCS3 and 3 µg MYC tagged WT USP15 or mutant USP15 (C269S). 48 hrs post transfection cells were treated with MG132 for 2 hrs (37°C, 5% $C0_2$) prior to harvesting in denaturing IP buffer. SOCS3 was then immunoprecipitated from lysates, under denaturing conditions, with anti-FLAG coated Sepharose beads. IP samples (500 µg) were split over two gels (250 µg/gel) alongside 30 µg whole cell lysate. Samples were resolved by SDS-PAGE and transferred to nitrocellulose membrane for western blotting. (A) Immunoblotting of whole cell lysates and IP SOCS3 (αFLAG) with mouse anti-FLAG (1:1000) to detect FLAG tagged SOCS3. The membrane was stripped and re-probed with sheep anti-USP15 (1:1000). (B) Immunoblotting of whole cell lysates and IP SOCS3 with rabbit anti-HA (1:1000) to detect HA tagged ubiquitin. Membranes were then stripped and probed with mouse anti-GAPDH (1:20,000) to provide a loading control. (A-B) Immunoblot visualisation was achieved using protein G-HRP (1:250) and enhanced chemiluminescence. (C) Densitometry analysis was performed using Total lab by normalising SOCS3 polyubiquitylation (Ub-HA blot) to the amount of SOCS3 present in the FLAG-SOCS3 IP blot. The data were presented as mean ± SEM. One-way ANOVA with Bonferroni correction was performed using GraphPad software where $P < 0.05$ was deemed significant. (C) WT USP15 overexpression led to a slight decrease in SOCS3 poly-ubiquitylation compared to the mutant USP15 however this was not significant ($P > 0.05$) and suggests USP15 is not a major regulator of SOCS3de- ubiquitylation. The experiment was repeated to N=3 and representative immunoblot shown.

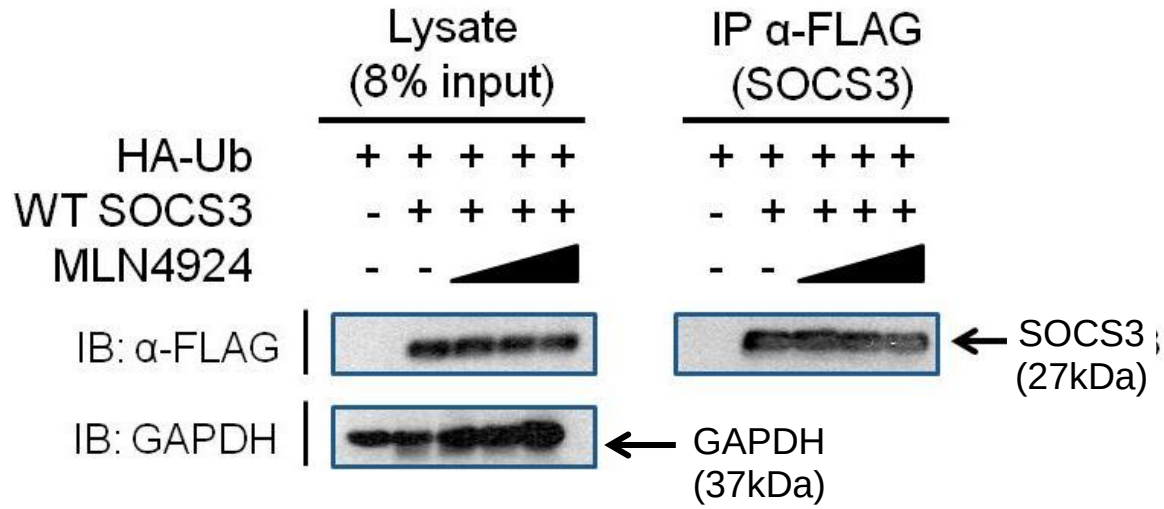

(A)

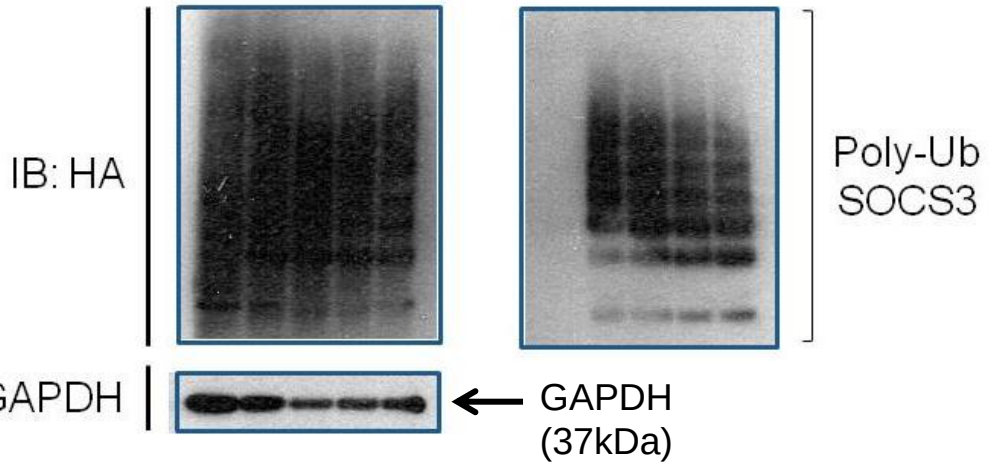

(B)

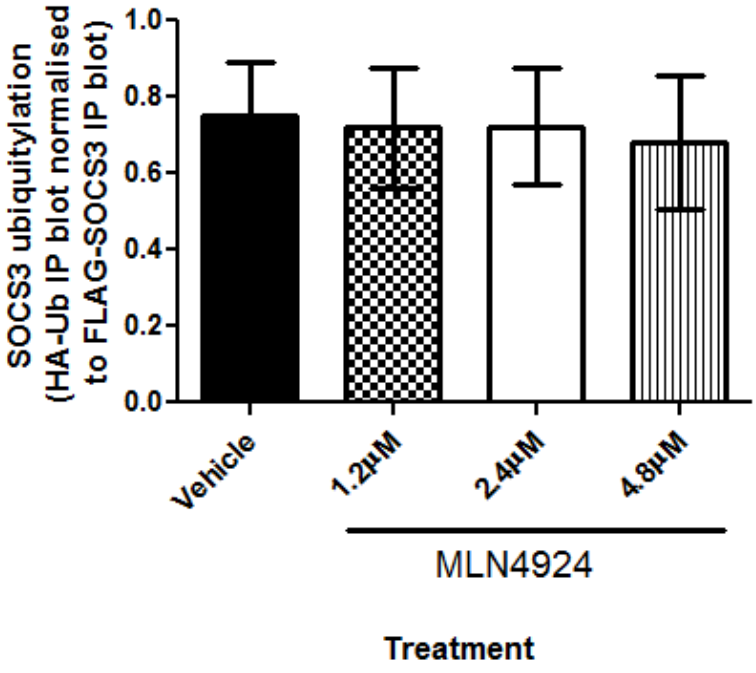

(C)

Figure 4-21: Inhibition of neddylation had no effect on SOCS3 ubiquitylation *(Continued overleaf)…*

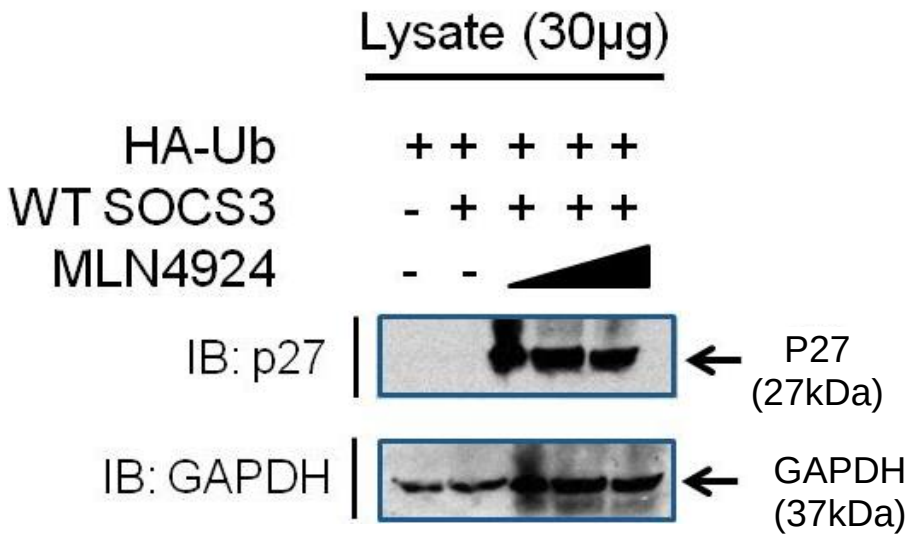

(D)

Figure 4-21: Inhibition of neddylation had no effect on SOCS3 ubiquitylation

HEK293 cells were transiently transfected with 2 µg HA tagged ubiquitin (HA-Ub) ± 1 µg FLAG tagged WT SOCS3. 24 hrs post transfection, cells were treated with DMSO vehicle or MLN4924 inhibitor (1.2 µM, 2.4 µM, 4.8 µM) for 24 hrs (37°C, 5% $C0_2$) before harvesting in denaturing IP buffer. SOCS3 was then immunoprecipitated from lysates, under denaturing conditions, with anti-FLAG coated Sepharose beads. IP samples (500 µg) were split over two gels (250 µg/gel) alongside 30 µg whole cell lysate. Samples were resolved by SDS-PAGE and transferred to nitrocellulose membrane for western blotting. (A) Immunoblotting of whole cell lysates and IP SOCS3 (αFLAG) with mouse anti-FLAG (1:1000) and protein G-HRP (1:1000) to detect FLAG tagged SOCS3 (B) Immunoblotting of whole cell lysates and IP SOCS3 with rabbit anti-HA (1:1000) with protein G-HRP (1:1000) to detect HA tagged ubiquitin. (C) Densitometry analysis was performed using Total lab by normalising SOCS3 polyubiquitylation (Ub-HA blot) to the amount of SOCS3 present in the FLAG-SOCS3 IP blot. The data were presented as mean ± SEM. One-way ANOVA with Bonferroni correction was performed using GraphPad software where $P < 0.05$ was deemed significant. (A-C) Inhibition of neddylation did not affect SOCS3 ubiquitylation status ($p>0.05$) suggesting the Cullin RING E3 ligase family may not regulate SOCS3 ubiquitylation and turnover in HEK293 cells. (D) Immunoblotting of whole cell lysates with mouse anti-p27 (1:300) and goat anti-mouse IgG-HRP (1:1000) secondary antibody to detect p27. Membranes were then stripped and probed with mouse anti-GAPDH (1:20,000) and goat anti-mouse IgG-HRP to provide a loading control. p27 degradation was blocked in the presence of MLN4924 confirming MLN4924 was active (D). The experiment was repeated to N=3 and representative immunoblot shown.

4.3 Discussion

SOCS3 is a poly-ubiquitylated protein with a relatively short half life (40-120 mins) that varies with cell type [97]. Gupta and colleagues [118] were the first to describe a significant reduction in SOCS3 expression in neointimal lesions derived from porcine coronary artery injury models. This led to our hypothesis that stabilising SOCS3 expression may limit the VSMC proliferation and migration contributing to NIH.

We aimed to identify the E3 ligase enzyme(s) responsible for the polyubiquitination of SOCS3 and therefore targeting it to the 26S proteasome. Knockdown of this E3 ligase gene *in vivo* may provide a useful tool for SOCS3 stabilisation and therefore reduction of NIH in patients undergoing PCI or CABGs. As such, we sought to develop an *in vitro* tool by which an E3 ligase siRNA library could be screened to identify the E3 ligase responsible for SOCS3 ubiquitylation.

First described in 2003, the AS-M.5 human endothelial cell line was derived from a male patient's scalp angiosarcoma (AS-M) [217]. For screening purposes, the use of an immortalised vascular cell line, as opposed to primary cells, would allow a degree of flexibility in terms of passage number and the risk of infection. As such we sought to characterise the ubiquitylation and turnover of SOCS3 in AS-M cells.

It was previously shown in human umbilical vein endothelial cells (HUVECs) that endogenous SOCS3 may be induced via a PKA independent cAMP route and not exclusively through the classic JAK/STAT pathway [177]. Interestingly, knockdown of the guanine nucleotide exchange factor (Epac1) in HUVECs abolished this cAMP mediated induction of SOCS3 and so elucidated a novel mechanism of SOCS3 induction in the vasculature [177]. As such, to investigate the proteasome as a route for endogenous SOCS3 turnover, we employed an adenylyl cyclase activator (Forskolin; Fsk) and a proteasome inhibitor (MG132) in AS-M and MEF cell lines. Consistent with the existing literature in HUVECs [177], FSK + MG132 stimulation significantly upregulated and stabilised the expression of endogenous SOCS3 in AS-M cells (Figure 4-1) and would therefore be amenable to an siARRAY screen for the SOCS3 E3 ligase(s).

In order to make a stable AS-M.5 cell line expressing the SOCS3-luciferase fusion protein, LV particles were generated using the p-lenti-CMV-SOCS3-Luc construct. LV vectors

have the advantage of incorporating the gene of interest into the host cell genome of both proliferating and non-proliferating cells [246]. Consequently, stable expression of the gene of interest may be achieved as opposed to the transient expression attained with non-viral vectors. It was important to select and expand an individual clone when generating a stable cell line to ensure the copy number of the SOCS3-luciferase gene was the same in all cells. If by chance, the cell population in one well of the assay had considerably more copies of the SOCS3-Luc gene this would suggest that the knockdown of an E3 ligase enhanced SOCS3 expression. As such, copy number variations between individual cells may result in false positive hits and therefore reduce the assay sensitivity (the ability of the assay to identify true positives) and specificity (the ability of the assay to identify true negatives).

Additionally, the linearity of the assay was assessed to ensure experiments were conducted within the linear range (Figure 4-4). Out with the linear range of the assay (signal plateau) other molecules such as luciferin [substrate] or ATP may be rate limiting factors.

Emetine is a protein synthesis inhibitor which blocks translation of mRNA at the ribosome and as previously mentioned MG132 is a peptide inhibitor of the proteasome. Our hypothesis was that in the AS-M.5 stable cell lines, SOCS3-Luc was transcribed and translated at such a high rate that any degradation at the proteasome was concealed in the luciferase assays. As such, treatment with Emetine would inhibit nascent translation of the SOCS3-Luc protein, at the same time MG132 treatment blocking proteasome degradation. Consequently, due to the inherent variability of the luciferase assay data and limited size of the AW for the most promising AS-M.5 stable clone E (Figure 4-6 and Figure 4-7) a luciferase based screening platform was considered unsuitable for the si-ARRAY.

An alternative strategy investigated was to develop a high content biology platform to screen the E3 ligase si-ARRAY (Figure 4-8). Immunofluorescence visualisation of endogenous SOCS3 may be performed in an automated, high throughput setting. Many of the high content imaging platforms have centred around small molecule drug discovery and predicting compound toxicity in man by quantifying an immunofluorescence signal using computer generated algorithms [249, 250]. The si-ARRAY to identify an E3 ligase controlling SOCS3 turnover would be amenable to a high content biology screen on the basis that knockdown of the E3 ligase would increase SOCS3 stability and therefore the intensity of the immunofluorescent signal. Initially, immunofluorescence visualisation of endogenous SOCS3 was investigated in WT vs SOCS3 KO MEFs however staining for

SOCS3 was observed in the SOCS3 KO MEFs (Figure 4-8 A). Conversely, immunoblotting of lysates, generated in parallel, showed SOCS3 expression was exclusive to WT MEFs (Figure 4-8 B). Moreover, a non-specific band, below that of SOCS3, was observed across all lanes in the western blot image (Figure 4-8 B). This further supports non-specific interaction of the Abcam 16030 primary antibody which may explain the ambiguous immunofluorescence result.

To determine whether this non-specific immunoreactivity was a cell specific problem in MEFs, we performed a Fsk/MG132 time course in HUVECs employing the Abcam 16030 and SantaCruz SC-7009 SOCS3 primary antibodies (Figure 4-9). Similarly, the HUVEC immunofluorescence data suggested the vehicle treatment group expressed SOCS3 to comparable levels as Fsk + MG132 treatment groups (Figure 4-9 A-B). Of note, immunoblot analysis using the ab16030 (Figure 4-9 C), in-house (Figure 4-9 D) and sc-7009 (data not shown) SOCS3 primary antibodies also revealed non-specific bands. Together, these data suggested non-specific immunoreactivity of the ab16030 and sc-7009 antibodies used for immunofluorescence in HUVECs. For that reason, the immunofluorescent visualisation of SOCS3 approach was deemed unsuitable for screening an E3 ligase siARRAY. In the absence of a suitable tool to screen the E3 ligase siARRAY alternative methods to identify an E3 ligase were investigated including LC-MS-MS.

In 2008, a genome wide study described 617 distinct E3 ligases [251]. As such, screening an E3 ligase si-ARRAY via immunoblot analysis of whole cell lysates was not deemed time or cost effective. In the absence of a suitable luciferase assay or high content biology tool to screen the si-ARRAY, LC-MS-MS analysis of a SOCS3 co-immunoprecipitate was investigated. These data were searched for E3 ligase or DUB enzymes that may interact with SOCS3 in HEK293 cells (Table 4-1) with the view to conduct functional validation in a vascular cell type in the future. Co-IP and immunoblot validation of these targets in HEK293 cells (a useful overexpression system) identified two promising candidates i) an E3 ligase known as HectD1 (Figure 4-15) and ii) a DUB known as USP15 (Figure 4-18).

Lys48(K^{48})-linked ubiquitylation targets proteins for proteasomal degradation [148]. In contrast, K^{63}-linked ubiquitylation is generally associated with a non-proteolytic role including the regulation of NF-κB signalling [140], DNA damage repair [141] and immune responses within the cell [142]. However, the literature describes the endocytosis and lysosomal degradation of cell surface proteins following K^{63}-linked ubiquitylation, a

modification that for some proteins required only two ubiquitin moieties in the chain [252]. Interestingly, Zhang and co-workers recently described the formation of mixed K^{48} and K^{63} polyubiquitin chains by the E3 ligase IDOL (inducible degrader of the LDL receptor) [146]. Consequently, the LDL receptor was degraded via the lysosomal or proteasomal route illustrating the complexity of ubiquitin signalling within the cell.

HectD1 has been described as a lys63(K^{63})-specific E3 ubiquitin ligase [247, 248]. In order to validate the HectD1-SOCS3 interaction, a co-IP was performed immunoblotting for HectD1 (Figure 4-15). Due to problems with the availability of a WT HectD1 construct, the co-IP was performed with the catalytically inactive point mutant (ΔHectD1; cys^{2579}gly). Nevertheless, ΔHectD1 was shown to interact with WT SOCS3. Upon the arrival of the WT HectD1 construct future investigations employed WT HectD1 where appropriate.

The literature on HectD1 is relatively sparse with only 29 publications cited by PubMed (http://www.ncbi.nlm.nih.gov/pubmed). As such, interpreting the role of a potential interaction with SOCS3 proved challenging. Denaturing IP experiments revealed that HectD1 slightly increased the poly-ubiquitylation of SOCS3 when compared to the catalytically inactive HectD1 mutant (cys^{2579}gly) in HEK293 cells (Figure 4-17). Immunoblotting with a K^{63}-linked ubiquitin antibody confirmed this subtle change in ubiquitylation status was attributed to an increase in K^{63}-linked ubiquitin chains specifically (Figure 4-17 A). However, as poly-ubiquitin chains appear as a black laddering down the immunoblot membrane, densitometry analysis to quantify this change in ubiquitylation status was not possible. Accordingly, caution should be warranted when interpreting these raw data by eye.

Recently, HectD1 was shown to conjugate K^{63}-linked poly-ubiquitin chains to the adenomatous polyposis coli (APC) protein [247]. Investigators treated cells with HectD1 siRNA and performed an IP using a K^{63}-linkage specific ubiquitin antibody to pull down Lys^{63} modified proteins only. Immunoblotting for APC revealed that siRNA mediated knockdown of HectD1 resulted in an obvious decrease in APC poly-ubiquitylation (lighter poly-ubiquitin smear on the blot) [247]. To confirm HectD1 induced changes to the ubiquitylation status of SOCS3 observed in the present study were not due to loading error (IP sample split over two gels) a similar method should be employed (Figure 4-17). A

GAPDH protein loading control for whole cell lysates was performed on the same gel as the IP samples.

To our knowledge, no E3 ligase for SOCS3 has been described in the literature and the identification of an E3 ligase controlling SOCS3 turnover may provide a useful therapeutic target. The development of a peptide disruptor to specifically disrupt the interaction between SOCS3 and the E3 ligase may avoid the off target effects associated with an E3 ligase inhibitor. In order to generate a peptide disruptor it is important to map the residues on both SOCS3 and the E3 ligase involved in the protein-protein interaction. Though HectD1 has been shown to be a K^{63} linked-ubiquitin E3 ligase ([247, 248]), and therefore may not control proteasomal turnover, it was still of interest to map the interaction site with SOCS3. As such, we assessed the ability of progressive SOCS3 truncation mutants to interact with WT HectD1. Loss of 84 or 40 residues at the C-terminus of SOCS3 did not affect the interaction with HectD1 (Figure 4-16). Similarly, loss of 36 residues at the n-terminus of SOCS3 did not affect the interaction with HectD1 (Figure 4-16). Interestingly, loss of 20 residues at the n-terminus of SOCS3 impaired its ability to interact with HectD1 as only a faint band was detected in the co-IP. Similarly, the band for HectD1 in the WT SOCS3 co-IP was not as prominent as the ΔN36 ΔC40 or ΔC84 SOCS3 mutants. These data suggested that a region between residues 20-36 on SOCS3 may be a strong repressor of the HectD1 interaction. A possible mechanism of the SOCS3-HectD1 interaction is depicted in Figure 4-22.

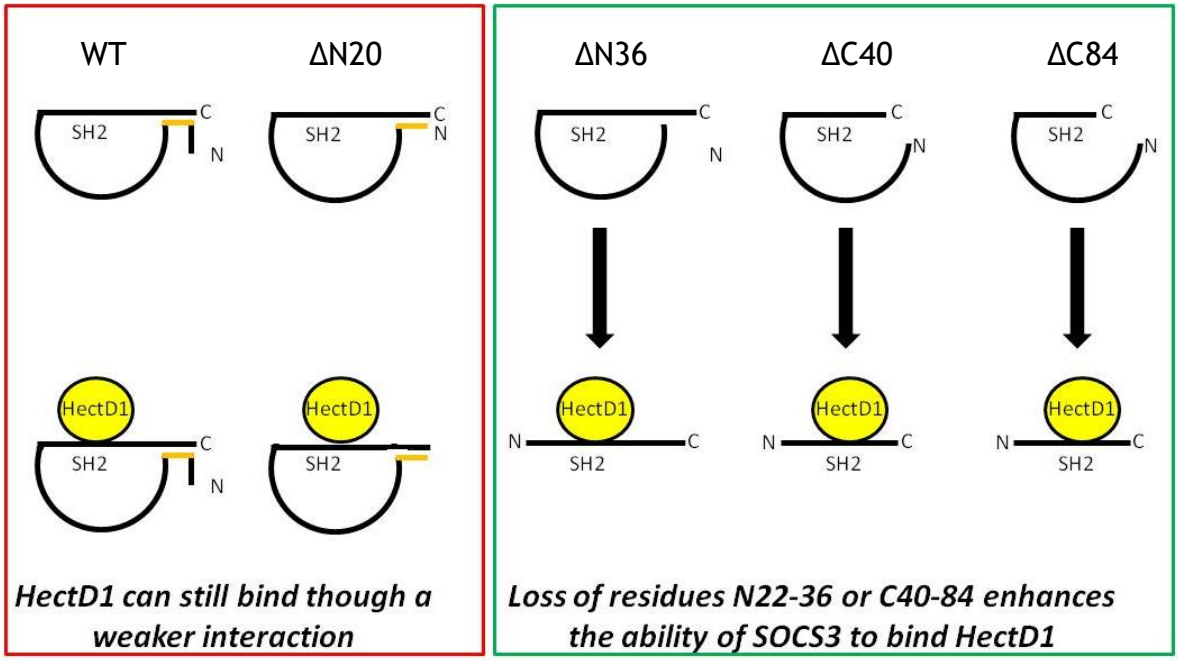

Figure 4-22: Possible mechanism to explain why SOCS3 mutagenesis enhanced the ability of SOCS3 to interact with HectD1.

Considering WT SOCS3 and ΔN20 SOCS3 did not interact as well with HectD1, the region between the n-terminal 20-36 residues may act as a repressor of this interaction. One possible explanation is that the n-terminal 20-36 residues interacts with the extreme c-terminus in such a way to occlude the central region which governs the interaction with HectD1. Therefore, loss of the n-terminus or c-terminus would enhance the ability to bind the E3 ligase HectD1.

As mentioned previously, the limited literature on HectD1 meant that predicting the functional significance of the SOCS3 interaction was challenging. Interestingly, knockout mouse models for both the HectD1 [253] and SOCS3 [45] were shown to be embryonic lethal due to malformation of the placenta during development. Though HectD1 may not be responsible for marking SOCS3 for proteasomal degradation, both proteins may be involved in a complex developmental signalling pathway. Conversely, SOCS3 was previously shown to interact with IRS-1/2 [88], Siglec-7 [90] and CD33 [91] targeting them for ubiquitin-mediated proteasomal degradation. As such, it is possible SOCS3 could target HectD1, and other interactors identified in the LC-MS-MS screen (Table 4-1), for proteasomal degradation.

Sequence alignment analysis has predicted that the human genome encodes ~79 DUB enzymes [254]. Ubiquitin-specific protease 15 (USP15) was initially described in 1999 [255] and is a member of the DUB family that contain a conserved “Cys” and “His” motif involved in the cleavage of ubiquitin [254]. The identification of a DUB regulating the ubiquitylation and therefore stability of SOCS3 would be a novel discovery. We

hypothesised that enhancing the stability and therefore expression of SOCS3 would reduce the development of NIH in CABG or PCI vessels. Interestingly, upregulation of the DUB for SOCS3 may provide a therapeutic strategy to achieve this. To identify the region of SOCS3 required for the interaction with USP15, progressive SOCS3 truncation mutants were assessed for their ability to interact with USP15 *in vitro*. Interestingly WT SOCS3 and the ΔN36 SOCS3 truncation mutant were able to interact with USP15 however the band for USP15 appeared to be more prominent in the ΔN36 lane (Figure 4-19). Of note, deletion of the N-terminal 20 residues (ΔN20) resulted in a loss of SOCS3-USP15 interaction (Figure 4-19). These data suggested that a region between residues 20-36 on SOCS3 may be a strong repressor of USP15 interaction. Additionally, loss of this interaction with the SOCS3 truncation mutants ΔC84 and ΔC40 suggested the C-terminal region of SOCS3 plays a major role in the interaction with USP15 (Figure 4-19).

To examine the functional significance of the SOCS3-USP15 interaction, a denaturing IP was performed to investigate the effect of USP15 on SOCS3 ubiquitylation. The poly-ubiquitin laddering in the WT SOCS3 only or WT SOCS3 + mutant USP15 lanes were more prominent than in the presence of the WT USP15 DUB (Figure 4-20). These data suggested that though USP15 appeared to de-ubiquitylate SOCS3 (Figure 4-20 B) this was not significant (Figure 4-20 C). Poly-ubiquitylation was still present and it is therefore likely that multiple DUBs may be involved in this process: a further example of functional redundancy within the system.

Moreover, USP15 was recently shown to de-ubiquitylate and stabilize the expression of an E3 ligase (Mdm-2) which in turn regulates the stability of the tumour suppressor p53 [256]. In the study conducted by Zou *et al* 2014, IP of Mdm-2 and immunoblotting for total ubiquitin revealed a striking decrease in Mdm-2 poly-ubiquitylation in the presence of WT USP15 but not in the presence of the catalytically inactive USP15. We have assessed the role of USP15 on SOCS3 ubiquitylation by a similar method however the USP15-mediated reduction in SOCS3 ubiquitylation was more subtle (Figure 4-20) than that observed for Mdm-2 by Zou *et al* [256]. This further supports the hypothesis that more than one DUB may be responsible for the de-ubiquitylation and therefore stabilisation of SOCS3.

Interestingly, Hetfeld and colleagues demonstrated that USP15 could de-ubiquitylate and stabilise the RING-domain E3 ligase Rbx1 [257]. The authors showed that USP15

enhanced the stability of Rbx1 following 6 hrs cycloheximide treatment (an alternative protein synthesis inhibitor to Emetine) [257]. Densitometry analysis confirmed a significant stabilising effect of WT USP15 on Rbx1, when compared to a catalytically inactive USP15 mutant (C783A). However, examination of the raw data (immunoblot) shows that these results appeared to be more subtle than Rbx1 turnover in cells transfected with Rbx1 + empty vector. Our data revealed a similar pattern where the WT SOCS3 +pcDNA3.1 empty vector lane appeared to show more poly-ubiquitylation than in the presence of catalytically inactive USP15 (C269S) (Figure 4-20).

The literature describes how SOCS3 provides a platform for the formation of an E3 ligase complex that subsequently ubiquitylates substrates bound by SOCS3 (Figure 1-11). It is possible that USP15 interacts with Rbx1 within this E3 ligase complex and not directly with SOCS3 as the co-IP technique involved a less stringent lysis buffer and aimed to preserve protein-protein interactions. Rbx1 may bind USP15 and therefore bring this DUB in close proximity with SOCS3 however confirmation of this would require further investigation. To test this hypothesis a co-IP for SOCS3 and USP15 in the presence of siRNA mediated knockdown of Rbx1 should be performed.

Previously we described the formation of a multi-protein E3 ligase complex on SOCS3 (Figure 1-11) that involved Elongin B, Elongin C, Rbx1 and Cul5 proteins. We have provided evidence to support the hypothesis that SOCS3 does not auto-ubiquitylate and that an external E3 ligase(s) controls the ubiquitylation of SOCS3 (Chapter 3: Figure 3.4-3.5). Accordingly, the ubiquitylation of SOCS3 by an external E3 ligase would still require the assembly of an E3 ligase complex to catalyse the ubiquitylation of SOCS3. Over 600 E3 ubiquitin ligases have been described in the literature including the cullin-RING ligase (CRL) family, of which there are around 350 members.

Neddylation is a post translational modification which describes the covalent attachment of a ubiquitin like protein (NEDD8) to a substrate (reviewed by [258]). Interestingly, in 1999 the human cullin protein family (cul1-5) were shown to be subject to neddylation[259]. In order for neddylation of cullins to proceed an E1 NEDD8 activating enzyme (NAE)[260] and an E2 NEDD8-conjugating enzyme (Ubc12)[261] are required. Importantly, cullin neddylation is required for the activation of the CRL E3 ubiquitin ligase family. Following its activation, a CRL is then available to participate in the formation of an E3 ubiquitin ligase complex and catalyse the ubiquitylation of its target substrate. With this in mind, we

employed a neddylation inhibitor (MLN4924) to assess whether members of the CRL family were responsible for the ubiquitylation and therefore proteasomal turnover of SOCS3. MLN4924 inhibits the E1 NAE and therefore cullin activation cannot proceed. In the presence of this neddylation inhibitor, there was a slight decrease in the laddering of SOCS3 ubiquitylation however this was a subtle observation and densitometry analysis confirmed there was no significant effect on SOCS3 ubiquitylation (Figure 4-21 B-C). These data suggested that though a CRL E3 ligase may be involved in the regulation of SOCS3 turnover it is unlikely to play a major role. The overall aim of this PhD was to identify a key E3 ligase or DUB with a significant contribution to SOCS3 stability and would therefore provide a useful therapeutic target. As such, future work should not focus on the role of the CRL family of E3 ligases in the regulation of SOCS3 turnover at the proteasome.

Furthermore, in 2000, Podust and colleagues confirmed that the CRL (SCF^{Skp2}) mediated degradation of a protein called $p27^{Kip1}$ required neddylation activity [262]. More recently, a study conducted in a pro-B cell line (Ba/F3) revealed that stimulation of cells with MLN4924 inhibited p27 turnover [164]. For that reason, as a positive control for MLN4924 activity, whole cell lysates were immunoblotted for p27 (Figure 4-21 D). The absence of p27 expression in the vehicle treatment group confirmed that the DMSO vehicle used to dissolve MLN4924 was not responsible for the enhanced stability of p27 observed in the MLN4924 treatment group only (Figure 4-21 D).

To summarise, the development of luciferase and immunofluorescence based assays to screen an E3 ligase si-ARRAY was unsuccessful due to technical limitations such as poor assay window and non-specific immunoreactivity of the SOCS3 antibodies available. As such, LC-MS-MS analysis of a SOCS3 co-immunoprecipitate was performed and identified >700 SOCS3 interacting proteins including seventeen E3 ligases and four DUBs. HectD1, a K^{63}-linked E3 ligase, was shown to interact with WT SOCS3 and truncation studies suggested that the SH2 domain of SOCS3 may facilitate this protein-protein interaction. Moreover, HectD1 appeared to slightly increase the ubiquitylation status of SOCS3 though these changes were subtle and not amenable to densitometry analysis. Additionally, USP15 (DUB) was also shown to interact with and decrease the ubiquitylation status of SOCS3 suggesting a role in the regulation of SOCS3 turnover. It is possible that the N-terminal 20 residues of SOCS3 serve as a repressor of USP15 interaction. Investigating the effect of HectD1 and USP15 on SOCS3 stability in a vascular setting is vital to explore therapeutic strategies in the vasculature specifically. Moreover,

validation of the remaining E3 ligase and DUBs identified in the LC-MS-MS screen is warranted as it is likely multiple E3s and DUBs regulate the ubiquitylation status and therefore stability of SOCS3. Ultimately, we would aim to identify candidate E3s or DUBs with a significant contribution to the regulation of SOCS3 turnover. One therapeutic strategy would be to develop a peptide disruptor to specifically target the E3-SOCS3 interaction, enhancing SOCS3 stability, and therefore expression. Similarly, candidate DUBs may be amenable to gene therapy strategies reducing K^{48}-linked ubiquitylation and therefore the proteasomal turnover of SOCS3. The advent of drug eluting stents and CABG procedures, employing virus infected conduits, may facilitate such therapies in the future.

4.3.1 Investigating non-specific immunoreactivity of primary antibodies

I hypothesised that the immunofluorescence investigations failed due to non-specific immunoreactivity of the SOCS3 primary antibody. To confirm this future experiments would involve i) siRNA-mediated knockdown of SOCS3 in MEFs/HUVECs and testing whether the so called "non-specific" bands were detected on an immunoblot of whole cell lysates and ii) assess whether the SOCS3 antibody binds the peptide sequence it was raised against *in vitro*. It is possible that the detergent Triton X-100 was too stringent and impaired the ability of the SOCS3 primary antibody to interact with the epitope on SOCS3 specifically. Future experiment should involve following the data sheet of the primary antibody as opposed to in-house protocols optimised for specific cell types.

4.3.2 Limitations of the study

There were some limitations of this study. Firstly, the SOCS3 immunoprecipitation experiments used for LC-MS/MS analysis to identify the novel E3/DUBs were performed in a non-vascular cell line (HEK293). HEK293 cells were selected as they provided an immortalised cell system that allowed reproducible and robust expression of FLAG tagged SOCS3 and ensured isolation of sufficient SOCS3 protein quantities for LC-MS/MS analysis (as a rough guide, pull down proteins visible by Coomassie staining following SDS-PAGE). The efficiency of plasmid expression in primary vascular cells, using standard transfection reactions, is often substantially lower versus HEK293 cells. In fact, the standard transfection reagent employed in the Palmer lab (PolyFect) does not document the efficiency of "hard to transfect" primary cells instead highlighting the success rate in

immortalised cell lines. More recently, transfection kits such as Nucleofector™ and Cytofect™ have reported improved efficiencies in primary smooth muscle cells however the cost associated is much higher than standard reagents. Using electroporation one group reported a 98% transfection efficiency in HUVECs [263] and this method warrants further investigation in primary VSMCs or ECs derived from HSV tissue. It was imperative that overexpression of SOCS3 was high to avoid insufficient SOCS3 protein content in the co-IP sample, thereby reducing the sensitivity of detection of interacting proteins in the LC-MS-MS analysis.

5 Investigating SOCS3 in the vasculature

5.1 Introduction

Procedures such as CABG and coronary angioplasty/stent implant are standard treatment options for patients presenting with asymptomatic coronary artery disease for whom pharmacological therapy is no longer effective [264]. However the patency of surgical and percutaneous intervention is limited by the accelerated re-narrowing of these vessels (neointima thickening) and susceptibility to atherosclerosis [264] (section 1.1).

In section 1.6 of this thesis we describe the role of JAK/STAT signalling in the vascular disease. Constitutive activation of the JAK2/STAT3 pathway was reported in an animal model of carotid artery balloon injury and provided the rationale that SOCS3 mediated inhibition of JAK may attenuate restenosis and the prevalence of NIH [172]. Similarly, Xiang and co-workers observed an increased in activated STAT3 and SOCS3 in a rat model of vein grafting suggesting a role for the JAK/STAT3 pathway in vessel remodelling [216].

SOCS3 is also thought to protect against the development of atherosclerosis. Ortiz-Munoz and co-workers described SOCS regulation of JAK/STAT signalling in vascular cells and their contribution to the progression of atherosclerosis [181]. SOCS3 was shown to limit the proliferative capacity of VSMCs *in vitro* whilst siRNA-mediated knockdown of SOCS3 *in vivo* increased atherosclerotic lesion size in apoE$^{-/-}$ mice [181]. Collectively, these data suggested that SOCS3 may serve as a negative regulator for VSMC activation and therefore a protective role against atherogenesis (section 1.6.3).

Interestingly, SOCS3 may play a role in the regulation of VSMC proliferation and migration which are key features of NIH (section 1.7). In a pig model of NIH SOCS3 expression was significantly reduced in the expanding NI lesion itself [118]. These data suggested that loss of this negative regulator *in vivo* promotes VSMC proliferation and migration from the media to the expanding intimal layer [118]. Additionally, in 3T3 fibroblasts [93] and a hepatocellular carcinoma (HCC) cell line [114], SOCS3 was shown to target activated FAK1 to the proteasome for degradation and therefore inhibited cellular migration. Similarly, knockdown of SOCS3 in a HCC cell line resulted in the up-

regulation of MMP-2/9 expression and increased cell proliferation, migration and invasion in a panel of *in vitro* assays [199].

SOCS3 is a critical negative regulator of JAK/STAT signalling. As such, it would be interesting to assess whether SOCS3 has the ability to limit STAT3-driven proliferation and migration of VSMCs responsible, in part, for NIH and vessel stenosis.

5.1.1 Aims

In the current study the localisation of SOCS3 within the various layers of a human blood vessel, specifically the human saphenous vein, was assessed. Moreover, preliminary functional investigations were conducted to assess the effect of SOCS3 overexpression on HSV SMC proliferation and migration *in vitro*.

5.2 Results

5.2.1 SOCS3 localised to the media, intima and endothelium of HSV tissue

Human saphenous vein (HSV) conduits are commonly used in coronary artery bypass procedures as an alternative to the internal mammary artery (IMA). Though the patency of HSV conduits is generally lower than the IMA, the HSV has the advantage of length and accessibility in patients. To investigate SOCS3 protein expression within the various layers of a human blood vessel, immunohistochemistry was performed in HSV tissue derived from patients undergoing CABG procedures. SOCS3 localised to the medial, intimal and endothelial layers of the blood vessel (Figure 5-1 a-b). SOCS3 appeared to be less abundant in the intimal region compared to the medial layer (Figure 5-1a-b). The isotype IgG control revealed faint background staining using DAB (Figure 5-1 c-d). The intima was pronounced and the blood vessel lumen appeared narrowed (Figure 5-1).

5.2.2 Investigating the effect of SOCS3 overexpression on HSV SMC proliferation

Before conducting experiments with primary vascular cells, we tested the ability of a GFP LV to overexpress a tractable gene (GFP) in HSVECs. The GFP virus was titrated (0-20IFU/cell) and imaged using a fluorescent microscope. At an MOI of 2, the efficiency of infection was ~100%, which decreased slightly at the higher MOIs (MOI 5 = 82%, MOI 10 = 88% and MOI 20 = 93%) (Figure 5-2 A). Immunoblot analysis performed in parallel revealed increasing the concentration of GFP virus correlated with an increase in GFP protein expression (Figure 5-2 B).

To assess whether the overexpression of SOCS3 in the SMCs would limit proliferation, a BrdU incorporation assay was performed. HSV segments left over from coronary bypass procedures were obtained, with ethical approval, and SMC cultures obtained from these. HSV SMCs were quiesced and infected with or without GFP or SOCS3-Luc LV particles. The BrdU assay revealed a trend toward decreased SMC proliferation in the presence of the SOCS3-Luc LV when compared to the no virus and GFP virus controls (Figure 5-3). In the absence of virus, serum starvation for 120 hrs resulted in an obvious reduction in BrdU

incorporation compared to the no virus control returned to serum containing media (Figure 5-3). Moreover, when viewed microscopically cell death was evident in the no virus, serum starved wells (data not shown).

5.2.3 Overexpression of SOCS3 in SMCs did not limit cell migration

To determine whether the overexpression of SOCS3 in SMCs would limit cell migration, a scratch-wound assay was performed. Initially, HSV SMCs were quiesced before creating a scratch using a p200 tip. The growth medium was then replaced with fresh low serum media (0.2%FBS) or SMC media containing 15% FBS (Figure 5-4). At this point cells were infected with SOCS3-Luc or GFP LV particles and cell migration at the wound site observed at 12 hrs and 24 hrs post infection time point. SOCS3 overexpression appeared to have no influence on VSMC migration when compared to GFP infected or no virus controls (Figure 5-4). In wells in which 15% FBS SMC media was replenished, at the time of virus infection, cell migration appeared to be more obvious than the groups maintained in 0.2%FBS for 96 hrs (Figure 5-4). Cell death was not observed after 96 hrs in 0.2% FBS (Figure 5-4).

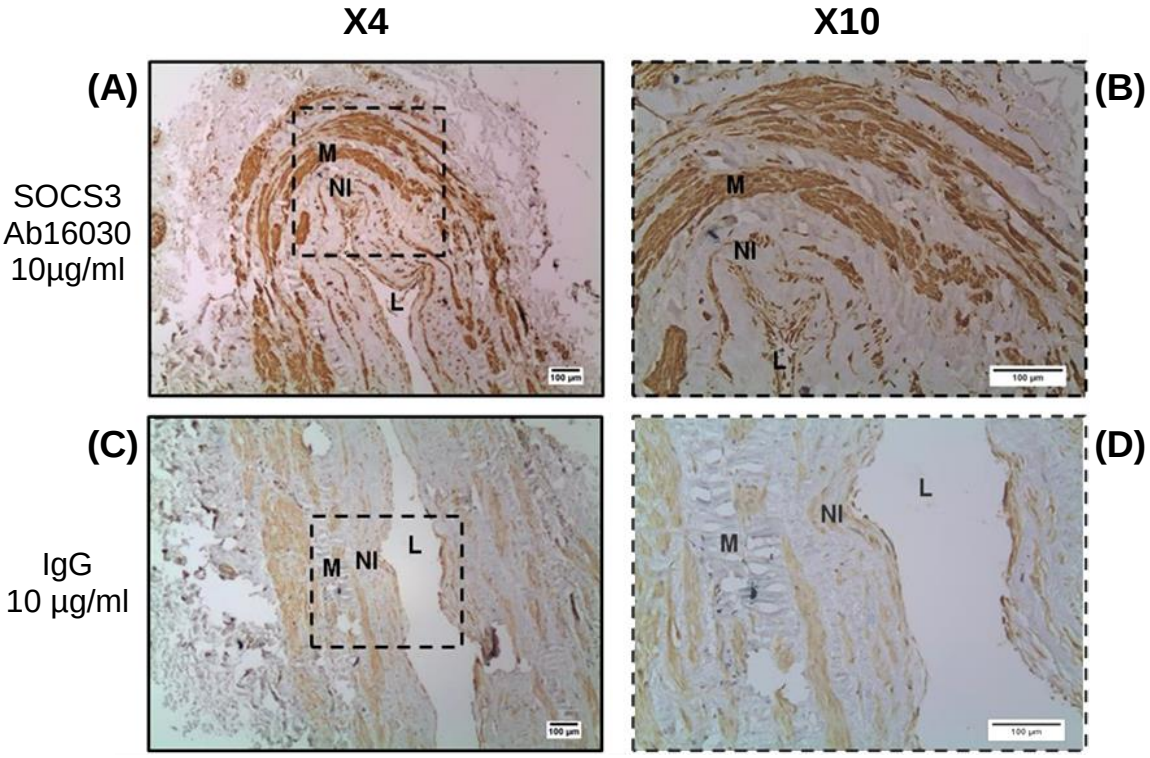

Figure 5-1: Immunolocalisation of SOCS3 in human saphenous vein tissue.

Paraffin embedded veins were cut to 4 µm sections, deparaffinised and probed with rabbit anti-SOCS3 (10 µg/ml) (A and B) or rabbit IgG (C and D) and biotinylated goat anti-rabbit (1:300) secondary antibody. SOCS3 was visualised using DAB and nuclei counterstained with haematoxylin. HSV tissue from three individual patients were analysed via IHC and representative images shown. Scale bar = 100 µm. (A) (x4) and (B) (x10) SOCS3 localised to the media (M), neointima (NI) and endothelium of HSV tissue though some adventitial fibres also showed positive staining. The lumen (L) appeared narrow. (C) (x4) and (D) (x10) rabbit IgG control revealed faint background staining with DAB.

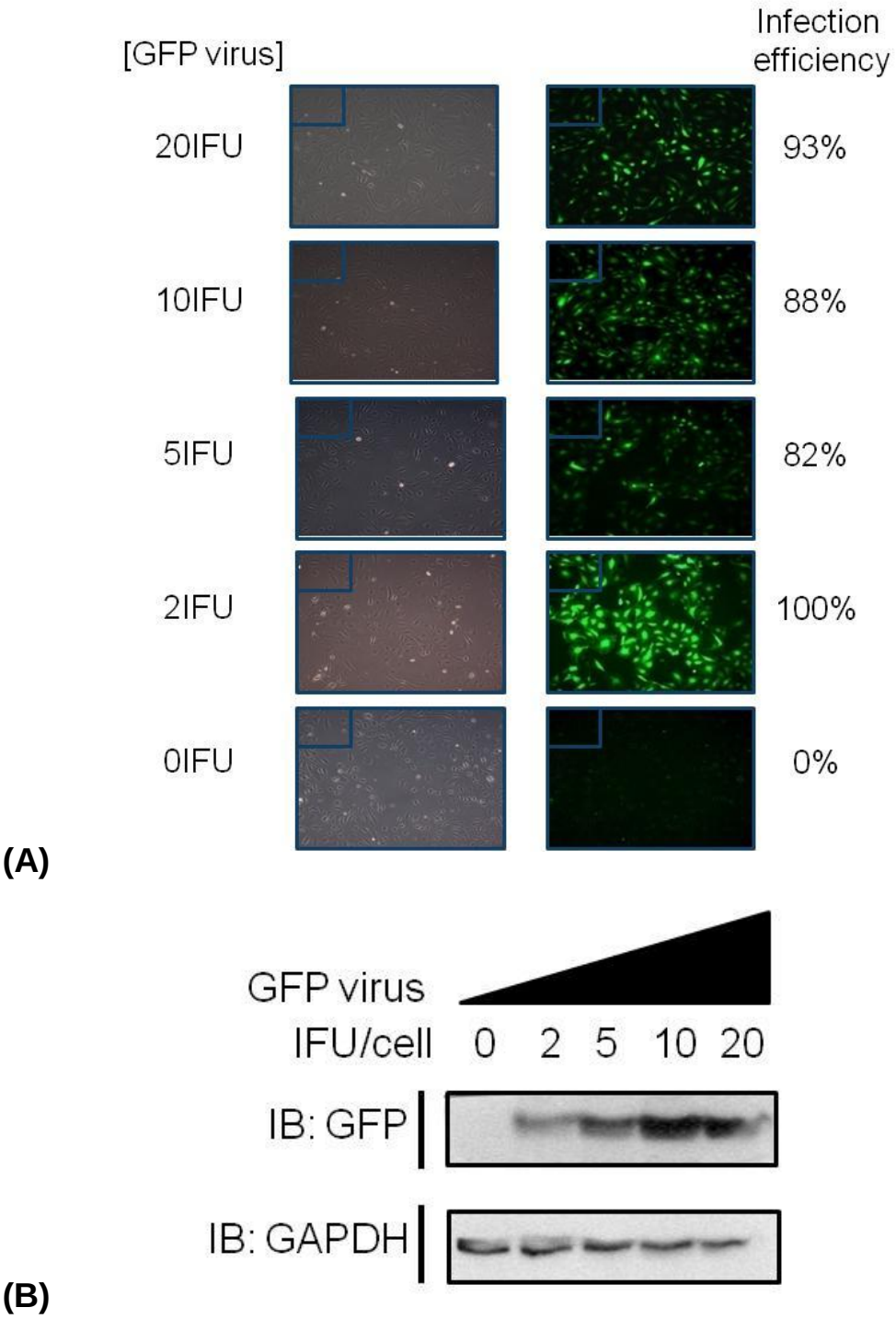

Figure 5-2: Optimising the MOI of the Sffv-GFP lentivirus in HSVECs.

HSVECs were infected with 0-20 IFU/cell of the Sffv-GFP lenti virus for 48 hours. (A) GFP expression was visualised using a fluorescent microscope. The infection efficiency at each MOI was calculated by counting the proportion of cells expressing GFP in a select region of each dish. (B) Whole cell lysates were prepared in parallel and immunoblotting for GFP and GAPDH was used as a loading control. The virus infection efficiency was greatest at an MOI of 2 (100%) (A). As the concentration of virus increased, the expression level of GFP increased as shown in the GFP immunoblot (B). The HSVEC primary cell cultures were susceptible to Sffv-GFP lentivirus infection with a high efficiency over the MOI concentration range 2-20. Experiment was performed to N=1.

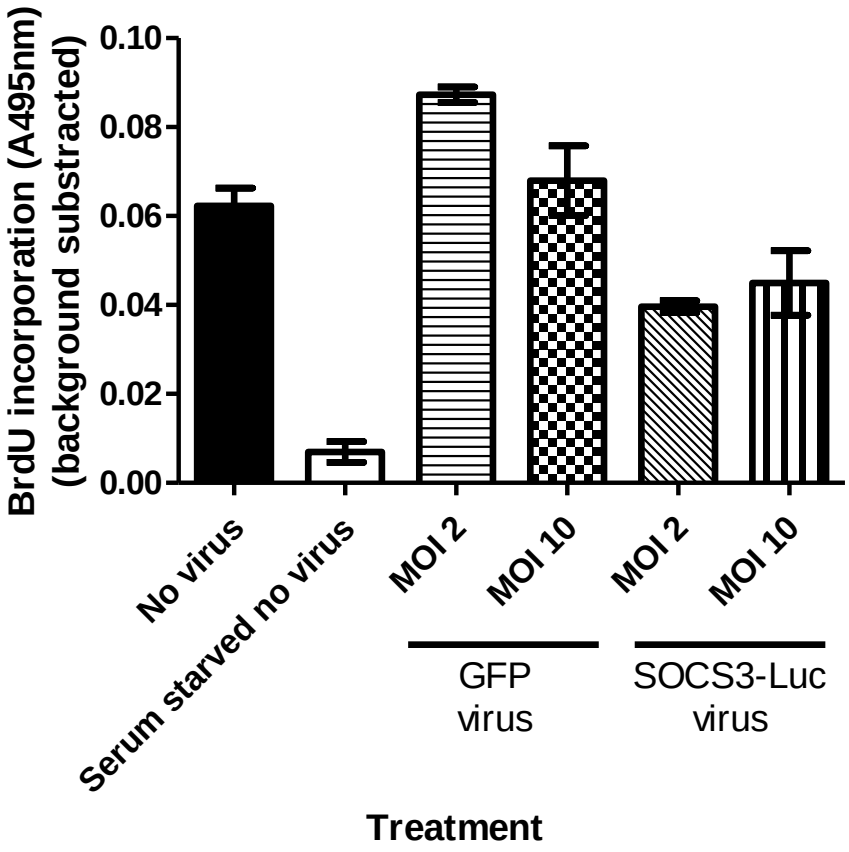

Figure 5-3: The effect of SOCS3 overexpression on HSV SMC proliferation.

HSV SMCs were serum starved for 72 hrs in 0.2%FBS. Cells were then infected with 0-10 MOI Sffv-GFP lentivirus or CMV-SOCS3-Luciferase lentivirus for 48 hrs. 31 hrs post virus infection, BrdU label was added to the cells according to manufacturer's instruction. BrdU incorporation was then measured using a fluorescent plate reader (POLARstar OPTIMA). Samples were prepared in technical replicates of 3 and the mean BrdU incorporation plotted with SEM error bars. A "cells only control" was included, in triplicate, on the plate and the average BrdU incorporation subtracted to provide a background subtraction. N=1 preliminary data shows a trend toward a decrease in HSV SMC proliferation following SOCS3-Luciferase overexpression when compared to the GFP virus and no virus controls. Serum starvation (in 0.2% FBS) for 120 hrs resulted in cell death. Experiment was performed to N=1.

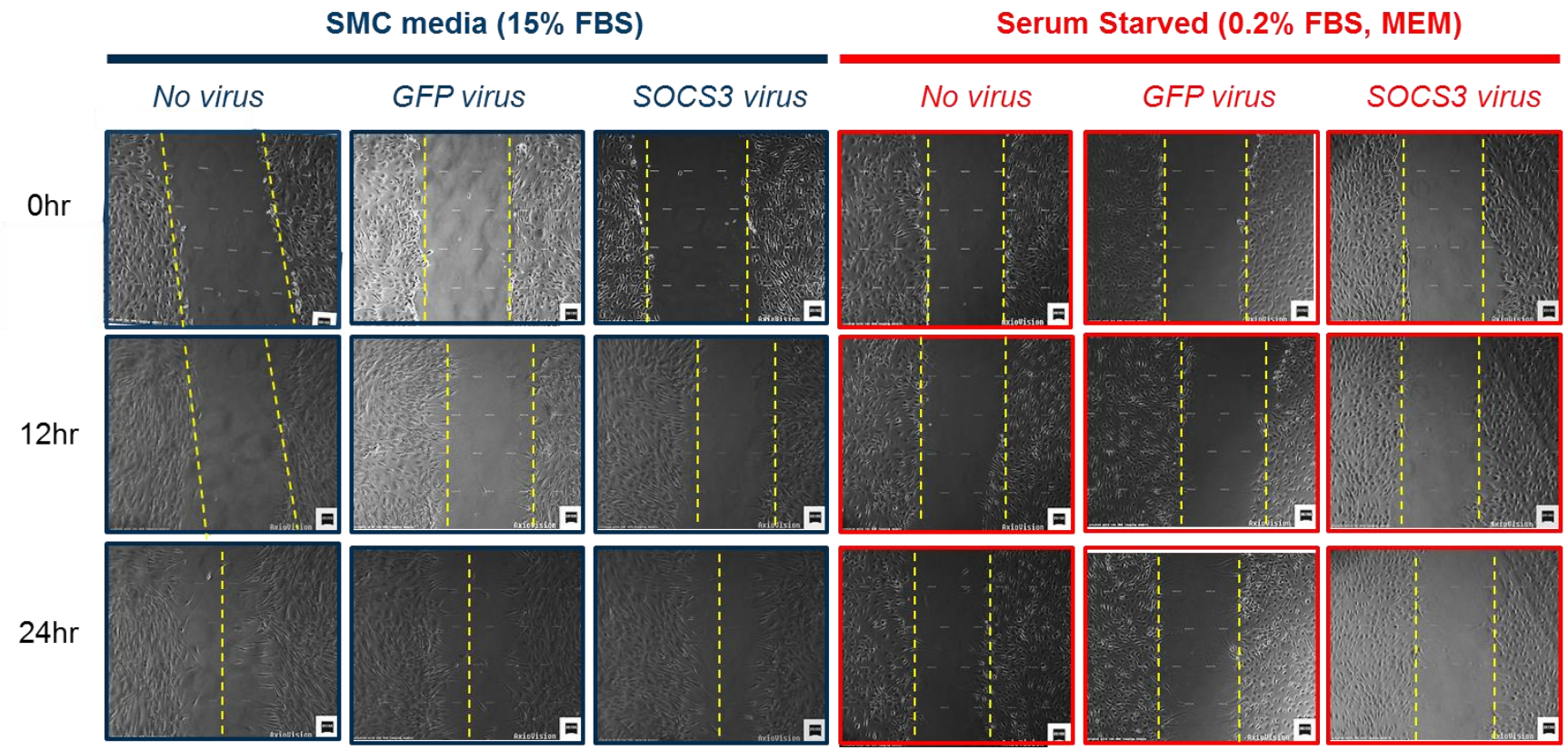

Figure 5-4: The effect of SOCS3 overexpression on HSV SMC migration.

HSV SMCs were serum starved for 72 hrs in 0.2%FBS. Cells were then infected with 20 MOI Sffv-GFP lentivirus or CMV-SOCS3-Luciferase lentivirus for 48 hrs and returned to 15% FBS or maintained in 0.2% FBS for wound assay. Images were taken at 0, 12 and 24 hr post wound time points. Samples were prepared in 3 technical replicates and representative images shown. The dotted lines show areas where cells were mostly absent. Preliminary data shows no effect of SOCS3 overexpression on the migration of HSV SMCs. Experiment was repeated to N=2 and representative images shown.

5.3 Discussion

SOCS3 has been implicated in vascular pathologies. Notably, adenoviral delivery of the SOCS3 gene in a rat model of vein grafting (autologous jugular vein-to-carotid-artery) recently confirmed that SOCS3 overexpression significantly reduced NI thickness at 2 weeks and 4 weeks post procedure [216]. SOCS3 has also been implicated in other vascular pathophysiologies such as atherosclerosis [181]. Interestingly, SOCS3 expression was significantly elevated in the inflammatory shoulder region when compared to the fibrous cap of human atherosclerotic plaques [181]. Furthermore, IL-6 or low-density lipoprotein **(**LDL) stimulation of VSMCs has been shown to promote proliferation *in vitro* [181]. However, the transient overexpression of SOCS3 in these cells was sufficient to block this proliferative response [181]. Together these data support our hypothesis that enhancing the stability of SOCS3 may limit the VSMC proliferation that contributes to NI lesion formation following CABG or PCI.

As such, we sought to investigate the expression of SOCS3 protein within the various layers of the HSV blood vessel. IHC revealed SOCS3 localised to the medial, intimal and endothelial layers of the blood vessel though some staining was observed in the adventitial fibres (Figure 5-1 a-b). Importantly, SOCS3 expression appeared to be reduced in the intimal region compared to the media (Figure 5-1 a-b). This would support the hypothesis that loss of SOCS3 expression in SMCs of the medial layer facilitates the proliferation and migration to the intimal layer. However, in the absence of co-localisation with cell specific markers (αSMA) we cannot confirm SOCS3 expression in the SMCs. Interestingly, Gupta *et al* showed SOCS3 expression was significantly downregulated in the NI of porcine arteries subject to wire injury [118]. Though our data showed positive staining for SOCS3 at the NI, using the DAB system it was not possible to quantify expression. Future experiments should involve the use of fluorescent antibodies and co-localisation of SOCS3 with VSMC cell specific markers. Previously α-smooth muscle actin (α-SMA) and smooth muscle-myosin heavy chain (SM-MHC) have been employed to distinguish VSMC from other cell types [265]. Additionally, staining for endothelial cell specific markers such as von Willebrand factor (vWf) or vascular cell adhesion molecule (VCAM1) would confirm whether SOCS3 expression was altered in the endothelium specifically [266]. We hypothesise that cells within the NI lesion would stain negative for vWF and VCAM1 due to the absence of endothelial cells. Additionally, we would expect the NI to contain a large proportion of SMCs (stain positive for α-SMA and SM-MHC) and that co-localisation of

SOCS3 with these cell specific markers would be reduced in the NI lesion compared to the medial layer of the blood vessel.

As mentioned previously, the HSV tissue was obtained from patients undergoing CABG procedures. HSV tissue sections were not subject to culture *ex vivo* and were instead formalin fixed on day 0. As such, we did not expect the NI of these vessels to be as enlarged and with reduced luminal diameters. One consideration is that the patients were undergoing a CABG procedure due to significant pathology of the coronary artery therefore it is possible other vessels within the body, including the saphenous vein, may be diseased.

Before conducting proliferation and migration assays in primary vascular cells the ability of a GFP LV to infect primary HSVECs was performed. At an MOI of 2, the efficiency of infection was ~100%, which decreased slightly at MOIs 5-20 though still >80% (Figure 5-2Figure 5-2). As such, the MOI of the SOCS3 virus progressed to proliferation and migration assays was within this range to ensure high efficiency of infection. The use of a Fluorescence-Activated Cell Sorting (FACS) platform would provide a more accurate assessment of infection efficiency however for the purpose of this project this was not essential.

Human saphenous vein (HSV) conduits are commonly used in coronary artery bypass procedures as an alternative to the internal mammary artery (IMA) due to accessibility and increased length. Our hypothesis was that overexpression of SOCS3 in the SMCs, derived from HSV tissue, would limit proliferation via inhibition of the JAK/STAT pathway. To test this hypothesis, we serum starved HSV SMCs for 72 hrs inducing quiescence and synchronising all cells to the same stage of the cell cycle (G_0) (Figure 5-3). Failure to synchronise all cells to the same stage of the cell cycle would otherwise introduce an additional variable that may skew these data output. It was essential to return serum at the time of virus infection to avoid cell death as seen in the no virus, serum starved control (Figure 5-3). Furthermore, the return of serum containing growth media facilitates exit from the stationary G_0 phase of the cell cycle which is required to measure DNA replication during the S phase of the cell cycle.

The BrdU incorporation assay (Chemicon®) was used to indirectly assess proliferation and relies on the incorporation of a modified nucleotide base (5-bromo-2'deoxyuridine), in

place of thymidine, into nascently synthesised DNA. The first generation BrdU assay was described in 1975 [267] though today employs more sophisticated monoclonal antibodies and a colourimetric plate reader to accurately quantify BrdU base incorporation [268]. Alternative methods such as the MTT assay relies on the reduction of a tetrazolium salt (MTT) to the coloured formazan and quantification this colour change [269]. However the MTT assay may not be a reliable indicator of cell proliferation as it measures the metabolic activity of viable cells as opposed to DNA synthesis or cell number: cells may be metabolically active but not proliferating. Moreover, since it was first described in 1957 [270], the incorporation of tritiated (H^3)-thymidine has widely been accepted as the gold standard for measuring DNA synthesis [268, 271]. However, use of the BrdU incorporation assay avoids the costs and hazards associated with handling radiolabelled products therefore this was used to investigate the effect of SOCS3-Luc overexpression on HSV SMC proliferation (Figure 5-3Figure 5-3). These preliminary data revealed a trend toward decreased SMC proliferation when SOCS3-LUC was compared to the GFP virus control (Figure 5-3Figure 5-3). However, the overexpression of a SOCS3-Luc fusion protein raised the argument that the luciferase tag (~59kDa) introduced a variable to the experiment and may be responsible for the reduction in proliferation observed (Figure 5-3Figure 5-3). For that reason, we generated a CMV-SOCS3 LV (Chapter 3, Figure 3-12 b) however due to time constraints of this project it was not possible to complete proliferation assays using the CMV-SOCS3 LV. Future investigations will employ the SOCS3 LV in three independent proliferation assays. Moreover, the effect of SOCS3 on SMC proliferation should be confirmed using an additional method such as the xCELLligence system (ACEA Biosciences. Inc). The xCELLigence platform employs tissue culture plates that have been coated with gold electrodes. An electrical current is then applied across the plate and any increase in cell number impedes this electrical current. The resulting change in current flow can be quantified and used to measure cell proliferation in real-time.

Recently, it has been shown that the overexpression of SOCS3 limited the migration of rat thoracic aorta VSMCs [216]. SOCS3 was overexpressed using an adenoviral vector and migration was stimulated with the addition of PDGF-BB [216]. SOCS3 overexpression significantly inhibited rat VSMC migration therefore we sought to replicate this result in human saphenous vein SMCs. These preliminary data suggested SOCS3-Luc did not reduce SMC migration when compared to the GFP control virus (Figure 5-4). However, similar to the proliferation assay, the overexpression of a SOCS3-Luc fusion protein to investigate migration was not deemed appropriate As such, the migration assay was not

progressed beyond N=2. Future work will involve the SOCS3 LV to remove the argument that the 59kDa luciferase tag may influence the result. It will be important to quantify the distance of the "scratch closure" from three independent experiments using analysis software (e.g. Image J) as described in the literature [231]. Again, assessing the effect of SOCS3 overexpression on SMC migration should be confirmed via an additional method such as 2D trans-well migration assays in which chemotaxis toward an inflammatory stimuli may also be introduced [272].

Interestingly, the Xiang *et al* publication, in which SOCS3 overexpression was shown to significantly limit rat VSMC migration and proliferation (MTT and BrdU assay), did not include a serum starvation period to induce quiescence prior to the experiment [216]. Our experimental design for both proliferation and migration assays incorporated a serum starvation to synchronise the population of cells plated to the same stage of the cell cycle. Moreover, the stimulus for migration in the Xiang paper was the PDGF-BB ligand only. This may be considered an oversimplification of the *in vitro* experiment as during vascular injury *in vivo* multiple mitogenic stimuli would drive the proliferation and migration of VSMC in the media to the intimal layer.

6 Final Discussion

Since the year 2002, the number of PCI procedures performed in the UK each year has more than doubled from ~44,000 to 92,000 [2]. Though the number of CABG procedures has declined from ~25,000 to 17,000 during this time, this method of surgical intervention remains an important strategy for more complex coronary lesions [2]. However, the patency of these revascularisation procedures remains relatively poor with >50% CABG procedures failing within 10 years [4] and ISR observed in ~12% of stent implants [3]. DESs though effective at reducing VSMC proliferation and therefore NIH, have an off target effect of inhibiting re-endothelialisation of the injured vessel and so patients are at risk of late in-stent thrombosis [28]. As such, there is an unmet clinical need for a therapy to reduce the incidence of NIH following CABG, balloon angioplasty or stent implant procedures. To address this problem we must generate novel therapies that maximise the benefit of these interventions while reducing the risk of adverse effects such as late in-stent thrombosis. We must identify new targets specifically involved in the development of NIH in these settings. The literature provides evidence in support of strategies to stabilise the expression of SOCS3 in VSMCs and therefore limit NIH without interfering with re-endothelialisation of injured vessels (section 1.6-1.7). The primary aim of this thesis was to investigate the mechanism of SOCS3 turnover and identify therapeutic targets that would facilitate the stabilisation of SOCS3.

SOCS3 is an important inhibitory regulator of the JAK/STAT pathway and its expression is, in part, driven by STAT transcription factors to form a non-redundant negative feedback loop (section 1.3). Loss of SOCS3 expression has been described in various cancers [113-116] and animal models of NIH (coronary balloon angioplasty of atherosclerotic pigs) [118]. Moreover, therapeutic strategies to enhance the expression of SOCS3 have been described for acute inflammation following staphylococcal enterotoxin B or LPS exposure [110], rheumatoid arthritis [244] and collagen induced arthritis [273]. SOCS3 delivery appeared to be an effective therapy reducing the detrimental effects of the acute inflammatory response to SEB or LPS [110] and also in reducing the pathology of arthritic joints [244, 273].

Ubiquitylation is a reversible PTM in which a ubiquitin moiety is covalently attached to a target Lys (K) residue on its substrate [127] (section 1.5). Amongst many functions, this PTM has been shown target proteins for degradation at either the proteasome or lysosomes,

play a role in DNA damage repair and regulate immune responses. Interestingly, Sasaki and co-workers reported that the ubiquitylation of Lys6 was a key regulator of SOCS3 stability in a pro B (Ba/F3) cell line and that the proteasome was a major route for SOCS3 degradation [95] (section 1.3.9). In Chapter 3 of this thesis, it was demonstrated that Lys6 was not required for SOCS3 ubiquitylation and therefore turnover in HEK293 cells. In fact, pharmacological inhibition of the proteasome had no obvious effect on SOCS3 expression suggesting an alternative route for SOCS3 degradation in this cell type. Babon and co-workers also demonstrated that pharmacological inhibition of the proteasome, lysosome or calpain degradation pathway had no significant effect on the stability of WT SOCS3 in HEK293T cells [100]. However, it is likely that the mechanism of SOCS3 turnover is dependent on the cell system under investigation which would explain the disparity between the results in this thesis and Sasaki *et al* [95].

To identify the residues required for the ubiquitylation of SOCS3, the ubiquitylation status of a panel of SOCS3 truncation mutants was assessed in transfected HEK293 cells. Initially, these data suggested that a C-terminal 44 amino acid region was required for SOCS3 ubiquitylation. However mutagenesis of the single Lys173 to Arg in this region had no discernible effect on either SOCS3 ubiquitylation or stability. Accordingly, we conducted LC-MS-MS analysis of SOCS3 isolated by immunoprecipitation following expression in HEK293 cells to directly identify putative sites of ubiquitylation. These revealed 8 distinct sites of ubiquitylation (K23, K28, K40, K85, K91, K173, K195, K206) confirming functional redundancy exists within this system. These novel data provided the rational for the generation of a so-called “Lys-less” SOCS3 mutant, in which all 8 Lys residues were mutated to Arg. Compared to WT SOCS3, Lys-less SOCS3 was shown to be significantly more stable whilst retaining its function as a negative regulator of JAK/STAT signalling *in vitro*.

The C-terminus of SOCS3 contains a 40 residue SOCS box region [49, 84] which provides a platform for the assembly of an ECS^{SOCS3} ubiquitin ligase complex (section 1.3.8). To date, the literature has described seven SOCS3 substrates that are subsequently targeted for proteasomal or lysosomal degradation (section 1.3.8). It had previously been reported that deletion of the C-terminal SOCS box stabilised SOCS3 similar to the Lys6 (K6Q) SOCS3 mutant [95]. Though deletion of the SOCS box may render SOCS3 resistant to ubiquitylation and therefore turnover, this may also enhance the stability of SOCS3 substrates. For example, stabilisation of the SOCS3 substrate FAK1 may promote cell

migration and contribute to disease progression. It is likely that additional SOCS3 substrates will emerge in future, therefore mutated SOCS3 which are resistant to ubiquitylation but cannot assemble an ECS^{SOCS3} ubiquitin ligase complex may have a detrimental effect on SOCS3 function. It is important that therapies to enhance the stability of SOCS3 do not compromise the functionality of SOCS3, interfere with phoso-tyrosine/substrate binding and permit the formation of the ECS^{SOCS3} ubiquitin ligase complex.

Sasaki and colleagues proposed that SOCS3 may autoubiquitylate to regulate its own turnover at the proteasome [95]. However, this thesis has provided evidence to support the role of an external E3 ligase for SOCS3 (Chapter 3). The L189A SOCS3 mutant was previously described by Babon and co-workers [100] and was unable to interact with the elongins (components of the E3 ligase machinery). Interestingly, despite an inability to form the E3 ligase complex at the C-terminal SOCS box, we have demonstrated that the L189A SOCS3 mutant was polyubiquitylated to the same degree as WT SOCS3 in HEK293 cells. These data suggested that formation of the E3 ligase complex at the SOCS box domain was not essential for SOCS3 ubiquitylation and that one or more separate E3 ligases may be responsible for this modification.

The current study investigated the mechanism of SOCS3 turnover in a human endothelial (AS-M.5) cell line (Chapter 4). The proteasome was identified as the major route of endogenous SOCS3 turnover in this vascular cell type. Our initial strategy to identify the E3 ligase controlling proteasome-mediated SOCS3 turnover was to develop *in vitro* tools to screen an E3 ligase siRNA library (siARRAY). As such, AS-M.5 stable cell lines were developed that expressed a SOCS3-Luc fusion protein that theoretically could be used in a luciferase-based siARRAY screen to identify E3 ligases which, when knocked down, would have produced an increase in SOCS3-Luc activity. However, during optimisation of this assay the calculated assay window was low (<2) and was deemed unsuitable for screening purposes. As an alternative approach, a previously developed *in vitro* fluorescence and cell-based high throughput screen for inhibitors of virus mediated gene transfer [249] was investigated as a platform to screen the E3 ligase siARRAY. However, this was also deemed unsuitable due to non-specific immunoreactivity of commercially available and in-house SOCS3 primary antibodies in immunofluorescence applications.
In the absence of a suitable tool to screen the si-ARRAY, LC-MS-MS and bioinformatic analysis of SOCS3 isolated by immunoprecipitation following expression in HEK293 cells

was performed to identify any potential interacting E3 ligase and DUB enzymes that may control SOCS3 turnover (Chapter 4). This screen highlighted two promising candidates that co-immunoprecipitated with SOCS3 i) a Lys63 specific E3 ligase known as HectD1 and ii) a cysteine protease DUB known as USP15.

As discussed previously, little is known about the function of HectD1 with only 29 publications cited in PubMed (section 4.3). Interestingly, HectD1 was recently shown to catalyse the Lys63 linked polyubiquitylation of the APC protein involved in the negative regulation of Wnt signalling [247]. The Wnt pathway controls cell fate and plays a crucial role during embryogenesis [274]. As such, it is not surprising that deregulation of this pathway has deleterious effects and has been implicated in many cancers [274]. However, rather than target APC for degradation, ubiquitylation by HectD1 promoted the interaction of APC with another protein called axin that was required for the formation of a "destruction complex" [247]. This destruction complex phosphorylates β-catenin which is subsequently targeted for Lys48 linked polyubiquitylation and proteasomal turnover [247]. In Chapter 4, preliminary investigations suggested that HectD1 may catalyse the Lys63-linked ubiquitylation of SOCS3 when both were co-expressed in HEK293 cells. However, the significance of this modification is not clear and thus further research is required. It is possible that this PTM of is not involved in regulating the inherent stability of SOCS3 rather it is involved in regulating protein-protein interactions as described for APC [247]. Subsequent investigations employing a neddylation inhibitor have indicated the CRL E3 family are not involved in the ubiquitylation of SOCS3 which narrows the search for candidate E3s.

As discussed previously (section 1.5.1), DUB enzymes reverse the action of the E3 ubquitin ligases by cleaving ubiquitin chains, in a progressive manner, and may therefore promote substrate stabilisation [130]. USP15 was recently shown to deubiquitylate and stabilise the expression of an E3 ligase (Mdm-2) which in turn regulates the stability of the tumour suppressor p53 [256]. Interestingly, preliminary investigations suggested that USP15 may catalyse the deubiquitylation of SOCS3 when overexpressed in HEK293 cells (Chapter 4). Though it is likely multiple DUBs play a role in the stabilisation of SOCS3, USP15 warrants further investigation as a therapeutic target for SOCS3 stabilisation.

Chapter 5 contains preliminary data from preliminary investigations of SOCS3 expression in the vasculature. However due to the time constraints of this PhD, further work is required to complete the analysis. The literature suggests that SOCS3 plays an important

role in vascular pathology associated with CHD. In support of this, SOCS3 overexpression *in vitro* has been shown to reduce inflammatory gene expression and proliferation in VSMCs, while siRNA-mediated knockdown of SOCS3 *in vivo* was shown to enhance the progression of atherosclerosis in *ApoE*$^{-/-}$ mice [181]. Moreover, IHC analysis of neointimal lesions from a pig coronary artery injury model revealed a significant decrease in SOCS3 expression in proliferating neointimal smooth muscle *versus* normal media [118]. In Chapter 5, the expression of SOCS3 protein within the various layers of a human saphenous vein (HSV) taken from a patient undergoing bypass surgery was investigated. These experiments demonstrated that SOCS3 immunoreactivity localised to the media, intima and endothelium of HSV tissue derived from patients undergoing CABG. Interestingly, SOCS3 expression appeared to be reduced in the intimal region compared to the media, consistent with the *in situ* observations described by Gupta *et al* in the porcine coronary artery injury model [118]. Initial studies also revealed a trend toward decreased serum-stimulated HSVSMC proliferation in the presence of the SOCS3-Luc LV (SOCS3 overexpression) when compared to GFP LV and no virus controls. These data were consistent with proliferation studies conducted by Xiang *et al* that reported SOCS3 overexpression reduced rat VSMC proliferation [216] and the Ortiz-Munoz [181] study that demonstrated SOCS3 overexpression effectively blocked IL6/LDL induced proliferation in murine VSMCs.

By linking signals initiated by integrins and growth factor receptors to the actin cytoskeleton, focal adhesion kinase (FAK) is a critical mediator of VSMC migration and proliferation in NIH [275]. SOCS3 has been shown to specifically bind Tyr397-phosphorylated FAK1, thus targeting it for ubiquitylation and proteasomal degradation [93, 114]. In Chapter 5, preliminary investigations indicated that the overexpression of SOCS3 had no effect on HSVSMC migration in the scratch assay. However, Xiang and colleagues reported that SOCS3 overexpression reduced the migration of SMCs derived from rat thoracic aortas *in vitro*[216]. As noted previously, WT and Lys-less SOCS3 LV without the luciferase tag have now been generated and will be used in future proliferation/migration studies by the Palmer lab. This will remove the possibility that the ~59kDa luciferase tag might have been compromising SOCS3 function in the proliferation and migration assays.

Together these observations suggest SOCS3 expression in the vasculature has the potential to suppress localised inflammation resulting from perturbation of the vascular

endothelium, but also reduce VSMC migration and proliferation leading to the NIH responsible for graft failure and in-stent restenosis.

6.1 Current therapies for the treatment of ISR are limited

Revascularisation using DESs have reduced the incidence of ISR when compared to BMSs however neointimal lesions may still form within the DES [23] (Section 1.1.2). The release of non-selective cell cycle inhibitors from the DES limits the proliferation of endothelial cells and slows re-endothelialisation of the stented vessel [24]. This increases the risk of late in-stent thrombosis and is one of the major limitations of DESs. As such, many patients still receive BMSs which are associated with a high incidence of ISR. The treatment of ISR remains problematic and dual anti-platelet therapies such as aspirin and platelet $P2Y_{12}$ inhibitor are recommended in patients receiving a stent [25]. A recent review conducted by Alfonso *et al* summarised the pitfalls of the most common ISR treatment strategies [276]:

1. Balloon angioplasty – beneficial in the short term however often results in recurrent ISR.

2. Drug coated balloon angioplasty – shown to be more effective than balloon angioplasty alone for the treatment of ISR however repeat stenting with a DES may be the preferred treatment option.

3. Atherectomy to remove neointimal tissue within the stent – clinical trials suggested this did not improve the incidence of re-current ISR.

As such, there is an unmet clinical need for the treatment and prevention of ISR. I originally hypothesised that stabilising the protein levels of SOCS3 would be a useful therapeutic strategy to reduce NIH and improve the patency of revascularisation procedures (section 1.8). The following section summarises the advantages and disadvantaged of a therapy to stabilise SOCS3 protein levels (section 6.2).

6.2 The pros and cons of SOCS3 stabilising therapies

One of the main challenges of a therapy to stabilise SOCS3 protein levels is the ability to target this VSMCs specifically. In atherogenesis, the role of SOC3S appears to be cell type

dependent and highlights the potential for a non-selective SOCS3 stabilising therapy to promote disease progression (section 1.6.3). Table 6-1 summarises the pros and cons that may be associated with SOCS3 stabilising therapies to limit NIH.

Advantages	Disadvantages
Attenuate VSMC proliferation [181, 216] that contributes to neointima formation.	Inability to selectively target SOCS3 therapy to VSMCs: ➢ Inhibition of leptin signalling may result in patients becoming obese [65]. ➢ Inhibition of endothelial cell proliferation will prevent re-endothelialisation over the denuded are of the blood vessel following PCI or CABG. ➢ SOCS3 expression was associated with M1 macrophage polarisation (pro-inflammatory) in unstable atherosclerotic lesions [277]. ➢ SOCS3 overexpression in T cells was shown to promote the development of atherosclerosis [184].
Promote FAK1 degradation [93, 114] and therefore limit migration of VSMCs from the media to the intima that drives expansion of the neointima and reduction in lumen diameter.	
Reduce the expression of STAT3 responsive genes such as MMP2 and MMP9 involved in vascular remodelling and VSMC migration [195].	
Reduce inflammatory gene expression in VSMCs [181, 216] and suppress localised inflammation induced by stent deployment.	
Targeting the E3 ligase/DUB for SOCS3 may enhance the specificity of therapeutic intervention and the effectiveness of the therapy [278].	

Table 6-1: Advantages and disadvantages that may be associated with stabilising SOCS3 protein levels to limit NIH.

In 2005, Jo *et al* generated a modified, cell penetrable form of SOCS3 (CP-SOCS3) that dampened the inflammatory response in animal disease models [110] (section 1.3.9). CP-SOCS3 was modified to include a hydrophobic sequence that facilitated crossing of the plasma membrane phospholipid bilayer [97, 110]. This cell penetrable feature would be required for any future SOCS3 therapy employed in the vasculature.

As discussed in chapter 1, SOCS1 and SOCS3 are the best characterised members of the SOCS family. SOCS1 is pre-dominantly associated with the negative regulation of IFNγ

signalling events [44]. In contrast, SOCS3 is largely involved in the non-redundant negative regulation of other cytokines including IL-6, LIF, IL-11, leptin and G-CSF [71]. As such, it would not be anticipated that a SOCS3 stabilising therapy would have an impact other SOCS signalling pathways.

6.3 How this thesis has advanced our scientific knowledge

The aim of this PhD was to investigate the mechanism of SOCS3 turnover and develop a functional SOCS3 that is resistant to degradation (section 1.9). As discussed previously, Sasaki *et al* showed that Lys6 was required for the recognition and degradation of SOCS3 at the proteasome in Ba/F3 cells [95]. However, in the HEK293 system I have shown for the first time that K6 is not required for the ubiquitylation of SOCS3 and that loss of this residue did not significantly enhance the stability of the protein (chapter 3). Using LC-MS-MS analysis of a SOCS3 coIP I have identified 8 putative sites of ubquitylation (K^{23}, K^{28}, K^{40}, K^{85}, K^{91}, K^{173}, K^{195} and K^{206}). To our knowledge, these data are a novel contribution to the literature and for the first time suggest that functional redundancy among the lysine acceptors on SOCS3 exists. To date, no further investigations of Lys6 as a master regulator of SOCS3 stability have been published and the LC-MS-MS data I have generated suggests that the regulation of SOCS3 stability is cell type dependent.

Failure to identify a single lysine residue controlling SOCS3 turnover led to the generation of a novel “Lys-less SOCS3” that was functional and resistant to degradation (chapter 3). Lys-less SOCS3 may provide a useful candidate for adenovirus mediated gene therapy to reduce the incidence of NIH lesions following CABG or PCI. Alternatively delivery of Lys-less SOCS3 into joints affected by rheumatoid arthritis may prevent disease progression and warrants further investigation [244].

Moreover, the identity of the E3 ubiquitin ligase(s) responsible for catalysing ubiquitylation of SOCS3 is unclear providing a gap in the literature. I have provided evidence to support the role of an external E3 ligase controlling SOCS3 stability and now challenge the existing hypothesis of SOCS3 autoubiquitylation that was proposed by Sasaki *et al* in 2003 [95] (chapter 3). Moreover, LC-MS-MS analysis of a SOCS3 co-IP identified 17 candidate E3 ligases and 4 DUBs that may interact with SOCS3 (chapter 4). To our knowledge, the DUB(s) responsible for cleaving poly-ubiquitin chains from SOCS3 are yet to be identified. As such, the candidate E3 and DUB enzymes identified in chapter

4 warrant functional validation and may provide novel targets for the design of small molecule inhibitors or peptide disruptors in the future.

Finally, preliminary data presented in chapter 5 suggests that SOCS3 may limit the proliferation of VSMCs derived from HSV tissue consistent with Xiang *et al*'s work in rat thoracic aorta VSMCs [216]. Immunolocalisation performed in HSV tissue also revealed SOCS3 localised to the medial, intimal and endothelial layers of the blood vessel. Interestingly, SOCS3 appeared to be less abundant in the intimal region compared to the medial layer. These data were consistent with Gupta and co-workers findings in a porcine coronary artery injury model [118] and provide further evidence in support a SOCS3 therapy to reduce the incidence of ISR in man.

6.4 Future work

In chapter 4 of this thesis, we confirmed HectD1 and USP15 were *bona fide* SOCS3 interactors and not simply an artefact of LC-MS-MS analysis. However, denaturing IPs revealed that the overexpression of HectD1 or USP15 did not have a significant impact on SOCS3 ubiquitylation status *in vitro*. Nevertheless, functional assessment of HectD1 and USP15 should still be considered and the effect on SOCS3 protein levels investigated. In addition to this, screening the remaining E3 ligase and DUB candidates described in Table 4-1 is vital.

As discussed previously SMC proliferation and migration contribute to the expansion of NI lesions following CABG or stent deployment (section 1.1.2). Moreover, these revascularisation procedures are often associated with endothelial denudation. Loss of the endothelium means there is no barrier to limit this SMC proliferation and migration in addition increasing the risk of thrombosis. As such, the functional role of candidate E3 ligases or DUBs should be investigated in primary VSMCs and ECs prepared from human saphenous vein (HSV) tissue and human coronary arteries (available commercially).

Initial experiments would involve reconstituting SOCS3 ubiquitylation in the above VSMCs and ECs via lentivirus-mediated overexpression of SOCS3 and the candidate E3 ligase or DUB *in vitro*. Exposure to the proteasome inhibitor MG132 would facilitate the accumulation of ubiquitylated SOCS3 prior to denaturing IP to assess the ubiquitylation status of SOCS3 (section 2.2.8). The identification of a *bona fide* E3 ligase for SOCS3

would result in a significant increase in SOCS3 polyubiquitylation. Conversely, the overexpression of a *bona fide* DUB would reduce the accumulation of polyubiquitylated SOCS3. Additionally, it would be interesting to assess the effect of siRNA-mediated knockdown of the endogenous E3 ligase or DUB for SOCS3 in both VSMCs and ECs. I hypothesis that knockdown of the E3 ligase(s) for SOCS3 would enhance SOCS3 protein levels and limit the proliferation and migration of VSMCs. Conversely, knockdown of the SOCS3 DUB(s) may further reduce SOCS3 protein levels and promote the proliferation and migration of these vascular cells.

Following this, it would be useful to generate and test catalytically inactive mutants of the E3 ligase and assess their ability to function as dominant-negative inhibitors of SOCS3 ubiquitylation in primary vascular cells. Depending on the class of E3 ligase responsible (HECT, single RING finger or multi-subunit RING finger [278]), mutations of specific conserved amino acids, critical for ubiquitin transfer to the substrate, are sufficient to inactivate the E3.

The expression of candidate E3 ligase and DUB genes at the molecular level may be assessed using quantitative reverse transcription real-time PCR (qRT-PCR) and at the protein level via immunoblot analysis. Following this, the effects of manipulating E3 ligase or DUB levels on the rate of SOCS3 turnover could be examined using some of the techniques employed in this thesis, such as Emetine chase assays as described in Chapter 3. It would be predicated that siRNA-mediated knockdown of a functionally significant E3 ligase targeting SOCS3, or transient expression of a catalytically inactive dominant-negative version, would reduce the rate of SOCS3 degradation/increase $t_{1/2}$, while overexpression of the E3 ligase should accelerate SOCS3 degradation and decrease $t_{1/2}$ and *vice versa* for a SOCS3 DUB.

Having examined the consequences for SOCS3 turnover and expression, it will be important to examine the impact of manipulating E3/DUB expression on key SOCS3-regulated functional endpoints in VSMCs and ECs that are relevant to the development of NIH. This would include measuring i) SMC proliferation in response to growth factors (e.g. PDGF), cytokines (e.g. IL-6) and proatherogenic lipoproteins; ii) pro-inflammatory signalling, as determined by assessment of IL-6-stimulated activation of STAT3 and expression of STAT3-responsive genes such as monocyte chemoattractant protein-1 (MCP-1/CCL2), MMP2/9, intracellular adhesion molecule-1 (ICAM-1), and vascular

endothelial growth factor (VEGF); and iii) cell migration in response to 10% (v/v) serum as described in Chapter 5.

The expression pattern of candidate E3/DUBs such as HectD1 or USP15 *in vivo* should be investigated. This would involve harvesting tissue from various organs of healthy rodents and performing qRT-PCR analysis of gene expression in addition to immunoblot analysis of protein levels. It would also be critical that manipulation of the E3/DUB controlling SOCS3 stability translates into reduced pathology in tissue and animal models of NIH. Using an *ex vivo* HSV organ culture model, surplus HSV tissue may be cultured for 0-14 days to allow formation of the neointima [279]. Tissue sections would then be embedded in paraffin wax and IHC performed to examine any changes in the expression of SOCS3 and its E3/DUBs over time. Additionally, the *in vivo* mouse model of in-stent re-stenosis may be used to generate tissue sections from stented vessels [280]. Again IHC to determine the localisation of SOCS3 and E3/DUB expression within the stented vessel would provide valuable information about the role of SOCS3 during NI lesion formation. The availability of a mouse model of in-stent re-stenosis would also allow genetic interrogation of the contributions of VSMC *versus* EC-derived SOCS3 in conferring protection from distinct aspects of the NIH phenotype by using Cre-lox technology to generate mice in which SOCS has been specifically deleted from smooth muscle cells ($SOCS3^{fl/fl}$; Tagln-Cre^{+}) or vascular ECs ($SOCS3^{fl/fl}$,; Cdh5-Cre^{+}). Others have employed a similar strategy, using the Cre-lox system, to generate conditional gene knockouts in SMCs [281-283] and ECs [188, 284, 285] specifically. Interestingly, Stahl and co-workers generated mouse models in which SOCS3 was specifically deleted in endothelial cells and revealed that SOCS3 was an important negative regulator of pathological angiogenesis [188].

6.5 Potential therapeutic strategies

In 2011, Stringer and Piper developed a DUB fusion protein that was resistant to ubiquitylation [286]. The group were investigating whether the ubiquitylation of a protein called ESCRT (endosomal sorting complexes required for transport) was required for its function [286]. As such, they fused the catalytic domain of various DUBs to ESCRT which effectively reversed the ubiquitylation of ESCRT [286]. Using a similar method, it may be possible to validate candidate DUBs regulating SOCS3 ubiquitylation. Moreover, if the SOCS3-DUB fusion protein significantly enhanced the stability of SOCS3 this may

provide a candidate for gene therapy. Stringer and Piper confirmed that DUB fusion did not alter the localisation of ESCRT nor did it impair the function of the protein [286] which would be an important feature of a SOCS3-DUB fusion protein. This approach would also be highly specific [287] and thus avoid detrimental side effects of global inhibitor therapies such as the proteasome inhibitor bortezomib [288].

Bortezomib is a non-specific proteasome inhibitor and in 2003 was FDA approved for the treatment of multiple myeloma (a myeloproliferative cancer) [288]. However, this non-selective inhibition of protein degradation is associated with undesirable side effects such as peripheral neuropathy (an extremely painful disease) upon subcutaneous injection [289]. In addition, the development of resistance to bortezomib in some cancer patients has been documented, further undermining the benefits as a therapy.

A targeted gene therapy employing a more stable form of SOCS3 may avoid the off target effects and toxicity associated with a global proteasome inhibitor therapy such as bortezomib. CABG procedures in man would facilitate the local delivery of adenoviral gene vectors containing Lys-less SOCS3 or SOCS3-DUB fusions. CUPID 1 (Calcium Up-Regulation by Percutaneous Administration of Gene Therapy In Cardiac Disease) is now a phase II clinical trial in which heart failure patients received an intracoronary infusion of an adenovirus containing the sarcoplasmic reticulum calcium ATPase gene 2a (SERCA2a) gene [243, 290]. At 3 year follow up, the results were promising with an 82% reduction in “pre-specified recurrent cardiovascular events” in patients who received the highest dose of the treatment when compared to control subjects [290]. As discussed previously, the endogenous MMP inhibitor TIMP3 provides another example of a candidate for gene therapy within the cardiovascular setting [205].

Alternatively, the identification of a separate E3 ligase that regulates SOCS3 ubiquitylation may provide a novel target for which specific disruptor peptides can be designed. Peptide disruptors specific for the regulatory I domain of protein kinase A (PKA) and A kinase-anchoring proteins (AKAP) have been developed based on peptide array data [291]. Peptide array technology allows the investigator to map the “minimal binding sequence” required for the protein-protein interaction and therefore defines the region a disruptor should target. Investigators subsequently screen peptides that selectively bind SOCS3 with higher affinity than the E3. The disruptor peptide would then effectively block the SOCS3-E3 interaction and therefore stabilise SOCS3 expression. In this way, the E3 ligase may

continue to regulate the ubiquitylation of other substrates. This feature would be lost if a small molecule inhibitor of the E3 were employed.

In conclusion, the role of SOCS3 in the vasculature warrants further investigation and provides a novel therapeutic target to alleviate the low patency of surgical intervention procedures to treat CHD.

7 References

1. *World Health Organization, Cardiovascular diseases (CVDs) Fact sheet N°317, 2013. [Online]. Available http://www.who.int/mediacentre/factsheets/fs317/en/.*
2. *British Heart Foundation, Coronary Heart Disease Statistics , 2015. [Online]. Available: https://www.bhf.org.uk/publications/statistics/cvd-stats-2015.*
3. Maluenda, G., et al., *Clinical outcomes and treatment after drug-eluting stent failure: the absence of traditional risk factors for in-stent restenosis.* Circ Cardiovasc Interv, 2012. **5**(1): p. 12-9.
4. Jeremy, J.Y., et al., *Platelets and saphenous vein graft failure following coronary artery bypass surgery.* Platelets, 1997. **8**(5): p. 295-309.
5. *British Heart Foundation, Cardiovascular Disease Statistics, 2014. [Online]. Available: https://www.bhf.org.uk/~/media/files/publications/research/bhf_cvd-statistics-2014_web_2.pdf*
6. Libby, P., P.M. Ridker, and G.K. Hansson, *Progress and challenges in translating the biology of atherosclerosis.* Nature, 2011. **473**(7347): p. 317-25.
7. Shah, P.K., *Biomarkers of plaque instability.* Curr Cardiol Rep, 2014. **16**(12): p. 547.
8. Bentzon, J.F., et al., *Mechanisms of plaque formation and rupture.* Circ Res, 2014. **114**(12): p. 1852-66.
9. Kolodgie, F.D., et al., *The thin-cap fibroatheroma: a type of vulnerable plaque: the major precursor lesion to acute coronary syndromes.* Curr Opin Cardiol, 2001. **16**(5): p. 285-92.
10. Hansson, G.K., *Inflammation, atherosclerosis, and coronary artery disease.* N Engl J Med, 2005. **352**(16): p. 1685-95.
11. Weber, C. and H. Noels, *Atherosclerosis: current pathogenesis and therapeutic options.* Nat Med, 2011. **17**(11): p. 1410-22.
12. Bonetti, P.O., et al., *Statin effects beyond lipid lowering--are they clinically relevant?* Eur Heart J, 2003. **24**(3): p. 225-48.
13. LaRosa, J.C., J. He, and S. Vupputuri, *Effect of statins on risk of coronary disease: a meta-analysis of randomized controlled trials.* JAMA, 1999. **282**(24): p. 2340-6.
14. Brautbar, A. and C.M. Ballantyne, *Pharmacological strategies for lowering LDL cholesterol: statins and beyond.* Nat Rev Cardiol, 2011. **8**(5): p. 253-65.
15. Goldman, S., et al., *Long-term patency of saphenous vein and left internal mammary artery grafts after coronary artery bypass surgery - Results from a department of veterans affairs cooperative study.* Journal of the American College of Cardiology, 2004. **44**(11): p. 2149-2156.
16. Lee, M.S., et al., *Saphenous vein graft intervention.* JACC Cardiovasc Interv, 2011. **4**(8): p. 831-43.
17. Parang, P. and R. Arora, *Coronary vein graft disease: pathogenesis and prevention.* Can J Cardiol, 2009. **25**(2): p. e57-62.
18. Moravej, M. and D. Mantovani, *Biodegradable metals for cardiovascular stent application: interests and new opportunities.* Int J Mol Sci, 2011. **12**(7): p. 4250-70.

19. Davies, M.G. and P.O. Hagen, *Pathobiology of intimal hyperplasia.* Br J Surg, 1994. **81**(9): p. 1254-69.
20. Bennett, M.R., *In-stent stenosis: pathology and implications for the development of drug eluting stents.* Heart, 2003. **89**(2): p. 218-24.
21. Robertson, K.E., et al., *Prevention of coronary in-stent restenosis and vein graft failure: does vascular gene therapy have a role?* Pharmacol Ther, 2012. **136**(1): p. 23-34.
22. Bennett, M.R. and M. O'Sullivan, *Mechanisms of angioplasty and stent restenosis: implications for design of rational therapy.* Pharmacol Ther, 2001. **91**(2): p. 149-66.
23. Dangas, G.D., et al., *In-stent restenosis in the drug-eluting stent era.* J Am Coll Cardiol, 2010. **56**(23): p. 1897-907.
24. Liu, H.T., et al., *Rapamycin inhibits re-endothelialization after percutaneous coronary intervention by impeding the proliferation and migration of endothelial cells and inducing apoptosis of endothelial progenitor cells.* Tex Heart Inst J, 2010. **37**(2): p. 194-201.
25. Warren, J., U. Baber, and R. Mehran, *Antiplatelet therapy after drug-eluting stent implantation.* J Cardiol, 2015. **65**(2): p. 98-104.
26. Bavry, A.A. and D.L. Bhatt, *Appropriate use of drug-eluting stents: balancing the reduction in restenosis with the concern of late thrombosis.* Lancet, 2008. **371**(9630): p. 2134-43.
27. Stone, G.W., et al., *Paclitaxel-eluting stents versus bare-metal stents in acute myocardial infarction.* N Engl J Med, 2009. **360**(19): p. 1946-59.
28. Joner, M., et al., *Pathology of drug-eluting stents in humans: delayed healing and late thrombotic risk.* J Am Coll Cardiol, 2006. **48**(1): p. 193-202.
29. Hirano, T., et al., *Complementary DNA for a novel human interleukin (BSF-2) that induces B lymphocytes to produce immunoglobulin.* Nature, 1986. **324**(6092): p. 73-6.
30. Schaper, F. and S. Rose-John, *Interleukin-6: Biology, signaling and strategies of blockade.* Cytokine Growth Factor Rev, 2015. **26**(5): p.475-87.
31. Rose-John, S., *IL-6 trans-signaling via the soluble IL-6 receptor: importance for the pro-inflammatory activities of IL-6.* Int J Biol Sci, 2012. **8**(9): p. 1237-47.
32. Hibi, M., et al., *Molecular cloning and expression of an IL-6 signal transducer, gp130.* Cell, 1990. **63**(6): p. 1149-57.
33. Muller-Newen, G., et al., *Purification and characterization of the soluble interleukin-6 receptor from human plasma and identification of an isoform generated through alternative splicing.* Eur J Biochem, 1996. **236**(3): p. 837-42.
34. Lust, J.A., et al., *Isolation of an mRNA encoding a soluble form of the human interleukin-6 receptor.* Cytokine, 1992. **4**(2): p. 96-100.
35. Mullberg, J., et al., *The soluble interleukin-6 receptor is generated by shedding.* Eur J Immunol, 1993. **23**(2): p. 473-80.
36. Matthews, V., et al., *Cellular cholesterol depletion triggers shedding of the human interleukin-6 receptor by ADAM10 and ADAM17 (TACE).* J Biol Chem, 2003. **278**(40): p. 38829-39.
37. Scheller, J., et al., *The pro- and anti-inflammatory properties of the cytokine interleukin-6.* Biochim Biophys Acta, 2011. **1813**(5): p. 878-88.
38. Krebs, D.L. and D.J. Hilton, *SOCS proteins: negative regulators of cytokine signaling.* Stem Cells, 2001. **19**(5): p. 378-87.

39. Trengove, M.C. and A.C. Ward, *SOCS proteins in development and disease*. Am J Clin Exp Immunol, 2013. **2**(1): p. 1-29.
40. Elliott, J. and J.A. Johnston, *SOCS: role in inflammation, allergy and homeostasis*. Trends Immunol, 2004. **25**(8): p. 434-40.
41. Yoshimura, A., et al., *A novel cytokine-inducible gene CIS encodes an SH2-containing protein that binds to tyrosine-phosphorylated interleukin 3 and erythropoietin receptors*. EMBO J, 1995. **14**(12): p. 2816-26.
42. Endo, T.A., et al., *A new protein containing an SH2 domain that inhibits JAK kinases*. Nature, 1997. **387**(6636): p. 921-4.
43. Starr, R., et al., *A family of cytokine-inducible inhibitors of signalling*. Nature, 1997. **387**(6636): p. 917-21.
44. Alexander, W.S., et al., *SOCS1 is a critical inhibitor of interferon gamma signaling and prevents the potentially fatal neonatal actions of this cytokine*. Cell, 1999. **98**(5): p. 597-608.
45. Roberts, A.W., et al., *Placental defects and embryonic lethality in mice lacking suppressor of cytokine signaling 3*. Proc Natl Acad Sci U S A, 2001. **98**(16): p. 9324-9.
46. Schindler, C. and J.E. Darnell, Jr., *Transcriptional responses to polypeptide ligands: the JAK-STAT pathway*. Annu Rev Biochem, 1995. **64**: p. 621-51.
47. Williams, J.J., K.M. Munro, and T.M. Palmer, *Role of Ubiquitylation in Controlling Suppressor of Cytokine Signalling 3 (SOCS3) Function and Expression*. Cells, 2014. **3**(2): p. 546-62.
48. Piessevaux, J., et al., *The many faces of the SOCS box*. Cytokine Growth Factor Rev, 2008. **19**(5-6): p. 371-81.
49. White, C.A. and N.A. Nicola, *SOCS3: An essential physiological inhibitor of signaling by interleukin-6 and G-CSF family cytokines*. JAKSTAT, 2013. **2**(4): p. e25045.
50. Sasaki, A., et al., *CIS3/SOCS-3 suppresses erythropoietin (EPO) signaling by binding the EPO receptor and JAK2*. J Biol Chem, 2000. **275**(38): p. 29338-47.
51. Hortner, M., et al., *A new high affinity binding site for suppressor of cytokine signaling-3 on the erythropoietin receptor*. Eur J Biochem, 2002. **269**(10): p. 2516-26.
52. Bjorbak, C., et al., *SOCS3 mediates feedback inhibition of the leptin receptor via Tyr985*. J Biol Chem, 2000. **275**(51): p. 40649-57.
53. Pedroso, J.A., et al., *Inactivation of SOCS3 in leptin receptor-expressing cells protects mice from diet-induced insulin resistance but does not prevent obesity*. Mol Metab, 2014. **3**(6): p. 608-18.
54. Dey, B.R., R.W. Furlanetto, and P. Nissley, *Suppressor of cytokine signaling (SOCS)-3 protein interacts with the insulin-like growth factor-I receptor*. Biochem Biophys Res Commun, 2000. **278**(1): p. 38-43.
55. Zong, C.S., et al., *Mechanism of STAT3 activation by insulin-like growth factor I receptor*. J Biol Chem, 2000. **275**(20): p. 15099-105.
56. Irandoust, M.I., et al., *Suppressor of cytokine signaling 3 controls lysosomal routing of G-CSF receptor*. EMBO J, 2007. **26**(7): p. 1782-93.
57. Nicholson, S.E., et al., *Suppressor of cytokine signaling-3 preferentially binds to the SHP-2-binding site on the shared cytokine receptor subunit gp130*. Proc Natl Acad Sci U S A, 2000. **97**(12): p. 6493-8.
58. Schmitz, J., et al., *SOCS3 exerts its inhibitory function on interleukin-6 signal transduction through the SHP2 recruitment site of gp130*. J Biol Chem, 2000. **275**(17): p. 12848-56.

59. Babon, J.J., et al., *Suppression of cytokine signaling by SOCS3: characterization of the mode of inhibition and the basis of its specificity.* Immunity, 2012. **36**(2): p. 239-50.
60. Richmond, T.D., M. Chohan, and D.L. Barber, *Turning cells red: signal transduction mediated by erythropoietin.* Trends Cell Biol, 2005. **15**(3): p. 146-55.
61. Hookham, M.B., et al., *The myeloproliferative disorder-associated JAK2 V617F mutant escapes negative regulation by suppressor of cytokine signaling 3.* Blood, 2007. **109**(11): p. 4924-9.
62. Elliott, J., et al., *SOCS3 tyrosine phosphorylation as a potential bio-marker for myeloproliferative neoplasms associated with mutant JAK2 kinases.* Haematologica, 2009. **94**(4): p. 576-80.
63. Haan, S., et al., *SOCS-mediated downregulation of mutant Jak2 (V617F, T875N and K539L) counteracts cytokine-independent signaling.* Oncogene, 2009. **28**(34): p. 3069-80.
64. Suessmuth, Y., et al., *A new polycythaemia vera-associated SOCS3 SH2 mutant (SOCS3F136L) cannot regulate erythropoietin responses.* Br J Haematol, 2009. **147**(4): p. 450-8.
65. Friedman, J.M. and J.L. Halaas, *Leptin and the regulation of body weight in mammals.* Nature, 1998. **395**(6704): p. 763-70.
66. Cullen, K.J., et al., *Insulin-like growth factor receptor expression and function in human breast cancer.* Cancer Res, 1990. **50**(1): p. 48-53.
67. Sayeed, A., et al., *IGF-IR promotes prostate cancer growth by stabilizing alpha5beta1 integrin protein levels.* PLoS One, 2013. **8**(10): p. e76513.
68. Wu, J. and E. Yu, *Insulin-like growth factor receptor-1 (IGF-IR) as a target for prostate cancer therapy.* Cancer Metastasis Rev, 2014. **33**(2-3): p. 607-17.
69. Lieschke, G.J., et al., *Mice lacking granulocyte colony-stimulating factor have chronic neutropenia, granulocyte and macrophage progenitor cell deficiency, and impaired neutrophil mobilization.* Blood, 1994. **84**(6): p. 1737-46.
70. Kershaw, N.J., et al., *SOCS3 binds specific receptor-JAK complexes to control cytokine signaling by direct kinase inhibition.* Nat Struct Mol Biol, 2013. **20**(4): p. 469-76.
71. Babon, J.J. and N.A. Nicola, *The biology and mechanism of action of suppressor of cytokine signaling 3.* Growth Factors, 2012. **30**(4): p. 207-19.
72. Asnani, A. and R.T. Peterson, *The zebrafish as a tool to identify novel therapies for human cardiovascular disease.* Dis Model Mech, 2014. **7**(7): p. 763-7.
73. Wilkinson, R.N., C. Jopling, and F.J. van Eeden, *Zebrafish as a model of cardiac disease.* Prog Mol Biol Transl Sci, 2014. **124**: p. 65-91.
74. Wilkinson, R.N. and F.J. van Eeden, *The zebrafish as a model of vascular development and disease.* Prog Mol Biol Transl Sci, 2014. **124**: p. 93-122.
75. Winston, L.A. and T. Hunter, *Intracellular signalling: putting JAKs on the kinase MAP.* Curr Biol, 1996. **6**(6): p. 668-71.
76. Ihle, J.N. and I.M. Kerr, *Jaks and Stats in signaling by the cytokine receptor superfamily.* Trends Genet, 1995. **11**(2): p. 69-74.
77. Shen, S.H., et al., *A protein-tyrosine phosphatase with sequence similarity to the SH2 domain of the protein-tyrosine kinases.* Nature, 1991. **352**(6337): p. 736-9.

78. Wormald, S. and D.J. Hilton, *Inhibitors of cytokine signal transduction.* J Biol Chem, 2004. **279**(2): p. 821-4.
79. Reth, M. and T. Brummer, *Feedback regulation of lymphocyte signalling.* Nat Rev Immunol, 2004. **4**(4): p. 269-77.
80. Mihara, M., et al., *IL-6/IL-6 receptor system and its role in physiological and pathological conditions.* Clin Sci (Lond), 2012. **122**(4): p. 143-59.
81. Chen, Y., et al., *Identification of Shp-2 as a Stat5A phosphatase.* J Biol Chem, 2003. **278**(19): p. 16520-7.
82. Rutherford, C., H.D. Woolson, and T.M. Palmer, *Cross-Regulation of JAK-STAT Signalling: Implications For Approaches to Combat Chronic Inflammatory Diseases and Cancers*, in *Protein Kinases / Book 2*. 2012, In-Tech Publishers.
83. Komander, D. and M. Rape, *The ubiquitin code.* Annu Rev Biochem, 2012. **81**: p. 203-29.
84. Hilton, D.J., et al., *Twenty proteins containing a C-terminal SOCS box form five structural classes.* Proc Natl Acad Sci U S A, 1998. **95**(1): p. 114-9.
85. Williams, J.J. and T.M. Palmer, *Unbiased identification of substrates for the Epac1-inducible E3 ubiquitin ligase component SOCS-3.* Biochem Soc Trans, 2012. **40**(1): p. 215-8.
86. Kershaw, N.J., et al., *Reconstruction of an active SOCS3-based E3 ubiquitin ligase complex in vitro: identification of the active components and JAK2 and gp130 as substrates.* Growth Factors, 2014. **32**(1): p. 1-10.
87. Pallotta, M.T., et al., *Proteasomal Degradation of Indoleamine 2,3-Dioxygenase in CD8 Dendritic Cells is Mediated by Suppressor of Cytokine Signaling 3 (SOCS3).* Int J Tryptophan Res, 2010. **3**: p. 91-7.
88. Kawaguchi, T., et al., *Hepatitis C virus down-regulates insulin receptor substrates 1 and 2 through up-regulation of suppressor of cytokine signaling 3.* Am J Pathol, 2004. **165**(5): p. 1499-508.
89. Rui, L., et al., *SOCS-1 and SOCS-3 block insulin signaling by ubiquitin-mediated degradation of IRS1 and IRS2.* J Biol Chem, 2002. **277**(44): p. 42394-8.
90. Orr, S.J., et al., *SOCS3 targets Siglec 7 for proteasomal degradation and blocks Siglec 7-mediated responses.* J Biol Chem, 2007. **282**(6): p. 3418-22.
91. Orr, S.J., et al., *CD33 responses are blocked by SOCS3 through accelerated proteasomal-mediated turnover.* Blood, 2007. **109**(3): p. 1061-8.
92. Boyle, K., et al., *Deletion of the SOCS box of suppressor of cytokine signaling 3 (SOCS3) in embryonic stem cells reveals SOCS box-dependent regulation of JAK but not STAT phosphorylation.* Cell Signal, 2009. **21**(3): p. 394-404.
93. Liu, E., J.F. Cote, and K. Vuori, *Negative regulation of FAK signaling by SOCS proteins.* EMBO J, 2003. **22**(19): p. 5036-46.
94. Haan, S., et al., *Tyrosine phosphorylation disrupts elongin interaction and accelerates SOCS3 degradation.* J Biol Chem, 2003. **278**(34): p. 31972-9.
95. Sasaki, A., et al., *The N-terminal truncated isoform of SOCS3 translated from an alternative initiation AUG codon under stress conditions is stable due to the lack of a major ubiquitination site, Lys-6.* J Biol Chem, 2003. **278**(4): p. 2432-6.

96. Zhang, J.G., et al., *The conserved SOCS box motif in suppressors of cytokine signaling binds to elongins B and C and may couple bound proteins to proteasomal degradation.* Proc Natl Acad Sci U S A, 1999. **96**(5): p. 2071-6.
97. Fletcher, T.C., A. DiGiandomenico, and J. Hawiger, *Extended anti-inflammatory action of a degradation-resistant mutant of cell-penetrating suppressor of cytokine signaling 3.* J Biol Chem, 2010. **285**(24): p. 18727-36.
98. Sommer, U., et al., *Mechanisms of SOCS3 phosphorylation upon interleukin-6 stimulation. Contributions of Src- and receptor-tyrosine kinases.* J Biol Chem, 2005. **280**(36): p. 31478-88.
99. Rogers, S., R. Wells, and M. Rechsteiner, *Amino acid sequences common to rapidly degraded proteins: the PEST hypothesis.* Science, 1986. **234**(4774): p. 364-8.
100. Babon, J.J., et al., *The structure of SOCS3 reveals the basis of the extended SH2 domain function and identifies an unstructured insertion that regulates stability.* Mol Cell, 2006. **22**(2): p. 205-16.
101. Storr, S.J., et al., *The calpain system and cancer.* Nat Rev Cancer, 2011. **11**(5): p. 364-74.
102. Goll, D.E., et al., *The calpain system.* Physiol Rev, 2003. **83**(3): p. 731-801.
103. Miyazaki, T., et al., *Calpastatin counteracts pathological angiogenesis by inhibiting suppressor of cytokine signaling 3 degradation in vascular endothelial cells.* Circ Res, 2015. **116**(7): p. 1170-81.
104. Donkor, I.O., *An updated patent review of calpain inhibitors (2012 - 2014).* Expert Opin Ther Pat, 2015. **25**(1): p. 17-31.
105. Neuhof, C., et al., *Reduction of myocardial infarction by calpain inhibitors A-705239 and A-705253 in isolated perfused rabbit hearts.* Biol Chem, 2004. **385**(11): p. 1077-82.
106. Saatman, K.E., J. Creed, and R. Raghupathi, *Calpain as a therapeutic target in traumatic brain injury.* Neurotherapeutics, 2010. **7**(1): p. 31-42.
107. Liu, S., et al., *The role of calpains in traumatic brain injury.* Brain Inj, 2014. **28**(2): p. 133-7.
108. Leloup, L. and A. Wells, *Calpains as potential anti-cancer targets.* Expert Opin Ther Targets, 2011. **15**(3): p. 309-23.
109. Donkor, I.O., *Calpain inhibitors: a survey of compounds reported in the patent and scientific literature.* Expert Opin Ther Pat, 2011. **21**(5): p. 601-36.
110. Jo, D., et al., *Intracellular protein therapy with SOCS3 inhibits inflammation and apoptosis.* Nat Med, 2005. **11**(8): p. 892-8.
111. Tannahill, G.M., et al., *SOCS2 can enhance interleukin-2 (IL-2) and IL-3 signaling by accelerating SOCS3 degradation.* Mol Cell Biol, 2005. **25**(20): p. 9115-26.
112. Egger, G., et al., *Epigenetics in human disease and prospects for epigenetic therapy.* Nature, 2004. **429**(6990): p. 457-63.
113. He, B., et al., *SOCS-3 is frequently silenced by hypermethylation and suppresses cell growth in human lung cancer.* Proc Natl Acad Sci U S A, 2003. **100**(24): p. 14133-8.
114. Niwa, Y., et al., *Methylation silencing of SOCS-3 promotes cell growth and migration by enhancing JAK/STAT and FAK signalings in human hepatocellular carcinoma.* Oncogene, 2005. **24**(42): p. 6406-17.

115. Tischoff, I., et al., *Methylation of SOCS-3 and SOCS-1 in the carcinogenesis of Barrett's adenocarcinoma.* Gut, 2007. **56**(8): p. 1047-53.
116. Isomoto, H., *Epigenetic alterations in cholangiocarcinoma-sustained IL-6/STAT3 signaling in cholangio- carcinoma due to SOCS3 epigenetic silencing.* Digestion, 2009. **79 Suppl 1**: p. 2-8.
117. Sutherland, K.D., et al., *Differential hypermethylation of SOCS genes in ovarian and breast carcinomas.* Oncogene, 2004. **23**(46): p. 7726-33.
118. Gupta, G.K., et al., *Suppressor of cytokine signaling-3 and intimal hyperplasia in porcine coronary arteries following coronary intervention.* Exp Mol Pathol, 2011. **91**(1): p. 346-52.
119. Dhar, K., et al., *SOCS3 promotor hypermethylation and STAT3-NF-kappaB interaction downregulate SOCS3 expression in human coronary artery smooth muscle cells.* Am J Physiol Heart Circ Physiol, 2013. **304**(6): p. H776-85.
120. Jenuwein, T. and C.D. Allis, *Translating the histone code.* Science, 2001. **293**(5532): p. 1074-80.
121. Tamaru, H., *Confining euchromatin/heterochromatin territory: jumonji crosses the line.* Genes Dev, 2010. **24**(14): p. 1465-78.
122. Qin, H., et al., *Molecular mechanism of lipopolysaccharide-induced SOCS-3 gene expression in macrophages and microglia.* J Immunol, 2007. **179**(9): p. 5966-76.
123. Chen, C.Q., et al., *Pure curcumin increases the expression of SOCS1 and SOCS3 in myeloproliferative neoplasms through suppressing class I histone deacetylases.* Carcinogenesis, 2013. **34**(7): p. 1442-9.
124. Gao, S.M., et al., *Histone deacetylases inhibitor sodium butyrate inhibits JAK2/STAT signaling through upregulation of SOCS1 and SOCS3 mediated by HDAC8 inhibition in myeloproliferative neoplasms.* Exp Hematol, 2013. **41**(3): p. 261-70 e4.
125. Xiong, H., et al., *Trichostatin A, a histone deacetylase inhibitor, suppresses JAK2/STAT3 signaling via inducing the promoter-associated histone acetylation of SOCS1 and SOCS3 in human colorectal cancer cells.* Mol Carcinog, 2012. **51**(2): p. 174-84.
126. Kuttan, R., et al., *Potential anticancer activity of turmeric (Curcuma longa).* Cancer Lett, 1985. **29**(2): p. 197-202.
127. Komander, D., *The emerging complexity of protein ubiquitination.* Biochem Soc Trans, 2009. **37**(Pt 5): p. 937-53.
128. Berndsen, C.E. and C. Wolberger, *New insights into ubiquitin E3 ligase mechanism.* Nat Struct Mol Biol, 2014. **21**(4): p. 301-7.
129. Sylvestersen, K.B., C. Young, and M.L. Nielsen, *Advances in characterizing ubiquitylation sites by mass spectrometry.* Curr Opin Chem Biol, 2013. **17**(1): p. 49-58.
130. Heideker, J. and I.E. Wertz, *DUBs, the regulation of cell identity and disease.* Biochem J, 2015. **467**(1): p. 191.
131. Singhal, S., M.C. Taylor, and R.T. Baker, *Deubiquitylating enzymes and disease.* BMC Biochem, 2008. **9 Suppl 1**: p. S3.
132. Cole, A.J., R.J. Clifton-Bligh, and D.J. Marsh, *Ubiquitination and cancer: Histone H2B monoubiquitination - roles to play in human malignancy.* Endocr Relat Cancer, 2014.
133. Haglund, K., et al., *Multiple monoubiquitination of RTKs is sufficient for their endocytosis and degradation.* Nat Cell Biol, 2003. **5**(5): p. 461-6.
134. Chau, V., et al., *A multiubiquitin chain is confined to specific lysine in a targeted short-lived protein.* Science, 1989. **243**(4898): p. 1576-83.

135. Adams, J., *The proteasome: structure, function, and role in the cell.* Cancer Treat Rev, 2003. **29 Suppl 1**: p. 3-9.
136. Saric, T., C.I. Graef, and A.L. Goldberg, *Pathway for degradation of peptides generated by proteasomes: a key role for thimet oligopeptidase and other metallopeptidases.* J Biol Chem, 2004. **279**(45): p. 46723-32.
137. Thrower, J.S., et al., *Recognition of the polyubiquitin proteolytic signal.* EMBO J, 2000. **19**(1): p. 94-102.
138. Boutet, S.C., et al., *Regulation of Pax3 by proteasomal degradation of monoubiquitinated protein in skeletal muscle progenitors.* Cell, 2007. **130**(2): p. 349-62.
139. Xu, P., et al., *Quantitative proteomics reveals the function of unconventional ubiquitin chains in proteasomal degradation.* Cell, 2009. **137**(1): p. 133-45.
140. Chen, J. and Z.J. Chen, *Regulation of NF-kappaB by ubiquitination.* Curr Opin Immunol, 2013. **25**(1): p. 4-12.
141. Sato, Y., et al., *Molecular basis of Lys-63-linked polyubiquitination inhibition by the interaction between human deubiquitinating enzyme OTUB1 and ubiquitin-conjugating enzyme UBC13.* J Biol Chem, 2012. **287**(31): p. 25860-8.
142. Bhoj, V.G. and Z.J. Chen, *Ubiquitylation in innate and adaptive immunity.* Nature, 2009. **458**(7237): p. 430-7.
143. Schreiber, A. and M. Peter, *Substrate recognition in selective autophagy and the ubiquitin-proteasome system.* Biochim Biophys Acta, 2014. **1843**(1): p. 163-81.
144. Nathan, J.A., et al., *Why do cellular proteins linked to K63-polyubiquitin chains not associate with proteasomes?* EMBO J, 2013. **32**(4): p. 552-65.
145. Olzmann, J.A., et al., *Parkin-mediated K63-linked polyubiquitination targets misfolded DJ-1 to aggresomes via binding to HDAC6.* J Cell Biol, 2007. **178**(6): p. 1025-38.
146. Zhang, L., et al., *Both K63 and K48 ubiquitin linkages signal lysosomal degradation of the LDL receptor.* J Lipid Res, 2013. **54**(5): p. 1410-20.
147. Rader, D.J., J. Cohen, and H.H. Hobbs, *Monogenic hypercholesterolemia: new insights in pathogenesis and treatment.* J Clin Invest, 2003. **111**(12): p. 1795-803.
148. Chen, Z.J. and L.J. Sun, *Nonproteolytic functions of ubiquitin in cell signaling.* Mol Cell, 2009. **33**(3): p. 275-86.
149. Ciechanover, A. and R. Ben-Saadon, *N-terminal ubiquitination: more protein substrates join in.* Trends Cell Biol, 2004. **14**(3): p. 103-6.
150. Breitschopf, K., et al., *A novel site for ubiquitination: the N-terminal residue, and not internal lysines of MyoD, is essential for conjugation and degradation of the protein.* EMBO J, 1998. **17**(20): p. 5964-73.
151. Liu, J., et al., *Targeting the ubiquitin pathway for cancer treatment.* Biochim Biophys Acta, 2015. **1855**(1): p. 50-60.
152. van der Veen, A.G. and H.L. Ploegh, *Ubiquitin-like proteins.* Annu Rev Biochem, 2012. **81**: p. 323-57.
153. Hannoun, Z., et al., *Post-translational modification by SUMO.* Toxicology, 2010. **278**(3): p. 288-93.
154. Tatham, M.H., et al., *Polymeric chains of SUMO-2 and SUMO-3 are conjugated to protein substrates by SAE1/SAE2 and Ubc9.* J Biol Chem, 2001. **276**(38): p. 35368-74.

155. Gareau, J.R. and C.D. Lima, *The SUMO pathway: emerging mechanisms that shape specificity, conjugation and recognition.* Nat Rev Mol Cell Biol, 2010. **11**(12): p. 861-71.
156. Matunis, M.J., E. Coutavas, and G. Blobel, *A novel ubiquitin-like modification modulates the partitioning of the Ran-GTPase-activating protein RanGAP1 between the cytosol and the nuclear pore complex.* J Cell Biol, 1996. **135**(6 Pt 1): p. 1457-70.
157. McMillan, L.E., et al., *Profiles of SUMO and ubiquitin conjugation in an Alzheimer's disease model.* Neurosci Lett, 2011. **502**(3): p. 201-8.
158. Seeler, J.S., et al., *SUMO, the three Rs and cancer.* Curr Top Microbiol Immunol, 2007. **313**: p. 49-71.
159. Steffan, J.S., et al., *SUMO modification of Huntingtin and Huntington's disease pathology.* Science, 2004. **304**(5667): p. 100-4.
160. Kho, C., et al., *SUMO1-dependent modulation of SERCA2a in heart failure.* Nature, 2011. **477**(7366): p. 601-5.
161. Enchev, R.I., B.A. Schulman, and M. Peter, *Protein neddylation: beyond cullin-RING ligases.* Nat Rev Mol Cell Biol, 2015. **16**(1): p. 30-44.
162. Osaka, F., et al., *A new NEDD8-ligating system for cullin-4A.* Genes Dev, 1998. **12**(15): p. 2263-8.
163. Bosu, D.R. and E.T. Kipreos, *Cullin-RING ubiquitin ligases: global regulation and activation cycles.* Cell Div, 2008. **3**: p. 7.
164. Soucy, T.A., et al., *An inhibitor of NEDD8-activating enzyme as a new approach to treat cancer.* Nature, 2009. **458**(7239): p. 732-6.
165. Luo, Z., et al., *The Nedd8-activating enzyme inhibitor MLN4924 induces autophagy and apoptosis to suppress liver cancer cell growth.* Cancer Res, 2012. **72**(13): p. 3360-71.
166. Kuo, K.L., et al., *MLN4924, a novel protein neddylation inhibitor, suppresses proliferation and migration of human urothelial carcinoma: In vitro and in vivo studies.* Cancer Lett, 2015. **363**(2): p. 127-36.
167. Milhollen, M.A., et al., *MLN4924, a NEDD8-activating enzyme inhibitor, is active in diffuse large B-cell lymphoma models: rationale for treatment of NF-{kappa}B-dependent lymphoma.* Blood, 2010. **116**(9): p. 1515-23.
168. Danielsen, J.M., et al., *Mass spectrometric analysis of lysine ubiquitylation reveals promiscuity at site level.* Mol Cell Proteomics, 2011. **10**(3): p. M110 003590.
169. Ordureau, A., C. Munch, and J.W. Harper, *Quantifying ubiquitin signaling.* Mol Cell, 2015. **58**(4): p. 660-76.
170. Phu, L., et al., *Improved quantitative mass spectrometry methods for characterizing complex ubiquitin signals.* Mol Cell Proteomics, 2011. **10**(5): p. M110 003756.
171. Marrero, M.B., et al., *Role of Janus kinase/signal transducer and activator of transcription and mitogen-activated protein kinase cascades in angiotensin II- and platelet-derived growth factor-induced vascular smooth muscle cell proliferation.* J Biol Chem, 1997. **272**(39): p. 24684-90.
172. Seki, Y., et al., *Role of the JAK/STAT pathway in rat carotid artery remodeling after vascular injury.* Circ Res, 2000. **87**(1): p. 12-8.
173. Barnes, T.C., M.E. Anderson, and R.J. Moots, *The many faces of interleukin-6: the role of IL-6 in inflammation, vasculopathy, and fibrosis in systemic sclerosis.* Int J Rheumatol, 2011. **2011**: p. 721608.

174. von der Thusen, J.H., et al., *Interleukins in atherosclerosis: molecular pathways and therapeutic potential.* Pharmacol Rev, 2003. **55**(1): p. 133-66.
175. Shah, P., et al., *Rapid Progression of Coronary Atherosclerosis: A Review.* Thrombosis, 2015. **2015**: p. 634983.
176. Pendyala, L.K., et al., *The first-generation drug-eluting stents and coronary endothelial dysfunction.* JACC Cardiovasc Interv, 2009. **2**(12): p. 1169-77.
177. Sands, W.A., et al., *Exchange protein activated by cyclic AMP (Epac)-mediated induction of suppressor of cytokine signaling 3 (SOCS-3) in vascular endothelial cells.* Mol Cell Biol, 2006. **26**(17): p. 6333-46.
178. Laurenza, A., E.M. Sutkowski, and K.B. Seamon, *Forskolin: a specific stimulator of adenylyl cyclase or a diterpene with multiple sites of action?* Trends Pharmacol Sci, 1989. **10**(11): p. 442-7.
179. Cullere, X., et al., *Regulation of vascular endothelial barrier function by Epac, a cAMP-activated exchange factor for Rap GTPase.* Blood, 2005. **105**(5): p. 1950-5.
180. Fishbein, M.C., *The vulnerable and unstable atherosclerotic plaque.* Cardiovasc Pathol, 2010. **19**(1): p. 6-11.
181. Ortiz-Munoz, G., et al., *Suppressors of cytokine signaling modulate JAK/STAT-mediated cell responses during atherosclerosis.* Arterioscler Thromb Vasc Biol, 2009. **29**(4): p. 525-31.
182. Grothusen, C., et al., *Role of suppressor of cytokine signaling-1 in murine atherosclerosis.* PLoS One, 2012. **7**(12): p. e51608.
183. Recio, C., et al., *Gene delivery of suppressors of cytokine signaling (SOCS) inhibits inflammation and atherosclerosis development in mice.* Basic Res Cardiol, 2015. **110**(2): p. 8.
184. Taleb, S., et al., *Loss of SOCS3 expression in T cells reveals a regulatory role for interleukin-17 in atherosclerosis.* J Exp Med, 2009. **206**(10): p. 2067-77.
185. Shah, P.K., *Inflammation, neointimal hyperplasia, and restenosis: as the leukocytes roll, the arteries thicken.* Circulation, 2003. **107**(17): p. 2175-7.
186. Phillips, J.W., et al., *Single injection of P-selectin or P-selectin glycoprotein ligand-1 monoclonal antibody blocks neointima formation after arterial injury in apolipoprotein E-deficient mice.* Circulation, 2003. **107**(17): p. 2244-9.
187. Pirvulescu, M., et al., *A novel pro-inflammatory mechanism of action of resistin in human endothelial cells: up-regulation of SOCS3 expression through STAT3 activation.* Biochem Biophys Res Commun, 2012. **422**(2): p. 321-6.
188. Stahl, A., et al., *SOCS3 is an endogenous inhibitor of pathologic angiogenesis.* Blood, 2012. **120**(14): p. 2925-9.
189. Sun, Y., et al., *Nuclear receptor RORalpha regulates pathologic retinal angiogenesis by modulating SOCS3-dependent inflammation.* Proc Natl Acad Sci U S A, 2015. **112**(33): p. 10401-6.
190. Wan, J., et al., *SOCS3 blocks HIF-1alpha expression to inhibit proliferation and angiogenesis of human small cell lung cancer by downregulating activation of Akt, but not STAT3.* Mol Med Rep, 2015. **12**(1): p. 83-92.

191. Mitra, S.K., D.A. Hanson, and D.D. Schlaepfer, *Focal adhesion kinase: in command and control of cell motility.* Nat Rev Mol Cell Biol, 2005. **6**(1): p. 56-68.
192. Gennaro, G., et al., *Inhibition of vascular smooth muscle cell proliferation and neointimal formation in injured arteries by a novel, oral mitogen-activated protein kinase/extracellular signal-regulated kinase inhibitor.* Circulation, 2004. **110**(21): p. 3367-71.
193. Muslin, A.J., *MAPK signalling in cardiovascular health and disease: molecular mechanisms and therapeutic targets.* Clin Sci (Lond), 2008. **115**(7): p. 203-18.
194. Bauvois, B., *New facets of matrix metalloproteinases MMP-2 and MMP-9 as cell surface transducers: outside-in signaling and relationship to tumor progression.* Biochim Biophys Acta, 2012. **1825**(1): p. 29-36.
195. Ghosh, A., et al., *Cigarette smoke-induced MMP2 and MMP9 secretion from aortic vascular smooth cells is mediated via the Jak/Stat pathway.* Hum Pathol, 2015. **46**(2): p. 284-94.
196. Johnson, C. and Z.S. Galis, *Matrix metalloproteinase-2 and -9 differentially regulate smooth muscle cell migration and cell-mediated collagen organization.* Arterioscler Thromb Vasc Biol, 2004. **24**(1): p. 54-60.
197. Galis, Z.S., et al., *Targeted disruption of the matrix metalloproteinase-9 gene impairs smooth muscle cell migration and geometrical arterial remodeling.* Circ Res, 2002. **91**(9): p. 852-9.
198. Wu, Z.S., et al., *Prognostic significance of phosphorylated signal transducer and activator of transcription 3 and suppressor of cytokine signaling 3 expression in human cutaneous melanoma.* Melanoma Res, 2011. **21**(6): p. 483-90.
199. Wu, W.Y., et al., *Loss of suppressors of cytokine signaling 3 promotes aggressiveness in hepatocellular carcinoma.* J Invest Surg, 2014. **27**(4): p. 197-204.
200. Gao, W., et al., *Tofacitinib regulates synovial inflammation in psoriatic arthritis, inhibiting STAT activation and induction of negative feedback inhibitors.* Ann Rheum Dis, 2016. **75**(1): p. 311-5.
201. Grote, K., et al., *Mechanical stretch enhances mRNA expression and proenzyme release of matrix metalloproteinase-2 (MMP-2) via NAD(P)H oxidase-derived reactive oxygen species.* Circ Res, 2003. **92**(11): p. e80-6.
202. Bendeck, M.P., et al., *Smooth muscle cell migration and matrix metalloproteinase expression after arterial injury in the rat.* Circ Res, 1994. **75**(3): p. 539-45.
203. Newby, A.C., *Dual role of matrix metalloproteinases (matrixins) in intimal thickening and atherosclerotic plaque rupture.* Physiol Rev, 2005. **85**(1): p. 1-31.
204. Southgate, K.M., et al., *Increased secretion of basement membrane-degrading metalloproteinases in pig saphenous vein into carotid artery interposition grafts.* Arterioscler Thromb Vasc Biol, 1999. **19**(7): p. 1640-9.
205. George, S.J., et al., *Sustained reduction of vein graft neointima formation by ex vivo TIMP-3 gene therapy.* Circulation, 2011. **124**(11 Suppl): p. S135-42.
206. Shah, P.K. and Z.S. Galis, *Matrix metalloproteinase hypothesis of plaque rupture: players keep piling up but questions remain.* Circulation, 2001. **104**(16): p. 1878-80.

207. Owens, G.K., M.S. Kumar, and B.R. Wamhoff, *Molecular regulation of vascular smooth muscle cell differentiation in development and disease.* Physiol Rev, 2004. **84**(3): p. 767-801.
208. Loppnow, H. and P. Libby, *Proliferating or interleukin 1-activated human vascular smooth muscle cells secrete copious interleukin 6.* J Clin Invest, 1990. **85**(3): p. 731-8.
209. Podor, T.J., et al., *Human endothelial cells produce IL-6. Lack of responses to exogenous IL-6.* Ann N Y Acad Sci, 1989. **557**: p. 374-85; discussion 386-7.
210. Interleukin-6 Receptor Mendelian Randomisation Analysis, C., A.D. Hingorani, and J.P. Casas, *The interleukin-6 receptor as a target for prevention of coronary heart disease: a mendelian randomisation analysis.* Lancet, 2012. **379**(9822): p. 1214-24.
211. Liu, Z., N. Dronadula, and G.N. Rao, *A novel role for nuclear factor of activated T cells in receptor tyrosine kinase and G protein-coupled receptor agonist-induced vascular smooth muscle cell motility.* J Biol Chem, 2004. **279**(39): p. 41218-26.
212. Wang, D., et al., *An essential role for gp130 in neointima formation following arterial injury.* Circ Res, 2007. **100**(6): p. 807-16.
213. Sherr, C.J., *G1 phase progression: cycling on cue.* Cell, 1994. **79**(4): p. 551-5.
214. Liao, X.H., et al., *STAT3 Protein Regulates Vascular Smooth Muscle Cell Phenotypic Switch by Interaction with Myocardin.* J Biol Chem, 2015. **290**(32): p. 19641-52.
215. Gomez-Guerrero, C., et al., *Suppressors of cytokine signaling regulate Fc receptor signaling and cell activation during immune renal injury.* J Immunol, 2004. **172**(11): p. 6969-77.
216. Xiang, S., et al., *Suppressor of cytokine signaling 3 is a negative regulator for neointimal hyperplasia of vein graft stenosis.* J Vasc Res, 2014. **51**(2): p. 132-43.
217. Krump-Konvalinkova, V., et al., *Establishment and characterization of an angiosarcoma-derived cell line, AS-M.* Endothelium, 2003. **10**(6): p. 319-28.
218. Chick, H.E., et al., *Integrase-deficient lentiviral vectors mediate efficient gene transfer to human vascular smooth muscle cells with minimal genotoxic risk.* Hum Gene Ther, 2012. **23**(12): p. 1247-57.
219. Sasaki, A., et al., *Cytokine-inducible SH2 protein-3 (CIS3/SOCS3) inhibits Janus tyrosine kinase by binding through the N-terminal kinase inhibitory region as well as SH2 domain.* Genes Cells, 1999. **4**(6): p. 339-51.
220. Smith, P.K., et al., *Measurement of Protein Using Bicinchoninic Acid.* Analytical Biochemistry, 1985. **150**(1): p. 76-85.
221. Hjerpe, R., et al., *Efficient protection and isolation of ubiquitylated proteins using tandem ubiquitin-binding entities.* EMBO Rep, 2009. **10**(11): p. 1250-8.
222. Demaison, C., et al., *High-level transduction and gene expression in hematopoietic repopulating cells using a human immunodeficiency [correction of imunodeficiency] virus type 1-based lentiviral vector containing an internal spleen focus forming virus promoter.* Hum Gene Ther, 2002. **13**(7): p. 803-13.
223. Yanez-Munoz, R.J., et al., *Effective gene therapy with nonintegrating lentiviral vectors.* Nat Med, 2006. **12**(3): p. 348-53.

224. Butler, S.L., M.S. Hansen, and F.D. Bushman, *A quantitative assay for HIV DNA integration in vivo.* Nat Med, 2001. **7**(5): p. 631-4.
225. Neuhoff, V., et al., *Improved staining of proteins in polyacrylamide gels including isoelectric focusing gels with clear background at nanogram sensitivity using Coomassie Brilliant Blue G-250 and R-250.* Electrophoresis, 1988. **9**(6): p. 255-62.
226. Perkins, D.N., et al., *Probability-based protein identification by searching sequence databases using mass spectrometry data.* Electrophoresis, 1999. **20**(18): p. 3551-67.
227. Searle, B.C., *Scaffold: a bioinformatic tool for validating MS/MS-based proteomic studies.* Proteomics, 2010. **10**(6): p. 1265-9.
228. Cox, J. and M. Mann, *Computational principles of determining and improving mass precision and accuracy for proteome measurements in an Orbitrap.* J Am Soc Mass Spectrom, 2009. **20**(8): p. 1477-85.
229. Tyanova, S., et al., *Visualization of LC-MS/MS proteomics data in MaxQuant.* Proteomics, 2015. **15**(8): p. 1453-6.
230. Udeshi, N.D., et al., *Large-scale identification of ubiquitination sites by mass spectrometry.* Nat Protoc, 2013. **8**(10): p. 1950-60.
231. Liang, C.C., A.Y. Park, and J.L. Guan, *In vitro scratch assay: a convenient and inexpensive method for analysis of cell migration in vitro.* Nat Protoc, 2007. **2**(2): p. 329-33.
232. Babon, J.J., et al., *The SOCS box domain of SOCS3: structure and interaction with the elonginBC-cullin5 ubiquitin ligase.* J Mol Biol, 2008. **381**(4): p. 928-40.
233. Hochstrasser, M., *New structural clues to substrate specificity in the "ubiquitin system".* Mol Cell, 2002. **9**(3): p. 453-4.
234. King, R.W., M. Glotzer, and M.W. Kirschner, *Mutagenic analysis of the destruction signal of mitotic cyclins and structural characterization of ubiquitinated intermediates.* Mol Biol Cell, 1996. **7**(9): p. 1343-57.
235. Powers, E.T., et al., *Biological and chemical approaches to diseases of proteostasis deficiency.* Annu Rev Biochem, 2009. **78**: p. 959-91.
236. Narendra, D., et al., *Parkin is recruited selectively to impaired mitochondria and promotes their autophagy.* J Cell Biol, 2008. **183**(5): p. 795-803.
237. Marder, K.S., et al., *Predictors of parkin mutations in early-onset Parkinson disease: the consortium on risk for early-onset Parkinson disease study.* Arch Neurol, 2010. **67**(6): p. 731-8.
238. Kim, W., et al., *Systematic and quantitative assessment of the ubiquitin-modified proteome.* Mol Cell, 2011. **44**(2): p. 325-40.
239. Reich, N., et al., *Interferon-induced transcription of a gene encoding a 15-kDa protein depends on an upstream enhancer element.* Proc Natl Acad Sci U S A, 1987. **84**(18): p. 6394-8.
240. Kaiser, P. and J. Wohlschlegel, *Identification of ubiquitination sites and determination of ubiquitin-chain architectures by mass spectrometry.* Methods Enzymol, 2005. **399**: p. 266-77.
241. Spence, J., et al., *A ubiquitin mutant with specific defects in DNA repair and multiubiquitination.* Mol Cell Biol, 1995. **15**(3): p. 1265-73.
242. Valkevich, E.M., et al., *Middle-down mass spectrometry enables characterization of branched ubiquitin chains.* Biochemistry, 2014. **53**(30): p. 4979-89.
243. Jessup, M., et al., *Calcium Upregulation by Percutaneous Administration of Gene Therapy in Cardiac Disease (CUPID): a phase 2 trial of*

intracoronary gene therapy of sarcoplasmic reticulum Ca2+-ATPase in patients with advanced heart failure. Circulation, 2011. **124**(3): p. 304-13.
244. Shouda, T., et al., *Induction of the cytokine signal regulator SOCS3/CIS3 as a therapeutic strategy for treating inflammatory arthritis.* J Clin Invest, 2001. **108**(12): p. 1781-8.
245. Herman, A.G., et al., *Discovery of Mdm2-MdmX E3 ligase inhibitors using a cell-based ubiquitination assay.* Cancer Discov, 2011. **1**(4): p. 312-25.
246. Park, F., *Lentiviral vectors: are they the future of animal transgenesis?* Physiol Genomics, 2007. **31**(2): p. 159-73.
247. Tran, H., et al., *HectD1 E3 ligase modifies adenomatous polyposis coli (APC) with polyubiquitin to promote the APC-axin interaction.* J Biol Chem, 2013. **288**(6): p. 3753-67.
248. Sarkar, A.A. and I.E. Zohn, *Hectd1 regulates intracellular localization and secretion of Hsp90 to control cellular behavior of the cranial mesenchyme*. J Cell Biol, 2012. **196**(6): p. 789-800.
249. Duffy, M.R., et al., *Identification of novel small molecule inhibitors of adenovirus gene transfer using a high throughput screening approach.* J Control Release, 2013. **170**(1): p. 132-40.
250. Persson, M., et al., *High-content analysis/screening for predictive toxicology: application to hepatotoxicity and genotoxicity.* Basic Clin Pharmacol Toxicol, 2014. **115**(1): p. 18-23.
251. Li, W., et al., *Genome-wide and functional annotation of human E3 ubiquitin ligases identifies MULAN, a mitochondrial E3 that regulates the organelle's dynamics and signaling*. PLoS One, 2008. **3**(1): p. e1487.
252. Katzmann, D.J., M. Babst, and S.D. Emr, *Ubiquitin-dependent sorting into the multivesicular body pathway requires the function of a conserved endosomal protein sorting complex, ESCRT-I.* Cell, 2001. **106**(2): p. 145-55.
253. Sarkar, A.A., et al., *Hectd1 is required for development of the junctional zone of the placenta*. Dev Biol, 2014. **392**(2): p. 368-80.
254. Nijman, S.M., et al., *A genomic and functional inventory of deubiquitinating enzymes.* Cell, 2005. **123**(5): p. 773-86.
255. Baker, R.T., et al., *Identification, functional characterization, and chromosomal localization of USP15, a novel human ubiquitin-specific protease related to the UNP oncoprotein, and a systematic nomenclature for human ubiquitin-specific proteases.* Genomics, 1999. **59**(3): p. 264-74.
256. Zou, Q., et al., *USP15 stabilizes MDM2 to mediate cancer-cell survival and inhibit antitumor T cell responses.* Nat Immunol, 2014. **15**(6): p. 562-70.
257. Hetfeld, B.K., et al., *The zinc finger of the CSN-associated deubiquitinating enzyme USP15 is essential to rescue the E3 ligase Rbx1.* Curr Biol, 2005. **15**(13): p. 1217-21.
258. Rabut, G. and M. Peter, *Function and regulation of protein neddylation. 'Protein modifications: beyond the usual suspects' review series.* EMBO Rep, 2008. **9**(10): p. 969-76.
259. Hori, T., et al., *Covalent modification of all members of human cullin family proteins by NEDD8.* Oncogene, 1999. **18**(48): p. 6829-34.
260. Huang, D.T. and B.A. Schulman, *Expression, purification, and characterization of the E1 for human NEDD8, the heterodimeric APPBP1-UBA3 complex.* Methods Enzymol, 2005. **398**: p. 9-20.

261. Kamura, T., et al., *The Rbx1 subunit of SCF and VHL E3 ubiquitin ligase activates Rub1 modification of cullins Cdc53 and Cul2.* Genes Dev, 1999. **13**(22): p. 2928-33.
262. Podust, V.N., et al., *A Nedd8 conjugation pathway is essential for proteolytic targeting of p27Kip1 by ubiquitination.* Proc Natl Acad Sci U S A, 2000. **97**(9): p. 4579-84.
263. Jordan, E.T., et al., *Optimizing electroporation conditions in primary and other difficult-to-transfect cells.* J Biomol Tech, 2008. **19**(5): p. 328-34.
264. Yahagi, K., et al., *Pathophysiology of native coronary, vein graft, and in-stent atherosclerosis.* Nat Rev Cardiol, 2016. **13**(2): p. 79-98.
265. Rensen, S.S., P.A. Doevendans, and G.J. van Eys, *Regulation and characteristics of vascular smooth muscle cell phenotypic diversity.* Neth Heart J, 2007. **15**(3): p. 100-8.
266. Deng, D.X., et al., *Molecular signatures determining coronary artery and saphenous vein smooth muscle cell phenotypes: distinct responses to stimuli.* Arterioscler Thromb Vasc Biol, 2006. **26**(5): p. 1058-65.
267. Gratzner, H.G., et al., *The use of antibody specific for bromodeoxyuridine for the immunofluorescent determination of DNA replication in single cells and chromosomes.* Exp Cell Res, 1975. **95**(1): p. 88-94.
268. Cavanagh, B.L., et al., *Thymidine analogues for tracking DNA synthesis.* Molecules, 2011. **16**(9): p. 7980-93.
269. Mosmann, T., *Rapid colorimetric assay for cellular growth and survival: application to proliferation and cytotoxicity assays.* J Immunol Methods, 1983. **65**(1-2): p. 55-63.
270. Taylor, J.H., P.S. Woods, and W.L. Hughes, *The Organization and Duplication of Chromosomes as Revealed by Autoradiographic Studies Using Tritium-Labeled Thymidinee.* Proc Natl Acad Sci U S A, 1957. **43**(1): p. 122-8.
271. Duque, A. and P. Rakic, *Different effects of bromodeoxyuridine and [3H]thymidine incorporation into DNA on cell proliferation, position, and fate.* J Neurosci, 2011. **31**(42): p. 15205-17.
272. Kramer, N., et al., *In vitro cell migration and invasion assays.* Mutat Res, 2013. **752**(1): p. 10-24.
273. Veenbergen, S., et al., *Splenic suppressor of cytokine signaling 3 transgene expression affects T cell responses and prevents development of collagen-induced arthritis.* Arthritis Rheum, 2008. **58**(12): p. 3742-52.
274. Komiya, Y. and R. Habas, *Wnt signal transduction pathways.* Organogenesis, 2008. **4**(2): p. 68-75.
275. Romer, L.H., K.G. Birukov, and J.G. Garcia, *Focal adhesions: paradigm for a signaling nexus.* Circ Res, 2006. **98**(5): p. 606-16.
276. Alfonso, F., et al., *Current treatment of in-stent restenosis.* J Am Coll Cardiol, 2014. **63**(24): p. 2659-73.
277. Shaikh, S., et al., *Macrophage subtypes in symptomatic carotid artery and femoral artery plaques.* Eur J Vasc Endovasc Surg, 2012. **44**(5): p. 491-7.
278. Nalepa, G., M. Rolfe, and J.W. Harper, *Drug discovery in the ubiquitin-proteasome system.* Nat Rev Drug Discov, 2006. **5**(7): p. 596-613.
279. Kranzhofer, A., et al., *Expression of tissue inhibitor of metalloproteinase-1, -2, and -3 during neointima formation in organ cultures of human saphenous vein.* Arterioscler Thromb Vasc Biol, 1999. **19**(2): p. 255-65.

280. Ali, Z.A., et al., *Increased in-stent stenosis in ApoE knockout mice: insights from a novel mouse model of balloon angioplasty and stenting.* Arterioscler Thromb Vasc Biol, 2007. **27**(4): p. 833-40.
281. Sheen, C.R., et al., *Pathophysiological role of vascular smooth muscle alkaline phosphatase in medial artery calcification.* J Bone Miner Res, 2015. **30**(5): p. 824-36.
282. Zhang, J., et al., *Generation of an adult smooth muscle cell-targeted Cre recombinase mouse model.* Arterioscler Thromb Vasc Biol, 2006. **26**(3): p. e23-4.
283. Hu, D., et al., *Artery Tertiary Lymphoid Organs Control Aorta Immunity and Protect against Atherosclerosis via Vascular Smooth Muscle Cell Lymphotoxin beta Receptors.* Immunity, 2015. **42**(6): p. 1100-15.
284. Han, C., et al., *SMAD1 deficiency in either endothelial or smooth muscle cells can predispose mice to pulmonary hypertension.* Hypertension, 2013. **61**(5): p. 1044-52.
285. Xu, Y., et al., *Endothelial PFKFB3 plays a critical role in angiogenesis.* Arterioscler Thromb Vasc Biol, 2014. **34**(6): p. 1231-9.
286. Stringer, D.K. and R.C. Piper, *A single ubiquitin is sufficient for cargo protein entry into MVBs in the absence of ESCRT ubiquitination.* J Cell Biol, 2011. **192**(2): p. 229-42.
287. Stringer, D.K. and R.C. Piper, *Terminating protein ubiquitination: Hasta la vista, ubiquitin.* Cell Cycle, 2011. **10**(18): p. 3067-71.
288. Chen, D., et al., *Bortezomib as the first proteasome inhibitor anticancer drug: current status and future perspectives.* Curr Cancer Drug Targets, 2011. **11**(3): p. 239-53.
289. Dou, Q.P. and J.A. Zonder, *Overview of proteasome inhibitor-based anti-cancer therapies: perspective on bortezomib and second generation proteasome inhibitors versus future generation inhibitors of ubiquitin-proteasome system.* Curr Cancer Drug Targets, 2014. **14**(6): p. 517-36.
290. Zsebo, K., et al., *Long-term effects of AAV1/SERCA2a gene transfer in patients with severe heart failure: analysis of recurrent cardiovascular events and mortality.* Circ Res, 2014. **114**(1): p. 101-8.
291. Burns-Hamuro, L.L., et al., *Designing isoform-specific peptide disruptors of protein kinase A localization.* Proc Natl Acad Sci U S A, 2003. **100**(7): p. 4072-7.